ACTIVATION OF SMALL MOLECULES BY A TUNGSTEN ACETYLENE COMPLEX

by

SEAN A. LUMB

B.Sc.(Hons), Queen's University, 1993

A THESIS SUBMITTED IN PARTIAL FULFILLMENT OF
THE REQUIREMENTS FOR THE DEGREE OF
DOCTOR OF PHILOSOPHY

in

THE FACULTY OF GRADUATE STUDIES

(Department of Chemistry)

We accept this thesis as conforming

to the required standard

THE UNIVERSITY OF BRITISH COLUMBIA

November 1998

In presenting this thesis in partial fulfilment of the requirements for an advanced degree at the University of British Columbia, I agree that the Library shall make it freely available for reference and study. I further agree that permission for extensive copying of this thesis for scholarly purposes may be granted by the head of my department or by his or her representatives. It is understood that copying or publication of this thesis for financial gain shall not be allowed without my written permission.

Department of CHEMISTRY

The University of British Columbia
Vancouver, Canada

Date 11.27.98

Abstract

A series of η^1- and η^2-vinyl-containing complexes of the form Cp*W(NO)(η^x-CPh=CH_2)(E) [x = 1 or 2, E = CH_2SiMe_3, Cl, η^2-O_2CPh, OTf, NH^{t}Bu, and (H)(PPh_3)] has been prepared, and the solid-state metrical parameters and solution NMR spectroscopic properties of these complexes have been examined. The hapticity of the vinyl ligand in these complexes is dependent of the electron donicity of the ancillary ligand E. Ligands which function as three-electron (3e) donors (such as η^2-O_2CPh and NH^{t}Bu) enforce a monohapto bonding mode for the vinyl ligand, whereas ligands that function as 1e donors (such as CH_2SiMe_3) permit the dihapto coordination of the vinyl ligand. A search of the Cambridge Structural Database (CSD) reveals a paucity of structurally characterized η^2-vinyl complexes of tungsten. Comparisons of the solid-state metrical parameters determined for the η^2-vinyl complexes described in this Thesis and those found in the CSD are made which shed light on the nature of the vinyl interaction in the nitrosyl-containing complexes described herein.

Thermolysis of the alkyl vinyl complex Cp*W(NO)(CH_2SiMe_3)(CPh=CH_2) (**1**) at 54 °C in the presence of unsaturated, heteroatom-containing compounds such as esters, nitriles or acetone quantitatively affords metallacyclic products of subtrate-alkyne coupling. The nature of these metallacycles is consistent with the intermediacy of the acetylene complex Cp*W(NO)(η^2-CPh≡CH) (**A**) derived *in situ* from the reductive elimination of $SiMe_4$ from **1**. With esters ROAc [R = Me, Et], coupling and C-O bond cleavage yield the alkoxide-containing oxametallacyclopentadiene complexes Cp*W(NO)(η^2-*O*=C(Me)CH=*C*Ph)(OR) R = Me, Et]. Thermolysis of **1** in RCN [R = Me, Et, ^{i}Pr] containing trace amounts of R′OH yields the respective hydroxide or alkoxide compounds Cp*W(NO)(η^2-*N*H=C(R)CH=*C*Ph)(OR′) [R = Me,

R' = H; R = Et, R′ = H; R = ^{i}Pr, R′ = H; R = Me, R′ = C_3H_5]. Utilization of cyclopentadiene (CpH) as the trapping agent in MeCN affords the aminopentafulvene complex Cp*W(NO)(HNC(=C(C_4H_4))(Me))(η^2- *N*H=C(Me)CH=*C*Ph). Thermolysis of **1** in RCN [R = Me, ^{i}Pr] containing trace amounts of acetone gives the bicyclic species Cp*W(NO)(η^3-*O*C(Me)$_2$*N*=C(R)CH=*C*Ph). In the absence of added trapping reagent, thermolysis of **1** in RCN [R = Me, Et] yields the vinyl amidinate complexes Cp*W(NO)(η^3-*N*HC(R)=*N*C(=C(R^1)(R^2))CH=*C*Ph) [R = Me, R^1 = R^2 = H; R = Et, R^1 = H, R^2 = Me]. The results of labelling studies corroborate mechanistic proposals that account for the observed chemistry. The results of a kinetic study involving several of these transformations substantiate the proposal for a rate-limiting generation of acetylene intermediate **A** in a dissociative mechanism under saturation conditions (ie. a "saturation" mechanism) via $SiMe_4$ elimination followed by the rapid trapping of **A** in coupling reactions with organic substrates. A qualitative molecular-orbital overlap rationale is given to account for the observed chemistry.

The quantitative decomposition of Cp*W(NO)(η^2-CPh=CH_2)(CH_2SiMe_3) (**1**) at 54 °C in neat hydrocarbon solutions transiently generates Cp*W(NO)(η^2-CPh≡CH) (**A**) which activates solvent C-H bonds *in situ*. For example, the thermolysis of **1** in benzene solution quantitatively generates Cp*W(NO)(η^2-CPh=CH_2)(Ph). The thermolysis of **1** in solutions of methyl-substituted arenes such as toluene and *p*-, *m*-, or *o*-xylene affords mixtures of aryl and benzyl vinyl complexes of the general formulae Cp*W(NO)(η^2-CPh=CH_2)(aryl), Cp*W(NO)(η^2-CPh=CH_2)(η^1-benzyl), or Cp*W(NO)(η^1-CPh=CH_2)(η^2-benzyl). During these conversions, no products of *ortho*-C-H bond activation are observed. The thermolysis of **1** in $(Me_3Si)_2O$ under identical conditions quantitatively affords Cp*W(NO)(η^2-

CPh=CH_2)($CH_2SiMe_2OSiMe_3$). The mechanism by which RH is eliminated from Cp*W(NO)(R)(CPh=CH_2) to generate the proposed acetylene-containing intermediate **A** is considered in detail. Deuterium-labelling experiments support the intermediacy of **A** along the reaction pathway. The results of kinetic studies are indicative of a mechanism involving the rate-limiting generation of **A** under saturation conditions via vinyl-H elimination and RH extrusion, in accord with those of the kinetic study described above. Mechanistic studies provide evidence for the transiency of hydrocarbon σ-complexes along the reaction coordinate prior to both hydrocarbon elimination and substrate C-H bond activation. Competition studies employing mixtures of hydrocarbon substrates reveal a lack of selectivity by **A** towards the nature of the activated C-H bond, consistent with the proposed mechanism. An MO scheme depicting the W-acetylene valence orbital interactions in **A** aids in rationalizing the activity of acetylene-containing **A** towards substrate C-H bonds. Dual C-H bond activation of the aliphatic substrate occurs during the thermal generation of **A** from **1** in aliphatic hydrocarbon solutions. Consequently, metallacycles of the form Cp*W(NO)(η^2-*C*H(η^2-Ph)CH_2CH(R)*C*H_2) [R = ^{n}Pr, ^{n}Bu, ^{t}Bu, OEt] result from the dehydrogenation of *n*-pentane, *n*-hexane, 2,2-dimethylbutane and diethyl ether, respectively. This dual C-H activation process displays a selectivity for linear substrates that contain an ethyl substituent. Dual C-H bond activation of 2,3-dimethyl-2-butene in the presence of **1** under thermolysis conditions regioselectively affords Cp*W(NO)(η^3-*endo*-*C*H_2*C*(Me)*C*(Me)CH_2(η^1-*C*PhMe)). Plausible mechanisms are proposed for the formation of these metallacyclic complexes, and a rationale for the regioselectivities extant in these conversions is also presented.

Table of contents

List of Tables

List of Figures

List of Schemes

List of Abbreviations

The following list of abbreviations employed in this Thesis are commonly used in the chemical literature.

°	degree (of angle or temperature)	**EI**	electron-impact
∞	infinity	**EtOAc**	ethyl acetate
α	the position once removed from a reference position (i.e. from a metal centre)	η	hapto, denotes ligand hapticity
$\mathbf{A_t}$	absorbance at time t	**FAB**	fast-atom bombardment
$\mathbf{A_\infty}$	absorbance at infinite time	**g**	gram(s)
Å	angstrom, 10^{-10} m	γ	the position thrice removed from a reference position (i.e. a metal centre)
anal	analysis	**h**	hour(s)
atm	atmosphere(s)	$\mathbf{^1H}$	proton
avge	average	**HMBC**	heteronuclear multiple-bond coherence
β	the position twice removed from a reference position (i.e. from a metal centre)	**HMQC**	heteronuclear multiple quantum coherence
br	broad (spectral)	**HOMO**	highest occupied molecular orbital
^{n}Bu	$CH_3CH_2CH_2CH_2$, "normal" butyl	**HPLC**	high-performance liquid chromatography
^{t}Bu	*tert*-butyl	**Hz**	Hertz (s^{-1})
Bz	benzyl	**IR**	infrared
°C	degree Celsius	**J**	coupling constant
$\mathbf{^{13}C}$	carbon-13	$\mathbf{^nJ_{AB}}$	n-bond J between atoms A and B
$\mathbf{^{13}C\{^1H\}}$	proton-decoupled ^{13}C	$\mathbf{k_n}$	rate constant for the nth elementary step
cal	calorie	$\mathbf{k_{obs}}$	observed rate constant
calcd	calculated	**K**	degree Kelvin
$\mathbf{cm^{-1}}$	wavenumbers	$\mathbf{K_{eq}}$	equilibrium constant
COSY	correlation spectroscopy	**KIE**	kinetic isotope effect
CSD	Cambridge Structural Database	λ	wavelength (nm)
Cp	η^5-C_5H_5, cyclopentadienyl	**L**	ligand or litre
CpH	C_5H_6	**LUMO**	lowest unoccupied molecular orbital
Cp*	η^5- C_5H_5, pentamethyl Cp	**m**	multiplet
Cp'	Cp or Cp*	**M**	molar or mega
δ	chemical shift in ppm	**m/z**	mass-to-charge ratio
d	doublet or day(s)	**Me**	CH_3, methyl
$\boldsymbol{d_n}$	deuterated in n positions	**MeCN**	acetonitrile
D	deuterium, ^2H	**MeOAc**	methyl acetate
DFT	density-functional theory	**mg**	milligram(s)
DIPP	bis(diisopropyl)phosphinoethane	**mL**	millilitre
DMSO	dimethyl sulfoxide	**mmol**	millimole
Δ	heat (in thermolysis) or a difference (between two states)	**mol**	mole
Et	C_2H_5, ethyl	**MS**	mass spectrum
EtCN	propionitrile	**NMR**	nuclear magnetic resonance

NOE	nuclear Overhauser effect	**R**	hydrocarbyl
Nu	nucleophile	**RT**	room temperature
ν	stretching frequency	**s**	singlet or second
OTf	SO_3CF_3, Triflate	**t**	Triplet or time (s)
ORTEP	Oak Ridge Thermal Ellipsoid Program	$\mathbf{t_{1/2}}$	half-life
^{31}**P**	phosphorus-31	**T**	temperature
$[P]^+$	parent molecular ion	**Temp**	temperature
Ph	C_6H_5, phenyl	**TBE**	*tert*-butylethylene
PhCN	benzonitrile	**THF**	tetrahydrofuran
ppm	parts per million	**THF-d_8**	C_4D_8O
^{i}**Pr**	$(CH_3)_2CH$, isopropyl	**TMS**	$SiMe_4$, tetramethylsilane
^{i}**PrCN**	isobutyronitrile	**Tp'**	Tris(3,5-dimethylpyrazolyl)hydroborate
^{n}**Pr**	$CH_3CH_2CH_2$, "normal" propyl	**UV-vis**	ultraviolet-visible
q	quartet	**VT**	variable temperature

Acknowledgments

Several individuals deserve acknowledgment for their contribution in one form or another to the success of this research project. Many thanks to Peter Legzdins for providing a stimulating research environment that promotes academic freedom and self-discipline, and for inspiration and expertise when my own failed me. Many past Legzdins group members deserve recognition. These include Jeff Debad for getting me started, Kevin Ross, my early A254 benchmate, Michelle Young for advice and adventures in the mountains, and Steve (Sonny-boy) Sayers, the irreplaceable housemate. Steve McNeil and Kevin Smith I thank for their bountiful ideas and warped humour. My thanks go to present group members: to P. Jamieson Daff (Daffy), a one-of-a-kind post-doctoral fellow, for endless discussions of kinetics and mechanism and for heartfelt Northerner-style cameraderie. Brett Sharp (Sharpie), the ultimate flatmate, helped to keep it all in perspective – "off you go, then". Way to go, Eric Jandciu, for keeping the A246 dream alive. My thanks go to Elizabeth Tran, Craig Adams, Rob Poe, and Trevor Hayton for their ideas, input, and general lab cameraderie, and to Jane Kuzelka and Trevor Hayton for allowing me to play "supervisor".

I thank Steve Rettig (UBC), Ray Batchelor and Fred Einstein (SFU), and Victor Young, Jr. (U. Minn.) for the solid-state X-ray crystallographic determinations presented in this Thesis. Peter Borda is to be commended for an unsurpassed level of excellence in the elemental analysis service. Likewise, many thanks go to Steve Rak for glass-blowing and Marshall Lapawa for mass spectrometry. Marietta Austria, Lianne Darge, and Nick Burlinson deserve recognition for their help in collecting some of the NMR spectra described in this Thesis. Brian James and Ed Piers also deserve my thanks for their constructive criticisms during the revising of this Thesis.

Thanks go to Rich Haworth, the Best Man, for sharing mountaineering adventures and for the occasional use of the Saturn. You're so money...

Ron and Mary Elliott, my second parents, have given me a home away from home over these past five years, for which I give them my thanks and love.

To my parents, Bev and Paul , I give my love and thanks for their enduring encouragement and support of all my pursuits over the years.

Well, Karen, this is it...Thanks for enduring the past five years and for helping to keep it all in perspective. Here's to a lifetime of adventures together.

"Be bold and courageous. When you look back
on your life, you'll regret the things you didn't
do more than the ones you did."

- H. Jackson Brown Jr.

"One day
I am going to grow wings
A chemical reaction...".

- Thom Yorke

"If we knew what it was we were doing,
it would not be called research, would
it?"

- Albert Einstein

Chapter 1. A General Introduction

1.1 Study in the Field of Organometallic Chemistry

The study of homogenous organometallic chemistry can be described in broad strokes as being motivated by two driving forces. The first is the desire to prepare new organometallic compounds either of academic interest or of potential synthetic or industrial utility. The competent synthetic organometallic chemist may often design on paper a synthesis utilizing a particular set of reagents, and, by employing established protocols or developing new strategies during a synthetic investigation, successfully prepare the desired target compound in the laboratory. While such directed synthetic studies very often prove fruitful,[1] examples exist in the repertoire of most practicing organometallic chemists in which a chemical reaction serendipitously affords an unexpected, but no less interesting, organometallic transformation.[2] When such an unanticipated and potentially useful transformation is discovered, questions naturally arise regarding the nature of the chemistry involved. Thus, restating the first impetus as being a motivation to answer the question "what can be made?", the second may be characterized as a desire to know "how?" and "why?" a particular transition-metal-mediated conversion occurs.

1.2 Organometallic Research in the Legzdins Research Group

Historically, the research conducted in the Legzdins group has been focused largely towards the syntheses of new types of organometallic complexes containing the nitrosyl (NO) ligand. In this regard, the synthetic endeavours of past Legzdins group members over the last fifteen years have yielded an expansive catalogue of new organometallic compounds containing the Cp'M(NO) fragment [Cp' = Cp or Cp*, M = Cr, Mo, W].[3,4] In the first decade of this period,

however, comparatively less emphasis has been placed on the study of how and why many of these compounds are generated. Since this time, and naturally following on the heels of their syntheses, the study of the unusual and often unexpected chemistry effected by certain of these Cp'M(NO)-containing species has increasingly become central to our investigations.[4] In this regard, the focus of this Thesis is different from that of many Legzdins doctoral projects which precede it: comparatively less emphasis is given to the rational synthesis of new organometallic compounds. This fact notwithstanding, the preparation of an interesting class of vinyl-containing complexes bearing the general formula Cp*W(NO)(CPh=CH_2)(X) [X = 1e or 3e donor ligand, e.g. Cl, CH_2SiMe_3, η^2-O_2CPh] is an important component of this Thesis. However, a large proportion of this Thesis is also devoted to the discussion of how and why the transformations that are presented in the following Chapters are effected by the unobserved acetylene intermediate Cp*W(NO)(η^2-PhC≡CH) (**A**), a species that is thermolytically generated from these vinyl complexes in solution.

1.3 Organometallic Vinyl Complexes

Before outlining the particular goals of this Thesis and the chemistry that is presented in each chapter, it is prudent to consider in more general terms the nature of the vinyl ligand in organometallic complexes and its characteristic chemistry.

1.3.1 The Nature of the Vinyl Ligand and the Metal-Vinyl Bond

Much of the academic interest in vinyl complexes of the transition metals stems from the ability of the vinyl ligand to bind to a metal centre in a mono- or dihapto manner, thereby contributing either one or three electrons to the valence shell of the organometallic complex. To illustrate this fact, two vinyl-containing complexes are depicted in Figure 1.1 below. Both are 18e complexes bearing an inert-gas electronic configuration, yet the vinyl ligand in each case is bound to the metal centre in a different manner and each contributes a different number of valence electrons to the complex's valence shell. In the first case, the 15-valence-electron count of the $CpRe(PPh_3)(Br)$ fragment in **A**[5] permits an η^2-coordination of the vinyl ligand. This interaction involves a 3e contribution to the valence shell, resulting in a closed-shell electronic configuration. In contrast, the $Cp^*W(NO)(PPh_3)(H)$ fragment in **B**[6] contains 17 valence electrons. The vinyl ligand therefore is limited to contributing only 1e in the monohapto form, yielding an electronically saturated complex.

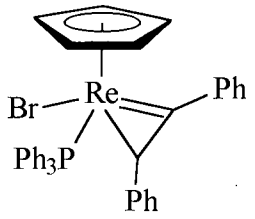

A
18e
η^2-vinyl ligand

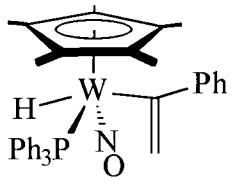

B
18e
η^1-vinyl ligand

Figure 1.1. Two electronically saturated vinyl complexes.

Both the η^1 and η^2 bonding modes of the vinyl ligand can be described in simple molecular-orbital terms. The monohapto vinyl ligand is isolobal to simpler aliphatic hydrocarbyl ligands, such as the methyl ligand, in that it contributes 1e to the valence-electron count of the organometallic complex and is bound to the metal through a single σ-bond. This single bond results from the orbital overlap between a σ-symmetric metal orbital and a σ-symmetric, sp^2-hybridized ligand orbital. The dihapto form of the vinyl ligand, in contrast, contributes 3e to the metal valence electron count and is bound to the metal centre in a more involved, three-centre interaction. The two alternate forms depicted in Figure 1.2 below can be considered as representing this bonding interaction.

Figure 1.2. Alternate representations of the η^2-vinyl bonding mode. M = transition metal.

The molecular orbitals required to describe the η^2-vinyl-M interaction are depicted in Figure 1.3.[7] The vinyl ligand MOs and the electrons that populate them are shown on the left side of this Figure, and the corresponding organometallic fragment orbitals of the correct symmetry for constructive orbital overlap are depicted on the right side. The relative energies of these orbitals and the identities of the metal-based orbitals are not implied in this depiction. Indeed, such information cannot be known without mathematically modeling a specific organometallic complex. The depicted metal orbitals simply serve to illustrate that one M-vinyl σ-interaction and two M-vinyl π-bonds are required to fully describe the η^2-vinyl-M interaction in the metallacyclopropene unit.

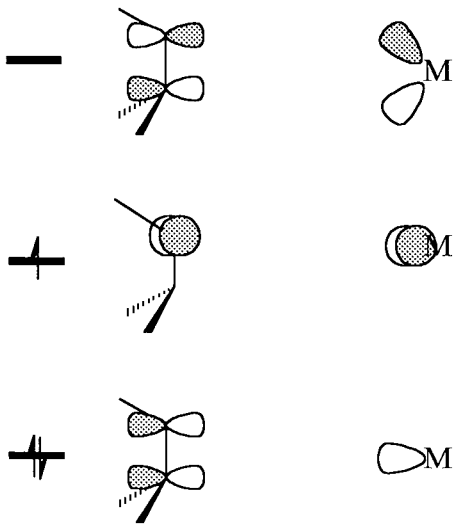

Figure 1.3. The valence molecular orbitals of the neutral vinyl fragment, their occupancies, and the complementary metal orbitals required to complete the η^2-vinyl-metal bonding interaction.

1.3.2 The Industrial Significance of Organometallic Vinyl Complexes

While organometallic vinyl complexes have not found widespread industrial application, much research has been conducted into the role of vinyl fragments in Fischer-Tropsch chemistry on metal surfaces. It has been shown recently that vinyl ligands on metal surfaces play an important role in Fischer-Tropsch chain propagation because they have a propensity to migrate into adjacent methylene units.[8] Thus, vinyl migration and isomerization can be envisioned to facilitate hydrocarbon chain propagation in a catalytic cycle known as the alkenyl mechanism, depicted in Scheme 1.1.

Scheme 1.1

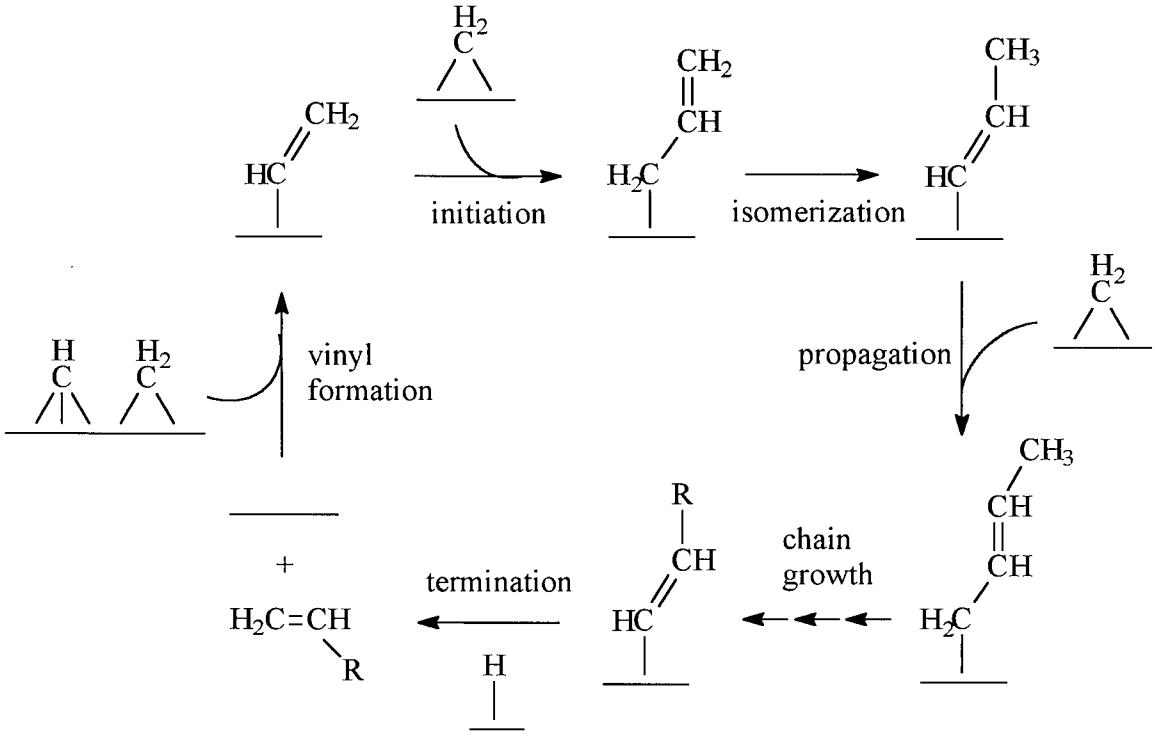

1.3.3 Common Methods for the Preparation of Organometallic Vinyl Complexes

The vinyl ligand can be introduced into an organometallic complex in a variety of ways. Figure 1.4 illustrates three common synthetic methods employed to prepare organometallic vinyl complexes.

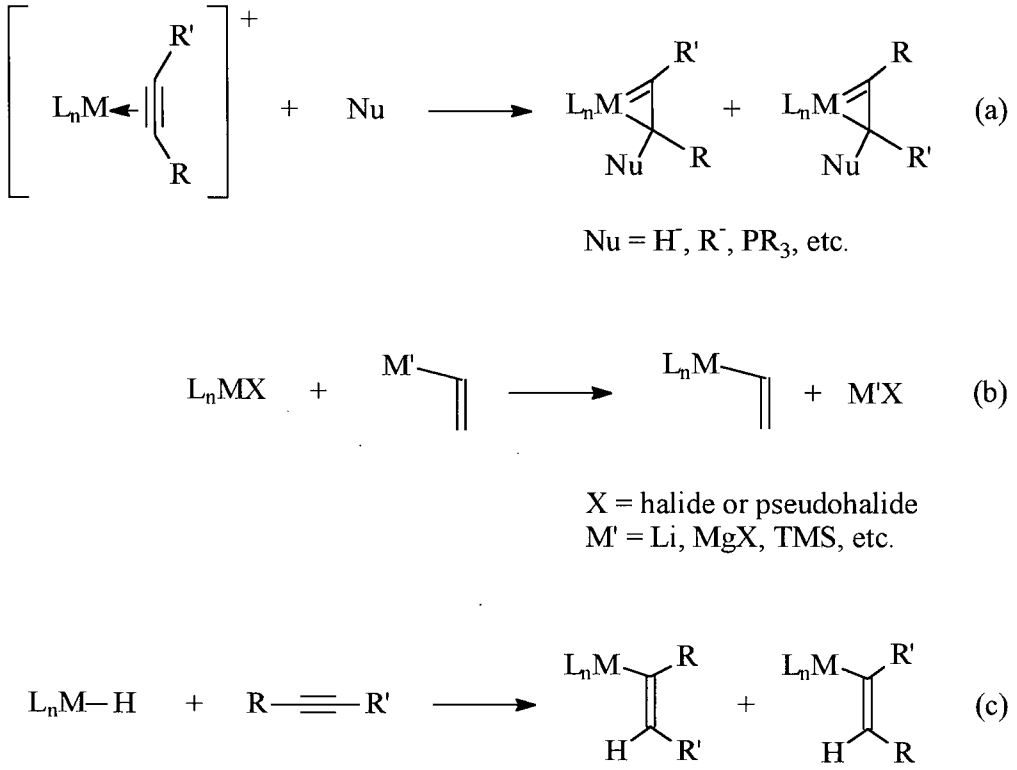

Figure 1.4. Three common synthetic routes to vinyl complexes of the transition elements.

In (a), attack of a nucleophile at an electrophilic acetylene carbon in a cationic acetylene complex results in the formation of a neutral η^2-vinyl species. Templeton[9] and Green[10] and their respective co-workers have applied this methodology to the synthesis of a wide range of η^2-vinyl complexes of the Group 6 transition metals. The regiochemistry of the reaction depends upon the relative electron-withdrawing character of the R and R' substituents, with nucleophilic attack predominating at the more electrophilic acetylene carbon. The vinyl ligand can also be introduced via a simple vinyl-for-halide metathesis reaction utilizing a suitable vinyl transfer reagent in the presence of the appropriate organometallic halide or pseudo-halide complex (Figure 1.4, (b)). This is the method commonly employed in the preparation of the vinyl complexes discussed in this Thesis. Probably the most ubiquitous of the three methods is that

depicted in (c), involving the addition of a metal-hydride bond across an acetylene linkage.[11] Similar to (a) described above, the regioselectivity of the reaction depicted in (c) depends upon the polarity of the acetylene substrate, although the additional influence of the M-H polarity also determines the proportion of products that is obtained. In this case, a hydridic H ligand attacks preferentially at the electropositive terminus of an acetylene bond, whereas a more protonic M-H linkage will add across an acetylene bond with the opposite regioselectivity. In a related reaction, Huggins and Bergman have reported the addition of both a Ni-Me and a Ni-Ph bond across an acetylene linkage to afford vinyl complexes of Ni.[12] Likewise, LaPointe and Brookhart in a recent contribution to the literature describe the addition of Pd-Me and Pd-vinyl bonds across the unsaturation in an acetylene ligand.[13]

1.3.4 Some Characteristic Chemistry of the Vinyl Ligand

Vinyl complexes have been reported to undergo a variety of chemical transformations, most of which are variations of the examples depicted in Figure 1.5. The unsaturated nature of the vinyl ligand permits the formulation of a carbene resonance contributor that imparts nucleophilic character to the β-carbon of the vinyl ligand (Figure 1.5, (a)). As such, the vinyl ligand has been reported to react with unsaturated substrates via nucleophilic attack at an electrophilic site, an example being the formation of a metallapyrrole as depicted in (a).[14] A variation is depicted in (b) in which attack occurs at the quaternary carbon in an acetylene ligand.[11a] In this case, however, it is the α-vinyl C that attacks the coordinated ligand to yield the resultant olefinic vinyl ligand. As noted previously, the vinyl β-carbon can be nucleophilic in character, and thus, the vinyl ligand is often subject to protonation, yielding cationic carbene complexes (Figure 1.5, (c)).[9b,15].

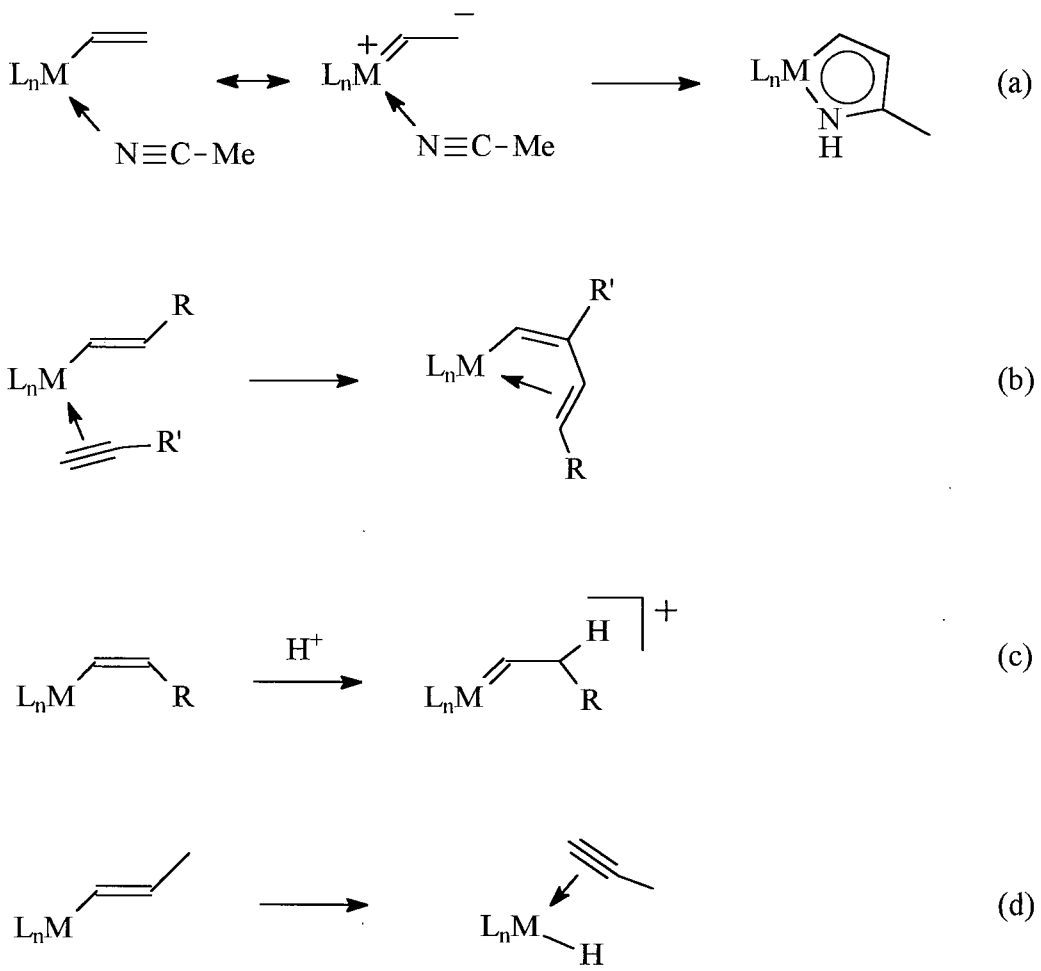

Figure 1.5. Some reactions of vinyl ligands in organometallic complexes.

Finally, in a reaction more commonly observed for alkyl complexes of the transition metals, β-vinyl-H elimination has been reported for a few types of vinyl complexes (Figure 1.5, (d)). In cases where an alkyl ligand, R, is also present in the metal's coordination sphere (as shown below), subsequent reductive elimination of RH yields a coordinatively unsaturated acetylene complex which can undergo further reactions.[16]

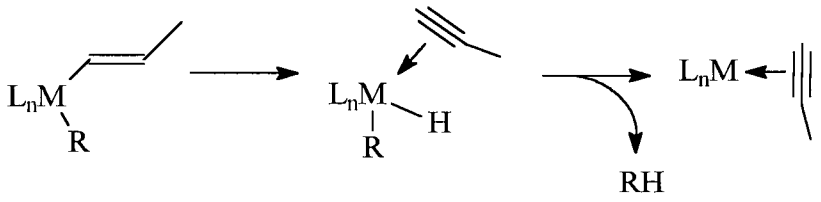

This last reaction is interesting in that it is formally the microscopic reverse of that depicted in Figure 1.4(c), in which a vinyl ligand is generated via hydrometallation of an alkyne ligand. More importantly, almost all of the chemistry described in this Thesis is derived from the analogous generation of the acetylene-containing complex Cp*W(NO)(η^2-PhC≡CH) (**A**) and its subsequent reactivity towards unsaturated organic substrates and hydrocarbon C-H bonds.

1.4 The Scope of this Research Project and Format of this Thesis

1.4.1 Preliminary Results

This project originated with the observation by Dr. Jeff Debad (formerly of our research group) that the vinyl-containing tungsten complex Cp*W(NO)(CPh=CH_2)(CH_2SiMe_3), known throughout this Thesis as complex **1**, is thermally unstable in solution. The scope of his preliminary investigation into this thermal activation chemistry is summarized in Scheme 1.2 and eqs 1.1 and 1.2. In the first instance, Dr. Debad observed that the thermolysis of **1** in benzene yields the phenyl vinyl analogue. This reaction requires two weeks for completion when conducted at room temperature, however, warming to 50 °C results in complete conversion after 24 h. Note that the activation of a benzene C-H bond in this reaction requires the formal exchange of an aryl C-H bond for an alkyl C-H bond, and the exchange of an alkyl C-W bond for

an aryl C-W bond. Monitoring the reaction in benzene-d_6 in a sealed NMR tube revealed that $SiMe_4$ (δ 0.00) was being generated and that deuterium label was being incorporated into the vinyl positions of the vinyl ligand. These observations suggested that the formation of the deutero-vinyl analogue results from the activation of solvent C-D bonds during the thermal activation of **1**. The identification of the deuterated analogue is made by utilizing its EI mass spectrum and by the conspicuous absence of both vinyl-proton signals in the ^1H NMR spectrum of the reaction mixture.

Scheme 1.2

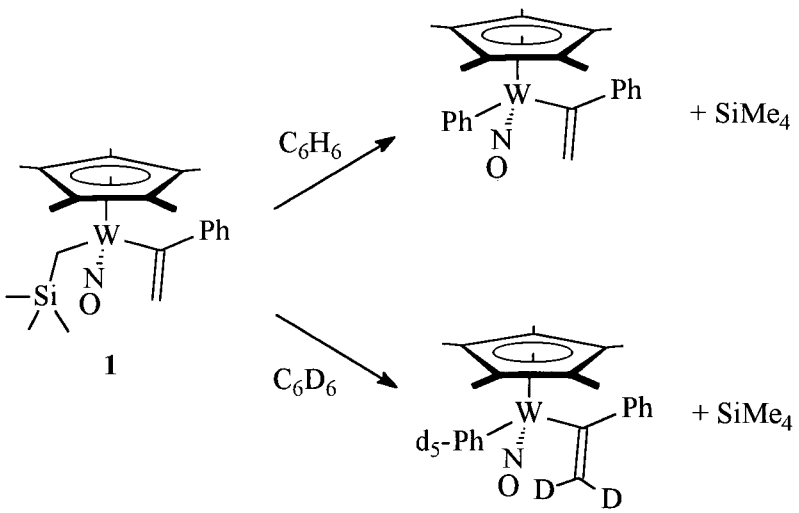

Three important conclusions can be drawn from the observations made by Dr. Debad. The incorporation of benzene into the coordination sphere of W during the formation of the phenyl vinyl product requires the conversion of a benzene C-H bond to an aryl C-W bond. Thus, cleavage of the benzene C-H bond (otherwise known as C-H bond activation) by an intermediate and unobserved W complex is implicated in this transformation. Because the only source of $SiMe_4$ is the precursor Me_3SiCH_2 ligand in **1**, free $SiMe_4$ in the reaction mixture is indicative of an alkane elimination process. Finally, and most importantly, the incorporation of deuterium-

label into the vinyl-H positions is a very strong indication that the vinyl ligand is intimately involved in the ligand exchange process that links benzene C-H bond activation and $SiMe_4$ elimination. Knowing that an alkyne ligand may be generated via β-elimination from a vinyl ligand (Figure 1.5(d)) and that a vinyl ligand may be generated in the microscopic reverse by the addition of H across the unsaturation in an alkyne link (Figure 1.4(c)), has led us to propose that this C-H activation chemistry is facilitated by an unobserved acetylene complex $Cp^*W(NO)(\eta^2$-PhC≡CH) (**A**), generated via reductive elimination of $SiMe_4$ from the parent complex(eq 1.1).[17]

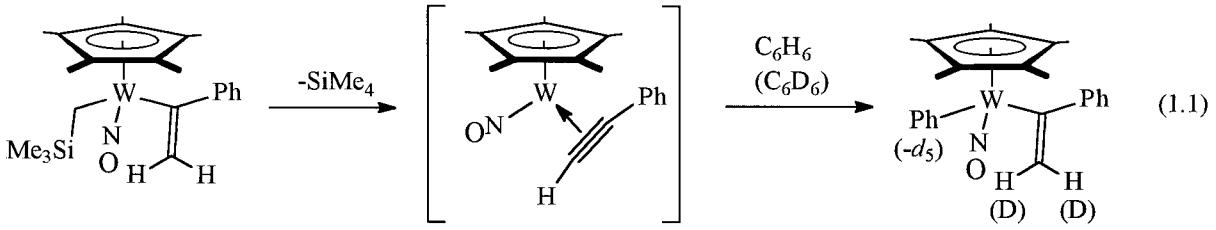

1 **A** (1.1)

Substrate C-H bond activation and H-transfer back to the acetylene ligand result in solvent incorporation into the metal's coordination sphere and regeneration of the vinyl ligand. In the presence of labeled substrate, deuterium-label is incorporated into the vinyl positions.

With this experimental information and a proposed mechanism in hand, a number of thermolysis experiments involving vinyl-containing **1** were performed by Dr. Debad designed to trap the proposed acetylene-containing intermediate with substrates known to react with acetylene ligands. In each case, hexanes was chosen as the inert solvent in which to conduct the experiments, with the serendipitous result that the same product was obtained in each case. Performing the thermolysis of **1** in hexanes in the absence of a trapping reagent also gave the identical result. Repeating the experiment in neat *n*-pentane, *n*-hexane or diethyl ether afforded the complexes depicted below (eq 1.2). The solid-state molecular structure of the product

derived from *n*-pentane activation was determined by X-ray diffraction methods and facilitated the structural assignment of these metallacycles. Inspection of the molecular structure of these complexes reveals that two C-H bonds of the hydrocarbon substrate have been cleaved during the process that fuses the vinyl and hydrocarbyl fragments together in the coordination sphere of the W centre.

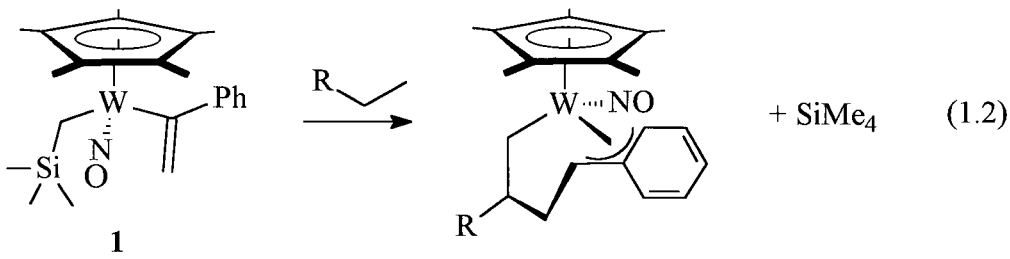

1

R = ^{n}Pr, ^{n}Bu, OEt

In a final attempt to trap acetylene-containing **A**, a thermolysis reaction involving **1** in the presence of PMe_3 was conducted by Dr. Debad. Interestingly, instead of the expected PMe_3-trapped acetylene adduct, a zwitterionic metallacyclopropane complex is obtained, purportedly as a result of nucleophilic attack at the α-carbon of the vinyl ligand (eq 1.3).

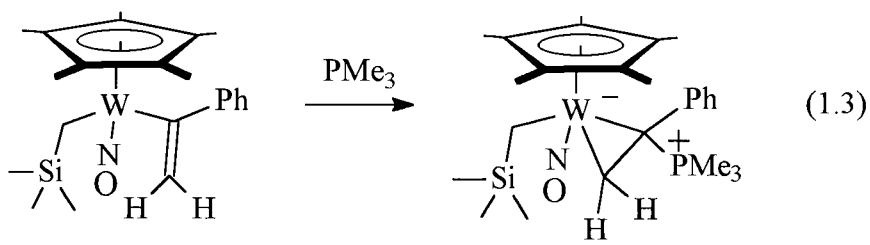

1

It is at this point where Dr. Debad halted his research activity and where I commenced my experimental investigations into the characteristic chemistry of this vinyl-containing system.

1.4.2 The Scope of the Work Presented in this Thesis

Following the serendipitous discovery that C-H bond activation of hydrocarbon substrates is effected upon the thermal activation of the vinyl-containing species **1** in solution, it was decided that a survey of the reactivity of this system was required to determine the scope of the accessible chemistry. In addition, kinetic and mechanistic studies were to be performed where appropriate in the hopes of identifying both the underlying mechanisms governing this chemistry and the factors that determine the chemo- and regioselectivity in any new chemistry observed. This Thesis presents the details of these investigations.

Chapter 2 begins with a description of the experimental evidence for the interesting W-vinyl bonding interaction in complex **1** in terms of its solid-state metrical parameters and solution NMR spectroscopic features. Because the preliminary experimental evidence suggested that the vinyl binding mode in **1** lies intermediate to the η^1- and η^2-limiting forms described in Section 1.3.1, it was postulated that the vinyl ligand may be induced to assume a particular bonding mode by the electronic properties of the remaining ancillary ligands in the organometallic fragment. In this regard, a series of compounds of the general formula $Cp^*W(NO)(CPh{=}CH_2)(E)$ [E = 1e or 3e ligand] has been prepared, and their syntheses and physical properties are described. Comparisons are made of the solid-state metrical parameters and solution NMR spectroscopic characteristics obtained for these compounds to those of a sample of structurally-characterized η^1- and η^2-vinyl complexes compiled from the Cambridge Structural Database (CSD). The results of these studies are described in detail in Chapter 2.

An unsuccessful attempt was made by Dr. Debad to trap the proposed acetylene intermediate **A** with PMe_3. However, acetylene complexes are known to react with a variety of unsaturated organic substrates such as olefins, ketones, and nitriles, affording metallacycles of varying composition. This chemistry has been particularly well studied for the Group 4 metallocenes by the research groups of Buchwald, Negishi, and others.[16] Comparison of the alkyne complex **A** to the analogous Group 4 acetylene complexes studied previously reveals striking structural and electronic similarities. Indeed, one method of access to these vinyl metallocene complexes involves the metathesis of chloride in the methyl chloride precursor with the appropriate vinyllithium reagent, followed by *in situ* elimination of methane to afford the desired metallocene acetylene complex (eq 1.4). This chemical transformation is identical to that proposed for the generation of acetylene-containing **A** from vinyl-containing **1**.

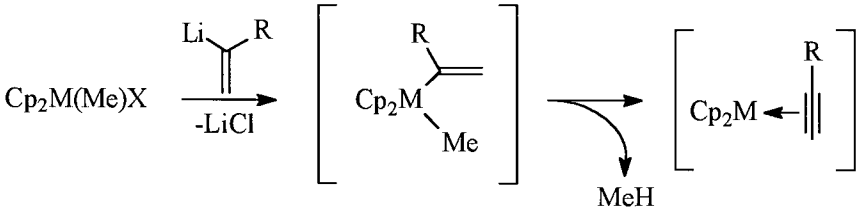

(1.4)

M = Group 4 metal
X = halide

Given the similarity between the Group 4 metallocenes and the Group 6 title system, thermolyses of complex **1** in the presence of various unsaturated, heteroatom-containing organic substrates such as esters, nitriles and acetone have been conducted, with a view to trapping the acetylene-containing intermediate **A** in coupling reactions that generate nitrosyl-containing metallacycles. Indeed, the thermolysis of **1** in these solvents *does* lead to the formation of a range of metallacycles in a manner similar to the Group 4 system. However, the ultimate products of these reductive coupling reactions are unlike the Group 4 complexes obtained under the

analogous reaction conditions. The scope of this chemistry and the products that result are the focus of Chapter 3. In addition to NMR and solid-state structural studies of these compounds, a qualitative molecular-orbital picture of the bonding in these metallacycles is proposed to help rationalize the formation of the Group 6 metallacycles in the context of the reported Group 4 system. Kinetic and mechanistic studies are described which lend insight into both the generation of **A** and into the formation of these metallacycles that result from the reaction of **A** with various organic substrates.

Chapter 4 is concerned with a study of the C-H bond-activation chemistry effected during the thermal decomposition of alkyl vinyl **1** in hydrocarbon solutions. A survey of the reactivity of **A** toward a variety of hydrocarbon substrates reveals the scope and limitations of the C-H bond activation process described in Section 1.4.1. Thermolyses of **1** in methyl-substituted arenes such as toluene and xylenes quantitatively yield distributions of aryl and benzyl C-H activation products that are dependent on the relative sites of methyl substitution. The results of kinetic and mechanistic studies permit the formulation of a mechanistic picture of the C-H activation process. The results of thermolyses of **1** conducted in aliphatic hydrocarbons lend insight into the regio- and stereoselectivity controlling the dual C-H bond activation of these substrates. NMR studies of the resultant metallacycles are described, the results of which impart information regarding the fluxional nature of the η^3-benzyl interaction that stabilizes these metallacycles as 18e complexes. Finally, a qualitative examination of the frontier molecular orbitals in acetylene **A**, made by analogy to well-defined systems, aids in rationalizing the reactivity of **A** towards C-H bonds in hydrocarbon substrates.

Two appendices follow Chapter 4, the first containing tables of X-ray data for each structurally-characterized complex presented in this Thesis. The second contains an algebraic derivation of the rate law applied to a saturation mechanism.

1.4.3 Thesis Format

This Thesis is formatted with Chapters 2 through 4 possessing five major Sections. If X is the chapter number, then the Sections appear as **X.1** Introduction, **X.2** Results and Discussion, **X.3** Epilogue and Future Work, **X.4** Experimental Procedures, and **X.5** Notes and References. Subsections of these categories are numbered using legal outlining procedures, e.g. X.1.1, X.1.2, X.1.2.1, X.1.3, etc. Except for compound **1** and acetylene-containing **A**, from which all of the chemistry discussed in this Thesis originates, all compounds discussed in each chapter are catalogued numerically, e.g. in chapter X, compounds appear as X.1, X.2, X.3, etc. Schemes, Tables, Figures and Equations are similarly sequenced. The standard experimental methodologies employed in the research described in this Thesis are outlined in detail in Chapter 2, Section 2.4.1.

1.5 Notes and References

(1) For example: (a) Daff, P. J.; Legzdins, P. *J. Am. Chem. Soc.* **1998**, *120*, 2688. (b) Kuzelka, J.; Legzdins, P.; Rettig, S. J.; Smith, K. M. *Organometallics* **1997**, *16*, 1997. (c)

Nicolaou, K. C.; Yang Z.; Ouellette M.; Shi G.-Q.; Gärtner P.; Gunzner J. L.; Agrios, R. Huber, R. Chadha K. A.; Huang D. H. *J. Am. Chem. Soc.* **1997**, *119*, 8105. (d) Danishefsky, S. J.; Masters, J. J.; Young, W. B.; Link, J. T.; Snyder, L. B.; Magee, T. V.; Jung, D. K.; Isaacs, R. C. A.; Bornmann, W. G.; Alaimo, C. A.; Coburn, C. A.; Di Grandi, M. J. *J. Am. Chem. Soc.* **1996**; *118*; 2843.

(2) The chemistry described in Section 1.4, the results of which are the primary motivation for this entire Thesis, is an excellent example of a serendipitous discovery.

(3) Legzdins, P.; Veltheer, J. E. *Acc. Chem. Res.* **1993**, *26*, 41.

(4) (a) Legzdins, P; Rettig, S. J.; Ross, K. J. *Organometallics* **1994**, *13*, 569. (b) Legzdins, P.; Rettig, S. J.; Sayers, S. F. *J. Am. Chem. Soc.* **1994**, *116*, 12105. (c) Legzdins, P.; Veltheer, J. E.; Young, M. A.; Batchelor, R. J.; Einstein, F. W. B. *Organometallics* **1995**, *14*, 407. (d) Legzdins, P.; Young, M. A.; Batchelor, R. J.; Einstein, F. W. B. *J. Am. Chem. Soc.* **1995**, *117*, 8798. (e) Burkey, D. J.; Debad, J. D.; Legzdins, P. *J. Am. Chem. Soc.* **1997**, *119*, 1139. (f) Legzdins, P.; McNeil, W. S.; Rettig, S. J.; Smith, K. M. *J. Am. Chem. Soc.* **1997**, *119*, 3513. (g) Legzdins, P.; MacNeil, W. S.; Smith, K. M.; Poli, R. *Organometallics* **1998**, *17*, 615. (h) Legzdins, P.; Lumb, S. A.; Young, V. G. *Organometallics* **1998**, *17*, 854.

(5) Carfagna, C.; Carr, N.; Deeth, N. J.; Dossett, S. J.; Green, M.; Mahon, M. F.; Vaughan, C. *J. Chem. Soc., Dalton Trans.* **1996**, 415.

(6) Compound **2.7**, Chapter 2.

(7) Feng, S. G.; Templeton, J. L. *Organometallics* **1992**, *11*, 2168.

(8) (a) Torkelson, J. R.; McDonald, R.; Cowie, M. *J. Am. Chem. Soc.* **1998**, *120*, 4047. (b) Turner, M. L.; Long, H. C.; Shenton, A.; Byers, P. K.; Maitlis, P. M. *Chem. Eur. J.* **1995**, *1*, 549. (c) Maitlis, P. M.; Long, H. C.; Quyoum, R.; Turner, M. L.; Wang, Z.-Q. *Chem. Commun.* **1996**, 1.

(9) (a) Morrow, J. R.; Tonker, T. L.; Templeton, J. L. *J. Am. Chem. Soc.* **1985**, *107, 6956.* (b) Feng, S. G.; Gamble, A. S.; Templeton, J. L. *Organometallics* **1989**, *8*, 2024. (c) reference 7.

(10) (a) Allen, S. R.; Beevor, R. G.; Green, M.; Norman, N. C.; Orpen, A. G.; Williams, I. D. *J. Chem. Soc., Dalton Trans.* **1985**, 435. (b) Allen, S. R.; Green, M.; Orpen, A. G.; Williams, I. D. *J. Chem. Soc., Chem. Comm.* **1982**, 826. (c) Conole, G. C.; Green, M.; McPartlin, M.; Reeve, C.; Woolhouse, C. M. *J. Chem. Soc., Chem. Comm.* **1988**, 1310. (d) reference 5.

(11) (a) Herberich, G. E.; Mayer, H. *Organometallics* **1990**, *9*, 2655. (b) van der Zeijdan, A. A. H.; Bosch, W.; Berke, H. *Organometallics* **1992**, *11*, 563. (c) Werner, H.; Esteruelas, M. A.; Otto, H. *Organometallics* **1986**, *5*, 2295. (d) Koike, M.; Hamilton, D. H.; Wilson, S. R.; Shapley, J. R. *Organometallics* **1996**, *15*, 4930.

(12) Huggins, J. M.; Bergman, R. G. *J. Am. Chem. Soc.* **1979**, *101*, 4410.

(13) LaPointe, A. M.; Brookhart, M. *Organometallics* **1998**, *17*, 1530.

(14) Alvarado, Y.; Daff, P. J.; Pérez, P. J.; Poveda, M. L.; Sánchez-Delgado, R.; Carmona, E. *Organometallics* **1996**, *15*, 2192.

(15) (a) Feng, S. G.; White, P. S.; Templeton, J. L. *Organometallics* **1993**, *12*, 2131. (b) Sterenberg, B. T. McDonald, R.; Cowie, M. *Organometallics* **1997**, *16*, 2297.

(16) (a) Buchwald, S. L.; Nielsen, R. B. *Chem. Rev.* **1988**, *88*, 1047. (b) Broene, R. D.; Buchwald, S. L. *Science* **1993**, *261*, 1696. (c) Negishi, E.-I.; Takahashi, T. *Acc. Chem. Res.* **1994**, *27*, 124. (d) Schwartz, J.; Hart, D. W.; McGiffert, B. *J. Am. Chem. Soc.* **1974**, *96*, 5613. (e) Johnson, B. F. G.; Lewis, J.; Nordlander, E.; Raithby, P. R. *J. Chem. Soc., Dalton Trans.* **1996**, 3825.

(17) Debad, J. D., Legzdins, P.; Lumb, S. A.; Batchelor, R. J.; Einstein, F. W. B. *J. Am. Chem. Soc.* **1995**, 117, 3288.

Chapter 2. The Variable Bonding Mode of the Vinyl Ligand in the Cp*W(NO)(CPh=CH_2) Fragment

2.1 Introduction

The tungsten-mediated chemical transformations described in the latter two Chapters of this Thesis result from the thermal conversion of $Cp^*W(NO)(CPh{=}CH_2)(CH_2SiMe_3)$ (**1**) to $Cp^*W(NO)(\eta^2\text{-}PhC{\equiv}CH)$ (**A**) in solution. In a preliminary communication of this chemistry, Debad, Lumb and Legzdins reported the solid-state molecular structure of **1** determined by X-ray diffraction methods at ambient temperature.[1] The vinyl H atoms were not located, and the structure showed large anisotropic displacement parameters which represented unresolved disorder, most notably in the Cp* ligand. The result was a structure of relatively low precision representing a somewhat blurred image of the molecule. As a result, conclusions regarding the nature of the W-vinyl interaction were difficult to make. Having reported the basic characterization details for **1**,[1] the solid-state metrical parameters and the solution NMR spectroscopic characteristics of the vinyl ligand in **1** have since been investigated in greater detail; the results of these investigations are presented in this Chapter.

In addition, the interesting vinyl-tungsten interaction observed in **1** has prompted an investigation into the nature of the W-vinyl interaction as a function of the ancillary ligands present in the metal's coordination sphere. As noted in Chapter 1, Section 1.3.2, the metal-vinyl bonding interaction may be manifested in either the mono- or dihapto forms. In vinyl complexes containing another donor ligand also capable of donating multiple numbers of electrons (e.g. $^-NR_2$, ^-OR, ^-O_2CR) to a metal centre, it is reasonable to assume that the vinyl bonding mode is dependent upon the strength of this donor ligand. To test this hypothesis, a series of vinyl-containing species of the general formula $Cp^*W(NO)(\eta^x\text{-}CPh{=}CH_2)(E)$ [x = 1 or 2, E = 1e or 3e donor ligand] has been prepared, and the solid-state metrical parameters and solution NMR

spectroscopic properties of these complexes have been examined. The details of these studies are also presented in this Chapter.

2.2 Results and Discussion

2.2.1 The Vinyl-Tungsten Bonding Interaction in $Cp^*W(NO)(\eta^2\text{-}CPh{=}CH_2)(CH_2SiMe_3)$ (1)

The solid-state molecular structure of **1** has been re-determined by X-ray crystallographic methods at –93 °C, and the vinyl hydrogen atoms have been located in the process.[2] The results of this new diffraction study are depicted in Figure 2.1. In describing the unusual W-vinyl bonding interaction evident in Figure 2.1 it is prudent to make note of the key structural features that identify an η^2-bonding mode in an $M(C_\alpha R{=}C_\beta R_2)$ metal-vinyl fragment. These include the $M{=}C_\alpha$ and $M\text{-}C_\beta$ bond distances, the $M{=}C_\alpha\text{-}C_\beta$ bond angle, and the $M{=}C_\alpha\text{-}R$ angle. The W-C(11) bond distance of 2.076 (5) Å in the molecular structure of **1** borders on those typically found for M=C η^2-vinyl linkages [M = Mo, W] (1.9 – 2.0 Å)[3] and is comparable in magnitude to many W=CH(Ar) alkylidene linkages (1.86 - 2.15 Å).[4] In addition, this interatomic distance is substantially shorter than the W-C single-bond distance observed for typical 16e $Cp^*W(NO)(aryl)_2$ complexes (ca. 2.15 Å)[5] and η^1-vinyl complexes of W (ca. 2.2 Å).[6] Indeed, the W-C(11) distance is nearly identical to the W-C contact in a $W(\eta^2\text{-}C(O)R)$ acyl fragment,[5c] a

linkage previously described as containing substantial carbene character.[7] The W(1)-C(11)-C(13) angle is expanded to 137.1 (3)°.

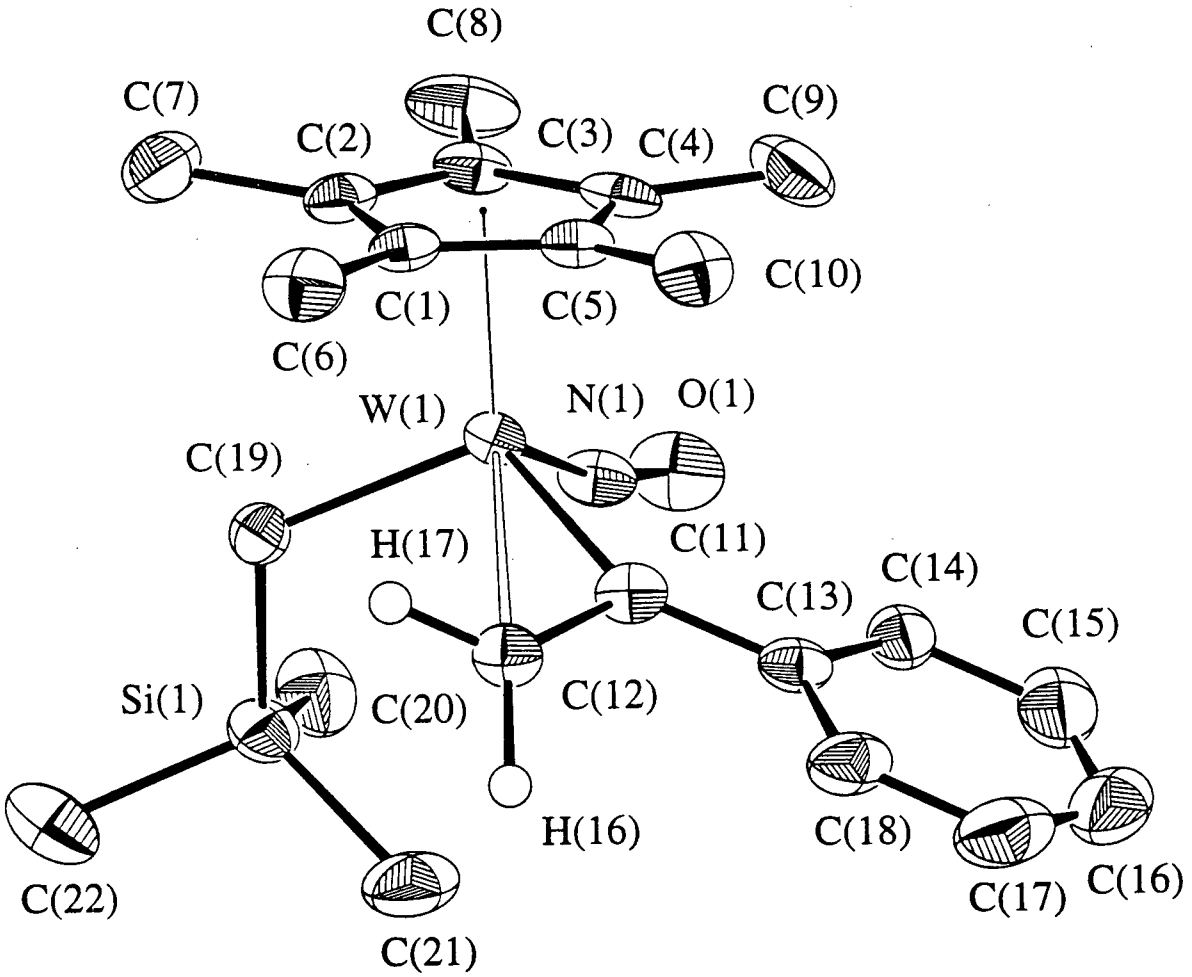

Figure 2.1. The solid-state molecular structure of complex **1** determined at –93 °C. 50% probability thermal ellipsoids are depicted.

A perspective view down the C(12)-C(11) bond in the molecular structure of **1** (Figure 2.2) reveals that the vinyl plane embodied by C(11), C(12), H(17) and H(16) is tilted towards W by an angle of 25° with respect to the plane defined by W(1), C(11), C(12) and C(13). This feature

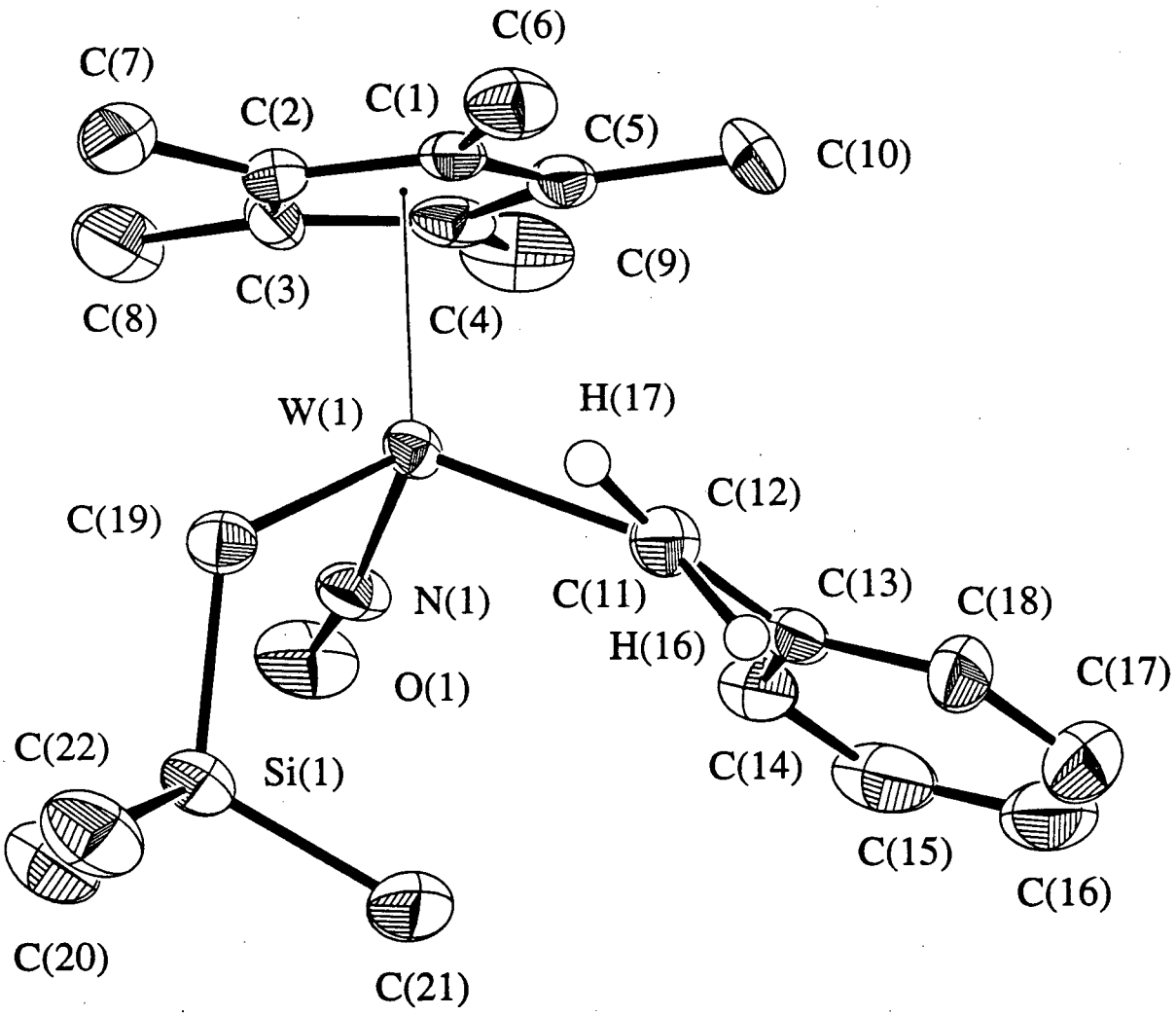

Figure 2.2. A perspective view of the solid-state molecular structure of complex **1** determined at –93 °C.

is indicative of a dihapto metal-vinyl interaction, although the degree of interaction between C(12) and W is reduced as compared to that observed for other structurally characterized η^2-vinyl complexes.[3a,d] The W-C(11)-C(12) bond angle is acute (97.5 (4)°), yet remains larger than the M=C-C angles observed for other η^2-vinyl complexes (70 - 85°). The long W-C(12) contact (2.615(5) Å) and the short C(11)-C(12) bond (1.342 (6) Å) are distances that also deviate from those typically found for the η^2-vinyl limiting form.

While the latter solid-state structural parameters for the vinyl ligand in **1** do not conclusively define the bonding mode to W, its solution properties are distinctly characteristic of an η^2-vinyl group.[3] For example, the vinyl α-C signal in the ^{13}C NMR spectra of **1** manifests itself in the carbene region (δ 228), typical of these nuclei in dihapto vinyl ligands. In addition, the β-C signal lies considerably upfield (82 ppm) in the region normally associated with metallated, sp^3- or sp^2-hybridized, σ-bound carbon nuclei in W nitrosyl complexes.[8] The vinyl proton signals in the ^1H NMR spectrum of **1** likewise appear upfield at about 3.5 ppm, near the region normally attributed to the sp^3-hybridized-alkyl-W magnetic environment. In addition, the magnitude of the one-bond C_β-H coupling constant ($^1J_{CH_a} \approx {}^1J_{CH_b} \approx 146$ Hz) is comparable to those determined for other η^2-vinyl complexes of W.[3b,c,9] The results of an NOE experiment involving **1** implicate the proximity of one of the vinyl protons to the Cp* methyl substituents, while the other is near to the Ph *ortho* protons. This information indicates that the vinyl proton environments are not equally disposed in space and that one is oriented nearer to the Cp* ring, while the other is oriented nearer to the vinyl Ph substituent. All of these pieces of data, together with the measured coupling of the vinyl-C and vinyl-H nuclei to the W metal center, imply a solution structure for **1** that includes an η^2-vinyl ligand. Variable temperature (VT) ^1H NMR spectroscopy of **1** in both THF-d_8 and toluene-d_8 reveals little shift (<0.5 ppm) in the signals for

the vinyl protons over the range –80 °C to +60 °C. These results indicate that the metal-vinyl-bonding interaction is a ground-state or that a very rapid equilibrium is occurring between η^1- and η^2-bonding modes over the temperature range measured.

Though the NMR spectroscopic parameters exhibited by the vinyl ligand in **1** are clearly a manifestation of a dihapto-vinyl-bonding mode, the metrical parameters determined for this ligand in the solid-state are intriguing in that they seemingly represent an outer limit to the η^2-vinyl-W interaction. A qualitative MO rationale that rationalizes the observed reduction in the W-vinyl(C_β) bonding interaction in the solid state may be developed. However, to do so requires a review of the valence molecular-orbitals in 16e Cp'M(NO)(R^1)(R^2) species [Cp' = Cp or Cp*, R^1, R^2 = 1e hydrocarbyl ligands] (Figure 2.3). To a first approximation, the Cp' ligand can be considered to occupy three cofacial sites of the octahedral coordination geometry, as indicated by the triangular "cap" in Figure 2.3(a). The three remaining coordination sites are occupied by 1e σ-donor ligands such as the methyl ligand. The focus of this rationale is primarily on the set of metal d-orbitals of π-symmetry with respect to the R ligands, namely those referred to as the t_{2g} set in a rigorously octahedral environment. The remaining d-orbitals ($d_{x^2-y^2}$, d_{z^2}) are involved in the ligand σ-bonding framework and are unaffected by the presence of π-donor ligands. In addition, the simplifying assumption is made that there is little influence by the Cp' ligand on the energies of the "t_{2g} set" of metal d-orbitals. Therefore, to a first approximation, these orbitals are nearly degenerate and are occupied by two of the fourteen valence electrons in this tris(alkyl) complex.

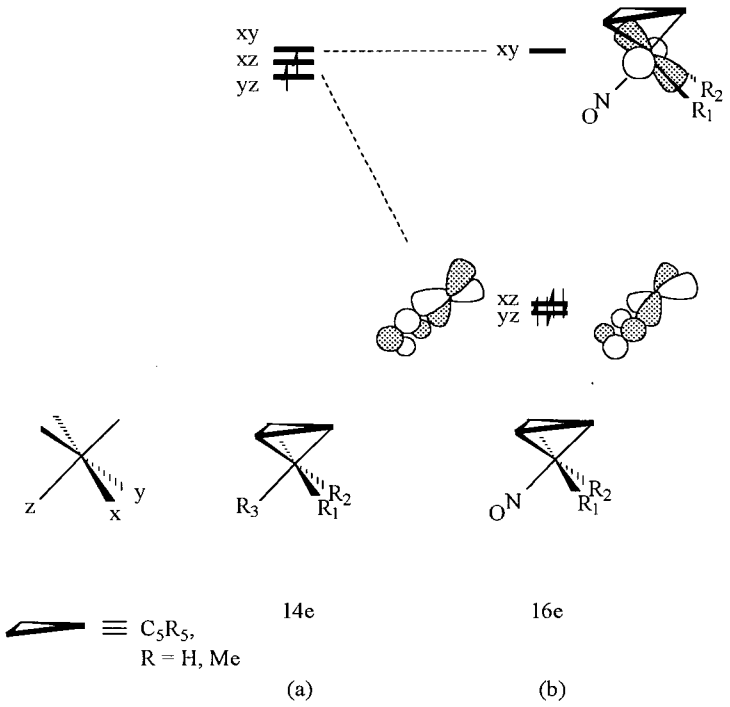

Figure 2.3. A qualitative frontier MO scheme for the 14e Cp'M(NO)(R^1)(R^2)(R^3) species and the 16e Cp'M(NO)(R^1)(R^2) species [Cp' = Cp or Cp*, M = Mo, W, R^1, R^2, R^3 = 1e hydrocarbyl ligands].

Replacement of the 1e alkyl ligand in the z coordinate axis in (a) with the strongly π-acidic, 3e NO ligand affords a 16e complex and effects a marked change in the degeneracy of the metal d-orbitals (Figure 2.3(b)). Strong backbonding interactions between the metal d_{xz} and d_{yz} orbitals and the complementary π-symmetric, mutually orthogonal NO π* orbitals result in the stabilization of the d_{xz} and d_{yz} orbitals relative to the non-bonding, metal-based d_{xy} LUMO. This qualitative MO depiction is consistent with the results of Fenske-Hall calculations based on the $CpW(NO)(Me)_2$ system.[10] The π-stabilization of the d_{xz} and d_{yz} orbitals through W-NO π-

bonding affords diamagnetic, electronically unsaturated complexes that are thermally stable as 16e species. The presence of the high-energy, metal-centred LUMO in these complexes renders the metal centre Lewis acidic and leads to a rich chemistry that is facilitated by adduct formation in the presence of a variety of Lewis bases.[11] An interesting intramolecular case illustrating this general phenomenon is depicted below. In heteroatom-containing analogues of the 16e dialkyl complexes described above, the π- or σ-donor site is oriented so as to effect the stabilization of the LUMO via a bonding interaction, affording 18e complexes.[12]

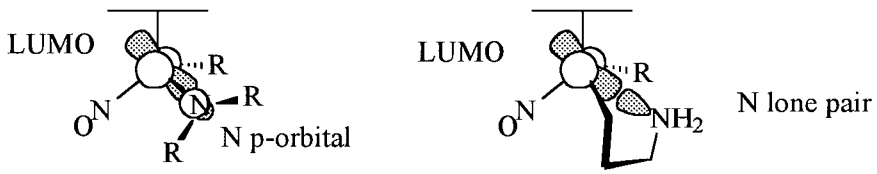

I II

In a similar vein, it is proposed that a bonding interaction between the vinyl C_β p-orbital and the metal-centred LUMO leads to the observed η^2-vinyl interaction in solution and the unusual W-vinyl interaction in the solid-state molecular structure of **1**. Tilting of the vinyl plane in the 16e $Cp^*W(NO)(CH_2SiMe_3)(\eta^1\text{-}CPh{=}CH_2)$ orients the vinyl β-carbon p-orbital towards the LUMO, as depicted below. The vinyl π-bond is not completely broken as a result of this W-C_β interaction and the vinyl C-C bond retains much of its double-bond character as evinced by the short C(11)-C(12) contact (1.346(2) Å) in the solid-state molecular structure of **1**.

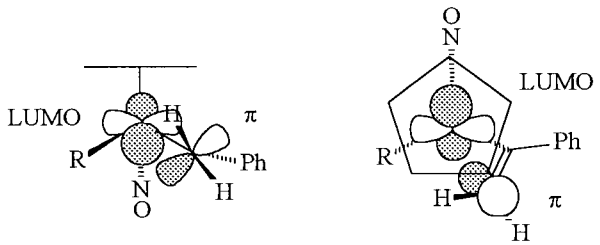

R = CH_2SiMe_3

The unusual solid-state and solution NMR properties of the vinyl ligand in **1** suggest that the W-(η^2-vinyl) interaction lies intermediate to the two representations depicted below. For reasons of clarity and consistency, the $CPh=CH_2$ ligand in the η^2-vinyl complexes described throughout this Thesis will be depicted as in **I** below.

I **II**

[W] = Cp*W(NO)(CH_2SiMe_3)

Armed with these proposals, the synthesis of a number of vinyl-containing analogues, Cp*W(NO)($CPh=CH_2$)(E), was devised with a view to investigating the nature of the W-vinyl interaction as a function of the ancillary donor ligands in the coordination sphere of W. At this point, and throughout the remainder of this chapter, "ancillary ligand" refers to the ligand E that is introduced to the Cp*W(NO)($CPh=CH_2$) fragment, the Cp* and NO ligands being ubiquitous to this series of compounds. Thus, if the original hypothesis is correct, a strong, 3e donor ligand E should impose an η^1-coordination mode on the vinyl ligand, whereas a weak 3e donor or a 1e

donor E ligand might allow for variation in the bonding mode of the vinyl ligand. The results of this study are presented in the following sections.

2.2.2 Preparation of Cp*W(NO)(η^x-CPh=CH_2)(E) Complexes [x = 1 or 2, E = Cl, η^2-O_2CPh, OTf, NH^{t}Bu, (H)(PPh_3), (D)(PPh_3)] and their Solid-state Structural and Solution NMR Spectroscopic Properties

In the ensuing discussion, the synthesis of each new vinyl complex will be considered in turn, along with the relevant structural and spectroscopic data that identify the vinyl bonding mode in each. Tables of analytical data (Table 2.2), mass spectrometric and infra-red spectroscopic data (Table 2.3), and ^{1}H and ^{13}C NMR spectroscopic data (Table 2.4) for all compounds discussed in this Chapter are found at the end of Section 2.4.

2.2.2.1 Preparation of Cp*W(NO)(η^2-CPh=CH_2)(Cl) (2.1)

A simple metathesis reaction between the parent dichloride complex Cp*W(NO)$(Cl)_2$ and Mg(CPh=$CH_2)_2$•x(dioxane) (1 equiv) at low temperature affords in good yields air-sensitive, burgundy crystalline **2.1** after work-up and recrystallization (eq 2.1).

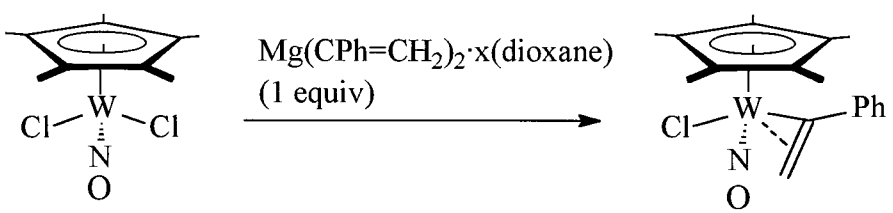

(eq 2.1)

2.1

The identification of the η^2-bonding mode for the vinyl ligand in **2.1** is made on the basis of solution NMR spectroscopic data and the solid-state molecular structure determined by Dr. S. J. Rettig (Figure 2.4 below).[13] The ^1H and ^{13}C NMR spectra for complex **2.1** in solution contain signals attributable to the paraffinic vinyl protons (δ 4.43 and 4.25) and the carbene C_α (δ 220.8) and alkyl C_β (δ 83.6) nuclei of an η^2-vinyl ligand.

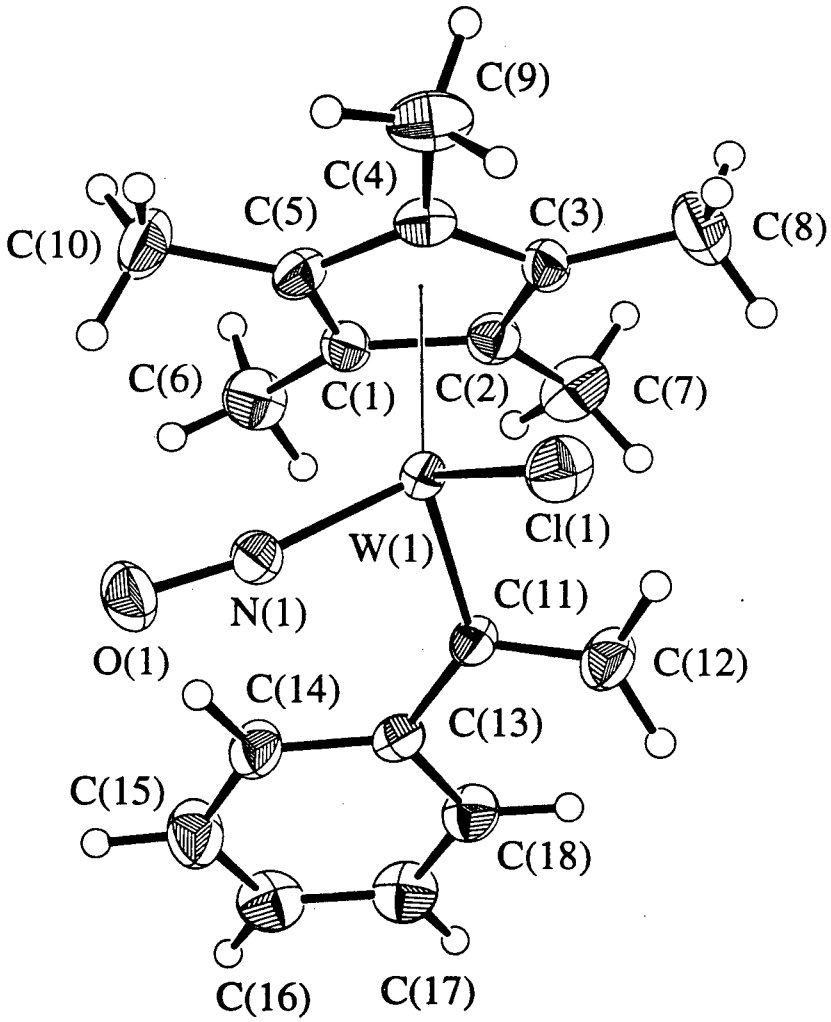

Figure 2.4. The solid-state molecular structure determined for complex **2.1**. The thermal ellipsoids depict the 50% probability level.

Though the vinyl hydrogens were not located during the solution of this structure, the short W(1)-C(11) contact (2.071(4) Å), the acute W(1)-C(11)-C(12) angle (96.4(3)°) and the expanded W(1)-C(11)-C(13) angle (137.0(3)°) are nearly identical to those of the vinyl ligand in the structure of complex **1** and implicate the existence of an η^2-vinyl interaction in the molecular structure of complex **2.1**. Again, the C(11)-C(12) contact is unusually short (1.331(6) Å) for the η^2-vinyl bonding mode, but this seemingly aberrant structural feature can be attributed to the reduced interaction of C_β with the tungsten centre.

2.2.2.2 Reaction of Cp*W(NO)(η^2-CPh=CH$_2$)(Cl) (2.1) with AgX Salts [X = O$_2$CPh, OTf]

Silver salts have long been known to abstract halide ligands from Cp'M(NO)-containing complexes.[14] For example, when such a reaction is conducted in MeCN utilizing $AgBF_4$, MeCN-solvated cations are typically isolated.[15] Likewise, treatment of Cp'M(NO)$_2$Cl [M = Group 6 metal] with $AgBF_4$ in CH_2Cl_2 generates Cp'M(NO)$_2$(FBF$_3$) species which can be used to prepare lactones and pyrones.[16] In a similar reaction, metathesis of the chloride in **2.1** by AgO_2CPh results in the formation of η^2-benzoate-containing **2.2,** as depicted in eq 2.2.

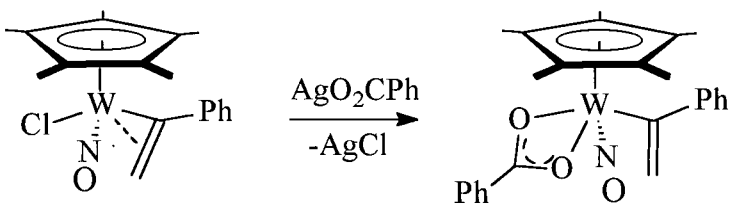

2.1 **2.2** (eq 2.2)

This air-stable compound is isolated as orange needles in good yields by crystallization from diethyl ether. Signals for the vinyl protons in the ^{1}H NMR spectrum of this compound lie in the alkenyl region of the spectrum at δ 6.40 and 5.63, considerably downfield of the analogous signals for the vinyl protons in complexes **1** and **2.1**. The vinyl C_{α} and C_{β} signals appear in the ^{13}C NMR spectrum at δ 189.5 and 122.5, respectively, and are characteristically olefinic in nature. Finally, $^{1}J_{C_{\beta}H}$ has a magnitude of 157.5 Hz, a value that is somewhat larger than the analogous coupling constants determined for complexes **1** and **2.1**. These data taken together implicate an η^{1}-vinyl bonding interaction with the metal centre in complex **2.2**.

The solid-state molecular structure determined for complex **2.2** permits the unambiguous identification of an η^{1}-vinyl ligand in the metal's coordination sphere (Figure 2.5).[17] Key structural features include the W-C(6) contact (2.188(8) Å) that is substantially longer than those in the structures of the η^{2}-vinyl-containing complexes, the W-C(6)-C(7) angle (115.7(6)°) and the W-C(6)-C(61) angle (126.6(6)°). These data taken together implicate a metal-carbon single bond to an sp^{2}-hybridized centre at C(6). The remaining structural features are unremarkable.

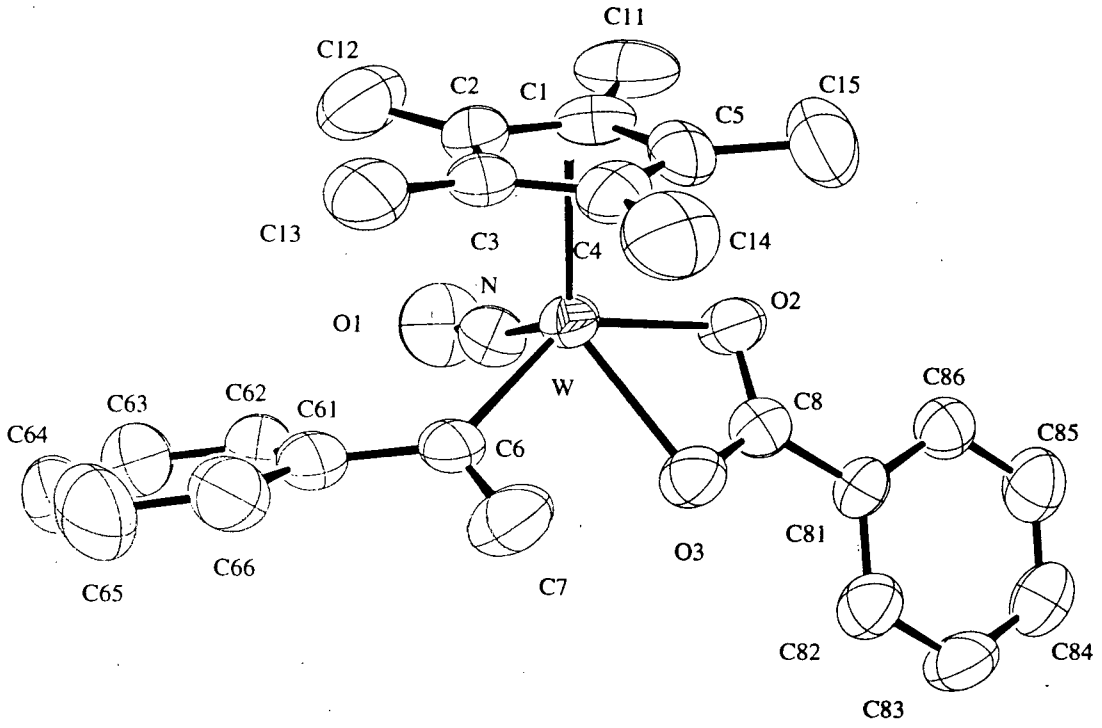

Figure 2.5. The solid-state molecular structure determined for complex **2.2**, 50% probability thermal ellipsoids being depicted.

By analogy to the conversion depicted in eq 2.2, the reaction of **2.1** with 1 equiv of AgOTf affords triflate-containing **2.3** in relatively good yields as a red crystalline solid following work-up and crystallization (eq 2.3).

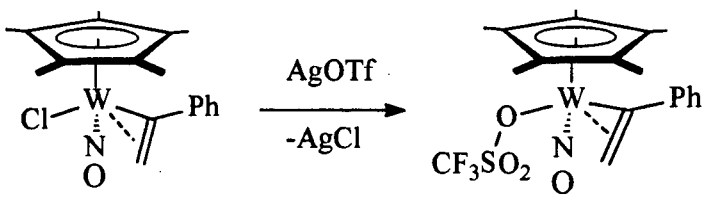

(eq 2.3)

2.1 **2.3**

Considerable spectroscopic evidence exists in support of the formulation of an inner-sphere triflate ligand in complex **2.3**. It has been shown previously that the coordination mode of the triflate ligand can be identified from the IR spectrum of the complex in question, the highest energy absorption of the S-O link occurring in the 1200 – 1280 cm^{-1} range for an ionic triflate group or in the 1300-1380 cm^{-1} range of the IR spectrum for a covalent triflate ligand.[18] Bands attributable to the S-O stretch (1355 cm^{-1}) and C-F stretch (1237 cm^{-1}) of a covalently-bound triflate ligand are evident in the Nujol IR spectrum of complex **2.3.** In addition, ν_{NO} occurs at 1609 cm^{-1}, in the region normally associated with neutral organometallic nitrosyl complexes,[19] a further indication of a covalently-bound triflate ligand in solid-state **2.3**.

While it is conceivable that the covalent triflate ligand could bind to W in a bidentate fashion to afford an 18e complex analogous to benzoate-containing **2.2**, the solution NMR data obtained for **2.3** are inconsistent with the requisite η^1-vinyl bonding mode that would also result. The signals attributable to vinyl C_α and C_β nuclei appear at 258.0 and 77.6 ppm, respectively, in the ^{13}C NMR spectrum of **2.3**. The vinyl proton signals appear in the ^1H NMR spectrum for **2.3** at 4.90 and 4.99 ppm, in the region associated with those of an η^2-vinyl ligand. Interestingly, the upfield vinyl H signal is broadened and lower in intensity than the downfield signal (Figure 2.6), suggestive of a fluxional process or an interaction involving the η^2-vinyl ligand and the metal centre that is absent in the case of **1** and **2.1**.

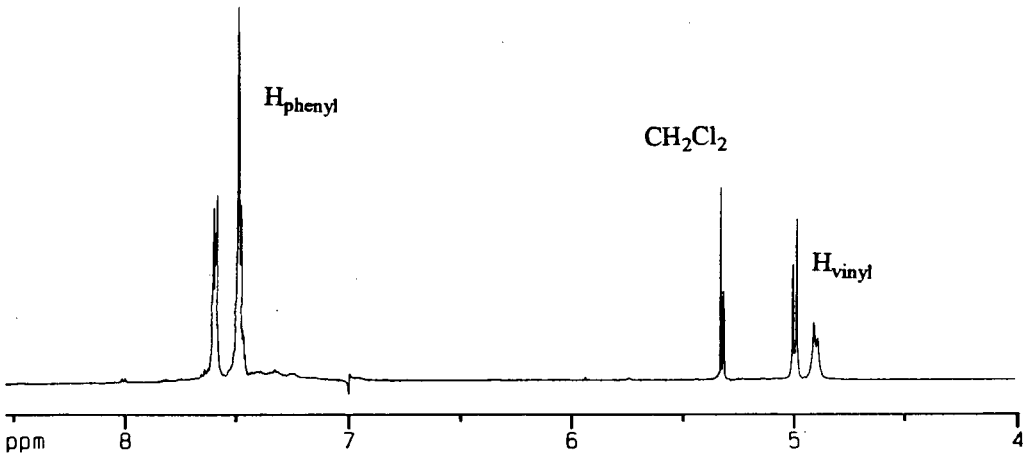

Figure 2.6. The upfield region of the ^1H NMR spectrum (CD_2Cl_2) of complex **2.3** recorded at ambient temperature.

The signals in the RT ^{13}C NMR spectrum of **2.3** attributable to C_α and C_β of the vinyl ligand reinforce the η^2-vinyl assignment. The signal attributable to the C_β resonance is broad, this being further evidence for a fluxional process or unusual interaction involving the vinyl ligand (Figure 2.7). The gate-decoupled ^{13}C NMR spectrum of complex **2.3** reveals a broad, virtual triplet attributable to the vinyl C_β resonance. The C_β nucleus couples to the nearly-equivalent vinyl protons($^1J_{CH}$ = 148 Hz).

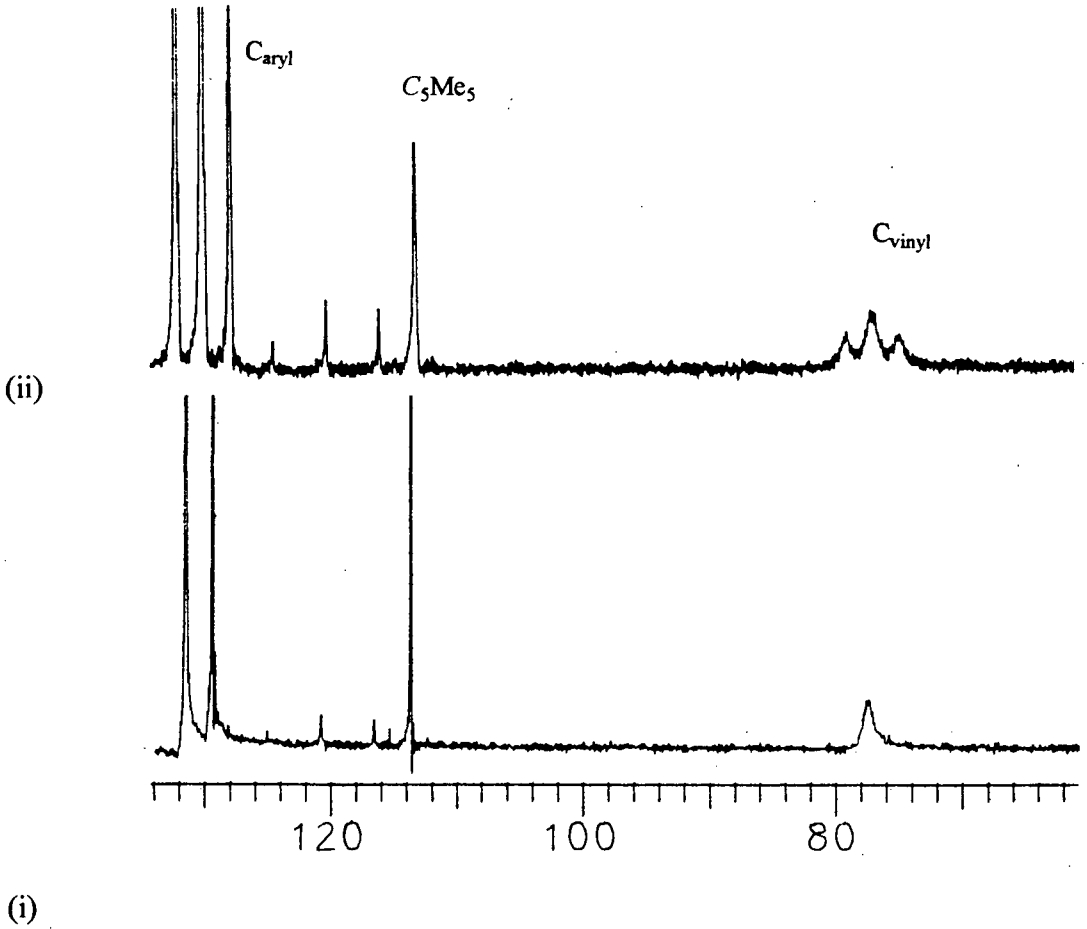

Figure 2.7. (i) The upfield region of the $^{13}C\{^{1}H\}$ NMR spectrum of triflate-containing **2.3**, and (ii) the gate-decoupled ^{13}C spectrum of **2.3** depicting the same region.

The variable-temperature behaviour of this compound in solution, as determined by ^{1}H NMR spectroscopy, is complicated and the processes governing it are unknown at the time of writing. In an analogous reaction, the combination of 1 equiv each of $AgBF_4$ and $Cp^*W(NO)(Cl)(\eta^2\text{-}CPh{=}CH_2)$in CD_2Cl_2 in an NMR tube affords one major product, presumably $[Cp^*W(NO)(\eta^2\text{-}CPh{=}CH_2)]^+[BF_4]^-$, the tetrafluoroborate analogue to **2.3.** The vinyl region in

the ^{1}H NMR spectrum of this reaction mixture contains signals attributable to two inequivalent vinyl protons that are identical to those observed for the triflate complex. Unfortunately, the ^{1}H NMR spectrum of the BF_4 analogue provides no further insight into the source of the unusual vinyl magnetic environment in these two complexes. The unusual signals observed for the vinyl protons could arise under the influence of either the tungsten centre or the weakly-coordinating ancillary ligand.

2.2.2.3 Reaction of 2.3 with MeCN to form $[Cp^*W(NO)(NCMe)_2(\eta^1\text{-}CPh{=}CH_2)]^+[OTf]^-$ (2.4)

The addition of acetonitrile to a red solution of **2.3** in CH_2Cl_2 results in a slow colour change to brown. Cooling of the solution to –30 °C for two weeks results in the deposition of the bis-acetonitrile adduct, $[Cp^*W(NO)(NCMe)_2(\eta^1\text{-}CPh{=}CH_2)]^+[OTf]^-$ (**2.4**) as a brown, crystalline solid. Signals in the ^{1}H and ^{13}C NMR spectra of this compound are readily attributable to the vinyl protons in an η^1-vinyl ligand. The signals in the ^{1}H NMR spectrum attributable to the vinyl protons are sharp and well-defined at room temperature, an observation that lends further support to the proposal for a fluxional W-vinyl interaction in complexes containing the weakly-coordinating OTf and BF_4 anions, as mentioned above.

2.2.2.4 Reaction of 2.1 with Excess ^{t}BuNH$_2$ and $(C_3H_5)_2NH$

A common method used to introduce an amide ligand into an organometallic complex involves the reaction of excess amine with an organometallic halide complex in an aminolysis

reaction.[20] Two equivalents of amine are consumed in this reaction as the halide is eliminated from the organometallic complex as the counteranion in an ammonium salt. The reaction of chloride-containing **2.1** with excess $^{t}BuNH_2$ in this way indeed affords the amide-containing **2.5** in moderate yields as yellow microcrystals following crystallization from diethyl ether (eq 2.4).

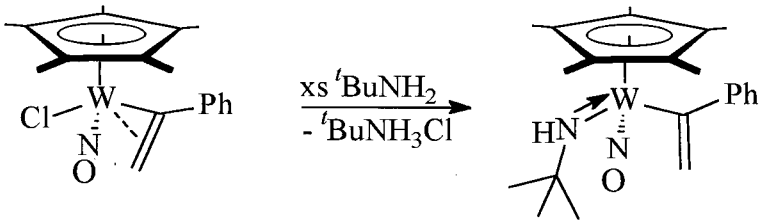

2.1 **2.5** (eq 2.4)

A broad singlet at 7.77 ppm in the ^{1}H NMR spectrum of **2.5** is attributable to the amine H resonance, and an intense singlet at 1.39 ppm that integrates for 9 H is identified as the methyl resonance of the *t*-butyl substituent. Analogous to the NMR signals observed for benzoate-containing **2.2**, the chemical shifts of the ^{1}H and ^{13}C resonances attributable to the respective vinyl protons (6.21 and 5.51 ppm) and the vinyl carbon nuclei (185.1 and 126.3 ppm) in **2.5** are indicative of an η^1-vinyl bonding interaction with W. Attempts to grow X-ray-quality crystals of complex **2.5** to this point have been unsuccessful.

Interestingly, exposure of **2.1** to an excess of diallyl amine does not yield the corresponding secondary-amide vinyl complex. Indeed, signals exist in the ^{1}H and ^{13}C solution NMR spectra of orange-brown crystalline **2.6** (eq 2.5) that are attributable to the allyl substituents of the amine group. However, signals assignable to either an η^1- or η^2-vinyl ligand are conspicuously absent. In addition, analytical and mass spectral data indicate that one equivalent of HCl remains in the coordination sphere of the complex. The solid-state molecular

structure determined for this complex, depicted in Figure 2.8 below,[21] reveals that the chloride ligand remains bound to W. In addition, the diallylamine unit is bound to W via a dative bond (W(1)-N(1) = 2.310(6) Å) and to the vinyl fragment through a single N-C bond (N(1)-C(11) = 1.491(8) Å) as a component of an azametallacyclobutane ring.[22] The vinyl ligand has been saturated, the C(11)-C(12) contact (1.51(1) Å) being the distance of a single C-C bond and the W(1)-C(12) distance (2.255(7) Å) being that of a typical W-C single bond.[23]

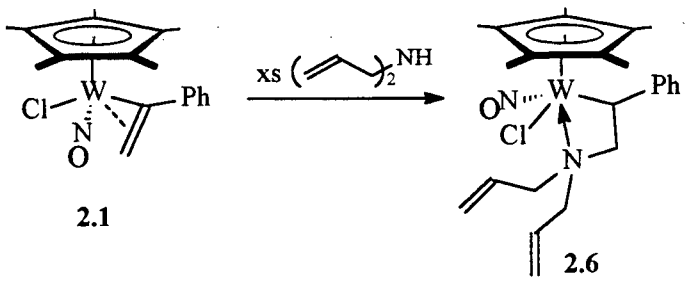

(eq 2.5)

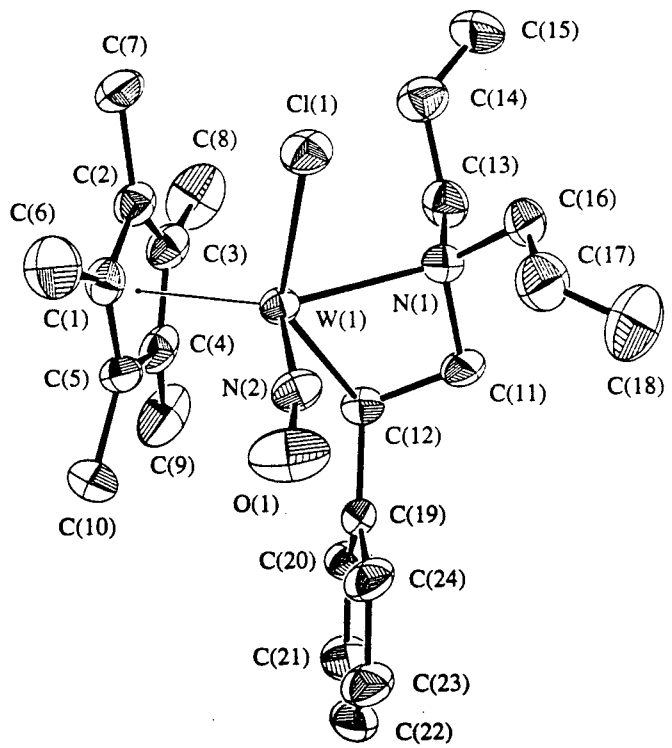

Figure 2.8. The solid-state molecular structure of complex **2.6.** The depicted ellipsoids represent the 50% probability level.

Scheme 2.1

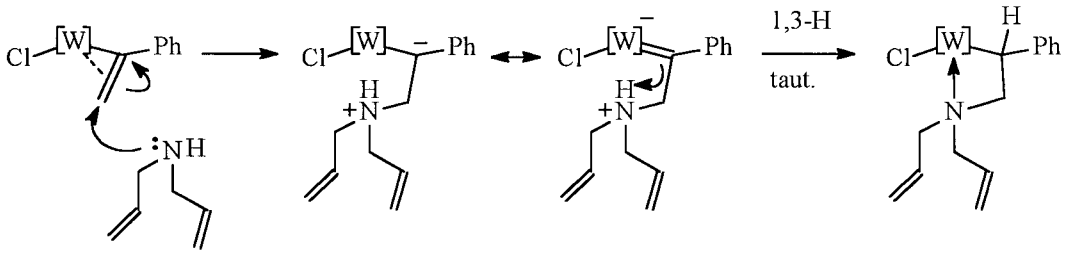

A reasonable mechanistic pathway for this reaction is shown in Scheme 2.1 above. Attack at the β-carbon of the vinyl ligand by diallyl amine affords the zwitterionic ammonium alkylidene complex which, upon tautomerization and coordination of the pendant amine, leads to the formation of the product compound. Support for this pathway is given by the report of an isolable zwitterionic phosphonium carbene complex that results from a similar reaction between a Ni(vinyl) complex and PPh_3 (eq 2.6).[24]

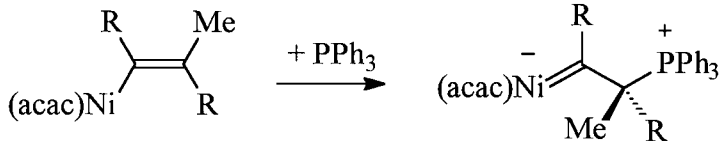

(eq 2.6)

A question naturally arises as to the reason why the reaction of **2.1** with diallylamine does not yield the desired amide vinyl complex, yet the reaction of *t*-butylamine with **2.1** does. In answering this question, the proposed mechanism of aminolysis must be considered (Scheme 2.2).

Scheme 2.2

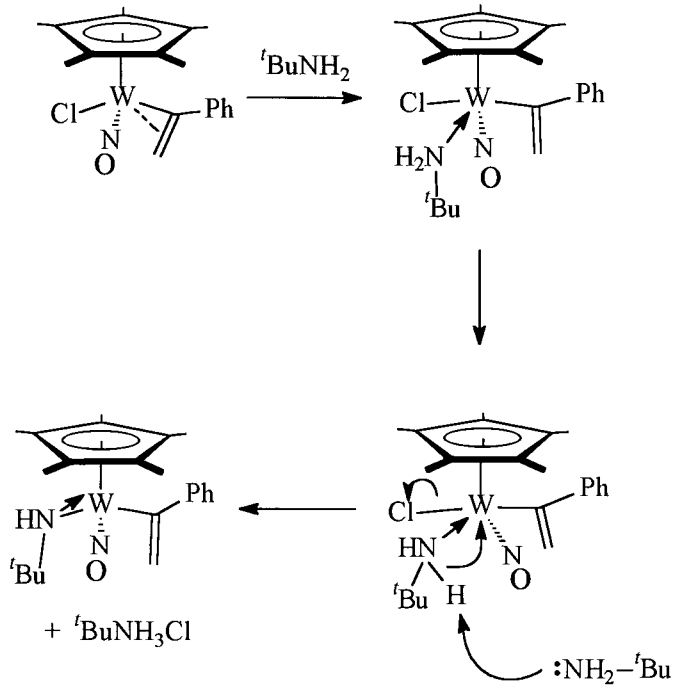

The aminolysis reaction is initiated with amine coordination at the Lewis acidic site in the 16e alkyl chloride complex. Deprotonation of the acidic coordinated amine by a second molecule of *t*-butylamine leads to covalent bond formation between the resultant 3e amide ligand and W. The chloride, being a good leaving group, is eliminated from the potentially 19e species to afford the 18e alkyl amide complex. The difference in the reactivity of *t*-butylamine and diallylamine with complex **2.1** is proposed to arise from a difference in the steric profile of the two reagents. The environment about W in complex **2.1** is considerably congested and, as a result, its accessibility is largely determined by the steric profile of an incoming reagent. *t*-Butylamine, while containing the bulkier hydrocarbyl substituent, is a primary amine and has a smaller steric cross-section than does the secondary diallylamine reagent. Thus, attack at the

metal centre by the diallylamine reagent is hindered by its bulkiness, and its reactivity with complex **2.1** is restricted to the kinetically more accessible vinyl ligand.

2.2.2.5 Synthesis and Properties of $Cp^*W(NO)(CH_2SiMe_3)(\eta^1\text{-}CPh{=}CH_2)(H)(PPh_3)$ (2.7)

Complexes of the form $Cp^*W(NO)(R)_2$ [R = alkyl] are known to be Lewis acidic and undergo reaction with a variety of Lewis bases, as described in Section 2.2.1. In particular, the reaction of $Cp^*W(NO)(CH_2SiMe_3)_2$ with H_2 has been investigated in great detail. At high pressures of dihydrogen, bimetallic tetrahydride complexes of tungsten are obtained in high yields following the extrusion of two equiv of $SiMe_4$.[25] On the other hand, the reaction of $Cp^*W(NO)(CH_2SiMe_3)_2$ with dihydrogen at low pressures leads to the extrusion of only 1 equiv of $SiMe_4$.[25] The hydride-containing species $Cp^*W(NO)(CH_2SiMe_3)(H)$ that is transiently generated undergoes a variety of hydrotungstenation reactions in the presence of unsaturated small molecules,[26] and can be trapped as an 18e adduct by PMe_3.[25]

The analogous reaction of $Cp^*W(NO)(CH_2SiMe_3)(\eta^2\text{-}CPh{=}CH_2)$ (**1**) with H_2 in the presence of PPh_3 affords the air-sensitive, ether-soluble vinyl hydride **2.7** (eq 2.7). Triphenylphosphine is chosen over trimethylphosphine in this reaction due to the reaction of the latter with the vinyl ligand in **1**, as described in Chapter 1, Section 1.4.1.

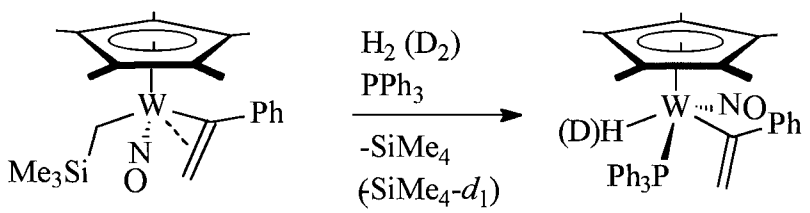

1 **2.7** **(2.7-d_1)** (eq 2.7)

The presence of a hydride ligand in **2.7** is made obvious by the W-H stretch evident in the Nujol IR spectrum (1824 cm^{-1}) and by the hydride resonance in the ^1H NMR spectrum (δ 1.04, $^2J_{PH}$ = 96.1 Hz) of **2.7**. These signals appear in the same regions of their respective spectra as those of other phosphine-trapped alkyl hydride complexes of tungsten.[27] The deuteride-containing **2.7-*d*$_1$** may be prepared under the identical conditions in the presence of D_2 gas. Evidence for the presence of a deuteride ligand in **2.7-*d*$_1$** is given by a W-D stretch in its Nujol IR spectrum (1318 cm^{-1}) that is shifted relative to the W-H stretch in **2.7**. The magnitude of this value is in good agreement with the expected theoretical value of 1290 cm^{-1}.[28] The signals in the ^1H and ^{13}C NMR spectra attributable to the vinyl ligand in these complexes are characteristic of an η^1-vinyl ligand. The vinyl protons resonate at 6.31 and 4.81 ppm and the C_α and C_β signals are identified in the olefinic region at 177.1 and 125.3 ppm, respectively.

The existence of a hydride ligand and the bonding mode of the vinyl ligand in complex **2.7** are confirmed by its solid-state molecular structure (Figure 2.9),[29] the hydride ligand having been located in the difference map. The W(1)-H(1) distance (1.73 Å) and W(1)-P(1) distance (2.519(3) Å) are comparable to those of other structurally characterized phosphine-trapped hydride complexes of the Cp*W(NO) fragment.[25,27] The vinyl ligand's metrical parameters are clearly characteristic of an η^1-vinyl ligand. For example, the W(1)-C(11) bond distance (2.21 Å) is that of a single W-C bond. In addition, the W(1)-C(11)-C(12) bond angle of 120(1)°, the W(1)-C(11)-C(13) angle of 123(1)°, and the C(11)-C(12) bond length of 1.33(2) Å are indicative of sp^2-hybridization at C(11) and double bond character in the C(11)-C(12) contact.

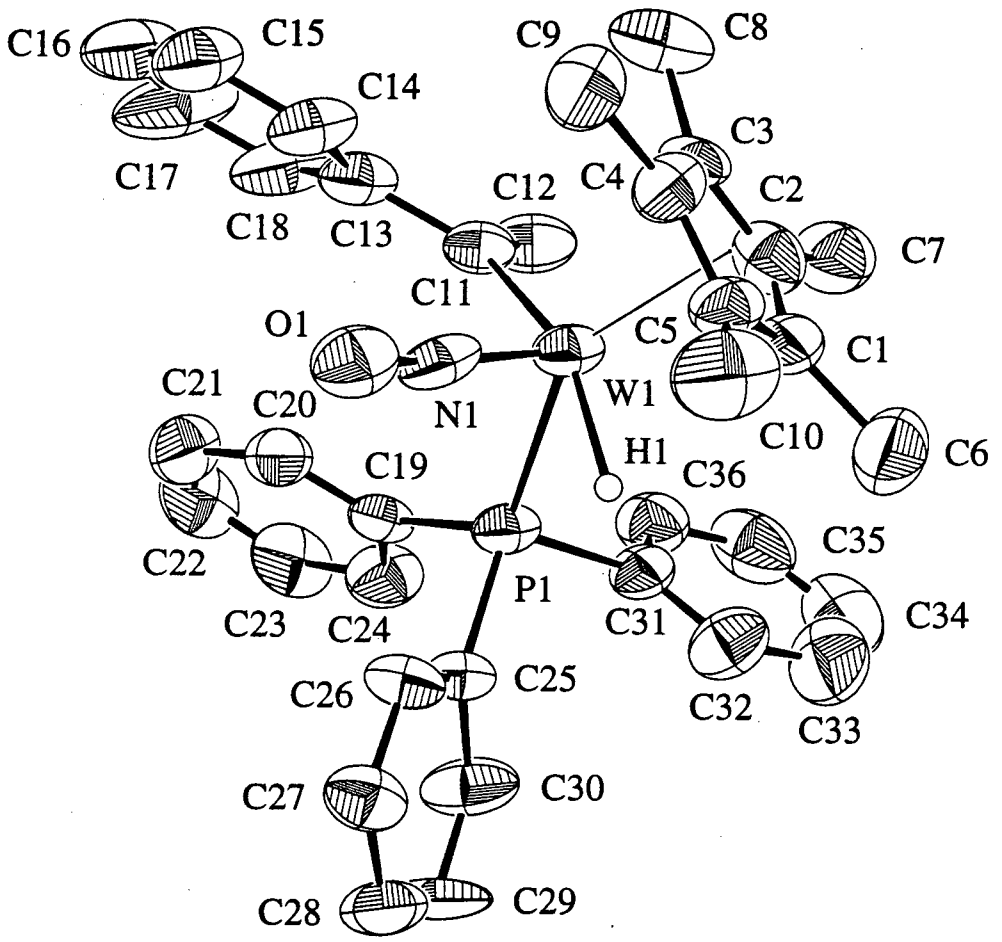

Figure 2.9. The solid-state molecular structure determined for complex **2.7**, 50% probability thermal ellipsoids being depicted.

2.2.3 NMR Spectroscopic and Solid-State Metrical Correlations for η^1- and η^2-Vinyl Complexes

In this final Discussion section of Chapter 2, graphical comparisons are made relating (1) the chemical shifts assigned to the vinyl C_α and C_β resonances in the ^{13}C NMR spectra obtained for compounds **1**, **2.1**, **2.2**, **2.3**, **2.5**, and **2.7**, and (2) the M-C_α bond lengths and the associated M-

C_α-C_β bond angles determined for these vinyl compounds with others taken from the literature for which solid-state metrical data are available. These comparisons illustrate pictorially the dependence of the vinyl NMR spectroscopic and metrical parameters on the W-vinyl bonding interaction. The established η^1-vinyl hydride-containing **2.7** and the known η^2-vinyl complexes, $CpRe(PMePh_2)(Br)(\eta^2\text{-}CPh{=}CHPh)$[3d] and $Tp'W(CO)_2(\eta^2\text{-}CPh{=}CH_2)$,[9] are taken as reference points which define the typical η^1- and η^2-vinyl bonding modes. Table 2.1 contains the solid-state metrical data and solution NMR spectroscopic data employed in these comparisons.

Table 2.1. Solid-state metrical and solution NMR spectroscopic data for selected vinyl-containing complexes.

Compound	d(M-C_α) (Å)	a(M-C_α-C_β) (°)	$\delta(C_\alpha)$ (ppm)	$\delta(C_\beta)$ (ppm)
$CpRe(PMePh_2)(Br)(\eta^2\text{-}CPh{=}CHPh)$	1.91(2)	79(1)	253.6	16.7
$Tp'W(CO)_2(\eta^2\text{-}CPh{=}CH_2)$	n/a	n/a	264.5	38.0
$Cp^*W(NO)(\eta^2\text{-}CPh{=}CH_2)(CH_2SiMe_3)$ (**1**)	2.076	98.7	227.9	83.1
$Cp^*W(NO)(\eta^2\text{-}CPh{=}CH_2)(Cl)$ (**2.1**)	2.071	96.4	220.8	83.6
$Cp^*W(NO)(\eta^1\text{-}CPh{=}CH_2)(O_2CPh)$ (**2.2**)	2.188	115.7	189.5	122.5
$Cp^*W(NO)(\eta^2\text{-}CPh{=}CH_2)(OTf)$ (**2.3**)	n/a	n/a	258.0	77.6
$Cp^*W(NO)(\eta^1\text{-}CPh{=}CH_2)(NH^tBu)$ (**2.4**)	n/a	n/a	185.1	126.3
$Cp^*W(NO)(\eta^1\text{-}CPh{=}CH_2)(H)(PPh_3)$ (**2.6**)	2.21	123	177.1	125.3

Thus, plotting $\delta(C_\alpha)$ against $\delta(C_\beta)$ affords the plot shown in Figure 2.10. Correlating these two parameters in this way does not imply that a mathematical relationship exists to describe one parameter as a function of the other. Such a plot simply serves to illustrate pictorially the NMR spectroscopic characteristics of the η^1- and η^2-vinyl bonding modes. Clearly, an η^2-vinyl ligand is typified by signals in the ^{13}C NMR spectrum at low and high field attributable to C_α and C_β, respectively, whereas those of the η^1-vinyl ligand appear mid-spectrum in the olefinic region.

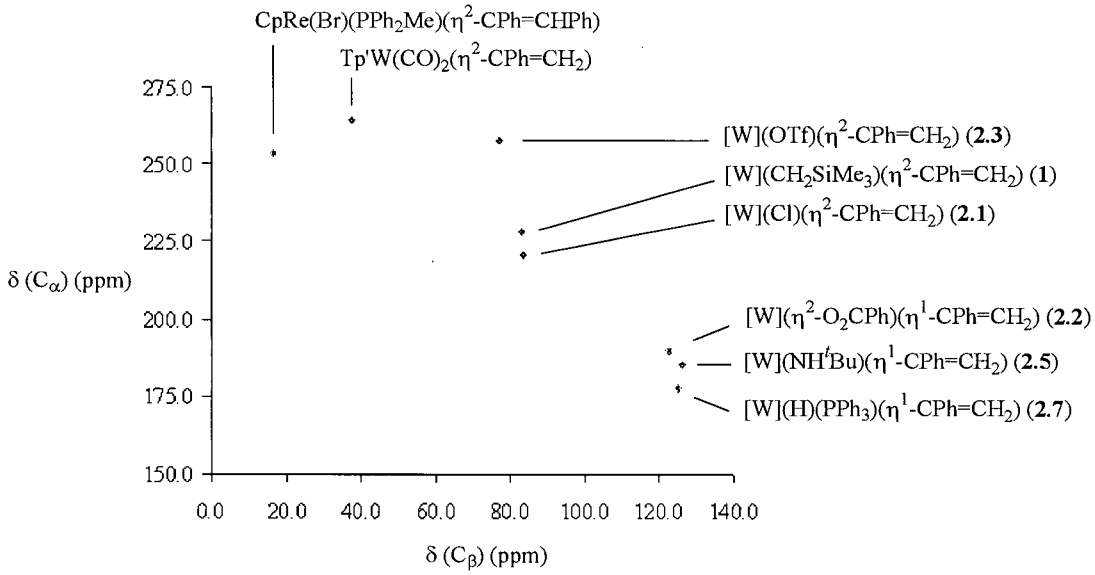

Figure 2.10. The correlation between vinyl ^{13}C shifts observed for η^1- and η^2-vinyl compounds. [W] = Cp*W(NO).

The vinyl C_α and C_β signals observed for complexes **1**, **2.1**, and **2.3** lie intermediate to the two regions defined by the η^1-vinyl- and η^2-vinyl-containing complexes. Though the C_α signals

are clearly carbenic in character, the C_β signals appear downfield of the region one might associate with a typical M-C(alkyl) resonance. A survey of the chemical shifts attributed to the sp^3-hybridized C_α nuclei in alkyl ligands in 18e Cp*W(NO) complexes (δ 30 – 60)[20,30] and those associated with their 16e alkyl-containing analogues (δ 60 – 100)[30c] reveals that the vinyl-C_β signals associated with **1**, **2.1**, and **2.3** also occur in the appropriate region to be assigned as σ-bound, metallated carbon nuclei in η^2-vinyl ligands. These observations permit the confident formulation of an η^2-vinyl ligand in the solution structures of **1**, **2.1**, and **2.3**.

A correlation of the M-C_α contacts and the associated M-C_α-C_β angles obtained for those vinyl complexes that have been structurally characterized is depicted in Figure 2.11.

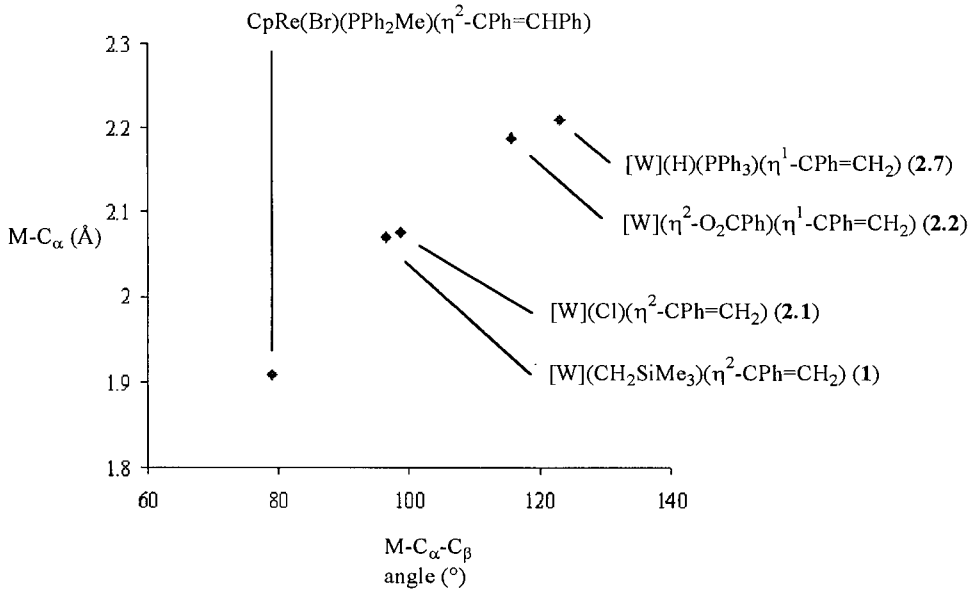

Figure 2.11. A comparison of the M-C_α-C_β angles and the associated M-C_α contacts in various η^1- and η^2-vinyl-containing complexes. [W] = Cp*W(NO).

It is apparent from this Figure that the vinyl parameters determined for **2.1** and **1** are seemingly intermediate to those typically observed for the two limiting bonding forms of the vinyl ligand. To broaden the scope of these structural comparisons, a correlation of the W-C_α and W-C_β distances obtained for **1** and **2.1** has been made with the averages of those obtained for other η^2-vinyl complexes of W that were compiled from the Cambridge Structural Database by Orpen *et al* in 1989,[31] as tabulated below.

	CSD[a]		**1** and **2.1**[b]	
	d (Å)	3σ	d (Å)	uncertainty
d(W-C_α)	1.918	0.09	2.074	0.010
d(W-C_β)	2.251	0.234	2.615	0.010

[a] denotes average values obtained from the Cambridge Structural Database (see ref 31). [b] denotes the average of the two distances obtained for **1** and **2.1**.

These values are plotted graphically in Figure 2.12 below. Interestingly, the variation in the statistical sample derived from the CSD and the variation in d(W-C_α) and d(W-C_β) observed for **1** and **2.1** are close in proximity (the 95% confidence limits nearly overlapping). This suggests that the solid-state geometry of the vinyl ligand in **1** and **2.1** potentially represents an outer limit for what may be considered an W-(η^2-vinyl) interaction.

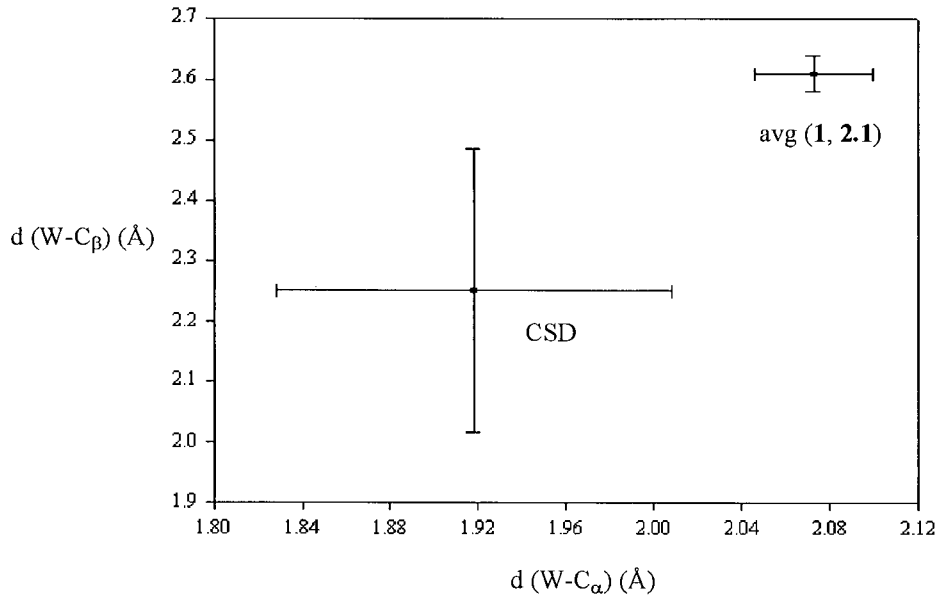

Figure 2.12. A correlation of average d(W-C_α) and d(W-C_β) determined for structurally-characterized η^2-vinyl complexes of W compiled from the Cambridge Structural Database (CSD), and those of **1** and **2.1** (avg(**1**, **2.1**)). Error bars represent 3 standard deviations in the average measurement.

Because the data obtained from reference 31 is dated, a search of the Cambridge Structural Database for more recent examples of the W(η^2-vinyl) fragment has been conducted utilizing the Quest[32] search program. Interestingly, no examples of structurally characterized tungsten complexes containing the simple vinyl fragment, CR=CR'$_2$, are identified in this search. Instead, each of the structures obtained in this way contains the vinyl fragment as a component of a larger multicyclic or multihapto unsaturated ligand, such as one of those depicted in Scheme

2.3. Therefore, the search has been broadened to identify complexes containing W-C bonding contacts of magnitude greater than 2.4 Å. This latter search yields a list of 75 crystal structures of various organotungsten complexes. Four of these compounds, whose solid-state molecular structures contain long W-C bonding contacts, are depicted in Scheme 2.3 below.[33] Common to all four of these examples is an unsaturated hydrocarbyl ligand that is coordinated to the W centre via at least one long W-C contact. The molecular structure depicted in case **III** is particularly noteworthy, the W-C contact of 2.61(2) Å in the ring system being strikingly similar to the η^2-vinyl W-C_β contact of 2.615(5) Å in **1**.

Scheme 2.3

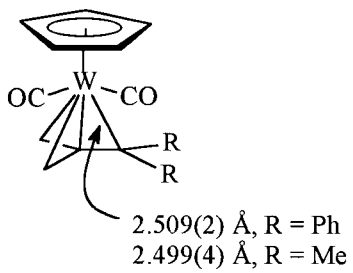

I

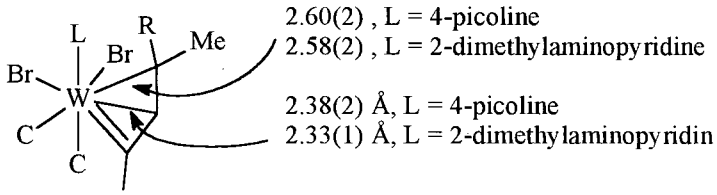

II

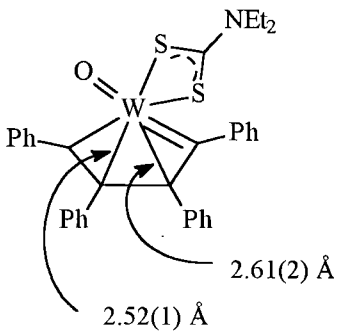

III

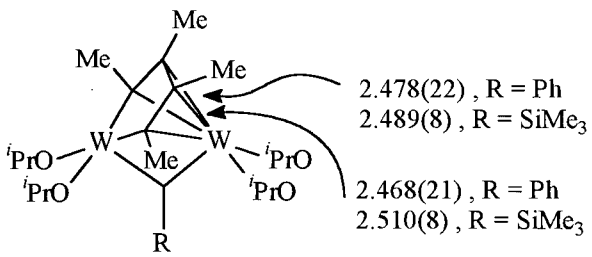

IV

From the results of these studies it can be concluded that the solution NMR spectroscopic properties observed for the η^2-vinyl ligand in complexes **1** and **2.1** are more closely allied to those of previously-reported η^2-vinyl complexes, more so than are the solid-state structural properties of the vinyl ligand in these two complexes to those of other vinyl complexes reported in the literature. However, a search of the Cambridge Structural Database immediately reveals that the number of structurally characterized η^2-vinyl complexes of tungsten reported in the literature is very small. In spite of this fact, at least one such complex of W has been reported which contains metrical parameters comparable to those determined for **1** and **2.1**.[33c] Thus, the solid-state molecular structures determined for the η^2-vinyl-containing complexes **1** and **2.1** may be considered as members of the set defining the W(η^2-vinyl) interaction, and the parameters determined for the η^2-vinyl fragment in these complexes probably represent outer limits for this interaction in the solid-state.

2.3 Epilogue and Future Work

Several η^1- and η^2-vinyl-containing complexes have been synthesized, and their solution NMR spectroscopic and solid-state metrical parameters have been investigated and compared to known η^1-vinyl and η^2-vinyl complexes. The results of these comparisons, as described above, imply that the vinyl ligand in complexes **1**, **2.1,** and **2.3** exists in an η^2 form best described as intermediate to the limiting η^2-CPh=CH_2 and metallacyclopropene forms. More generally, it can be stated by association that this description also applies to any Cp*W(NO)(E)(η^2-CPh=CH_2) complex where E is a 1e donor ligand. In cases where a stronger donor ligand exists in a vinyl-containing Cp*W(NO) complex, the ancillary donor ligand will donate the greater number of

electrons in completing the electronic saturation of the metal centre, thereby forcing the vinyl ligand into the η^1-bonding mode. In the ensuing chapters these general phenomena will be illustrated in a myriad of η^1-vinyl- and η^2-vinyl-containing complexes generated by reductive coupling reactions (Chapter 3) or by C-H bond activation reactions (Chapter 4).

While the vinyl-containing complexes presented in this chapter were prepared as a part of a study of the vinyl coordination mode at W, complexes **2.1** and **2.3** are interesting in their own right. Complex **2.1** may serve as a source of interesting vinyl-containing complexes in which the chloride ligand in the former has been replaced by an unsaturated ligand such as an acetylide or allyl ligand. Much research today is focused towards the regio- and stereoselective coupling of such unsaturated ligands in the coordination sphere of a transition metal.[34] The preparation of such compounds incorporating the Cp*W(NO)(CPh=CH_2) framework and an investigation into their thermal chemistry will undoubtedly lead to interesting chemistry. Complex **2.3** displays interesting temperature-dependent solution behaviour, the nature of which remains unknown at this time (although investigations continue at the time of writing). Speculation as to the nature of this behaviour is premature at this time. In addition to this temperature-dependent behaviour, it has been demonstrated that a cationic η^2-vinyl complex can be generated in the reaction of **2.3** with a neutral donor compound such as MeCN. The resultant cation is similar to those of the Group 4 metals that are receiving considerable attention at present for their ability to polymerize α-olefins in Ziegler-Natta processes.[35] As such, further investigation into the synthesis and reactivity of complex **2.3** and analogous cationic vinyl-containing complexes is warranted.

2.4 Experimental Procedures

2.4.1 General Methodologies

The general experimental procedures described in this Section apply to the entire Thesis. All reactions and subsequent manipulations involving organometallic reagents were performed under anhydrous conditions in an atmosphere of prepurified argon or dinitrogen. Purification of inert gases was achieved by passing them through two double-walled glass columns (10 × 70 cm), one containing MnO and the other activated 4Å molecular sieves.

Solvents were freshly distilled from the appropriate drying agents under nitrogen atmosphere and either purged for 10 min with argon prior to use or were directly transferred under vacuum from the appropriate drying agent. Tetrahydrofuran (THF) and diethyl ether were distilled from Na/benzophenone; hexanes, toluene and pentane were distilled from Na/benzophenone/tetraglyme; dichloromethane was distilled from CaH_2; acetone was distilled from CaH_2 and stored over 4Å molecular sieves and vacuum-transferred when required. C_6D_6, C_7D_8 and THF-d_8 were dried over Na and vacuum-transferred as required. $CDCl_3$, acetone-d_6, and CD_2Cl_2 were dried over 4Å molecular sieves and vacuum-transferred as required.

Conventional glovebox and vacuum line Schlenk techniques were utilized throughout.[36] The specific gloveboxes used in this work were a two-station IT/Braun Labmaster 130, a Vacuum Atmospheres HE-553-2, and a HE-43-2. The IT/Braun two-station glovebox was equipped with a cold well and freezer for low-temperature work. All IR samples were prepared as Nujol mulls sandwiched between KBr plates or as KBr pellets, unless otherwise noted. IR spectra were recorded on an ATI Mattson Genesis Series FT-IR spectrometer. All NMR spectra were recorded in parts per million (ppm) on a Varian Associates XL-300, Bruker AC-200,

Bruker WF-400 or Bruker AMX-500 spectrometer. All ^{1}H NMR spectra are referenced to the residual protio-isotopomer (~0.2%) present in a particular solvent. All ^{13}C NMR spectra are referenced to the natural abundance carbon signal of the solvent employed. Ms. M. T. Austria, Ms. L. K. Darge, and Drs. N. Burlinson and S. O. Chan assisted in obtaining some of the NMR spectra. Mass spectra were recorded by the staff of the UBC Chemistry Mass Spectrometry Laboratory. Low-resolution mass spectra (EI, 70 eV) were recorded on a Kratos MS50 spectrometer utilizing the direct-insertion sample introduction method. All elemental analyses were performed by Mr. P. Borda. X-ray crystallographic analyses were performed by Drs. R. J. Batchelor and F. W. B. Einstein of Simon Fraser University, Dr. S. J. Rettig of the UBC X-ray Crystallography Department, or Dr. V. G. Young, Jr., of The University of Minnesota X-ray Crystallography Laboratory.

2.4.2 Reagents

The organometallic reagents, namely $Cp^*W(NO)(Cl)_2$,[37] $Cp^*W(NO)(CH_2SiMe_3)(CPh{=}CH_2)$,[1] and $Mg(CPh{=}CH_2)_2{\bullet}x(dioxane)$[38] were prepared according to published procedures. H_2 (Linde, extra dry) and D_2 (CIL) was used as received. PPh_3 (Aldrich) was recrystallized from hexanes. $^{t}BuNH_2$ and $(C_3H_5)_2NH$ were dried over CaH_2 and vacuum-transferred as required. AgO_2CPh and AgOTf were stored under nitrogen in the glovebox and used as supplied without further purification.

2.4.3 Synthesis

Physical and spectroscopic data for each new organometallic complex discussed in this chapter are collected in tables that appear at the end of Section 2.4. A numbering scheme, list of yields, and analytical data for compounds **2.1** – **2.7** appear in Table 2.2. Mass spectrometric and IR spectroscopic data are collected in Table 2.3, and ^{1}H and ^{13}C NMR spectroscopic data appear in Table 2.4. Characterization data for the previously-characterized complex **1**[39] are included in each table for reference.

2.4.3.1 Preparation of Cp*W(NO)(CPh=CH$_2$)(Cl) (2.1)

Brown, powdery Cp*W(NO)(Cl)$_2$ (420 mg, 1 mmol) and white solid Mg(CPh=CH$_2$)$_2$•x(dioxane) (105 mg, 1 equiv) were placed in a 50-mL Erlenmeyer flask in an inert atmosphere glovebox. The flask was cooled to ~ -100 °C in a liquid-N_2-cooled cold well over 20 min. THF (10 mL) was placed in a stoppered vial and cooled to –35 °C in the glovebox freezer. After 15 min the vial was removed from the freezer and its contents were pipetted down the walls of the Erlenmeyer flask submerged in the cold well, forming a solid puck of THF on top of the solids in the base of the flask. The reaction vessel was left in the cold well until thermal equilibration was achieved (~5 min) and then removed and placed on a rotary evaporator. Warming the mixture slowly to room temperature was accompanied by a colour change to a deep burgundy-black. After being stirred at room temperature for 15 min, the THF was removed from the final reaction mixture under vacuum to leave a burgundy brown solid. The solid was washed with diethyl ether (3 × 2 mL) and then dried under high vacuum for another 5 min. Methylene chloride was added (7 mL) and the resulting burgundy suspension

was filtered through Celite. The filtrate was concentrated, hexanes added (3 mL), and the burgundy solution was placed in the freezer (-35 °C) overnight to induce the crystallization of pure **2.1** as burgundy blocks (280 mg). Concentration and cooling of the mother liquor to –35 °C overnight afforded a second crop of crystals (80 mg).

2.4.3.2 Preparation of Cp*W(NO)(CPh=CH_2)(η^2-O_2CPh) (2.2)

Burgundy **2.1** (244 mg, 0.5 mmol) was dissolved in CH_2Cl_2 (8 mL) in a 25-mL Erlenmeyer flask in an inert atmosphere glovebox. AgO_2CPh (115 mg, 1 equiv) was placed in a stoppered vial and dissolved in a minimum of diethyl ether. The flask and vial were both cooled to -35 °C in the glovebox freezer. After 15 min the two vessels were removed from the freezer and the contents of the vial were slowly added to the Erlenmeyer flask, with agitation of the resultant mixture. As the mixture warmed to room temperature a colour change to dark orange and the formation of a flocculent white precipitate occurred. After being stirred at room temperature for 15 min, the solvent was removed from the final reaction mixture under vacuum to leave an orange residue. Diethyl ether (20 mL)was added and the resulting orange suspension filtered through Celite. The orange filtrate was concentrated, hexanes (2 mL) were added, and the solution was placed in a freezer (-35 °C) overnight to induce the crystallization of pure **2.2** as orange needles (172 mg). Concentration and cooling of the mother liquor to –35 °C overnight afforded a second crop of crystals (66 mg).

2.4.3.3 Preparation of Cp*W(NO)(η^2-CPh=CH_2)(OTf) (2.3)

Burgundy **2.1** (244 mg, 0.5 mmol) was dissolved in CH_2Cl_2 (8 mL) in a 25-mL Erlenmeyer flask in an inert atmosphere glovebox. AgOTf (129 mg, 1 equiv) was placed in a vial and dissolved in a minimum of diethyl ether. The flask and vial were both cooled to -35 °C in the glovebox freezer, whereupon after 15 min the AgOTf solution was added slowly to the CH_2Cl_2 solution of compound **2.1**. Upon mixing, an immediate reaction occurred as evinced by the formation of a white flocculent precipitate and the lightening of the mixture to a red colour. After being stirred at room temperature for 15 min, the solvent was removed from the final reaction mixture under vacuum to leave a red residue. Methylene chloride (10 mL) was added and the resulting red suspension was filtered through Celite. The red filtrate was concentrated, hexanes (5 mL) were added, and the solution was placed in the freezer (-35 °C) overnight to induce the precipitation of pure **2.3** as red microcrystalline solid (175 mg).

2.4.3.4 Preparation of [Cp*W(NO)(η^1-CPh=CH_2)($NCMe)_2$][OTf] (2.4)

Red **2.3** (114 mg, 0.18 mmol) was dissolved in CH_2Cl_2 (4 mL) in a Schlenk tube and MeCN (0.5 mL) was added, thereby resulting in a brown solution. Maintaining this solution at a temperature of –35 °C for 2 weeks resulted in the deposition of 98 mg of analytically pure **2.4** as brown needles. The needles were isolated by removing the mother liquor and were dried under vacuum for 0.5 h.

2.4.3.5 Preparation of Cp*W(NO)(η^1-CPh=CH_2)(NH^{t}Bu) (2.5)

Burgundy **2.1** (244 mg, 0.5 mmol) was dissolved in THF (7 mL) in a Schlenk tube. The tube was connected to a vacuum-transfer bridge and cooled to –196 °C in a liquid N_2 bath. ^{t}BuNH_2 (excess) was vacuum transferred onto the resulting frozen solution. The mixture was allowed to warm to room temperature with stirring, whereupon a colour change to brown occurred. After being stirred at room temperature for 15 min, the solvent was removed from the final reaction mixture under vacuum to leave a yellow-brown residue. Methylene chloride/hexanes (1:2, 5 mL) was added and the resulting suspension was filtered through Celite. The yellow filtrate was concentrated, hexanes (3 mL) were added, and the solution was placed in a freezer (-35 °C) overnight to induce the precipitation of pure **2.5** as a yellow-brown analytically-pure crystalline aggregate (148 mg).

2.4.3.6 Preparation of Cp*W(NO)(η^2-*C*HPhCH_2*N*(C_3H_5)$_2$)(Cl) (2.6)

Complex **2.6** was prepared in a manner analogous to **2.5** except that excess diallylamine was vacuum-transferred onto the solid solution of complex **2.1**. An identical work-up procedure afforded large prismatic crystals of pure **2.6** (254 g) after the brown filtrate was kept at –35 °C for 3 d in the glovebox freezer.

2.4.3.7 Preparation of Cp*W(NO)(η^1-CPh=CH_2)(H)(PPh_3) (2.7)

Burgundy Cp*W(NO)(CPh=CH_2)(CH_2SiMe_3) (135 mg, 0.25 mmol) and PPh_3 (66 mg, 1 equiv) were dissolved in hexanes (20 mL) in a thick-walled glass reaction bomb. The bomb was

connected to a cylinder of H_2 and frozen in a liquid nitrogen bath. The bomb was submitted to three freeze-pump-thaw cycles, whereupon after the third evacuation dihydrogen (14 psig) was added. The bomb was then maintained at 0 °C in a constant temperature bath for 4 d, during which time gold needles of **2.7** deposited on the walls of the flask. After 4 d the H_2 was removed under vacuum and the mother liquor was cannulated away from the crystals. The bomb was evacuated and left under vacuum for 1h, after which time the gold crystals were isolated (58 mg). The mother liquor was concentrated and cooled in a freezer to induce further precipitation of an analytically pure straw yellow powder (**2.7**, 40 mg).

2.4.3.8 Preparation of Cp*W(NO)(η^1-CPh=CH_2)(D)(PPh_3) (2.7-d_1)

Complex **2.7**-d_1 was prepared in a manner analogous to complex **2.7** except that D_2 was employed in the place of H_2. An identical work-up procedure afforded the isolation of 90 mg of gold **2.7**-d_1.

Table 2.2. Numbering scheme, yield, and analytical data for complexes **2.1 – 2.7.**

Complex	Cpd no.	Colour (yield[a], %)	Anal. found (calcd) C	H	N
Cp*W(NO)(η^2-CPh=CH_2)(CH_2SiMe_3)	**1**	burgundy, (72)	49.30 (48.98)	6.29 (6.17)	2.52 (2.60)
Cp*W(NO)(η^2-CPh=CH_2)(Cl)	**2.1**	burgundy, (74)	44.56 (44.53)	4.49 (4.56)	2.89 (2.87)
Cp*W(NO)(η^1-CPh=CH_2)(O_2CPh)	**2.2**	orange, (83)	51.87 (51.37)	4.78 (4.77)	2.60 (2.44)
Cp*W(NO)(η^2-CPh=CH_2)(OTf)	**2.3**	red (58)	37.94 (37..96)	3.70 (3.69)	2.30 (2.33)
[Cp*W(NO)(η^1-CPh=CH_2)($NCMe)_2$][OTf]	**2.4**	Brown (80)	[b]		
Cp*W(NO)(η^1-CPh=CH_2)(NH^{t}Bu)	**2.5**	brown (56)	[c]		
Cp*W(NO)(η^2-*C*HPhCH_2*N*($C_3H_5)_2$)(Cl)	**2.6**	brown (87)	49.43 (49.29)	5.95 (5.69)	4.80 (4.79)
Cp*W(NO)(η^1-CPh=CH_2)(H)(PPh_3)	**2.7**	gold (55)	60.68 (60.43)	5.49 (5.75)	2.00 (1.96)
Cp*W(NO)(η^1-CPh=CH_2)(D)(PPh_3)	**2.7-d_1**	gold (51)	[b]		

[a] Isolated yield unless otherwise noted. [b] Not determined. [c] Satisfactory analysis could not be obtained.

Table 2.3. Mass spectroscopic and IR spectral data for complexes **2.1 – 2.7.**

Compd no.	MS (m/z)[a]	probe temp[b] (°C)	IR (Nujol, cm^{-1})
1	540	180	1539 (ν_{NO})
2.1	489	150	1580 (ν_{NO})
2.2	576	120	1574 (ν_{NO}) 1501 (ν_{CO})
2.3	601	120	1609 (ν_{NO}) 1355 (ν_{SO}) 1237 (ν_{CF})
2.4	686		
2.5	524	200	1588 (ν_{NO})
2.6	548[c]	150	1581 (ν_{NO})
2.7	715	150	1824 (ν_{WH}) 1541 (ν_{NO})
2.7-d_1	716	150	1543 (ν_{NO}) 1318 (ν_{WD})

[a] Values for the highest intensity peak of the calculated isotopic cluster (^{184}W). [b] Probe temperatures. [c] FAB^+ mass spectrum.

Table 2.4. ^{1}H and ^{13}C NMR spectroscopic data for complexes **2.1** – **2.7**.

cmpd no.	^{1}H NMR[a] δ / ppm	^{13}C NMR[a] δ / ppm
1[b]	7.87 (dd, $^{3}J_{HH}$ = 8.0 Hz, $^{4}J_{HH}$ = 1.2 Hz, 2H, Ph-H_{ortho}) 7.29 (t, $^{3}J_{HH}$ = 8.0 Hz, 2H, Ph-H_{meta}) 7.11 (t, $^{3}J_{HH}$ = 8.0 Hz, 1H, Ph-H_{para}) 3.88 (dd, $^{2}J_{HH}$ = 5.4 Hz, $^{5}J_{HH}$ = 1.2 Hz, 1H, CPh=CH_aH$_b$) 3.56 (dd, $^{2}J_{HH}$ = 5.4 Hz, $^{5}J_{HH}$ = 1.2 Hz, 1H, CPh=CH$_a$$H_b$) 1.50 (s, 15H, C_5Me_5) 0.69 (d, $^{2}J_{HH}$ = 12.6 Hz, 1H, CH_aH$_b$SiMe$_3$) 0.59 (s, 9H, SiMe$_3$) 0.21 (d, $^{2}J_{HH}$ = 12.6 Hz, 1H, CH$_a$$H_b$SiMe$_3$)	227.9 (s, $^{1}J_{WC}$ = 99 Hz, *C*Ph=CH$_2$) 145.3 (s, Ph-C_{ipso}) 129.6 (d, $^{1}J_{CH}$ = 157 Hz, Ph) 128.8 (d, $^{1}J_{CH}$ = 157 Hz, Ph) 127.6 (d, $^{1}J_{CH}$ = 157 Hz, Ph) 109.6 (s, *C*$_5$Me$_5$) 83.1 (dd, $^{1}J_{CH}$ = 146 Hz, $^{2}J_{WC}$ = 13 Hz, CPh=*C*H$_2$) 35.5 (t, $^{1}J_{CH}$ = 111 Hz, *C*H$_2$SiMe$_3$) 9.5 (q, $^{1}J_{CH}$ = 127 Hz, C$_5$*Me*$_5$) 3.4 (q, $^{1}J_{CH}$ = 126 Hz, CH$_2$Si*Me*$_3$)
2.1	7.72 (dd, $^{3}J_{HH}$ = 6.0 Hz, $^{4}J_{HH}$ = 1.2 Hz, 2H, Ph-H_{ortho}) 7.22 (t, $^{3}J_{HH}$ = 6.0 Hz, 2H, Ph-H_{meta}) 7.13 (t, $^{3}J_{HH}$ = 6.0 Hz, 1H, Ph-H_{para}) 4.43 (dd, $^{2}J_{HH}$ = 6.0 Hz, $^{5}J_{HH}$ = 1.2 Hz, 1H, CPh=CH_aH$_b$) 4.25 (dd, $^{2}J_{HH}$ = 6.0 Hz, $^{5}J_{HH}$ = 1.2 Hz, 1H, CPh=CH$_a$$H_b$) 1.51 (s, 15H, C_5Me_5)	220.8 (*C*Ph=CH$_2$) 142.7 (Ph-C_{ipso}) 129.6, 128.8, 127.6 (Ph) 112.1 (*C*$_5$Me$_5$) 83.6 (dd, $^{1}J_{CH}$ = 151 Hz, CPh=*C*H$_2$) 9.5 (C$_5$*Me*$_5$)
2.2	8.07 (d, $^{3}J_{HH}$ = 7.5 Hz, 2H, Ph-H_{ortho}) 7.61 (d, $^{3}J_{HH}$ = 7.8 Hz, 2H, Ph-H_{meta}) 7.45 (vt, 4H, Ph-H_{meta}, -H_{ortho}) 7.24 (t, $^{3}J_{HH}$ = 6.2 Hz, 2H, Ph-H_{para}) 7.12 (t, $^{3}J_{HH}$ = 7.8 Hz, 1H, Ph-H_{para}) 6.40 (d, $^{2}J_{HH}$ = 2.1 Hz, 1H, CPh=CH_aH$_b$) 5.63 (d, $^{2}J_{HH}$ = 2.1 Hz, 1H, CPh=CH$_a$$H_b$) 1.84 (s, 15H, C_5Me_5)	189.5 (Ph*C*O$_2$) 179.7 (*C*Ph=CH$_2$) 151.5 (Ph-C_{ipso}) 133.8 130.1, 129.1, 128.4, 128.2, 127.3, 125.5 (Ar) 122.4 (CPh=*C*H$_2$) 113.3 (*C*$_5$Me$_5$) 9.5 (C$_5$*Me*$_5$)
2.3	7.59 (m, 2H, Ph) 7.49 (m, 3H, Ph) 4.99 (d, $^{2}J_{HH}$ = 8.7 Hz, $^{2}J_{WH}$ = 3.1 Hz, 1H, CPh=CH_aH$_b$) 4.90 (br d, $^{2}J_{HH}$ = 8.7 Hz, $^{2}J_{WH}$ = 7.8 Hz, 1H, CPh=CH$_a$$H_b$) 1.98 (s, 15H, C_5Me_5)	[c]258.0 (*C*Ph=CH$_2$) 140.5 (Ph-C_{ipso}) 129.1 (Ph-C_{ortho}) 128.1, (Ph-C_{mta}) 125.3 (Ph-C_{para}) 119.1 (q, $^{1}J_{CF}$ = 315 Hz, CF_3) 112.8 (*C*$_5$Me$_5$) 77.6 (br t, $^{1}J_{CH}$ = 164 Hz, CPh=*C*H$_2$) 9.6 (q, $^{1}J_{CH}$ = 126 Hz, CH$_2$Si*Me*$_3$)

Table 2.4 continued.

cmpd no.	^{1}H NMR[a] δ / ppm	^{13}C NMR[a] δ / ppm
2.4[d]	7.28 (m, 2H, Ph-H_{meta}) 7.11 (m, 1H, Ph-H_{para}) 7.13 (d, $^3J_{HH}$ = 7.6 Hz, 1H, Ph-H_{ortho}) 6.38 (d, $^2J_{HH}$ = 2.3 Hz, 1H, CPh=C$H_a$$H_b$) 5.36 (d, $^2J_{HH}$ = 2.3 Hz, 1H, CPh=C$H_a$$H_b$) 2.05 (s, 15H, C_5Me_5) 1.96 (s, 6H, MeCN)	171.6 (*C*Ph=CH_2) 141.7 (Ph-C_{ipso}) 129.5 (Ph) 129.2 (Ph) 128.4 (Ph) 124.6 (CPh=*C*H_2) 115.2 (C_5Me_5) 11.2 (C_5Me_5)
2.5	7.77 (br, 1H, NH) 7.25 (m, 4H, Ph) 7.07 (m, 1H, Ph-H_{para}) 6.21 (d, $^2J_{HH}$ = 3.0 Hz, 1H, CPh=C$H_a$$H_b$) 5.51 (d, $^2J_{HH}$ = 3.0 Hz, 1H, CPh=C$H_a$$H_b$) 1.80 (s, 15H, C_5Me_5) 1.39 (s, 9H, ^{t}Bu)	[e]185.1 (*C*Ph=CH_2) 150.1 (Ph-C_{ipso}) 128.2 (Ph-C_{ortho}) 127.7 (Ph-C_{imeta}) 126.3 (CPh=*C*H_2) 125.6 (Ph-C_{para}) 111.6 (s, C_5Me_5) 33.4 (HNC*Me*$_3$) 29.7 (HN*C*Me$_3$) 10.0 (C_5Me_5)
2.6	7.69 (d, $^3J_{HH}$ = 7.8 Hz, 2H, Ar-H_{ortho},) 7.29 (t, $^3J_{HH}$ = 7.8 Hz, $^3J_{HH}$ = 7.8 Hz, 2H, Ar-H_{meta}) 7.03 (t, $^3J_{HH}$ = 7.8 Hz, 1H, Ar-H_{para}) 6.53 (m, 1H, NCH_2CH=CH_2) 5.70 (m, 1H, NCH_2CH=CH_2) 5.17 (d, $^3J_{HH}$ = 10.2 Hz, 1H, NCH_2CH=CH_2) 4.90 (m, 3H, NCH_2CH=CH_2, WCHPhCH_2) 4.29 (t, $^3J_{HH}$ = 12 Hz, 1H, WC*H*PhCH_2) 4.07 (m, 2H, NCH_2CH=CH_2) 3.26 (m, 1H, NCH_2CH=CH_2) 3.00 (m, 1H, NCH_2CH=CH_2) 2.74 (m, 1H, NCH_2CH=CH_2) 2.48 (m, 1H, NCH_2CH=CH_2) 1.59 (s, 15H, C_5Me_5)	148.7 (Ph-C_{ipso}) 133.6 (NCH_2*C*H=CH_2) 131.5 (Ph-C_{ortho}) 131.1 (NCH_2*C*H=CH_2) 128.3 (Ph-C_{meta}) 125.2 (Ph-C_{para}) 121.6 (NCH_2CH=*C*H_2) 120.8 (NCH_2CH=*C*H_2) 111.3 (C_5Me_5) 64.6 (W*C*HPhCH_2) 61.0 (N*C*H_2CH=CH_2) 60.8 (N*C*H_2CH=CH_2) 38.9 (WCHPh*C*H_2) 10.1 (C_5Me_5)

Table 2.4 continued.

cmpd no.	^{1}H NMR[a] δ / ppm	^{13}C NMR[a] δ / ppm
2.7[b]	7.72 (br t, $^3J_{HH}$ = 6.8 Hz, 6H, PPh_3) 7.43 (d, $^3J_{HH}$ = 7.2 Hz, 2H, Ph-H_{meta}) 7.34 (t, $^3J_{HH}$ = 7.5 Hz, 2H, Ph-H_{para}) 7.08 (t, $^3J_{HH}$ = 7.5 Hz, 1H, Ph-H_{para}) 6.98 (m, 9H, PPh_3) 6.31 (d, $^2J_{HH}$ = 3.0 Hz, 1H, CPh=CH_aH$_b$) 4.81 (d, $^2J_{HH}$ = 3.0 Hz, 1H, CPh=CH$_a$$H_b$) 1.71 (s, 15H, C_5Me_5) 1.04 (d, $^2J_{PH}$ = 96.1 Hz, WH)	177.1 (d, $^2J_{PC}$ = 21.8 Hz, *C*Ph=CH_2) 152.9 (Ph-C_{ipso}) 137.2 (d, $^1J_{PC}$ = 66.0 Hz, Ph-C_{ipso}) 134.5, 134.2, 129.6, 129.3, 128.8, 128.2 (Ar) 125.3 (CPh=*C*H$_2$) 106.7 (*C*$_5$Me$_5$) 10.5 (C$_5$*Me*$_5$)
2.7-d_1[b,f]	7.72 (br t, $^3J_{HH}$ = 6.8 Hz, 6H, PPh_3) 7.43 (d, $^3J_{HH}$ = 7.2 Hz, 2H, Ph-H_{meta}) 7.34 (t, $^3J_{HH}$ = 7.5 Hz, 2H, Ph-H_{para}) 7.08 (t, $^3J_{HH}$ = 7.5 Hz, 1H, Ph-H_{para}) 6.98 (m, 9H, PPh_3) 6.31 (d, $^2J_{HH}$ = 3.0 Hz, 1H, CPh=CH_aH$_b$) 4.81 (d, $^2J_{HH}$ = 3.0 Hz, 1H, CPh=CH$_a$$H_b$) 1.71 (s, 15H, C_5Me_5)	[g]

[a] ^{1}H NMR spectra recorded in $CDCl_3$ at RT unless otherwise noted, and ^{13}C NMR spectra recorded in $CDCl_3$ at RT unless otherwise noted. [b] ^{1}H and ^{13}C spectra recorded in C_6D_6. [c] Spectrum recorded at -70 °C in CD_2Cl_2 solvent. [d] ^{1}H and ^{13}C NMR spectra recorded in CD_3CN. [e] Spectrum recorded in acetone-d_6. [f] ^{31}P NMR spectrum (ref. $P(OMe)_3$): 27.1 ppm, d, $^2J_{HP}$ = 92.8 Hz. [g] not recorded.

2.5 Notes and References

(1) Debad, J. D.; Legzdins, P.; Lumb, S. A.; Batchelor, R. J.; Einstein, F. W. B. *J. Am. Chem. Soc.* **1995**, *117*, 3288.

(2) Crystals of **1** are triclinic of space group P*1*; Z = 2, V = 1162.0(2) Å^3, *a* = 8.4119(7) Å, *b* = 8.9053(9) Å, *c* = 16.717(2) Å, α = 89.106(4)°, β = 87.394(2)°, γ = 68.2654(9)°. Dr. S. J. Rettig solved the structure using the Patterson method and full-matrix least-squares refinement procedures to $R_F = 0.030$ for 4320 reflections with $I_o \geq 2.5\sigma(I_o)$. Tables of fractional atomic coordinates (Table A1), bond distances (Table A2) and bond angles (Table A3) in the solid-state structure determined for this compound are found in Appendix A.

(3) (a) Allen, S. R.; Beevor, R. G.; Green, M.; Norman, N. C.; Orpen, A. G.; Williams, I. D. *J. Chem. Soc., Dalton Trans.* **1985**, 435. (b) Morrow, J. R.; Tonker, T. L.; Templeton, J. L. *J. Am. Chem. Soc.* **1985**, *107, 6956*. (c) Feng, S. G.; Gamble, A. S.; Templeton, J. L. *Organometallics* **1989**, *8*, 2024. (d) Carfagna, C.; Carr, N.; Deeth, R. J.; Dossett, S. J.; Green, M.; Mahon, M. F.; Vaughan, C. *J. Chem. Soc., Dalton Trans.* **1996**, 415.

(4) Nugent, W. A.; Mayer, J. M. *Metal-Ligand Multiple Bonds*; John Wiley and Sons: New York, 1988.

(5) (a) Debad, J. D.; Legzdins, P.; Batchelor, R. J.; Einstein, F. W. B. *Organometallics* **1992**, *11*, 8. (b) Dryden, N. H.; Legzdins, P.; Rettig, S. J.; Veltheer, J. E. *Organometallics*

1992, *11*, 2583. (c) Debad, J. D.; Legzdins, P.; Batchelor, R. J.; Einstein, W. B. *Organometallics* **1993**, *12*, 2094.

(6) (a) van der Zeijden, A. A.; Bosch, H. W.; Berke, H. *Organometallics* **1992**, *11*, 563.

(7) (a) Rusik, C. A.; Collins, M. A.; Gamble, A. S.; Tonker, T. L.; Templeton, J. L. *J. Am. Chem. Soc.* **1989**, *111*, 2550. (b) Feng, S. G.; White, P. S.; Templeton, J. L. *Organometallics* **1993**, *12*, 2131.

(8) (a) Legzdins, P.; Rettig, S. J.; Sanchez, L. *Organometallics* **1988**, *7*, 2394. (b) reference 5c.

(9) Feng, S. G.; Templeton, J. L. *Organometallics* **1992**, *11*, 2168.

(10) (a) Legzdins, P.; Rettig, S. J.; Sánchez, L. J.; Bursten, B. E.; Gatter, M. G. *J. Am. Chem. Soc.* **1985**, *107*, 1411. (b) Bursten, B. E.; Cayton, R. H. *Organometallics* **1985**, *6*, 2004.

(11) Legzdins, P. Veltheer, J. E. *Acc. Chem. Res.* **1993**, *26*, 41.

(12) (a) Kuzelka, J.; Legzdins, P.; Rettig, S. J.; Smith, K. M. *Organometallics* **1997**, *16*, 3570. (b) Burkey, D. J.; Debad, J. D.; Legzdins, P. *J. Am. Chem. Soc.* **1997**, *119*, 1139. (c) Legzdins, P.; Lumb, S. A.; Young, V. G. *Organometallics* **1998**, *17*, 854. (d) Debad, J. D.; Legzdins, P.; Lumb. S. A. *Organometallics* **1995**, *14*, 2543. (e) Legzdins, P.; Rettig, S. J.; Sanchez, L. *Organometallics* **1988**, *7*, 2394.

(13) Crystals of **2.1** are triclinic of space group P*1*; Z = 2, V = 890.6(2) $Å^3$, a = 9.212(1) Å, b = 14.235(2) Å, c = 7.3792(8) Å, $\alpha = 95.72(1)°$, $\beta = 107.674(8)°$, $\gamma = 101.38(1)°$. Dr. S. J. Rettig solved the structure using the Patterson method and full-matrix least-squares refinement procedures to $R_F = 0.032$ for 4857 reflections with $I_o \geq 3\sigma(I_o)$. Tables of

fractional atomic coordinates (Table A4), bond distances (Table A5) and bond angles (Table A6) in the solid-state structure determined for this compound are found in Appendix A.

(14) Smith, K. M. Ph.D. Thesis, The University of Bristish Columbia, 1998.

(15) (a) Debad, J. D.; Legzdins, P.; Rettig, S. J.; Veltheer, J. E. *Organometallics* **1993**, *12*, 2714. (b) Legzdins, P.; Nurse, C. R. Inorg. Chem. **1982**, *21*, 3110. (c) Chin, T. T.; Legzdins, P.; Trotter, J.; Yee, V. C. *Organometallics* **1992**, *11*, 913. (d) Legzdins, P.; Rettig, S. J.; Sayers, S. F. *J. Am. Chem. Soc.* **1994**, *116*, 12105. (e) Dryden, N. H.; Legzdins, P.; Sayers, S. F.; Trotter, J.; Yee, V. C. *Can. J. Chem.* **1995**, *73*, 1035. (f) McCleverty, J. A.; Murray, A. J. *Trans. Met. Chem.* **1979**, *4*, 273.

(16) (a) Legzdins, P.; Martin, D. T. *Organometallics* **1983**, *2*, 1785. (b) Legzdins, P.; Richter-Addo, G. B.; Einstein, F. W. B.; Jones, R. H. *Organometallics* **1990**, *9*, 431. (c) Legzdins, P.; McNeil, W. S.; Vessey, E. G.; Batchelor, R. J.; Einstein, F. W. B. *Organometallics* **1992**, *11*, 2718.

(17) Crystals of **2.2** are orthorhombic of space group P_{cab}; a = 13.650(2) Å, b = 15.227(2) Å, c = 21.976(3) Å. Drs. R. J. Batchelor and F. W. B. Einstein solved the structure using the Patterson method and full-matrix least-squares refinement procedures to $R_F = 0.025$ for 1778 reflections with $I_o \geq 2.5\sigma(I_o)$. Tables of fractional atomic coordinates (Table A7), bond distances (Table A8) and bond angles (Table A9) in the solid-state structure determined for this compound are found in Appendix A.

(18) (a) Lawrance, G. A. *Chem. Rev.* **1986**, *86*, 17. (b) Otieno, T.; Rettig, S. J.; Thompson, R. J.; Trotter, J. *Can. J. Chem.* **1990**, *68*, 1901.

(19) Richter-Addo, G. B.; Legzdins, P. *Metal Nitrosyls*; Oxford University Press: New York, 1992.

(20) See: Legzdins, P.; Rettig, S. J.; Ross, K. J. *Organometallics* **1993**, *12*, 2103, and references cited therein.

(21) Crystals of **2.6** are monoclinic of space group C_2/c; a = 29.017(4) Å, b = 8.435(2) Å, c = 19.812(5) Å, β = 93.58(2)°. Dr. S. J. Rettig solved the structure using the Patterson method and full-matrix least-squares refinement procedures to $R_F = 0.033$ for 2815 reflections with $I_o \geq 3\sigma(I_o)$. Tables of fractional atomic coordinates (Table A10), bond distances (Table A11) and bond angles (Table A12) in the solid-state structure determined for this compound are found in Appendix A.

(22) For another example of a W nitrosyl complex containing both a W-N dative bond and C-N single bond, see: Debad, J. D.; Legzdins, P.; Lumb, S. A.; Batchelor, R. J.; Einstein, F. W. B. *Organometallics* **1995**, *14*, 2587.

(23) See, for example: Debad, J. D.; Legzdins, P.; Rettig, S. J.; Veltheer, J. E. *Organometallics* **1993**, *12*, 2714.

(24) Huggins, J. M.; Bergman, R. G. *J. Am. Chem. Soc.* **1979**, *101*, 4410.

(25) Legzdins, P.; Martin, J. T.; Einstein, F. W. B.; Jones, R. H. *Organometallics* **1987**, *6*, 1826.

(26) Debad, J. D.; Legzdins, P.; Lumb, S. A.; Batchelor, R. J.; Einstein, F. W. B. *Organometallics* **1995**, *14*, 2543.

(27) Martin, J. T., Ph.D. Thesis, The University of British Columbia, 1987.

(28) This calculation is based upon the assumption that the ground-state vibrational frequency of an X-H bond will have a frequency $\nu = 1/2\pi\bullet(k'/\mu)^{1/2}$, based on the simple harmonic oscillator model, where k' is the force constant and μ = reduced mass = $m_X m_H/(m_X+m_H)$. If $m_X >> m_H$, then $\mu \approx m_H$. Making the same argument for an X-D bond, and assuming that $\mu_H \approx m_H$, $\mu_D \approx m_D$, and $k'_H \approx k'_D$, then $\nu_H/\nu_D = (m_D/m_H)^{1/2} = 2^{1/2}$. For a more detailed analysis of isotope effects, see: Connors, K.A. *Chemical Kinetics*; VCH Publishers: New York, 1990.

(29) Crystals of **2. 7** are monoclinic of space group $P2_1/n$; a = 26.039(1) Å, b = 8.902(2) Å, c = 29.973(1) Å. Dr. S. J. Rettig solved the structure using the Patterson method and full-matrix least-squares refinement procedures to $R_F = 0.048$ for 4241 reflections with $I_o \geq 3\sigma(I_o)$. Minor disorder is evident in the vinyl ligand, however, Dr. Rettig has made no attempt to model or resolve it. Tables of fractional atomic coordinates (Table A13), bond distances (Table A14) and bond angles (Table A15) in the solid-state structure determined for this compound are found in Appendix A.

(30) (a) Dryden, N. H.; Legzdins, P.; Trotter, J. Yee, V. C. *Organometallics* **1991**, *10*, 2857. (b) Dryden, N. H.; Legzdins, P.; Lundmark, P. J. *Organometallics* **1993**, *12*, 2085. (c) Debad, J. D.; Legzdins, P.; Batchelor, R. J.; Einstein, F. W. B. *Organometallics* **1993**, *12*, 2094.

(31) Orpen, A. G.; Brammer, L.; Allen, F. H.; Kennard, O.; Watson, D. G.; Taylor, R. *J. Chem. Soc., Dalton Trans.* **1989**, S1.

(32) Quest search program utilized for searching the Cambridge Structural Database.

(33) (a) Case **I**: Wu, I.-Y.; Cheng, M.-C.; Lin, Y.-C.; Wang, Y. *Organometallics* **1993**, *12*, 1686. (b) Case **II**: Mayr, A.; Asaro, M. A.; Glines, T. J.; Van Engen, D.; Tripp, G. M. *J. Am. Chem. Soc.* **1993**, *115*, 8187. (c) Case **III**: Morrow, J. R.; Tonker, T. L.; Templeton, J. L. *J. Am. Chem. Soc.* **1985**, *107*, 5004. (d) Case **IV**: Chisholm, M. H.; Eichorn, B. W.; Huffman, J. C. *Organometallics* **1989**, *8*, 67.

(34) See, for example: Ipaktschi, J.; Mirzaei, F.; Demuth-Eberle, G. J.; Beck, J.; Serafin, M. *Organometallics* **1997**, *16*, 3965.

(35) For recent surveys of this chemistry, see: (a) Bochmann, M. *J. Chem. Soc., Dalton Trans.* **1996**, 255. (b) Brintzinger, H. H.; Fischer, D.; Mulhaupt, R.; Rieger, B.; Waymouth, R. M. *Angew. Chem., Int. Ed. Engl.* **1995**, *34*, 1143.

(36) Shriver, D. F.; Drezdzon, M. A. *The Manipulation of Air-Sensitive Compounds*, 2nd ed.; Wiley-Interscience: New York, 1986.

(37) Dryden, N. H.; Legzdins, P.; Rettig, S. J.; Veltheer, J. E. *Organometallics* **1992**, *11*, 2583.

(38) Dryden, N. H.; Legzdins, P.; Batchelor, R. J.; Einstein, F. W. B. *Organometallics* **1991**, *10*, 2077.

(39) Debad, J. D., Ph.D. Thesis, The University of British Columbia, 1994.

Chapter 3. Trapping of Thermally-generated $Cp^*W(NO)(\eta^2\text{-}PhC{\equiv}CH)$ in Coupling Reactions with Organic Substrates

3.1 Introduction

Of fundamental importance to synthetic chemistry is the bond-forming process involving the coupling of two unsaturated substrates. That a transition metal environment possesses the ability to act as a template for such bond formation represents one of the most significant applications of modern organotransition metal chemistry to synthesis.[1] Since the first report of Ni-induced alkyne cyclotrimerization and cyclotetramerization (eq 3.1),[2] transition-metal-induced coupling of unsaturated organic substrates has provided access to a wealth of polyfunctional cyclic hydrocarbons and heterocycles.[3]

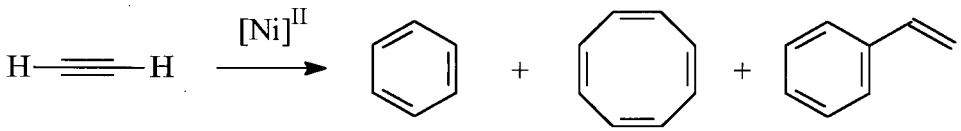

(eq 3.1)

Coupling is typically mediated by transition metal complexes containing a coordinatively-unsaturated, low-valent (electron-rich) metal centre, the former characteristic being prerequisite for the initial coordination of unsaturated substrate while the latter is required for the activation of the coordinated substrate towards coupling. Such low-valent, "naked" complexes of the early transition metals tend to be very unstable and must be generated *in situ* from higher-valent precursors. A particularly versatile method towards this end involves the reductive elimination of hydrocarbon from a parent hydrocarbyl complex (Scheme 3.1). Because one of the two unsaturated ligands involved in the coupling process is generated intramolecularly in the initial reductive elimination step, the presence of a *different* unsaturated substrate in the reaction mixture affords access to novel products of cross-coupling. Further variation can be introduced into the overall reaction by modifying the substituents R′ and E in the parent hydrocarbyl complex. The regiochemistry of such coupling reactions leading to a particular

distribution of products (as depicted in Scheme 3.1) depends upon the electronic characteristics of the unsaturated substrates employed in this reaction.

Scheme 3.1

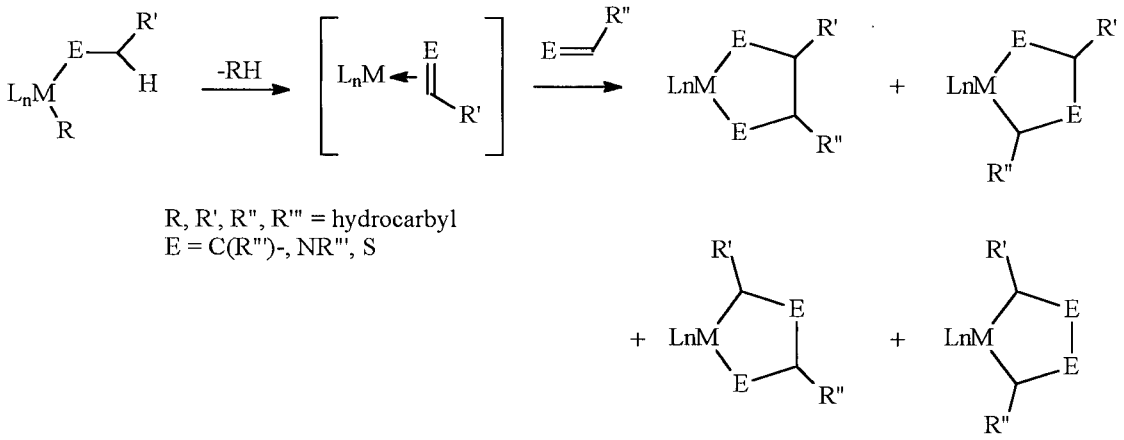

While current interest in this area spans a number of groups and ligand sets, its foundation is set in the chemistry developed for the Group 4 metallocenes.[3b,d] Initial reports by Erker's group described the thermal elimination of benzene from Cp_2ZrPh_2 and proposed the formation of a transient benzyne complex that is capable of coupling to olefins and acetylenes, yielding a plethora of functionalized aromatic zirconacycles (e.g. eq 3.2).[4]

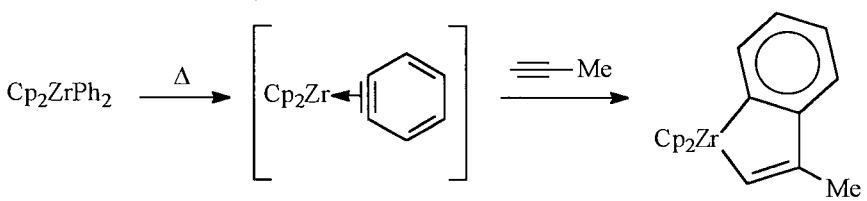

(eq 3.2)

Buchwald *et al.* subsequently characterized the phosphine-trapped benzyne complex in the solid state by X-ray diffraction methods and then extended the reactivity to heteroatom-containing substrates.[5] This method was then generalized so that a variety of alkyne complexes could be

obtained through β-H reductive elimination of methane from the appropriate methyl alkenyl precursor (e.g. eq 3.3).[6] The development of this particular methodology dramatically expanded the range of cyclic and heterocyclic compounds made accessible to the synthetic chemist.

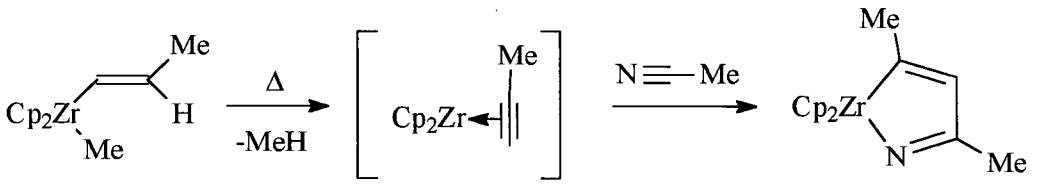

(eq 3.3)

In a communication describing the double C-H activation of *n*-pentane and *n*-hexane, Legzdins *et al.* proposed the formation of the η^2-acetylene-containing complex Cp*W(NO)(η^2-PhC≡CH) (**A**) by an analogous reductive elimination of $SiMe_4$ from Cp*W(NO)(CH_2SiMe_3)(η^2-$CPh=CH_2$) (**1**) under thermolysis conditions in the appropriate hydrocarbon solution (eq 1.1).[7] The similarity of **A** to the benzyne complex of Erker and Buchwald has prompted an investigation into the thermolytic chemistry of **1** in the presence of such unsaturated, heteroatom-containing substrates as esters and nitriles. The collection of nitrosyl-containing metallacycles that can be generated under these conditions lends considerable support to the proposal for the intermediacy of the acetylene-containing intermediate **A**. In this chapter, the full details of this study are presented, which include X-ray diffraction and NMR spectroscopic studies of the metallacycles generated under thermolysis conditions, a kinetic analysis of representative reactions, and mechanistic evidence and molecular orbital proposals to account for the chemistry observed.

3.2 Results and Discussion

The thermolysis of $Cp^*W(NO)(CH_2SiMe_3)(\eta^2\text{-}CPh{=}CH_2)$ (**1**) in the presence of several substituted esters and nitriles under differing experimental conditions affords the complexes depicted in Scheme 3.2. Each reaction portrayed is considered in turn in the following Sections. The numbering scheme for the new compounds isolated during this investigation is also indicated in Scheme 3.2, and their respective yields and analytical data are collected in Table 3.4 at the end of Section 3.4. Mass and IR spectroscopic data are presented in Table 3.5, and ^1H and ^{13}C NMR data are summarized in Table 3.6.

Scheme 3.2

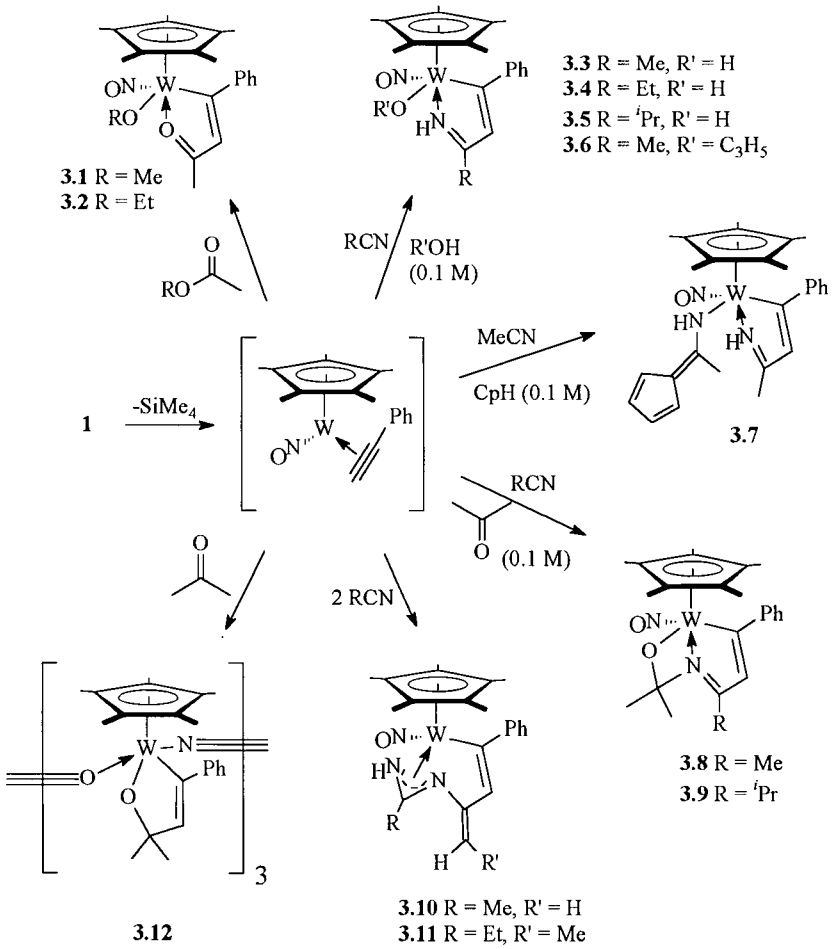

3.2.1 Coupling of Esters: Acyl C-O Bond Cleavage

Thermolysis of the red tungsten vinyl complex **1** at 45 °C in the presence of esters such as methyl or ethyl acetate affords the oxametallacyclopentadienyl complexes Cp*W(NO)(OMe)(η^2-*O*=C(Me)CH=*C*Ph) (**3.1**) and Cp*W(NO)(OEt)(η^2-*O*=C(Me)CH=*C*Ph) (**3.2**), respectively, in high yield and purity (eq 3.4).

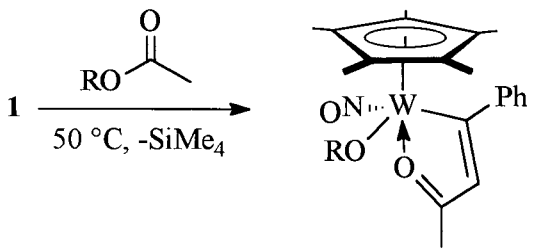

(eq 3.4)

3.1 R = Me
3.2 R = Et

These four-legged, piano-stool complexes are burgundy crystalline solids that are air-stable at ambient temperatures for periods up to a week. The Nujol-mull IR bands attributable to the NO stretch in **3.1** and **3.2** are located at 1532 and 1538 cm^{-1}, typical of 18-valence-electron (18e) alkoxide-containing complexes (Table 3.4).[8] Vibrational bands attributable to the acyl C-O moiety in these complexes are apparent as shoulders on the Nujol band located at 1460 cm^{-1}. The ^1H and ^{13}C NMR signals displayed by complexes **3.1** and **3.2** (Table 3.5) are readily assigned. For example, the resonances of the acyl methyl substituents in the ^1H NMR spectra are singlets that integrate for 3 protons at 2.32 and 2.44 ppm for **3.1** and **3.2**, respectively, and the signals for the analogous carbon nuclei are identifiable in the ^{13}C NMR spectra at about 26 ppm for both complexes. Likewise, the vinyl proton resonance is evident as a singlet at 7.18 ppm for complex **3.1** and 7.37 ppm for complex **3.2**. The assignment of the carbon backbone containing

the PhC=CH unit in these complexes is deduced from the combination of the gate-decoupled ^{13}C NMR results and from HMBC experiments.

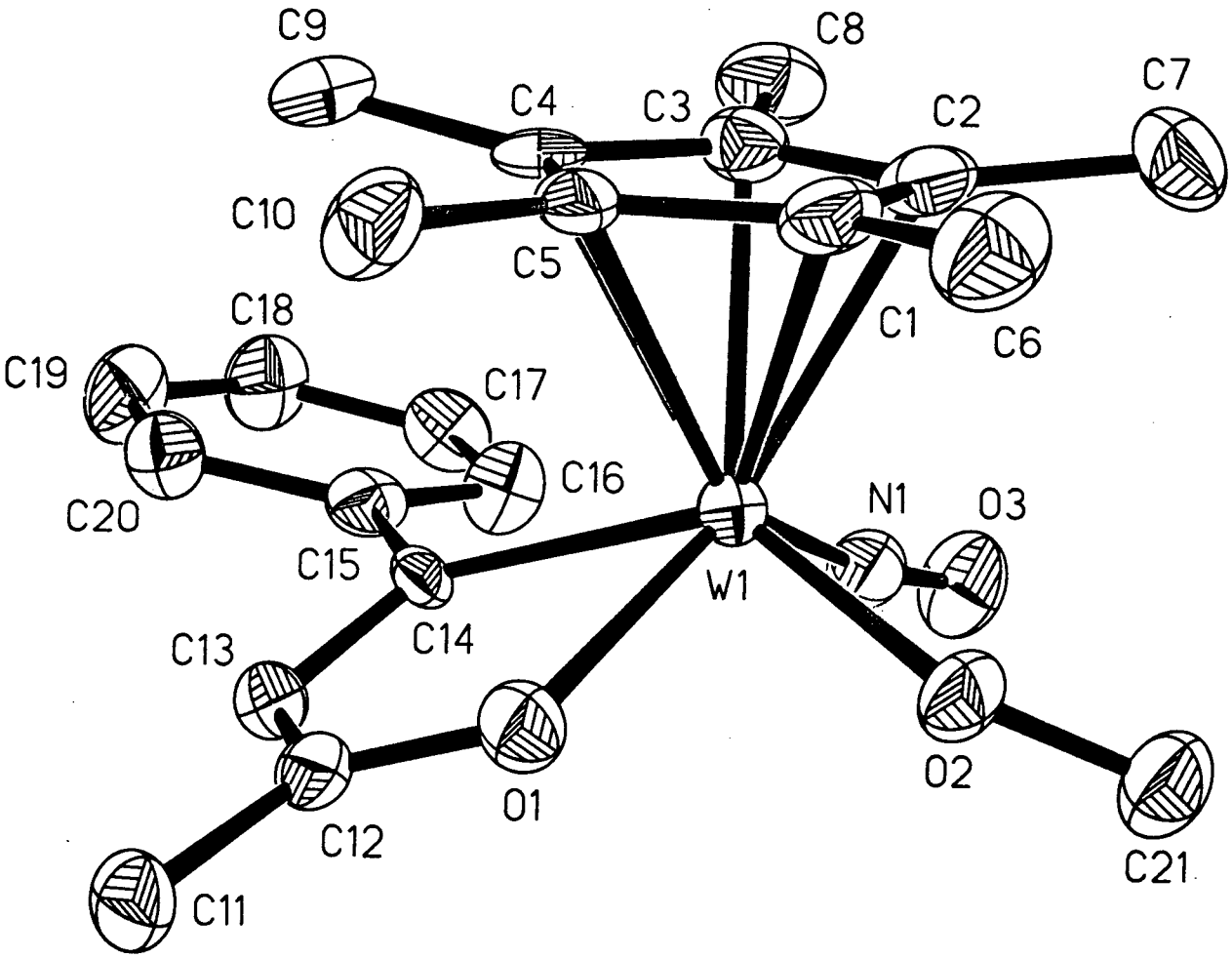

Figure 3.1. ORTEP plot of compound **3.1** with thermal ellipsoids depicting the 50% probability level.

The four-legged piano-stool arrangement of ligands in the solid-state molecular structure of **3.1** has been definitively established by an X-ray crystallographic analysis (Figure 3.1).[9] Of particular note is the existence of the tungsten-bound methoxy group (W-O bond length of 2.001(7) Å) that confirms that a C-O bond-cleavage process has occurred to afford the observed 18e products. The σ-bound methoxy and alkyl ligands are *trans*-disposed in the metal's coordination sphere, and the acyl function is coordinated in a cis fashion to both σ-ligands with a W-O dative bond length of 2.203(6) Å. Interestingly, this distance is shorter than the 2.535(7) Å Ni-O dative bond length in the late-metal complex $Ni(PMe_3)_2(Cl)(\eta^2\text{-}O{=}C(CH_2SiMe_3)C{=}CPh)$[10] as well as the 2.361(3) Å Zr-O bond length previously reported by Rosenthal and coworkers for related zirconacyclic complexes.[11] The C=O bond length of 1.277(12) Å is longer than a typical C-O double bond and is characteristic of a coordinated acyl function.[12] The oxametallacyclopentadiene ring is clearly evident from the short-long-short pattern of bond lengths for the O(1)=C(12)-C(13)=C(14) fragment (1.277(12) Å, 1.413(14) Å, and 1.337(12) Å, respectively), comparable to those found in the structure of the above-mentioned Ni (II) complex.

The mechanism that we propose for the overall process leading to **3.1** and **3.2** is depicted in Scheme 3.3. Intermediate **B,** formed by coordination of ester to W in **A**, is transformed into the oxametallacyclopentene **C** by the coupling of the two coordinated ligands. While the analogous Cp_2Zr oxametallacyclopentene complexes are readily isolable and have been studied extensively,[3b,d] the Cp*W(NO)-containing intermediate **C** cannot be isolated as such. Indeed, the metal-bound acetal O in 16e **C** has the capacity to function as a 3e donor to the metal centre in the correct orientation,[13] rendering the complex electronically saturated. However, the restrictive geometry of the five-membered ring enforces a conformation that leaves the filled O-centred orbitals pointed away from the metal. The O atom thus functions predominantly as a 1e donor, resulting in a build-up of electron density at the heteroatom and leaving the metal centre in **C** electronically unsaturated. Subsequent acetal C-O-bond cleavage yields the observed 18e complexes.

Scheme 3.3

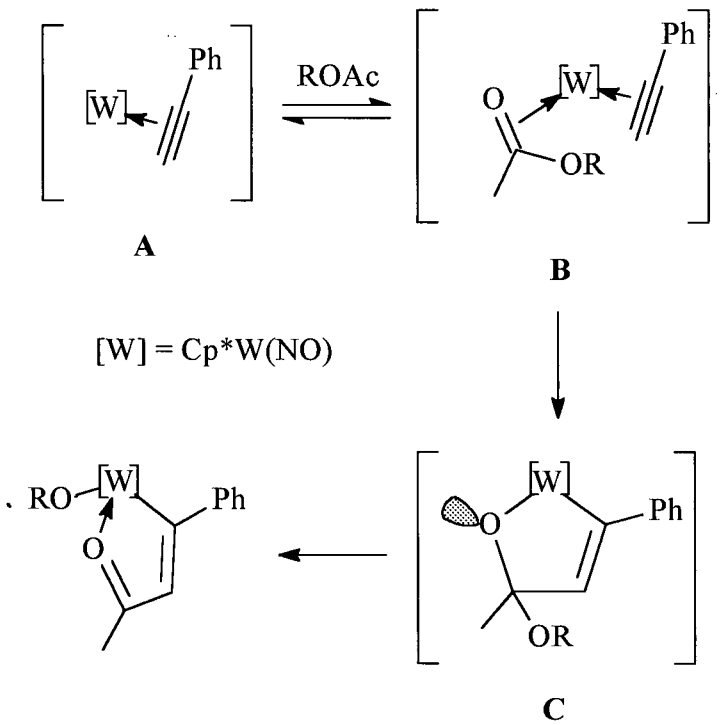

Only one of two possible routes to the observed products is presented in Scheme 3.3. An alternate path involving direct acyl C-O oxidative addition to the metal centre in **A** followed by acyl/acetylene coupling is conceivable, yet such examples involving alkyl carboxylate esters are rare and reports of this mode of reactivity seem limited to low-valent, late transition-metal systems. [14] On the other hand, coordination of ester is a prerequisite to coupling, and the recent observation of η^2-ester coordination in the related $Cp^*W(NO)(PPh_3)$ fragment[15] supports a pathway involving the intermediacy of **B**.

Acetal β-C-O bond cleavage by a TM complex is an area of considerable current interest, probably the most well-known example being the Kulinkovich reaction which generates

cyclopropanols enantioselectively following coupling of coordinated olefin and ester at Ti(II) centres (Scheme 3.4).[16]

Scheme 3.4

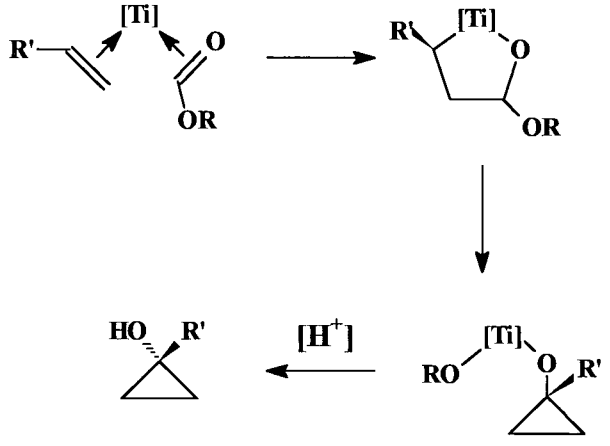

While the coupling leading to complexes **3.1** and **3.2** is reminiscent of the Kulinkovich reaction, the products of the two reactions are quite different. Displacement of RO^- in the putative acetal intermediate **C** (Scheme 3.3) via attack by the quaternary vinyl C at the electrophilic acetal carbon centre to give the O-bound cyclopropenyl ligand does not occur (in a manner analogous to that depicted in Scheme 3.4). That this is so presumably arises as a result of both the reduced oxophilicity of W(II) relative to Ti and the greater ring strain in cyclopropene relative to cyclopropane.[17]

In support of the mechanism depicted in Scheme 3.3, other examples of acetal β-C-O bond cleavage have been described in the literature. Yamamoto *et al.* have reported the generation of acetal complexes by the addition of a M-H bond [M = Rh,[18a] Co[18b]] across the carbonyl function of coordinated ester and subsequent β-C-O bond cleavage to produce the analogous aldehydes (eq 3.5).

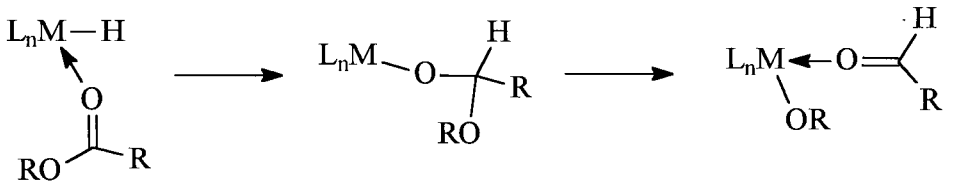

(eq 3.5)

M = Rh, Co

Grotjahn and coworkers have recently invoked acetal C-O bond cleavage to account for the thermal generation of an alkoxycarbene complex from a CpRu acetal complex.[19] Given these literature precedents, the pathway outlined in Scheme 3.3 appears to be the most reasonable. While numerous examples of ester coupling to olefin exist, the coupling of an ester to an acetylene in the coordination sphere of a metal appears to be unprecedented. Because the overall transformation involves the formal exchange of vinyl for alkoxide at the acyl carbon of the ester fragment, this reaction can be viewed as the conversion of a carboxylate ester to an α,β-unsaturated ketone via C-O bond cleavage.[10,20]

3.2.2 Coupling With Nitriles

Simple coupling of acetylene and coordinated nitrile in the tungsten's coordination sphere does not yield the expected azametallacycle, Cp*W(NO)(η^2-*N*=C(R)CH=*C*Ph), subsequent to the generation of the acetylene intermediate **A** in nitrile solvent. Instead, similar to the thermolysis of **1** in esters, the products are obtained from the resultant reactivity of an intermediate metallacyclic complex derived via coupling. Unlike the acetal intermediate **C**, however, this intermediate complex does not achieve electronic saturation by rearranging in an intramolecular fashion. Rather, intermolecular trapping of this intermediate by a variety of electrophilic sources can be effected.

3.2.2.1 Trapping by Protic Sources

The thermolysis of **1** in nitrile solvent containing 0.1 - 0.01 M H_2O or allyl alcohol affords complexes **3.3** – **3.6** quantitatively (eq 3.6).

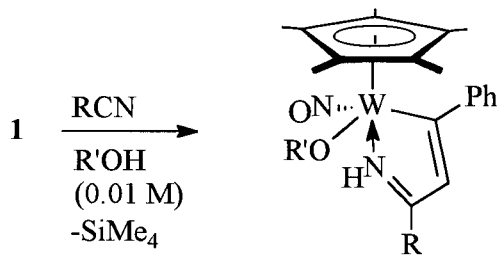

3.3 R = Me, R' = H
3.4 R = Et, R' = H
3.5 R = ^{i}Pr, R' = H
3.6 R = Me, R' = C_3H_5 (eq 3.6)

These products are orange-red crystalline solids that are air-stable for periods of up to two weeks at ambient temperatures, thereby attesting to the existence of an 18e, closed-shell configuration at the metal centre. The solid-state molecular structure of prototypal complex **3.3** is shown in Figure 3.2.[21] Analogous to the structure of complex **3.1**, imine N coordination to W diagonal to the NO ligand in these four-legged piano-stool complexes confers electronic saturation at the metal centre. Although the hydroxyl H was not located during the structure refinement, the W-O bond length of 2.064(2) Å is characteristic of a tungsten-oxygen single bond.[22] In addition, the W-N and N-C bonding distances are 2.150(3) Å and 1.295(5) Å, respectively. Thus, protonation at the coordinated imine must be invoked to support the hybridization at N and to preserve the electroneutrality of the complex.

The structural components highlighted in the preceding paragraph are also evident in the spectroscopic data for complexes **3.3** – **3.6** (Table 3.5). For example, signals for both the N-H and O-H protons are apparent in the ^{1}H NMR spectra ($CDCl_3$) of complexes **3.3** – **3.6,** the former appearing at approximately 8.65 ± 1.0 ppm and the latter in the range 0.84 ± 0.2 ppm. In addition, the singlet attributable to the vinyl H in all cases appears at about 7.1 ppm ($^1J_{CH} \approx 157$ Hz). Signals in the $^{13}C\{^1H\}$ NMR spectrum at about 228 ppm and 189 ± 7 ppm divulge the

presence of the carbenoid C_α atom of the vinyl moiety and the quaternary imine carbon, respectively. The downfield shift of the resonance due to the carbenoid C_α atom suggests a degree of electronic delocalization in the azametallacyclopentadienyl ring.[23]

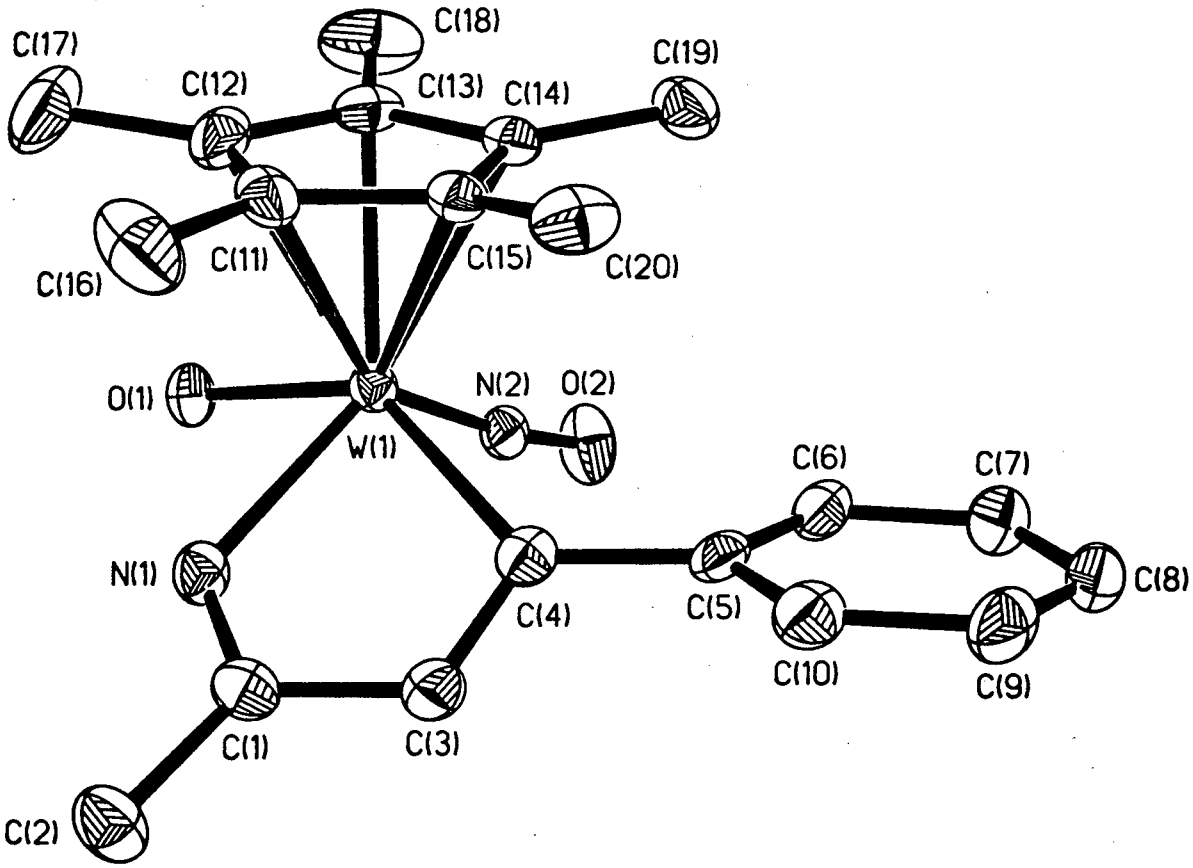

Figure 3.2. The solid-state molecular structure of complex **3.3**. The thermal ellipsoids depict the 50% probability level.

Interestingly, only the O-H stretch in the Nujol-mull IR spectrum of **3.3**, **3.4**, or **3.5** is readily observable, the N-H stretch being masked by the broad unsaturated C-H absorptions in the range 3000 - 3200 cm^{-1}. However, the isotopic shift of these absorptions in the IR spectrum can be examined for the complex in which a deuterium label is incorporated at the hydroxyl and imido sites (eq 3.7).

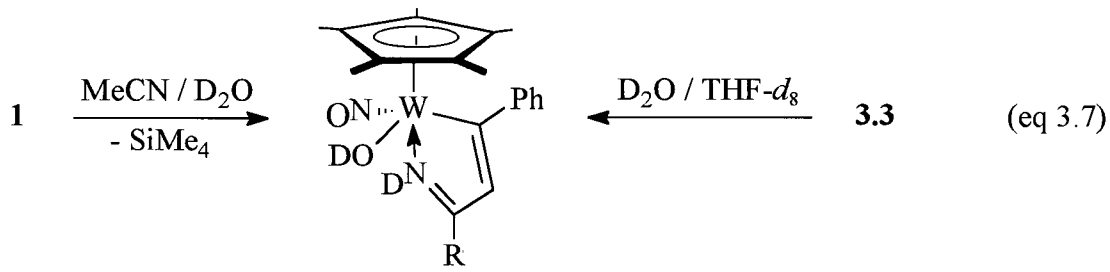

3.3-d_2

(eq 3.7)

The Nujol-mull IR spectrum of **3.3-d_2** reveals a band at 2282 cm^{-1} which can be attributed to the N-D stretch. Calculation of the expected N-H stretch for complex **3.3** based on isotopic substitution[24] gives a value of ν_{N-H} for **3.3** of 3195 cm^{-1}, in a region obscured by the bands resulting from the vinylic and aromatic C-H stretches. Prediction of the O-D stretch expected for **3.3-d_2** employing the same calculation based on the observed ν_{O-H} for **3.3** yields a value of 2544 cm^{-1}, which is in reasonable agreement with the experimentally observed value of 2630 cm^{-1}.

Other protic sources with pK_a values comparable to that of water can also be employed as trapping reagents in this reaction. For example, thermolysis of **1** in acetonitrile containing small amounts of allyl alcohol results in the formation of the alkoxide complex **3.6** which can be isolated in good yield as air-stable red crystals. The N-H proton resonance in the ^1H NMR spectrum of **3.6** is a singlet at 8.62 ppm, analogous to those exhibited by **3.3 - 3.5** (Table 3.5). Signals attributable to the allylic moiety of the alkoxide ligand are distinguishable as a series of multiplets in the characteristic range of δ 4.5 - 6.2.[25] The remaining spectroscopic data are

consistent with the formulated structure and are readily assigned by comparison to the data for complexes **3.3 – 3.5.**

The mechanism that is proposed to account for this reactivity is shown in Scheme 3.5. Coordination of RC≡N (R = Me, Et, ^{i}Pr) to **A** (forming **D**) and subsequent coupling of acetylene and nitrile in the metal's coordination sphere affords the azametallacyclopentadienyl intermediate **E**. The geometry of the resulting five-membered ring restricts donation to the metal centre from the nitrogen atom's sp^2 lone-pair electron density. Hence, the imide N only functions as a 1e donor, and the result is a 16e, Lewis acidic complex (containing a Lewis-basic N). Analogous to intermediate **C**, the build-up of lone pair electron density on the imido N in **E** renders it susceptible to protonation by the external protic source, R'OH. The hydration of **E** and coordination of the pendant imine N thus affords the observed 18e products. Similar protonated or alkylated azametallacyclopentadienyl complexes of Ti,[26a] Nb,[26b] Ta,[26c] W[26d,e] and Ir[26f] have been synthesized via analogous or other preparative routes.

Scheme 3.5

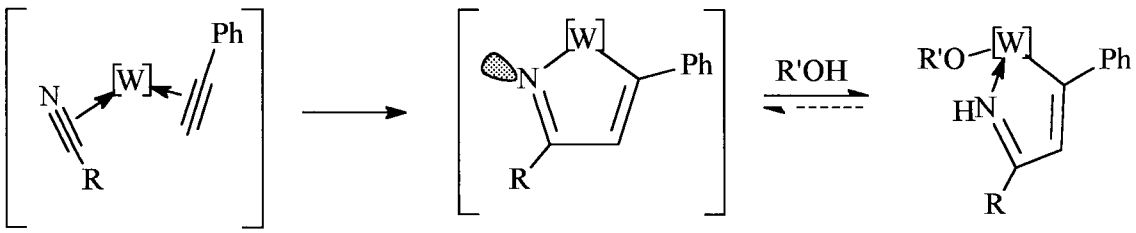

D **E**

[W] = Cp*W(NO)

Mechanistic studies have afforded evidence in support of the reaction pathway proposed in Scheme 3.5. That the thermolysis of **1** in MeCN doped with D_2O affords complex **3.3-*d*$_2$** indicates that the imine D and OD ligand are derived from D_2O, presumably via protonation of

the azametallacycle **C**. Incorporation of deuterium at the amine and hydroxyl positions also occurs during the thermolysis of **3.3** in THF-d_8 containing D_2O (vide supra), revealing that these two protons are labile. In addition, the thermolysis of allylalkoxide-containing **3.6** in wet THF-d_8 also results in its conversion to hydroxyl-containing complex **3.3**, though at a rate significantly slower than that observed for label exchange. Thus, while the hydroxyl and amine protons are labile and readily exchange in the presence of D_2O, the formation of complexes **3.3** - **3.6** by the addition of R'OH to **E** is presumably slower, by comparison. Such an exchange of alkoxide ligand in the presence of the appropriate ROH is presumably governed by the pK_a of the two protic sources.[27]

The formation of a strong C-C single bond and the conjugation within the ligand backbone upon coupling of the two organic fragments suggests that the **D** $\rightarrow$ **E** ring closure is irreversible. Consistent with this inference is the fact that complex **3.3** cannot be converted to **3.2** under thermolysis conditions in EtOAc, nor can **3.2** be converted to **3.3** under the identical thermolysis conditions in $MeCN/H_2O$ solution.

It is interesting that the thermolysis of **1** in wet ^{t}BuCN does not afford any tractable products. While an η^1 interaction of the bulkier ^{t}BuCN with the metal centre can presumably occur, unfavourable steric interactions probably slow the formation of intermediate **D** or the **D** $\rightarrow$ **E** ring-closing step, to an extent where decomposition pathways become competitive and no product is observed. Interestingly, the coupling of two ^{t}BuC≡CH units on the $(RO)_3Ta$ fragment [RO = 2,6-diisopropylphenoxide] reported by Wigley's group is facile at room temperature.[28] Even more striking is the fact that under thermolysis conditions ^{t}BuCN couples readily to coordinated benzyne in the Buchwald Cp_2Zr system.[29] It would thus appear that the substantial size of the Cp* and phenyl acetylene ligands in the Group 6 nitrosyl complexes is playing a significant role in the chemo- and regioselectivity leading to complexes **3.3** – **3.6**.

3.2.2.2 Trapping by CpH: Formation of an Aminopentafulvene Ligand

In light of the mechanism invoked to account for the formation of complexes **3.3** – **3.6**, cyclopentadiene (CpH) was chosen as an atypical protic source to probe the extent of this reactivity. In so doing, it was discovered that the unexpected result that under these experimental conditions a second molecule of acetonitrile is incorporated into the complex and a fulvene substituent is obtained from the cyclopentadienyl fragment (eq 3.8).

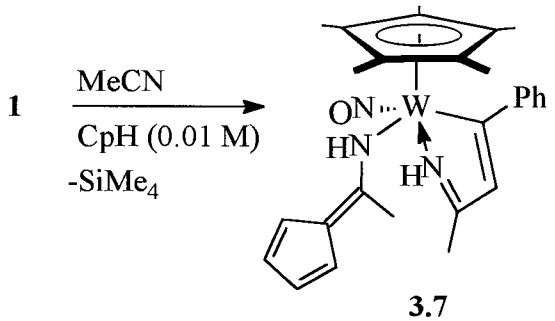

(eq 3.8)

3.7

Solution ^{1}H NMR data ($CDCl_3$) for this red-brown crystalline product are consistent with the existence of the protonated azametallacyclopentadienyl ring found in the molecular structures of complexes **3.3** – **3.6**. The results of a single-crystal X-ray diffraction study confirm the structure shown for complex **3.7** in eq 3.8.[30] The solid-state molecular structure depicted in Figure 3.3 reveals that the second molecule of MeCN is incorporated into the complex as a component of an aminopentafulvene ligand. In addition, the angles around both C(11) and C(13) sum to 360.0°, in accord with the proposed sp^2 hybridization at these centres, revealing the fulvene character in this five-membered ring. On the other hand, the C(11)-C(13) bond length and the fulvene ring bond lengths in **3.7** deviate substantially from those in the analogous 6,6-dimethylpentafulvene,[31] the $C(sp^2)=C(sp^2)$ bonds containing significant single-bond character and the single bonds being contracted relative to the accepted $C(sp^2)$-$C(sp^2)$ bond length.

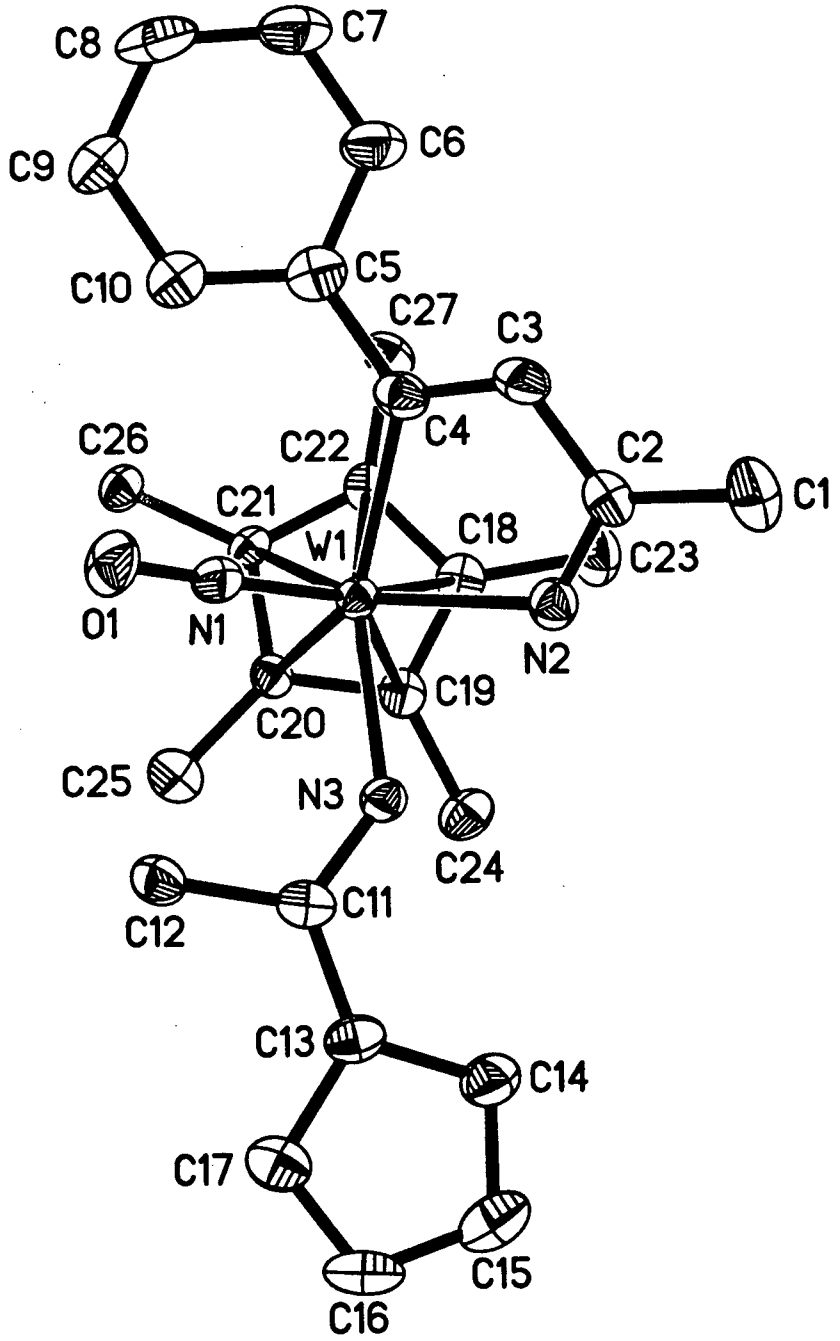

Figure 3.3. Solid state molecular structure of **3.7**. 50% probability ellipsoids are depicted.

A structural study of aminopentafulvenes conducted by Ammon has revealed that the resonance structures depicted in Figure 3.4 make a significant contribution to the ground state of the aminopentafulvene unit. This state of affairs arises due to the presence of the electron-releasing amine substituent that allows significant charge separation in the ground state of the molecule.[32]

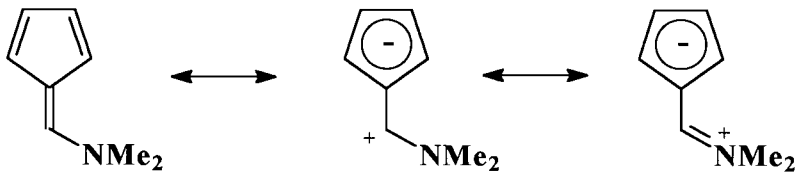

a b

Figure 3.4. Resonance contributors to the electronic structure of dimethylaminopentafulvene.

The aminopentafulvene N in **3.7** functions as a 1e donor as a result of the electronic saturation of the metal centre by the imine moiety of the metallacycle fragment. Thus, it reasonable to assume that the structural parameters determined for this fragment reflect a substantial contribution by resonance form **b** to the ground-state of the aminopentafulvene unit.

Examination of the solution behaviour of **3.7** by ^{1}H NMR spectroscopy reveals the intriguing fluxional nature of the aminofulvene ligand, further evidence for the electronic influence of the amine group (and resonance form **b**, Figure 3.4) on the structure of the fulvene ring. The four fulvene H resonances in the ^{1}H NMR spectrum ($CDCl_3$) appear in the region δ 6.5 - 6.1. The broadness of these signals and the lack of observed inter-proton coupling in the room temperature spectrum are both symptomatic of a fluxional process. Consistently, changing the

NMR solvent to toluene-d_8 results in a shift of the fulvene signals into the aromatic region and their coalescence into two broad singlets, implying a fluxional process that is faster in the less-polar solvent. Indeed, a VT-^{1}H NMR experiment (MeCN-d_3) reveals that at 60 °C the α- and α′-H signals coalesce to a broad singlet, as do the β- and β′-H signals. No further change occurs with an increase in temperature. Because the four sites are inequivalent in the static fulvene unit, coalescence implies that the α-site is equilibrating with the α′-site, as is the β- with the β′-site, through a rotation about the fulvene long axis (Scheme 3.6, A). In the low-temperature limiting spectrum (-38 °C) of complex **3.8**, the peak separation of the β and β' sites is 122.4 Hz. The approximate rotation rate of 272(5) s^{-1} at coalescence[33] (60 °C) based on this peak separation corresponds to a $\Delta G^{\ddagger}$ = 15.9(2) kcal(mol)$^{-1}$.[34] The source of this hindered rotation presumably lies in the partial reduction of the unique C=C bond order as highlighted in the structural discussion above.

Scheme 3.6

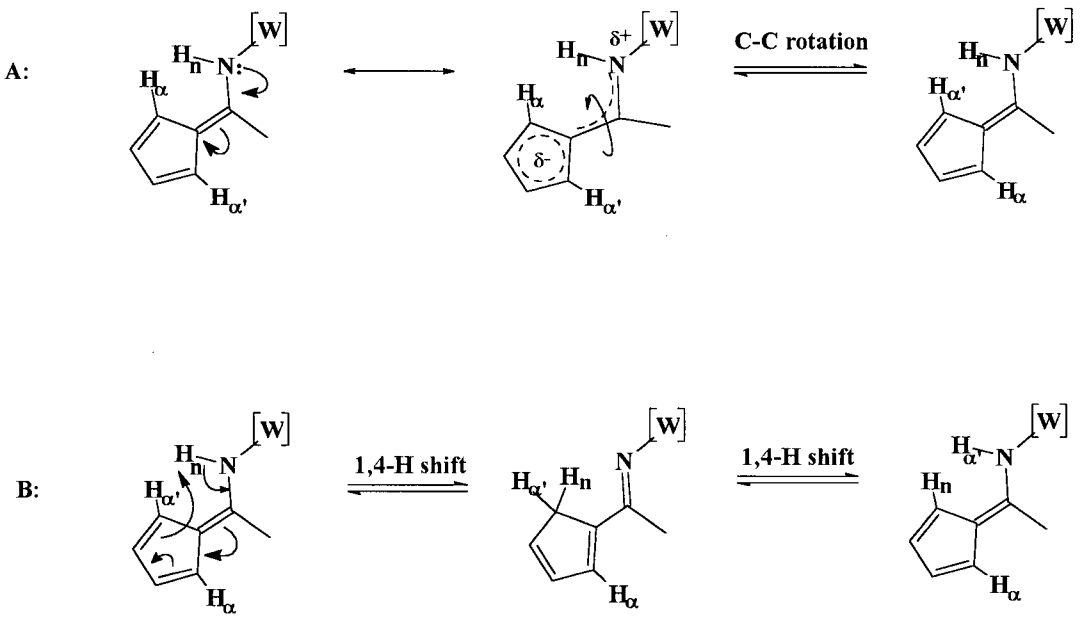

[W] = Cp*W(NO)(η²-H*N*=C(Me)CH=*C*Ph)

In addition, the ^{1}H NMR spectrum of **3.7** in $CDCl_3$ containing added D_2O shows the surprising result that ^{2}H-label is incorporated into the α- *and* α′-H positions (δ 6.50 and 6.44 in the ^{1}H NMR spectrum), but *not* into either of the β-H positions, in addition to the expected label-exchange at the two amine sites. Consistently, selective irradiation of the fulvene amine H signal during a magnetization transfer experiment results in a dramatic reduction in intensity of both α-H signals equally, indicative of an exchange process involving these three environments (Scheme 3.6, B). A 1,4-H shift transfers H_n to the α-position, yielding two equivalent α-H bound to the sp^3 α-C. In the microscopic reverse, either one of these two protons may be transferred back to the amine N. Since the amine N readily exchanges with D_2O, label is incorporated into the fulvene ring via mechanism B. Because label appears in *both* the α and α′ sites at the same time in the slow-exchange RT spectrum, the rotational mechanism (A) must be occurring at a much greater rate than, and independently of, the amine exchange mechanism (B).[35] The simultaneous intensity reduction of the H_α and $H_{\alpha'}$ signals upon irradiation of H_n supports the proposal that the rotational process is significantly faster than the exchange mechanism.

The mechanism to account for the formation of **3.7** is shown in Scheme 3.7 and is most easily expressed as a continuation of that presented in Scheme 4 for complexes **3.3** - **3.6**. Protonation by CpH at the basic imido site in **E** affords **F**, an intermediate analogous to compounds **3.3** - **3.6**. Acetonitrile insertion may then proceed via one of two pathways. Dissociation of either Cp^- or the pendant imine followed by MeCN coordination yields the adducts **G** or **H**, respectively. Attack at the quaternary nitrile carbon by Cp^- in an inter- or intramolecular fashion then affords the azomethine intermediate **I**, and a 1,3-H tautomerization yields the aminopentafulvene-containing product.

Scheme 3.7

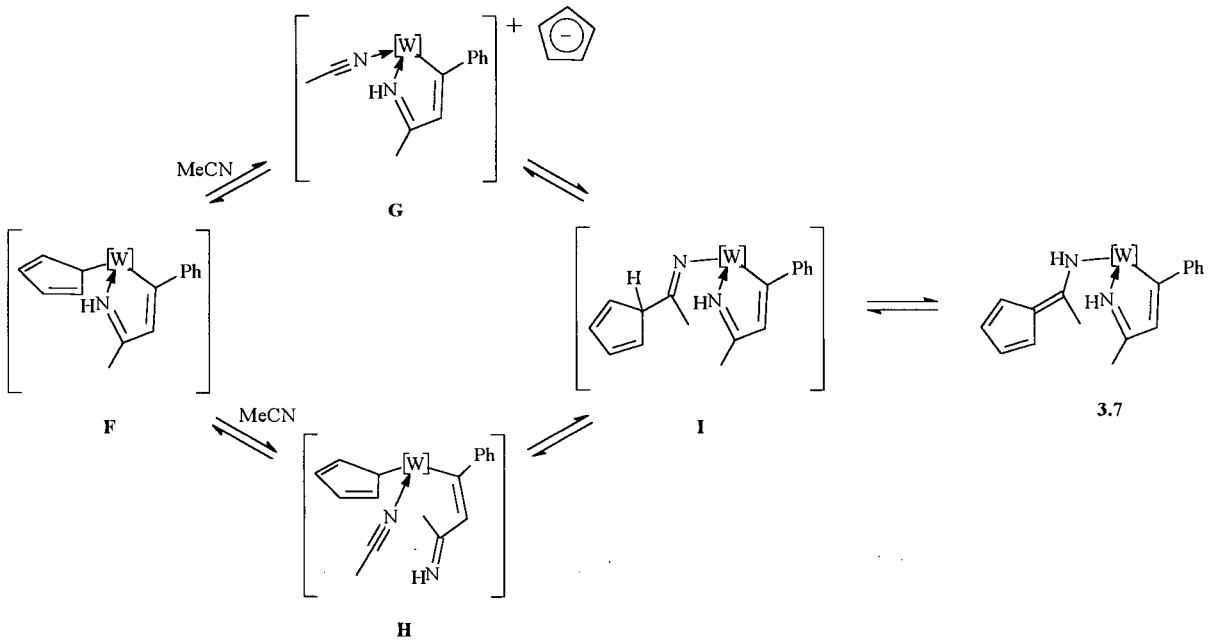

Either pathway leading to **I** is plausible. The pendant imine fragment certainly could possess a degree of lability under the thermolysis conditions employed. Likewise, outer-sphere "η^0" Cp^- anions have been reported, but these seem to predominate in conjunction with late transition-metal coordination compounds.[36] Considerable literature precedent exists for the η^1-bonding mode of the Cp ligand,[37] though examples of insertion chemistry into such metal-carbon linkages are scarce. Casey *et al.* have described the formation of an oxafulvene of rhenium by the insertion of CO into a Re-η^1-Cp bond in the presence of PMe_3.[36] More recently, Carmona and coworkers have reported the formation of the C-bound aminofulvene ligand [C(=C(C_4H_4))N(H)^{t}Bu] by invoking a 1,3 H shift in the imido ligand derived from the insertion of ^{t}BuNC into the Pd-C bond of an η^1-Cp ligand (eq 3.9).[38]

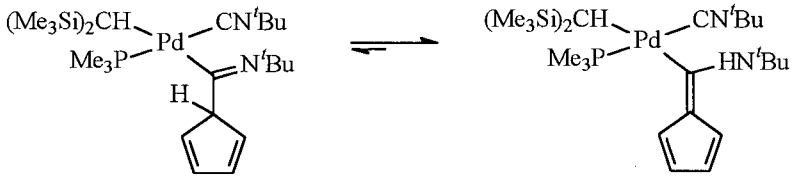

(eq 3.9)

3.2.2.3 Addition of the Carbonyl Function across the W-N Bond

It has been postulated in the previous Sections that the chemistry occurring beyond the initial coupling event (leading to compounds **3.1** - **3.7**) results because the heteroatom lone-pair in the resultant metallacycles (**C** and **E**) does not sufficiently stabilize the formally 16e W centre. The nature of products **3.3** – **3.7** derived from the thermolyses in nitrile solvents containing protic acids and the proposed pathway by which they form reflect both the nucleophilic character of the imido nitrogen atom conferred by a build-up of electron density at N and the electronic unsaturation of the metal centre in **E**.

Further evidence supporting this rationale is provided by the products derived from the thermolysis of **1** in 0.1 M solutions of acetone in MeCN or ^{i}PrCN. After 24 h at 45 °C in these solutions, the alkyl vinyl complex **1** is converted to **3.8** or **3.9**, respectively (eq 3.10). These complexes are isolable in relatively high yields from their respective reaction mixtures as red-brown crystalline blocks and are air-stable in the solid state for up to two weeks. Unlike the conversions described in the preceding discussion, these reactions are not quantitative, signals attributable to other unidentified products being apparent in the ^{1}H NMR spectra of the crude reaction mixtures.

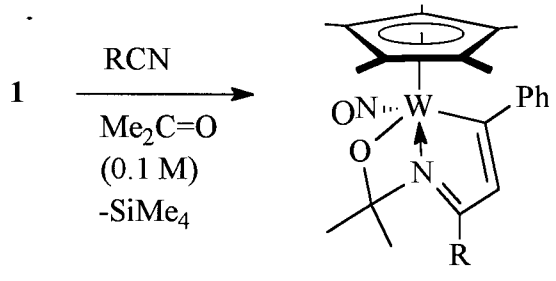

(3.10)

3.8 R = Me
3.9 R = ^{i}Pr

Analogous to complexes **3.3** – **3.7** described previously, the phenyl ring, vinyl proton, and methyl substituent are readily identified from their characteristic signals in the ^{1}H and ^{13}C NMR

spectra of **3.8** and **3.9** in $CDCl_3$ (Table 4.5). While these assignments are straightforward, there exist extra signals in the proton and carbon spectra which are in accord with the presence of two additional methyl substituents and an extra quaternary carbon nucleus. The masses of the parent ions in the mass spectra of **3.8** and **3.9** are consistent with the inclusion of one molecule of acetone in the molecular formulae for these complexes, a feature also corroborated by their elemental analyses.

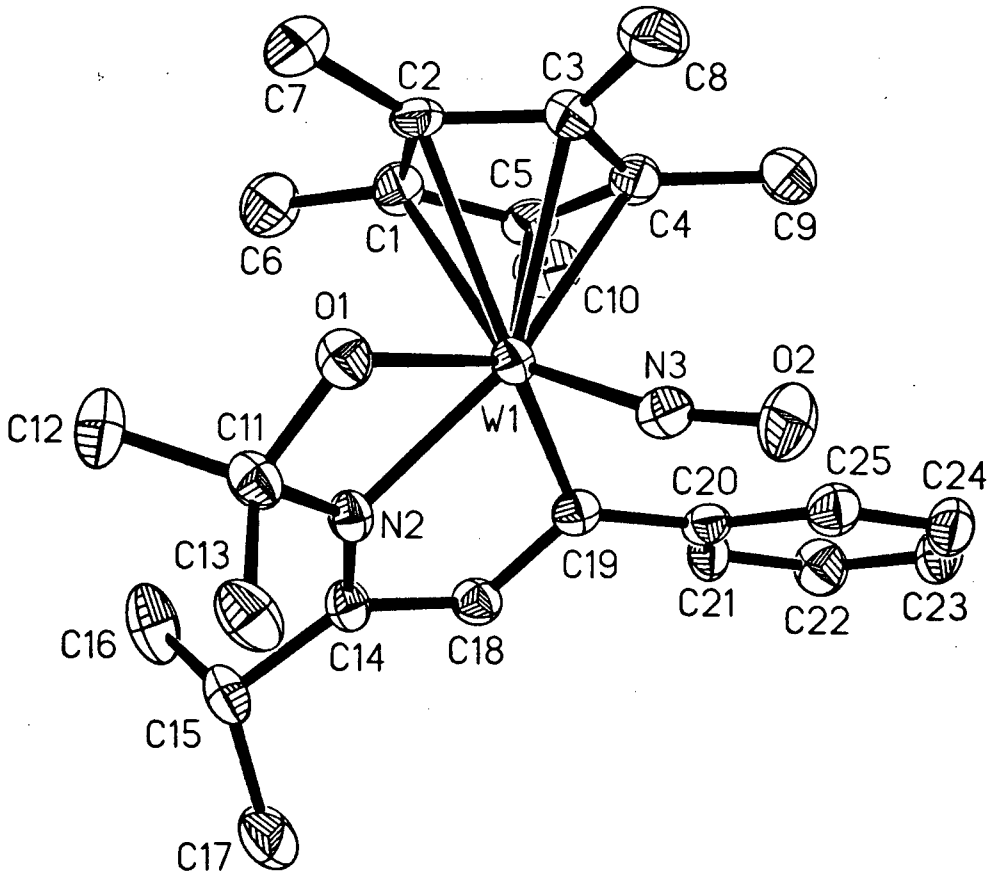

Figure 3.5. The solid-state molecular structure of complex **3.9**. The thermal ellipsoids depict the 50% probability level.

That acetone is incorporated into these extended ring systems is confirmed by the solid-state molecular structure detemined for complex **3.9** by X-ray crystallography (Figure 3.5).[39] The carbonyl unit has clearly added across the W-N bond, as evinced by the C(11)-N(2) single bond contact of 1.478 (5) Å and the W(1)-O(1) single bond length of 2.075 (3) Å. Likewise, the C(11)-O(1) distance of 1.425 (5) Å reflects the reduction of the C-O bond order to that of a single bond. The sum of the bond angles about N(2) (360.0°) reveals the sp^2 hybridization at the imine moiety, and the W(1)-N(2) distance of 2.095(3) Å is characteristic of dative N-coordination to W.[25]

The mechanism proposed to yield complexes **3.8** and **3.9** is depicted in Scheme 3.8. Following the formation of **E** via acetylene/nitrile coupling, acetone coordination (**J**) facilitates the addition of the W-N bond across the carbonyl fragment.

Scheme 3.8

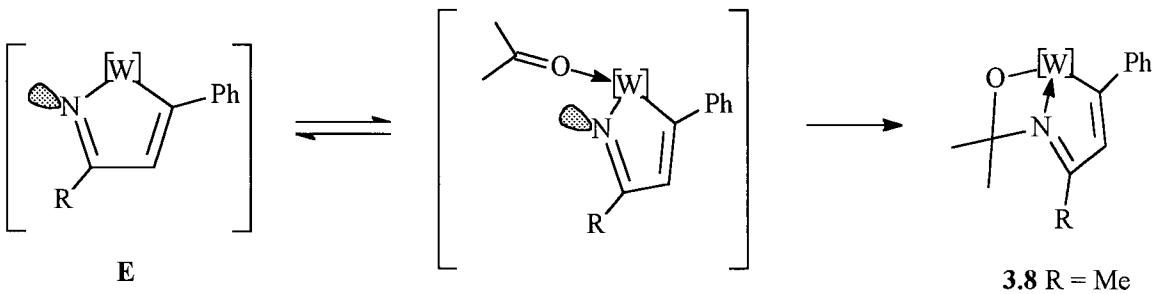

E **J** **3.8** R = Me, **3.9** R = ^{i}Pr

The regiochemistry of this addition reflects both the affinity of W for O[1a] as well as the polarity of the W-N linkage; the nucleophilic imido N attacks at the electrophilic quaternary carbonyl carbon with concomitant O attack at the electrophilic, electronically-unsaturated metal centre. That **3.8** and **3.9** are formed exclusively implies that the **J**→ product step is irreversible. In agreement with this supposition, **3.8** does not convert to **3.3** under thermolysis conditions in

wet MeCN-d_3. At present, this ring expansion seems to be limited to sterically unencumbered ketones and aldehydes. For example, an NMR-scale thermolysis of **1** in MeCN containing small amounts of acetaldehyde affords the analogous addition products as evinced in the ^{1}H NMR spectrum ($CDCl_3$) of the final reaction mixture. Two signals of equal intensity are observed for each environment, thereby implying the formation of two regioisomers in which the methyl substituent of the alkoxy fragment presumably is directed either towards or away from the Cp* ring. In contrast, the analogous thermolyses in acetonitrile solvent containing small amounts of larger substrates such as ethyl acetate, dimethyl acetamide, or benzaldehyde afford only complex **3.10** (vide infra) and small amounts of unidentified decomposition products.

The ring-expanding insertions of unsaturated hydrocarbons,[40] ketones,[41] and carbon monoxide[42] into metallacycle M-C sigma bonds are well known. Conversely, the addition of unsaturated molecules across metal-nitrogen bonds of amido complexes is quite rare.[43]

3.2.2.4 Nitrile Addition across the W-N Bond

In the absence of an added protic source or electrophile, the blood-red products resulting from the thermolysis of **1** in MeCN or EtCN at 45 °C over 24 h are generated in virtually quantitative yield (eq 3.11). These amidinate complexes are isolable as microcrystalline solids and are air-stable in solution or in the solid state for periods up to a month. As described for compounds **3.8** and **3.9** (vide supra), the imine N atom is correctly disposed relative to the NO ligand for dative bonding to W, thus rendering **3.10** and **3.11** electronically and coordinatively saturated at the metal centre.[25]

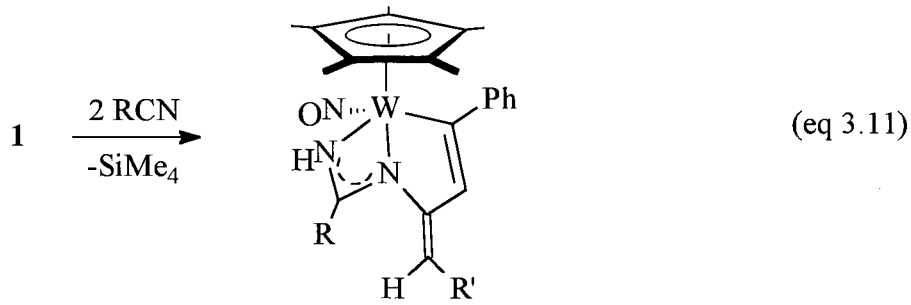

(eq 3.11)

3.10 R = Me, R' = H
3.11 R = Et, R' = Me

The close similarity of the azacyclic ring in these compounds to that established for the structurally-characterized **3.9** aids in the formulation of these compounds on the basis of their spectroscopic data. Utilizing compound **3.10** as an example, the characteristic signals of the azametallacyclopentenyl ring components are easily identified in the NMR spectral data. A broad singlet at 4.73 ppm in the ^{1}H NMR spectrum and a ν_{NH} at 3268 cm^{-1} in the KBr pellet IR spectrum reveal the presence of the amine H. Likewise, the signal attributable to the resonance of the ring vinyl proton is clearly discernible at 6.83 ppm. A short-range ^{1}H-^{13}C correlation experiment identifies the carbon signals to which the proton environments, particularly the vinyl signals, are coupled. For example, the endocyclic vinyl proton resonance at δ 6.83 couples to the carbon signal at 138.8 ppm with a coupling constant of 158 Hz, a value obtained from a gate-decoupled ^{13}C NMR experiment. Likewise, the exocyclic vinyl resonances at 4.73 and 4.45 ppm in the ^{1}H NMR spectrum couple to the carbon-13 signal at 90.6 ppm ($^1J_{CH}$ = 152 Hz). Hence, the ring substituents (the vinyl H, CH_2 vinyl group, methyl substituent, and phenyl group) are identifiable from these data, although their connectivity is not. The bicyclic structure of this ring system is implied by analogy to the solid-state molecular structure determined for complex **3.9**, but the location of the NH, methyl, and vinyl CH_2 units can only be assigned through the combination of NOE and long-range ^{1}H-^{13}C correlation data. The spatial arrangement of these substituents is revealed by the results of an NOE experiment (Figure 3.6).

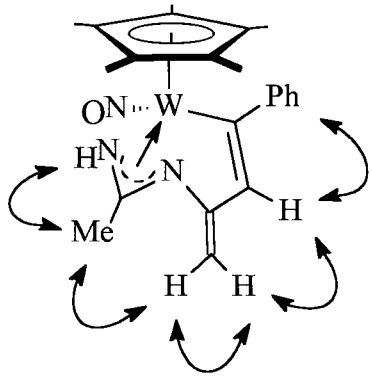

Figure 3.6. NOE results for the indicated environments in complex **3.10.** ↔ indicates an observed NOE.

It thus remains to assign the quaternary nuclei to which these substituents are bound, facilitated by the results of an HMBC ^{1}H-^{13}C correlation experiment. Thus, both the endocyclic vinyl H signal and that of the phenyl *ortho*-H couple via two-bond and three-bond interactions, respectively, to the quaternary signal at 191.9 ppm, which can be assigned as the carbon nucleus α to W. Likewise, the endocyclic vinyl H signal shows a two-bond coupling to the signal at 156.1 ppm, as does one of the signals atributable to the geminal vinyl protons. This signal is therefore attributed to the quaternary imine carbon. Both geminal vinyl proton signals couple via three-bond couplings to the endocyclic vinyl carbon signal at 138.8 ppm. Finally, the quaternary carbon signal at 171.1 ppm shows a coupling to the singlet assigned to the methyl substituent's resonance at 2.11 ppm, which permits its assignment as the quaternary amidinate carbon. Complex **3.11** is characterized in an analogous manner.

The mechanism leading to these complexes (Scheme 3.9) can be viewed as being analogous to that proposed for the formation of **3.8** and **3.9** (Scheme 3.6). The azametallacyclopentadiene **E** is first formed by coupling of the acetylene and RCN at W. A

second molecule of acetonitrile coordinates (**K**) and adds across the polar W-imine link (**L**), a process facilitated by attack at the electrophilic quaternary nitrile carbon nucleus by the nucleophilic imido N in **K**. A coordinatively saturated intermediate species (**L**) is thus generated. This species, an 18e analogue of **E**, contains a basic imido N centre that is quenched upon tautomerization via a formal 1,5-H shift to afford the observed products.

Scheme 3.9

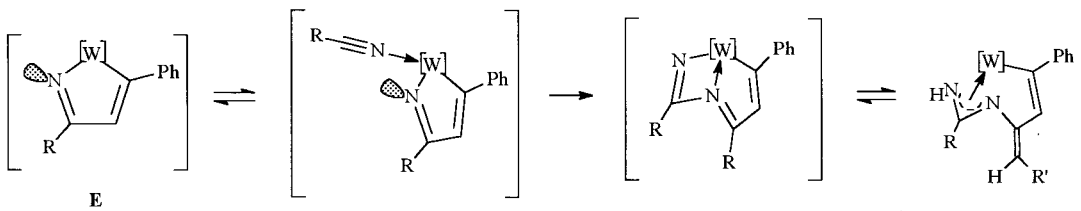

Interestingly, when either ^{t}BuCN, PhCN, or ^{i}PrCN is employed in this reaction, no tractable products are obtained. This is not surprising in the case of ^{t}BuCN, since no product was isolated in the presence of added water either, a result that is attributable to the inhibition of coupling due to unfavourable steric interactions between the metal complex and incoming solvent molecule. In the absence of steric arguments, a lack of accessible protons on the quaternary β-carbon in ^{t}BuCN or PhCN prohibits the tautomerization step which affords the final product in these transformations. In contrast, it is remarkable that no product is obtained with ^{i}PrCN as the isolation of **3.5** confirms that the coupling event does indeed occur. On the other hand, steric interactions prohibiting ring expansion by addition of the bulky ^{i}PrCN molecule across the W-N link might be responsible for the observed lack of reactivity, by analogy to the limitations of the ring expansions by ketone addition described in Section 3.2.2.3. Similar to the formation of compounds **3.8** and **3.9**, the insertion of a nitrile into a metal-N bond appears to be

unprecedented, constituting a novel regioselective coupling of two equivalents of nitrile with phenyl acetylene to give the vinyl amidinate complexes **3.10** and **3.11**.

Several other experiments have been performed to corroborate the structural and mechanistic proposals made above. For example, no ligand substitution chemistry occurs for **3.10** under thermolysis conditions in the presence of MeCN-d_3 and PMe_3.[44] This fact coupled to the absence of characteristic IR[45] and ^{13}C NMR[46] evidence for a nitrile group suggests that the second equivalent of acetonitrile indeed has added across the W-N linkage. A labeling study indicates that the tautomerization step is a reversible one. Thus, thermolysis of authentic **3.10** in THF-d_8 containing D_2O results in label incorporation at the amine position as well as at the exocyclic methyl position *and* the exocyclic vinyl position, affording **3.10-d_6**. Because the tautomerization is reversible, the ring expansion affording **L** must be irreversible to account for the fact that **3.10** is not converted to **3.3** in the presence of water.

The extensive deuteration in the ring substituents of **3.10-d_6** leads to the conclusion that tautomerization processes[47] occur during the formation of these amidinate complexes. To gain further insight into the nature of this tautomerization, a crossover experiment involving the thermolysis of an equimolar mixture of **3.10-d_6** and **3.11** at 65 °C in THF-d_8 was performed. Monitoring the progress of this thermolysis by ^1H NMR spectroscopy reveals that deuterium label is incorporated into the amine, ethyl and methylvinyl susbtituents in **3.11** and proton label is incorporated into the analogous sites in **3.10-d_6**, a clear indication of the *intermolecular* nature of this tautomerization process.[48] A striking feature of this experiment is its low rate of conversion. After 24 h the deuterium scrambling is approximately 50% complete as judged by integration of the methyl signals at 2.1 and 1.3 ppm in the ^1H NMR spectrum. Because the thermolyses to form complexes **3.1 - 3.11** require approximately 24 h at 45 °C, the dilution of the reaction mixture and an isotope effect presumably retard the rate of tautomerism, in accord with a bimolecular tautomerization mechanism.[49]

The competition by MeCN and water for reaction with intermediate **E** has been tested by conducting the thermolysis of **1** in MeCN containing 2, 5, and 10 equivalents of water ([H_2O] = 19, 46 and 93 mM, respectively) on an NMR scale. Formation of **3.10** (~5%) was observed only in the case where [H_2O] = 19 mM, as detected by ^{1}H NMR spectroscopy of the three mixtures after their thermolysis for 24h. Quantitative conversion to **3.3** was indicated in the ^{1}H NMR spectra of the final mixtures in the latter two cases. Thus, the ring expansion afforded by the insertion of a second acetonitrile molecule must be a more energetically-demanding process; only at very low water concentrations does this process become competitive with protonation of **E** by water.

3.2.2.5 Thermolysis of Complex 1 in Acetone

The thermolysis of complex **1** in acetone at 45 °C over 24 h affords red crystals of trimetallic **3.12** in moderate yields (eq 3.12). This compound resists analysis by mass spectrometry and combustion, affording irreproducible results when samples of this compound are subjected to either analytical technique. In its crystalline form this trimeric complex is insoluble in almost all common organic solvents. The ^{1}H NMR spectrum (DMSO) for this compound reveals one signal attributable to a vinyl H environment and two signals attributable to diastereotopic methyl substituents. Only one signal is observed for each proton environment, implying that either the symmetric structure of the trimer is maintained in solution, or that the trimer completely dissociates into its constituent monomers upon dissolution. Evidence in support for the former (and in contradiction with the latter) lies in the complete insolubility of **3.12** in very polar solvents such as MeCN and acetone-d_6. The observed insolubility in such solvents implies that the NO→W bonding interaction between organometallic units must be a

strong one and that strong donor solvents such as DMSO and MeCN[50] are unable to break this interaction and solubilize the monometallic units.

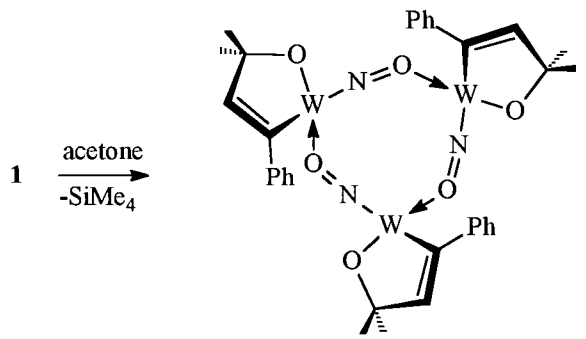

(eq 3.12)

3.12

(the Cp* ligand is omitted for reasons of clarity)

The solid-state molecular structure determined for **3.12** by X-ray diffraction methods permits the assignment of a trimetallic structure to this complex (Figure 3.7).[51] The structure of the oxametallacyclopentene unit is strikingly similar to that determined for complex **3.1**. Of note are the average C-O and W-O bond lengths in the three metallacycle units, the former being 1.404(34) Å and the latter being 1.958(18) Å. The C-O contacts clearly represent those of a single bond, and those of the W-O bond in this metallacycle are similar to the W-O single-bond distance of 2.001(7) Å observed in the solid-state structure of complex **3.1**. The average W-O bonding contact in the isonitrile link is 2.164(15) Å, and again this value is similar to the W-O dative bonding contact in the structure determined for complex **3.1** (2.203(6)°). The average W-N-O angle is 162.4(10)°, consistent with the linear W-NO angle of neutral monometallic nitrosyl complexes of W. The average N-O-W angle is 122.7(15)°, suggesting that O→W dative coordination occurs via lone pair donation from O to W. The average N-O bond length of

The average W-N distance of 1.754(21) Å is characteristic of the typical W-N bonding contact in linear nitrosyl complexes.[52]

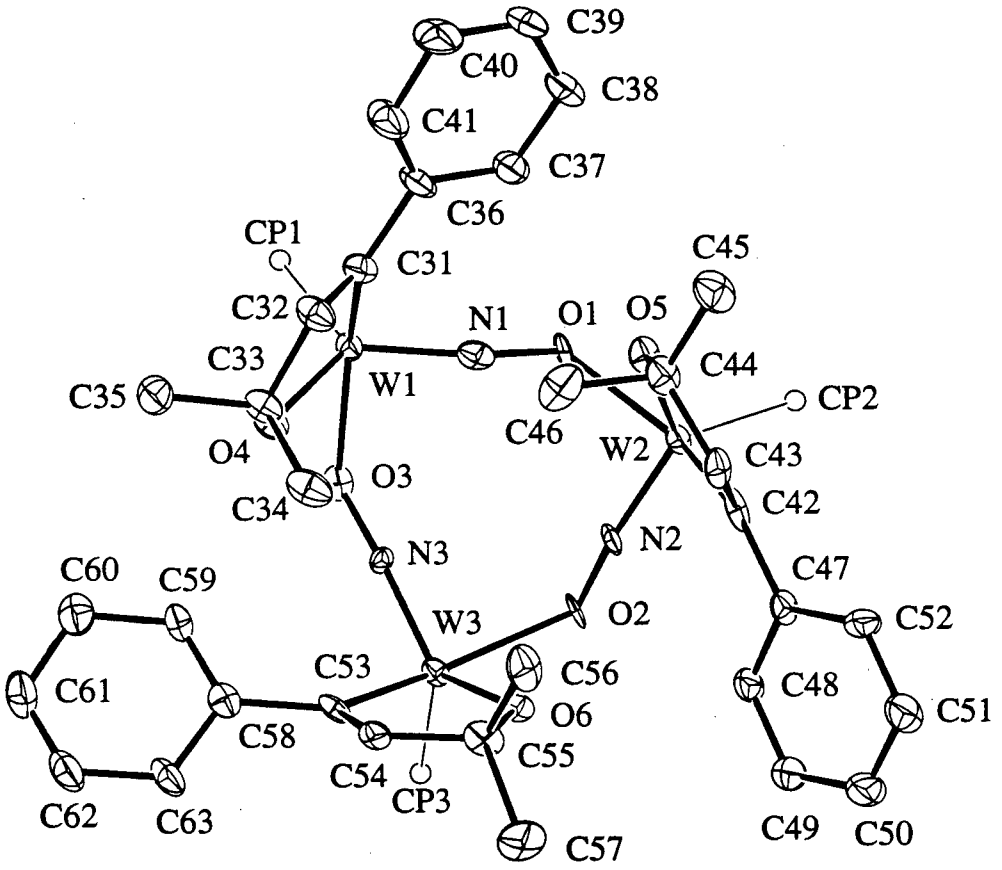

Figure 3.7. The solid-state molecular structure determined for complex **3.12**, with thermal ellipsoids depicting the 50% probability level.

The formation of **3.12** (Scheme 3.10) is consistent with the mechanistic proposals that rationalize the formation of complexes **3.1** – **3.11**. However, no external or internal agent is present to stabilize oxametallacyclopentenyl-containing **M** once it is formed, thus, dative coordination by the NO ligand of another monomeric unit stabilizes these complexes through the formation of an isonitrosyl link.

present to stabilize oxametallacyclopentenyl-containing **M** once it is formed, thus, dative coordination by the NO ligand of another monomeric unit stabilizes these complexes through the formation of an isonitrosyl link.

Scheme 3.10

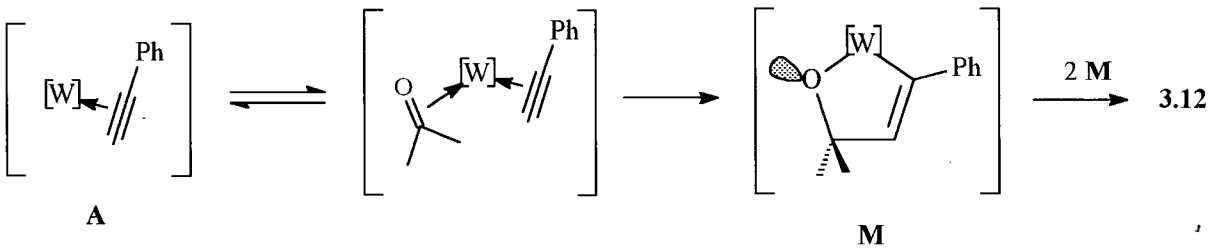

Such isonitrosyl complexes are rare: a search of the Cambridge Structural Database reveals that only two complexes containing an isonitrosyl bonding interaction have been structurally characterized previously, one of a Re tetrametallic complex and another of a Mo/Co tetrametallic complex.[50,53] No complexes containing the linear-bridging M-N-O-M link (M = transition metal) such as that extant in **3.12** have been structurally characterized previously.

3.2.3 Kinetic Studies

Many of the conversions described in this chapter are very clean, prompting a study of their reaction kinetics. UV-vis spectroscopy is the method of choice for collecting well-defined kinetic data. Quantification of these data is effected by monitoring the growth of the shoulder at 336 nm or 350 nm at regular time intervals in the UV-vis spectra of these reaction mixtures (e.g. Figure 3.8) and the observed rate constants were determined from a first-order analysis of the data (e.g. Figure 3.9).

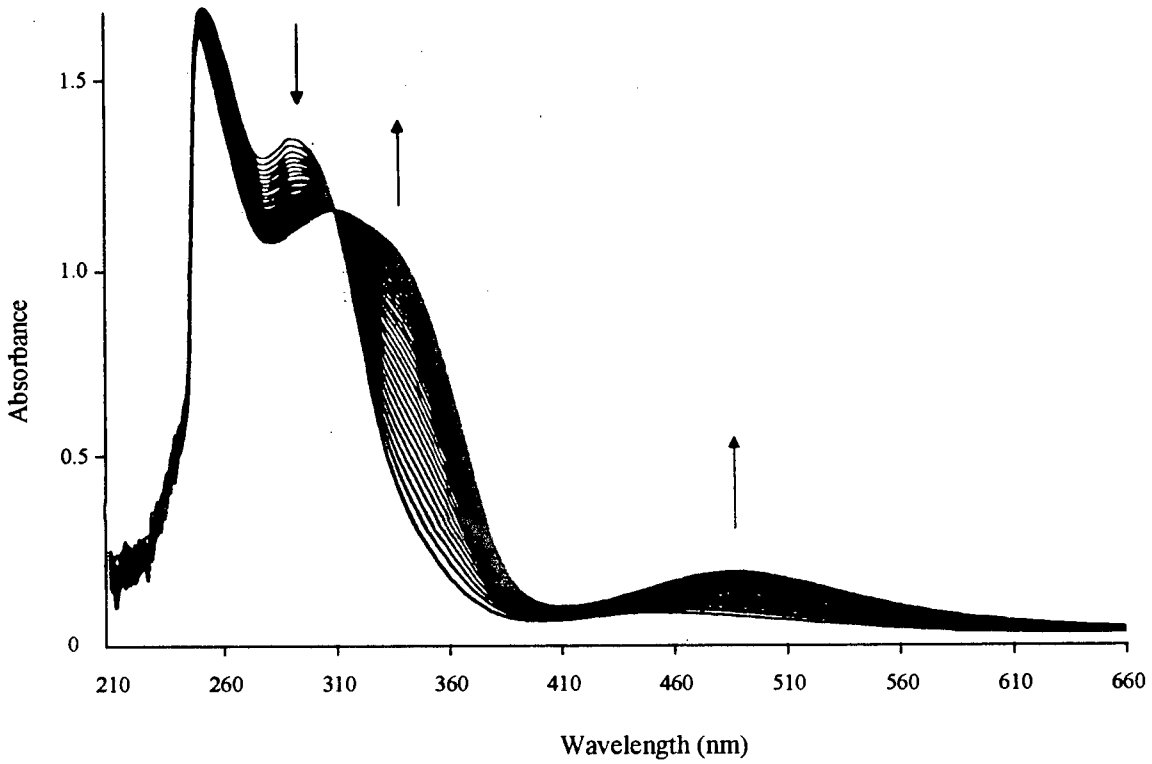

Figure 3.8. The thermolysis of **1** in EtOAc at 318 K, as monitored by UV-vis spectroscopy (210 nm < λ < 660 nm).

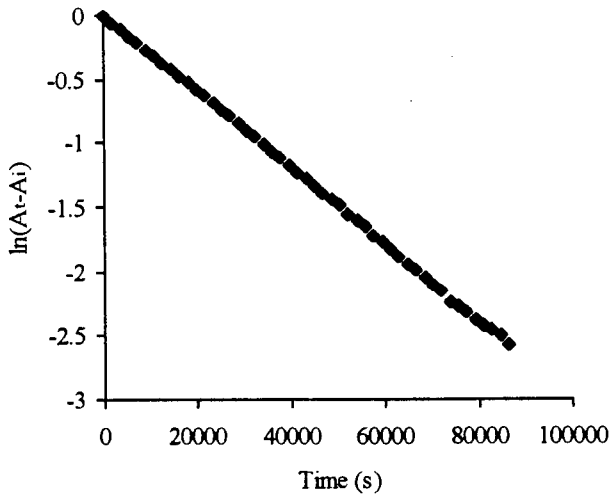

Figure 3.9. A plot of $\ln(A_t-A_i)$ vs. t (A_i = absorbance at infinite time, $R^2 = 0.9999$) for the **1** → **3.2** conversion conducted at 318 K ($k_{obs} = 2.9(1) \times 10^{-5}\ s^{-1}$).

The mechanism that was originally proposed[7] to account for the observed C-H activation of *n*-pentane and *n*-hexane included an initial reversible elimination of $SiMe_4$ from **1** to produce the η^2-acetylene intermediate **A**. Consistent with this inference, the addition of $SiMe_4$ to these reaction mixtures hinders the observed rate of C-H bond activation.[54] In addition, it has been demonstrated that the formation of the metallacyclic complexes discussed in this Chapter is irreversible. Thus, one can envision a dissociative mechanism under saturation conditions (ie. a "saturation" mechanism) governing these conversions. Such a mechanism utilizing EtOAc as the trapping agent is depicted in Scheme 3.11.

Scheme 3.11

$$\mathbf{1} \underset{k_{-1}}{\overset{k_1}{\rightleftharpoons}} \mathbf{A} + SiMe_4$$

$$\mathbf{A} + EtOAc \xrightarrow{k_2} \mathbf{3.2}$$

Preliminary evidence certainly exists in support of such a mechanism. Because added $SiMe_4$ hinders the rate at which C-H bonds are activated by **1**, it is feasible that, at a particular concentration of trapping agent, the trapping step (the k_2 step) could become rate-limiting. Utilizing EtOAc as the trapping agent, a study of the [EtOAc] dependence in the **1** → **3.2** conversion was warranted. Such a study would involve dissolving **1** in a solvent mixture of varying concentrations of EtOAc in $SiMe_4$ and monitoring the rate of conversion of **1** to **3.2**. However, the thermolysis conditions typically employed are unrealistic for a solvent system based on $SiMe_4$, whose boiling point is 26 °C. In contrast, the silyl ether analogue to **1**, $Cp^*W(NO)(CH_2SiMe_2OSiMe_3)(\eta^2\text{-}CPh{=}CH_2)$ (complex **4.9**), is similar to **1** in its solution

properties. Moreover, hexamethyldisiloxane, the solvent from which complex **4.9** is derived, has a more practical boiling point of 104 °C.

Thus, thermolyses of complex **4.9** in hexamethyldisiloxane containing varying amounts of EtOAc (in greater than ten-fold excess of the organometallic reagent in each case) were monitored by UV-vis spectroscopy and their rates of reaction determined through a first-order analysis (Table 3.1).

Table 3.1. Kinetic data for the rate dependence on [EtOAc] in the **4.9** $\rightarrow$ **3.2** conversion (T = 338 K).

[EtOAc] (M)	k_{obs} ($\times 10^4$, s^{-1})
0	0
0.938	1.7(2)
1.88	2.5(3)
3.28	3.3(1)
4.69	4.0(1)
7.51	5.4(3)
9.38	5.8(2)
11.7	6.2(1)
14.1 (neat)	6.2(1)

Indeed, the rate constant associated with this conversion *does* display a non-linear dependence on the concentration of EtOAc (Figure 3.10). Noteworthy of this plot is the high concentration of EtOAc (ca. 10 M) required to effect saturation kinetics, a clear indicator of the lack of selectivity on the part of **A** for EtOAc over hexamethyldisiloxane during this reaction.

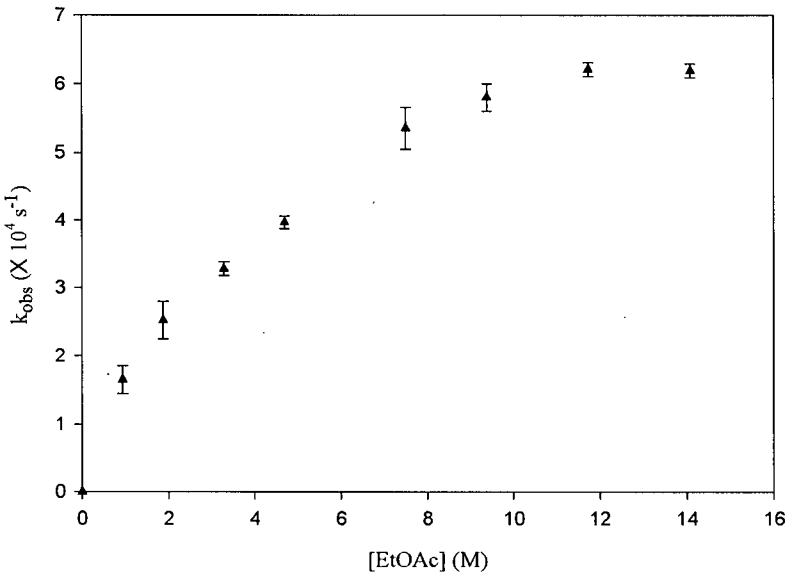

Figure 3.10. The [EtOAc] dependence of k_{obs} in the **4.9**→**3.2** conversion.

A rate equation for the loss of **4.9** can be derived from the mechanism depicted in Scheme 3.11, assuming a steady-state concentration of **A** (the full derivation of this rate law appears in Appendix B). Thus,

$$-d[\mathbf{4.9}]/dt = d[\mathbf{3.2}]/dt = \frac{k_1 k_2 [EtOAc][\mathbf{4.9}]}{k_{-1}[(Me_3Si)_2O] + k_2[EtOAc]},$$

and

$$k_{obs} = \frac{k_1 k_2 [EtOAc]}{k_{-1}[(Me_3Si)_2O] + k_2[EtOAc]}$$

The $(Me_3Si)_2O$ and [EtOAc] concentrations are known for each kinetic run, and inverting the expression for k_{obs} yields

$$1 / k_{obs} = \frac{k_{-1}[(Me_3Si_2)O]}{k_1 k_2[EtOAc]} + \frac{1}{k_1}$$

Thus, a plot of $1 / k_{obs}$ vs. $[(Me_3Si)_2O]/[EtOAc]$ should afford a line of slope k_{-1}/k_1k_2 and intercept of value $1/k_1$. Indeed, a plot of the experimental data collected (Figure 3.11) reveals a linear relationship; linear regression of these data yields a line of slope 694(33) and intercept of 1696(86) for $R^2 = 0.987$.

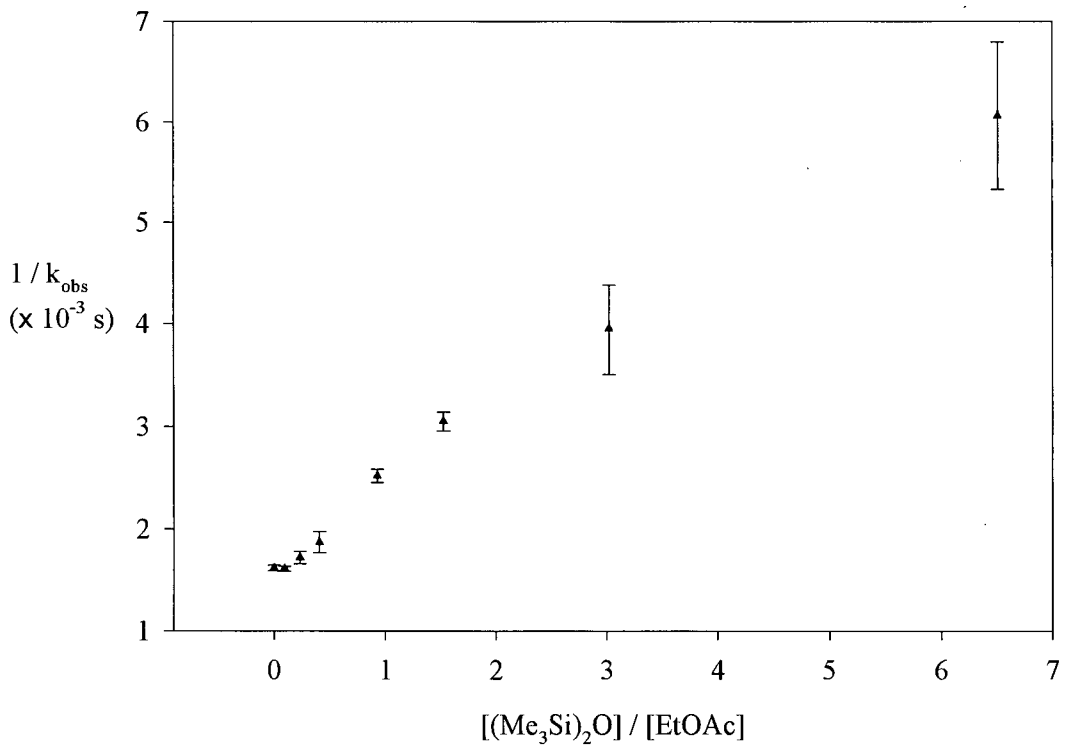

Figure 3.11. A plot of $1 / k_{obs}$ vs. $[(Me_3Si)_2O]/[EtOAc]$.

From the intercept, k_1 is calculated to be $5.9(3) \times 10^{-4}$ s^{-1}, in very good agreement with the experimentally determined value of $6.2(1) \times 10^{-4}$ s^{-1} (Table 3.1). Utilizing the calculated value in the expression for the slope of the line affords a value of 0.41(4) for the k_{-1}/k_2 ratio.

In considering the results of this saturation study, a proviso must be added that arises as a result of the large concentration of EtOAc required to effect saturation of the rate. Because saturation occurs at such a high concentration of EtOAc, the solvent mixture and its bulk properties vary greatly: from one in which EtOAc is dissolved in hexamethyldisiloxane to another in which hexamethyldisiloxane is the solute and EtOAc is the solvent. This is borne out in the slight deviation from linearity observed in the double reciprocal plot depicted in Figure 3.11. As a result, it is conceivable that the variation in the observed rates results from a dependence on [EtOAc] whose linearity varies as a result of the difference in the bulk properties of the solvent mixture (such as dielectric constant, dipole moment, and polarizability)[27] and not to a saturation mechanism. One method of testing this hypothesis requires the use of a solvent with bulk physical properties similar to those of EtOAc that is inert to activation by **1** or **4.9** under thermolysis conditions, giving access to a solvent mixture whose physical properties remain unchanged over a wide range of EtOAc concentrations. Unfortunately, it is difficult to find a solvent embodying both of these properties. At the time of writing such an inert solvent had not been discovered, and this study remains to be performed. Due to the variation in the composition of the solvent mixtures employed in this study, the bulk properties of these solvent mixtures undoubtedly have a measurable effect on the reaction rate. Hence, the absolute magnitude of k_{-1}/k_2 is best regarded as an approximation of the selectivity expressed by **A**. The order of magnitude of this ratio is probably a more accurate indicator of the minimal selectivity expressed by **A** for one substrate over the other in this study.

Having established that these conversions are probably governed by saturation kinetics, the thermolyses of **1** in the presence of EtOAc, MeCN, and MeCN/H_2O mixtures under pseudo-first-order conditions have been conducted. The kinetic data outlined in Table 3.2 (entries 1-6)

are consistent with the rate-controlling generation of **A** during these conversions. Thus, the rates of conversion of **1** in acetonitrile doped with water afford observed rate constants from 4.6×10^{-5} s^{-1} to 4.7×10^{-5} s^{-1} for water concentrations ranging from 0.006 M to 0.12 M (table entries 2-5), indicating an independence of the rate on $[H_2O]$. More importantly, the rate constants associated with the activation of **1** in the presence of different substrates are remarkably similar, ranging from 2.9×10^{-5} s^{-1} to 4.7×10^{-5} s^{-1} (table entries 1, 2, and 6). The slight variance in these observed rate constants can be ascribed to the differences in bulk properties of the MeCN and EtOAc solvents and not to any definable mechanistic discrepancies between the various reactions.[55]

Table 3.2. Kinetic data for the conversion of **1** to **3.10**, **3.3**, and **3.2**.

Table Entry	Solvent	Temp (K)	$[H_2O]$ (M)	Product Complex	Avge k_{obs} ($\times 10^5$, s^{-1})
1	MeCN	318	-	**3.10**	4.7(2)
2	MeCN	318	0.12	**3.3**	4.6(1)
3	MeCN	318	0.06	**3.3**	4.6(4)
4	MeCN	318	0.03	**3.3**	4.6(1)
5	MeCN	318	0.006	**3.3**	4.7(3)
6	EtOAc	318	-	**3.2**	2.9(1)
7	EtOAc	327	-	**3.2**	10(1)
8	EtOAc	336	-	**3.2**	50(1)
9	EtOAc	341	-	**3.2**	95(6)
10	EtOAc	348	-	**3.2**	276(16)

From a study of the temperature-dependence of the reaction rate (table entries 6 – 10, Figure 3.12 below), an Eyring analysis yields the enthalpy and entropy of activation of 31.8(6) $kcal(mol)^{-1}$ and 21(3) $cal(mol \bullet K)^{-1}$, respectively, for the **1** → **3.2** conversion. The magnitude of the enthalpy reflects considerable bond cleavage leading up to the transition state, and is

comparable to others determined for analogous eliminations of hydrocarbon from organometallic complexes.[56] More significant is the positive value of the activation entropy that implicates a rate- limiting step that is dissociative in character, consistent with the proposed rate-limiting, reversible formation of acetylene **A** by elimination of hydrocarbon in the saturation mechanism. Notably, the inclusion of the rate of formation of **A** from **4.9** (k_{obs} (338 K) = 6.2(1) × 10^{-4} s^{-1}) in the Eyring analysis of the formation of **A** from **1** affords a sixth data point that is coincident with the line obtained from the five original points, consistent with the proposed mechanism.

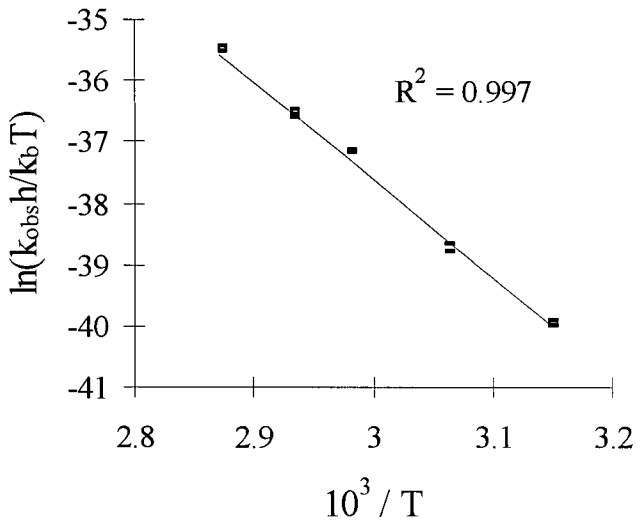

Figure 3.12. Eyring plot for the thermolysis of **1** in EtOAc, 318 < T < 348 K.

3.2.4 A Molecular-Orbital Rationale for Ring Expansion and Ligand Elaboration

In Schemes 3.5, 3.8, 3.9, and 3.10 it is proposed that the chemistry leading to complexes **3.3** – **3.11** arises from the specific incapability of the N atom in intermediate **E** to function as a 3e donor to W, an effect caused by the conformational restrictions of the metallacycle. Two salient consequences of this are (i) the electronic unsaturation of the metal centre in these intermediate complexes, and (ii) the resultant basicity or nucleophilicity conferred on the imido

N which affords a reactivity beyond the initial coupling event. The origin of these chemical characteristics in the azametallacycle **E** (and also in the O-containing analogue **C**) deserves further discussion in light of the fact that the analogous complexes for the Cp_2Zr system are readily isolated and have been extensively studied. In this regard, an orbital-overlap rationale for the observed reactivity can be made. As described in Chapter 2, Section 2.2.1, the Lewis acidity of the 16e model complexes $CpM(NO)Me_2$ [M = Mo, W] results from the presence of a metal-centred d_{xy}-type LUMO oriented perpendicular to the M-NO vector, with one of the lobes bisecting the R-M-R angle (Figure 3.13, case **I**). [57]

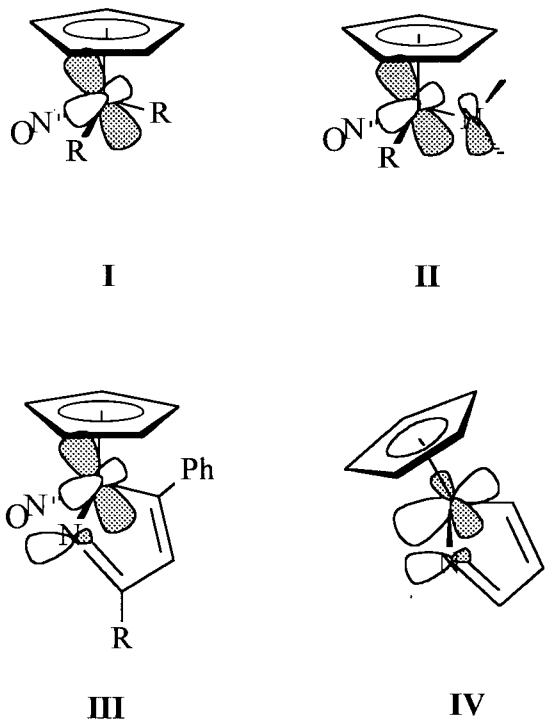

Figure 3.13. Frontier orbitals in isolobal CpW(NO) (**I** - **III**) and Cp_2Zr (**IV**) azametallacycles.

A similar metal-centred LUMO exists in the related complexes containing an NR_2 or OR ligand (case **II**, NR_2 ligand depicted), but in this case the heteroatom-containing ligand is typically oriented so as to stabilize the metal-centered LUMO via N(p)→W(LUMO) orbital overlap, thus

yielding an 18e, saturated metal centre. In the case of intermediate **E**, however, the filled orbital on N is forced to point away from the metal centre by the conformation of the ring (case **III**). Little orbital overlap is possible, which in turn leads to the Lewis basicity of the imido N and Lewis acidity of the metal centre. In comparison, the two larger, accessible lobes are exterior to the azametallacycle in the analogous zirconocene LUMO (case **IV**, lower Cp omitted for clarity).[58] One of the lobes is situated adjacent to the imide N, suggesting that significant N(p)-Zr(LUMO) overlap is possible, stabilizing these complexes towards reaction with electrophiles.

3.2.5 Towards Releasing the Organic Fragment from the Tungsten Centre

Unlike the Group 4 analogues which release the organic fragment readily under protonolysis conditions, these Group 6 heterocycles resist elimination from the tungsten centre under similar conditions. Exposure of NMR-scale samples of **3.2**, **3.3**, **3.8**, and **3.10** to gaseous HCl (excess) in gas-tight NMR tubes does result in a colour change in each case. However, the NMR spectra recorded for each of these samples reveals that the organic fragment remains bound to W, with characteristic signals for the metallacycle in each case being identifiable. The reactions of HCl with **3.2** and **3.3** are particularly clean, and brown crystalline solids are isolable from these two samples following cooling of their solutions for 2 d in a freezer. Mass spectral data for the solids indicate that the ethoxide ligand in the former and the hydroxyl ligand in the latter have been exchanged for a chloride ligand, presumably in a protonolysis reaction (eq 3.13).

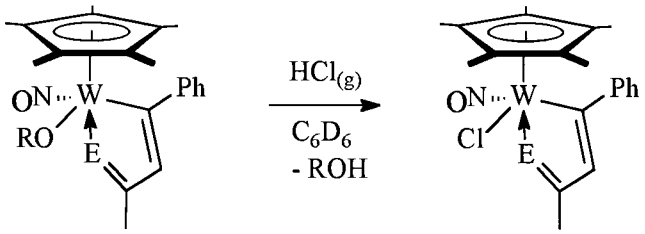

(eq 3.13)

3.2 R = Et, E = O
3.3 R = H, E = HN

EIMS (E = O): $[P^+] = 529$, $[P^+ - NO] = 499$
EIMS (E = HN): $[P^+] = 528$, $[P^+ - NO] = 498$

No further reaction occurs upon exposing these samples to a second excess of HCl, nor may any further reaction be induced by heating these latter samples to 50 °C, indicating that the congeneric chloride complexes of these metallacycles are both thermodynamically robust and stable towards further protonation.

3.3 Epilogue and Future Work

In this chapter, the products of coupling of esters, nitriles, and acetone with coordinated phenyl acetylene in the coordination sphere of the Cp*W(NO) template are described. An underlying theme of the chemistry, which is in contrast to previously published work involving the isolobal zirconocene system, is the quest for electronic saturation by the transient 16e intermediates so formed. A number of reaction pathways can be made available to this system dependent upon the reaction conditions employed. In the case involving coupling to esters, β-C-O bond cleavage in the putative 16e intermediate oxametallacyclopentene complex affords alkoxide-containing, 18e oxametallacyclopentadiene complexes. In nitrile solvent, the proposed 16e azametallacyclopentadiene complex is trapped by protonation of the basic imine N by water, allyl alcohol, or CpH. Coordination of the conjugate base thus fulfills the electronic requirements of the metal, yielding 18e compounds. In the last case, the tautomeric

aminopentafulvene ligand is formed, a ligand which exhibits interesting fluxional behaviour at room temperature in solution. In the presence of acetone, the intermediate azametallacyclopentadiene complex is trapped by a chemo- and regioselective ring-expanding addition of ketone. In the absence of any trapping agent, a second equivalent of RCN inserts in a manner analogous to acetone, and a subsequent intermolecular proton shift affords the observed vinyl amidinate complex. Coupling of coordinated acetylene and acetone yields a novel trimetallic complex, the monomeric units being connected by an unusual bridging isonitrosyl linkage. The products of these coupling reactions lend considerable support to the proposed intermediacy of acetylene-containing **A**. A kinetic study of these transformations implicates a mechanism involving rate-limiting elimination of $SiMe_4$ from the parent bis(hydrocarbyl) complex. In all cases studied, reaction ensues beyond the initial coupling event until electron saturation of the metal centre is achieved. This phenomenon has been rationalized through a qualitative discussion of frontier orbitals; an incompatibility of the heteroatom lone-pair orbital(s) with the metal-centred LUMO in the proposed 16e transient species results in a Lewis-acidic metal centre and nucleophilic heteroatom. This incompatibility is in direct contrast electronic configuration achievable by the analogous zirconocene system and reflects the difference in electronic structure of the two systems. The scope of the reactivity that results is an extension of, and provides an interesting contrast to, the body of work surrounding the analogous zirconocene system.

A number of small projects can be envisioned to stem from the chemistry described in this chapter. In particular, it is apparent from the results described above that the judicious addition of reagents affords novel metallacycles of new and interesting compositions. In light of the fact that coupling with acetone affords an electronically-unsaturated oxametallacycle complex which traps itself to form a trimetallic species, the thermolyses of **1** in acetone containing various trapping agents might afford different types of products relative to those derived from the analogous reactions with nitriles.

The formation of chloride-containing metallacycles by the reaction of HCl with **3.2**, **3.3**, **3.8**, and **3.10** is potentially useful if the resultant chloride ligand can be metathesized in the presence of organometallic transfer agents such as allyl Grignard or phenylvinyl Grignard. If such metathesis reactions are successful, a wealth of interesting metallacycles containing unsaturated organic ligands could be prepared, and their thermal stability towards further coupling investigated. Analogous coupling of acetylide and allyl ligands in the coordination sphere of the CpM(NO) fragment [M = Group 6 metal] is currently being investigated by Ipatkschi *et al.*[59]

3.4 Experimental Procedures

3.4.1 General Methods.

All reactions and subsequent manipulations were performed under anaerobic and anhydrous conditions using procedures described in Section 2.4.1 of Chapter 2.

3.4.2 Reagents

Ethyl acetate, methyl acetate, acetonitrile, propionitrile, isobutyronitrile, *t*-butyl nitrile, benzonitrile and allyl alcohol (Aldrich) were distilled or vacuum-transferred from CaH_2. Acetone was refluxed over anhydrous $CaSO_4$, distilled onto anhydrous $CaSO_4$, and vacuum-transferred as needed. CpH was cracked from cylopentadiene dimer and stored at –35 °C in the dark. Wet acetonitrile was prepared by deaerating HPLC-grade solvent obtained directly from Aldrich or by adding microliter amounts of distilled, deionized water to rigorously dried acetonitrile via a microsyringe. Acetonitrile-d_3 (CIL) was dried over CaH_2 and vacuum-transferred. Deuterated water (CIL) was deaerated under a flow of argon immediately prior to use. Where appropriate, NOE, HMQC, HMBC and gate-decoupled ^{13}C experiments were performed to facilitate ^{1}H and ^{13}C spectral assignments.

3.4.3 Kinetic Studies.

Kinetic studies were performed using gas-tight quartz cells and an HP8452 UV-vis spectrometer equipped with a thermostatted cell holder connected to a VWR 1150 constant-temperature bath which was accurate to ± 0.05 °C. Typical kinetic runs monitored the change in absorbance at

wavelengths of 336 or 360 nm arising from the thermolysis of 0.1 - 1 mg of **1** dissolved in 3 mL of solvent over not less than 3.5 half-lives. Reported k_{obs} values are the average of at least three replicate runs under identical conditions. Fresh solvent mixtures were prepared for each kinetic run performed as a part of the saturation study. Microsyringes were utilized to deliver the appropriate volume of solvent into the cuvette. In each case, the total volume of solvent was 3.00(15) mL. Absorbence values for t_∞ were obtained by optimization of the squared residual, R^2, for the regression line fitted to the data through a first-order analysis. The optimized A_∞ values agreed within 7% with those determined experimentally for selected runs.

3.4.4 Syntheses

Physical and spectroscopic data for each new organometallic complex discussed in this chapter are collected in tables that appear at the end of Section 3.4. A numbering scheme, list of yields, and analytical data for compounds **2.1** – **2.12** are collected in Table 3.3. Mass spectrometric and IR spectroscopic data are collected in Table 3.4, and ^1H and ^{13}C NMR spectroscopic data appear in Table 3.5.

3.4.4.1 Preparation of Cp*W(NO)(OMe)(η^2-*O*=C(Me)CH=*C*Ph) (3.1).

Cp*W(NO)(CH_2SiMe_3)(CPh=CH_2) (**1**, 135 mg, 0.250 mmol) was dissolved in MeOAc (10 mL) in a thick-walled bomb. The resulting deep red solution was heated at 45 °C for 24 h, during which time its colour changed to purple. Solvent was removed from the final solution in vacuo, and the purple residue was extracted with a minimum of a CH_2Cl_2/hexanes mixture (1:1). The extract was filtered through a plug of Celite (1.5 × 0.5 cm) supported on a frit, and the volume of the filtrate was reduced in vacuo. Cooling of the concentrated solution to -30 °C overnight induced the deposition of dark purple needles of complex **3.1** (89 mg) which were

isolated by removal of the supernatant solution. A second crop of crystals (28 mg) was obtained by reducing the volume of the supernatant solution and cooling for a further 24 h.

3.4.4.2 Preparation of Cp*W(NO)(OEt)(η²-*O*=C(Me)CH=*C*Ph) (3.2).

Complex **3.2** was prepared in a manner analogous to that described in the preceding paragraph for **3.1**. After having been heated for 24 h, the reaction mixture was reduced in volume, and the burgundy solution was cooled to -30 °C overnight to induce the deposition of **3.2** as analytically pure needles (112 mg) which were isolated by removal of the supernatant solution and subsequent drying under vacuum.

3.4.4.3 Preparation of Cp*W(NO)(OH)(η²-H*N*=C(Me)CH=*C*Ph) (3.3).

Reactant **1** (135 mg, 0.250 mmol) was dissolved in wet MeCN (10 mL) in a thick-walled bomb. The solution was heated for 24 h at 45 °C, whereupon it became light orange in colour and a red crystalline solid deposited in the bottom of the bomb. The orange supernatant solution was removed by pipette, and the crystals were dried under vacuum. The supernatant solution was filtered through a Celite plug (1.5 × 0.5 cm), and the volume of the filtrate was reduced in vacuo. The resulting dark orange solution was then cooled to -32 °C overnight to induce the deposition of a second fraction of **3.3** as orange microcrystals (107 mg) which were isolated as described above.

3.4.4.4 Preparation of Cp*W(NO)(OD)(η²-D*N*=C(Me)CH=*C*Ph) (3.3-d_2).

Complex **3.3-d_2** was prepared in a manner similar to that employed for **3.3** (vide supra) except that reactant **1** (135 mg, 0.250 mmol) was first dissolved in dry MeCN (10 mL), and the red solution was then doped with D_2O (25 μL, 1.4 mmol). After thermolysis, the dark orange solution was concentrated and cooled to induce crystallization. Red crystalline **3.3-d_2**, isolated by removal of the solvent and washing with Et_2O, was characterized by EI-MS and by comparison of its ^1H NMR spectroscopic properties to those displayed by **3.3**.

3.4.4.5 Preparation of Cp*W(NO)(OH)(η²-H*N*=C(Et)CH=*C*Ph) (3.4) and Cp*W(NO)(OH)(η²-H*N*=C(ⁱPr)CH=*C*Ph) (3.5).

Both complexes **3.4** and **3.5** were prepared in a manner similar to that employed for **3.3**. Following the thermolyses, the final reaction mixtures were concentrated and cooled to -32 °C overnight to induce the deposition of **3.4** as red needles (82 mg) and **3.5** as red blocks (87 mg). Further concentration and cooling of the supernatant solutions afforded second crops of the products (18 mg of **3.4** and 25 mg of **3.5**) which were isolated by removal of the mother liquor and drying under vacuum.

3.4.4.6 Preparation of Cp*W(NO)($OCH_2CH=CH_2$)(η²-H*N*=C(Me)CH=*C*Ph) (3.6).

Complex **3.6** was prepared in a manner identical to that for **3.4**, except that allyl alcohol (280 μL, 16 equiv) was added via microsyringe in place of the water. The final dark orange solution was concentrated and cooled twice to obtain red needles of **3.6** in two crops (78 mg and 33 mg). The crystals were isolated and dried in the usual fashion.

3.4.4.7 Preparation of Cp*W(NO)(HNC(=C(C_4H_4))(Me))(η^2-*N*H=C(Me)CH=*C*Ph) (3.7).

Complex **3.7** was prepared in a manner identical to that for **3.4**, except that excess CpH was added via syringe in the place of water. The thermolyzed dark red solution was concentrated and cooled to obtain **3.7** as dark red needles (112 mg) after isolation and drying under high vacuum.

3.4.4.8 Preparation of Cp*W(NO)(η^3-*O*C(Me)$_2$*N*=C(Me)CH=*C*Ph) (3.8).

Complex **3.8** was prepared in a manner identical to that for **3.7**, except that excess acetone was added by vacuum-transfer onto a frozen MeCN solution of **1** (135 mg, 0.250 mmol). After thermolysis, the resultant red-brown solution was concentrated and cooled to obtain **3.8** as brown irregular blocks (99 mg) after isolation and drying under high vacuum.

3.4.4.9 Preparation of Cp*W(NO)(η^3-*O*C(Me)$_2$*N*=C(^{i}Pr)CH=*C*Ph) (3.9).

Complex **3.9** was prepared in a manner analogous to that for **3.8** and was isolated in two crops as brown-red blocks (102 mg) by concentration and cooling of the final reaction mixture.

3.4.4.10 Preparation of Cp*W(NO)(η^3-H*N*C(Me)=*N*C(=CH_2)CH=*C*Ph) (3.10).

Reactant **1** (270 mg, 0.500 mmol) was dissolved in MeCN (20 mL) in a thick-walled bomb, and the solution was heated for 24 h at 50 °C. The final blood-red solution was taken to dryness under reduced pressure, and the residue was triturated with pentane (3 × 5 mL), washed

with Et_2O (3 × 5 mL), and dried under high vacuum. The remaining solid was dissolved in a minimum volume of CH_2Cl_2/hexanes (1:1), and the solution was filtered through Celite (1 × 2 cm plug). The filtrate was reduced in volume and cooled to -32 °C overnight. Complex **3.10** was isolated the next day as a dark red microcrystalline powder (207 mg) after removal of the supernatant solution and drying under vacuum.

3.4.4.11 Preparation of Cp*W(NO)(η³-D*N*C(CD₃)=*N*C(=CD₂)CH=*C*Ph) (3.10-d_6).

Complex **1** (30 mg, 0.056 mmol) was dissolved in MeCN-d_3 (0.5 mL) in an NMR tube and was heated at 45 °C for 24 h. The solvent was then removed in vacuo, and the red solid was washed twice with Et_2O and dried under high vacuum for 4 h. Characterization of **3.10-d_6** was effected by EI-MS and by comparison of its ^{1}H NMR spectrum ($CDCl_3$) to that exhibited by **3.10**.

3.4.4.12 Preparation of Cp*W(NO)(η³-H*N*C(Et)=*N*C(=CHMe)CH=*C*Ph) (3.11).

Complex **3.11** was prepared in a manner identical to that for **3.10** except that the dark red-brown solution produced by thermolysis was reduced in volume and cooled overnight twice to induce the deposition of two crops of **3.11** (96 mg total) as brown, analytically pure microcrystals.

3.4.4.13 Preparation of [Cp*W(η²-OC(Me)₂CHCPh)(σ,μ-NO)]₃ (3.12).

Complex **1** (45 mg, 0.083 mmol) was dissolved in acetone (2 mL) in a small thick-walled glass bomb and placed in a constant temperature bath at 45 °C for 28 h. After this time, the red

solution was transferred to a vial in the glovebox and its volume reduced (ca. 1 mL). Cooling of the solution to –35 °C for 8 days resulted in the deposition of **3.12** as red blocks (23 mg).

3.4.4.14 Reaction of 3.3 with D_2O.

Complex **3.3** (20 mg, 0.040 mmol) was dissolved in MeCN-d_3 (0.5 mL) in an NMR tube, and D_2O (10 mL, 0.56 mmol) was added. The resulting solution was heated at 45 °C overnight, and its ^1H NMR spectrum was then recorded. Quantitative formation of **3.3-d_2** was indicated by a comparison of this spectrum to that exhibited by an authentic sample of **3.3-d_2**.

3.4.4.15 Thermolysis of 4 in EtOAc.

Complex **3.3** (20 mg, 0.040 mmol) was dissolved in EtOAc (3 mL) in a glass bomb and heated for 24 h at 45 °C. The volatiles were removed under vacuum after cooling of the orange solution. Comparison of the ^1H NMR spectrum ($CDCl_3$ solution) of the resultant orange solid to that of authentic **3.3** indicated no reaction during thermolysis in EtOAc.

3.4.4.16 Thermolysis of 3.6 in CD_3NO_2 containing D_2O.

Complex **3.6** (15 mg) was dissolved in CD_3NO_2 and D_2O (2 μL) was added. After thermolysis at 50 °C for 16 h, the ^1H NMR spectrum of the mixture was recorded. Signals attributable to **3-d_2** and free allyl alcohol indicated partial conversion. Further heating for an additional 72 h resulted in ~35% conversion to **3**, as evinced in the ^1H NMR spectrum of the solution.

3.4.4.17 Thermolysis of 3.8 in THF-d_8 containing D_2O.

Complex **3.8** (15 mg) was dissolved in THF-d_8 and D_2O (2 μL) was added to the solution. After thermolysis of the mixture at 50 °C for 16 h, the ^1H NMR spectrum was recorded. Only signals attributable to **3.8** were evident, indicating no conversion to **3.3-d$_2$**.

3.4.4.18 Thermolysis of 1 in MeCN containing 2, 5, and 10 equiv of H_2O.

Reactant **1** (30.0 mg, 55.6 μmol) was dissolved in dry MeCN (6.0 mL), and the resulting solution was divided into three 2-mL aliquots which were placed into three glass bombs. Two, five, and ten equivalents of water (0.7 μL, 1.7 μL, and 3.5 μL) were added to the first, second, and third bombs, thereby affording solutions with $[H_2O]$ = 19, 47, and 95 mM, respectively. Following thermolyses at 45 °C for 24 h, the volatiles were removed from the final mixtures under high vacuum, and the red-orange residues were taken up in $CDCl_3$ (0.5 mL). The ^1H NMR spectra of the three resulting solutions were recorded and compared to the ^1H NMR spectrum ($CDCl_3$) of an equimolar mixture of authentic **3.10** and **3.3**, revealing that in only the case where $[H_2O]$ = 19 mM was **3.10** observed to form, in approximately 5%. The formation of **3.3** was quantitative for $[H_2O] \geq 47$ mM.

3.4.4.19 Thermolysis of 3.10 in THF-d_8 containing D_2O.

An excess of D_2O was added via microsyringe to a solution of pure **3.10** dissolved in THF-d_8. The solution was placed in a thermostatted water bath at 55 °C, and its ^1H NMR spectra were recorded at regular intervals over a 48 h period. The resulting spectra revealed quantitative conversion to **3.10-d$_6$** by comparison to the proton spectra of authentic **3.10** and **3.10-d$_6$**.

3.4.4.20 Thermolysis of 3.10-d_6 and 3.11 in THF-d_8.

The crossover experiment involving equimolar amounts of **3.10-d_6** and **3.11** dissolved in THF-d_8 was performed. An initial ^{1}H NMR spectrum was recorded, and the solution was then placed in a 65 °C oil bath for 72 h, during which time its ^{1}H NMR spectra were recorded at regular intervals. The progress of the experiment was followed by comparison of the resultant spectra to those for authentic **3.10** and **3.11** and revealed an intermolecular exchange process between the acidic sites in the two compounds.

Table 3.3.. Numbering scheme, yield, and analytical data for complexes **3.1 – 3.12**

Complex	compd no.	colour (yield, %)	anal. found (calcd) C	H	N
Cp*W(NO)(OMe)(η^2-*O*=C(Me)CH=*C*Ph)	**3.1**	purple (89)	47.96 (47.99)	5.09 (5.18)	2.50 (2.67)
Cp*W(NO)(OEt)(η^2-*O*=C(Me)CH=*C*Ph)	**3.2**	purple (83)	48.77 (49.00)	5.35 (5.42)	2.47 (2.60)
Cp*W(NO)(OH)(η^2-H*N*=C(Me)CH=*C*Ph)•0.5MeCN	**3.3•0.5MeCN**	orange (84)	47.52 (47.15)	5.27 (5.22)	7.04 (6.60)
Cp*W(NO)(OD)(η^2-D*N*=C(Me)CH=*C*Ph)	**3.3-d_2**	orange (>95)[a]	n/a[b]	n/a	n/a
Cp*W(NO)(OH)(η^2-H*N*=C(Et)CH=*C*Ph)	**3.4**	red-orange (92)	44.64 (48.99)	5.15 (5.79)	5.12 (5.19)
Cp*W(NO)(OH)(η^2-H*N*=C(^{i}Pr)CH=*C*Ph)	**3.5**	red-orange (83)	48.39 (48.11)	5.57 (5.38)	5.49 (5.34)
Cp*W(NO)(OCH$_2$CH=CH$_2$)(η^2-H*N*=C(Me)CH=*C*Ph)	**3.6**	red-orange (81)	47.52 (50.20)	5.00 (5.49)	4.65 (5.09)
Cp*W(NO)(HNC(=C(C$_4$H$_4$))(Me)) (η^2-H*N*=C(Me)N=C(Me)CH=*C*Ph)•1MeCN	**3.7•MeCN**	deep red (75)	54.63 (54.39)	5.75 (5.66)	8.82 (8.75)
Cp*W(NO)(η^3-*O*C(Me)$_2$*N*=C(Me)CH=*C*Ph)	**3.8**	red-brown (72)	[b]		
Cp*W(NO)(η^3-*O*C(Me)$_2$*N*=C(^{i}Pr)CH=*C*Ph)	**3.9**	red-brown (71)	52.56 (52.92)	5.94 (5.92)	5.01 (4.84)
Cp*W(NO)(η^3-H*N*C(Me)=*N*C(=CH$_2$)CH=*C*Ph)	**3.10**	dark red (77)	48.90 (49.52)	5.09 (5.10)	6.69 (7.88)
Cp*W(NO)(η^3-D*N*C(CD$_3$)=*N*C(=CD$_2$) CH=*C*Ph)	**3.10-d_6**	dark red (95)[a]	[b]		
Cp*W(NO)(η^3-H*N*C(Et)=*N*C(=CHMe)CH=*C*Ph)	**3.11**	red-brown (68)	51.59 (51.32)	5.53 (5.57)	7.55 (7.49)
[Cp*W(η^2-*O*C(Me)$_2$CH=*C*Ph)(σ,μ-NO)]$_3$	**3.12**	red (57)	[b]		

[a] yield as indicated in the ^{1}H NMR spectrum of the reaction mixture. [b] Satisfactory analysis was not obtained.

Table 3.4. Mass spectroscopic data and IR spectral data for complexes **3.1** - **3.12**.

Compd no.	MS (m/z)[a]	probe temp[b] (°C)	IR (Nujol, cm^{-1})
3.1	539	200	1532 (ν_{NO})
3.2	525	150	1538 (ν_{NO})
3.3	510	150	3562 (ν_{OH}) 1532 (ν_{NO})
3.3-d_2	512	120	2630 (ν_{OD}) 2282 (ν_{ND}) 1531 (ν_{NO})
3.4	494 [P^+-NO]	150	3580(ν_{OH}) 1587 ($\nu_{C=N}$) 1535 (ν_{NO})
3.5	508 [P^+-NO]	150	3578(ν_{OH}) 1733 ($\nu_{C=N}$) 1588 (ν_{NO})
3.6	550	150	1730 ($\nu_{C=N}$) 1589 (ν_{NO})
3.7	599	150	1730 ($\nu_{C=N}$) 1589 (ν_{NO})
3.8	550	150	
3.9	578	150	1598 ($\nu_{C=N}$) 1542 (ν_{NO})
3.10	533[c]	80	[d] 3268 (ν_{NH}) 1614 ($\nu_{C=N}$) 1590 ($\nu_{C=C}$) 1517 (ν_{NO})
3.10-d_6	539	n/a	n/a[e]
3.11	561	150	1598 ($\nu_{C=N}$) 1529 (ν_{NO})
3.12	[f]		

[a] Values for the highest intensity peak of the calculated isotopic cluster (^{184}W). [b] Probe temperatures. [c] High-resolution EI mass spectrum (150 °C), found (calcd): 533.16608 (533.16638), [$C_{22}H_{27}N_3O^{184}W$, P^+]; 503.16662 (503.16837), [P^+-NO]. [d] KBr pellet. [e] NMR tube reaction. [f] A satisfactory mass spectral analysis could not be obtained.

Table 3.5. ^{1}H and ^{13}C NMR spectroscopic data for complexes **3.1 – 3.12**.

compd no.	^{1}H NMR[a] δ	^{13}C NMR[a] δ
3.1	7.60 (d, 2H, $^{3}J_{HH}$ = 7.2 Hz, Ph o-H) 7.37 (s, 1H, CPh=C*H*) 7.31 (vt, 2H, $^{3}J_{HH}$ = 7.2 Hz, Ph m-H) 7.29 (vt, 1H, $^{3}J_{HH}$ = 7.5 Hz, Ph p-H) 4.42 (s, 3H, MeO) 2.44 (s, 3H, MeC=O) 1.72 (s, 15H, C_5Me_5)	251.3 (O=*C*Me) 204.8 (*C*Ph=CH) 150.1 (Ph i-C) 136.2 (CPh=*C*H) 128.5 (Ph) 127.9 (Ph) 127.0 (Ph) 112.7 (C_5Me_5) 62.6 (OMe) 26.3 (*Me*C=O) 9.2 (C_5Me_5)
3.2	7.50 (d, 2H, $^{3}J_{HH}$ = 8.4 Hz, Ph o-H) 7.19 (vt, 2H, $^{3}J_{HH}$ = 7.2 Hz, Ph m-H) 7.18 (s, 1H, CPh=C*H*) 7.17 (vt, 1H, $^{3}J_{HH}$ = 7.2 Hz, Ph p-H) 4.49 (dq, 1H, OCH_aH$_b$CH$_3$) 4.35 (dq, 1H, OCH$_a$$H_bCH_3$) 2.32 (s, 3H, O=CMe) 1.59 (s, 15H, C_5Me_5) 1.14 (t, 3H, OCH$_2$*Me*)	250.7 (O=*C*Me) 204.7 (*C*Ph=CH) 150.1 (Ph i-C) 136.2 (d, $^{1}J_{CH}$ = 158.6 Hz, CPh=*C*H) 128.5, 127.9, 127.2, (C_6H_5) 112.7 (C_5Me_5) 69.8 (t, $^{1}J_{CH}$ = 133.7 Hz, O*C*H$_2$Me) 26.2 (q, $^{1}J_{CH}$ = 127.4 Hz, *Me*C=O) 21.4 (q, $^{1}J_{CH}$ = 127.7 Hz, OCH$_2$*Me*) 9.4 (q, $^{1}J_{CH}$ = 127.7 Hz, 127.5, C_5Me_5)
3.3	8.69 (br s, 1H, NH) 7.55 (d, 2H, $^{3}J_{HH}$ = 6.9 Hz, Ph o-H) 7.27 (vt, 2H, $^{3}J_{HH}$ = 7.2 Hz, Ph m-H) 7.18 (vt, 1H, $^{3}J_{HH}$ = 6.9 Hz, Ph p-H) 7.06 (d, 1H, $^{4}J_{HH}$ = 3.5 Hz, CPh=C*H*) 2.25 (s, 3H, HN=C*Me*) 1.67 (s, 15H, C_5Me_5) 0.86 (br s, 1H, OH)	229.5 (s, *C*Ph=CH) 182.6 (s, HN=*C*Me) 150.9 (s, Ph i-C) 135.2 (d, $^{1}J_{CH}$ = 155.8 Hz, CPh=*C*H) 127.8 (d, $^{1}J_{CH}$ = 156.7 Hz, Ph) 127.7 (d, $^{1}J_{CH}$ = 156.7 Hz, Ph) 127.3 (d, $^{1}J_{CH}$ = 158.8 Hz, Ph) 112.0 (s, C_5Me_5) 23.6 (q, $^{1}J_{CH}$ = 132.0 Hz, HN=C(*Me*)) 9.7 (q, $^{1}J_{CH}$ = 127.4 Hz, C_5Me_5)

Table 3.5 continued.

compd no.	^{1}H NMR[a] δ	^{13}C NMR[a] δ
3.3-d_2	7.55 (d, 2H, $^3J_{HH}$ = 6.9 Hz, Ph o-H) 7.27 (vt, 2H, $^3J_{HH}$ = 7.2 Hz, Ph m-H) 7.18 (vt, 1H, $^3J_{HH}$ = 6.9 Hz, Ph p-H) 7.06 (s, 1H, CPh=C*H*) 2.25 (s, 3H, ND=C*Me*) 1.67 (s, 15H, C_5Me_5)	*b*
3.4	8.59 (br s, 1H, NH) 7.58 (d, 2H, $^3J_{HH}$ = 7.2 Hz, Ph o-H) 7.29 (vt, 2H, $^3J_{HH}$ = 7.2 Hz, Ph m-H) 7.18 (vt, 1H, $^3J_{HH}$ = 6.8 Hz, Ph p-H) 7.11 (d, 1H, $^4J_{HH}$ = 3.5 Hz, CPh=C*H*) 2.56 (mult, 2H, $^2J_{HH}$ = 2.0 Hz, $^3J_{HH}$ = 7.3 Hz, CH_2Me) 1.68 (s, 15H, C_5Me_5) 1.20 (dt, 3H, $^3J_{HH}$ = 7.3 Hz, CH_2*Me*) 0.83 (br s, 1H, OH)	228.9 (s, *C*Ph=CH) 187.7 (s, HN=*C*Et) 151.3 (s, Ph i-C) 134.5 (d, $^1J_{CH}$ = 157.8 Hz, CPh=*C*H_2) 127.7 (d, $^1J_{CH}$ = 157.2 Hz, Ph) 127.2 (d, $^1J_{CH}$ = 157.2 Hz, Ph) 127.0 (d, $^1J_{CH}$ = 157.2 Hz, Ph) 112.0 (s, C_5Me_5) 30.1 (t, $^1J_{CH}$ = 129.6 Hz, *C*H_2Me) 11.0 (q, $^1J_{CH}$ = 127.7Hz, CH_2*Me*) 9.6 (q, $^1J_{CH}$ = 127.8Hz, C_5*Me*$_5$)
3.5	8.71 (br s, 1H, NH) 7.45 (d, 2H, $^3J_{HH}$ = 6.9 Hz, Ph o-H) 7.26 (vt, 2H, $^3J_{HH}$ = 6.9 Hz, Ph m-H) 7.19 (vt, 1H, $^3J_{HH}$ = 6.8 Hz, Ph p-H) 7.01 (d, 1H, $^4J_{HH}$ = 3.0 Hz, CPh=C*H*) 2.76 (sept, 1H, $^3J_{HH}$ = 6.9 Hz, C*H*Me_2) 1.77 (s, 15H, C_5Me_5) 1.20 (d, 3H, $^3J_{HH}$ = 6.9 Hz, CH*Me*$_2$) 0.82 (br s, 1H, OH)	227.8 (*C*Ph=CH) 195.9 (HN=*C*^{i}Pr) 151.3 (Ph i-C) 132.2 (CPh=*C*H_2) 128.1 (Ph) 127.9 (Ph) 127.0 (Ph) 110.3 (s, C_5Me_5) 36.3 (*C*HMe_2) 20.7 (CH*Me*$_2$) 20.6 (CH*Me*$_2$) 10.3 (C_5*Me*$_5$)

Table 3.5 continued.

compd no.	^{1}H NMR[a] δ	^{13}C NMR[a] δ
3.6	8.62 (br s, 1H, NH) 7.62 (d, 2H, $^3J_{HH}$ = 7.2 Hz, Ph o-H) 7.29 (vt, 2H, $^3J_{HH}$ = 7.2 Hz, Ph m-H) 7.21 (vt, 1H, $^3J_{HH}$ = 7.2 Hz, Ph p-H) 7.14 (d, 1H, $^4J_{HH}$ = 3.0 Hz, CPh=C*H*) 6.01 (m, 1H, $OCH_2CH{=}CH_2$) 5.22 (m, 1H, $OCH_2CH{=}CH_2$) 4.92 (m, 1H, $OCH_2CH{=}CH_2$) 4.60 (m, 2H, $OCH_2CH{=}CH_2$) 2.31 (s, 3H, HN=N*Me*) 1.67 (s, 15H, C_5Me_5)	229.0 (s,*C*Ph=CH_2) 181.8 (s, HN=*C*Me) 151.1 (s, Ph i-C) 143.8 (d, $^1J_{CH}$ = 149.4 Hz, $OCH_2CH{=}CH_2$) 135.0 (d, $^1J_{CH}$ = 159.4 Hz, CPh=CH_2) 127.5 (d, $^1J_{CH}$ = 156.5 Hz, Ph) 127.1 (d, $^1J_{CH}$ = 156.5 Hz, Ph) 126.9 (d, $^1J_{CH}$ = 156.5 Hz, Ph) 112.1 (s, C_5Me_5) 111.6 (t, $^1J_{CH}$ = 153.8 Hz, $OCH_2CH{=}CH_2$) 74.9 (t, $^1J_{CH}$ = 131.4 Hz, $OCH_2CH{=}CH_2$) 23.4 (q, $^1J_{CH}$ = 128.1 Hz, HN=C*Me*) 9.5 (q, $^1J_{CH}$ = 127.3 Hz, C_5Me_5)
3.7	8.11 (br s, 1H, *H*N=CMe) 7.53 (d, 2H, $^3J_{HH}$ = 8.1 Hz, Ph o-H) 7.24 (vt, 2H, $^3J_{HH}$ = 8.1 Hz, Ph m-H) 7.21 (vt, 1H, $^3J_{HH}$ = 8.1 Hz, Ph p-H) 7.06 (d, 1H, $^4J_{HH}$ = 3.0 Hz, CPh=C*H*) 6.52 (br s, 1H, *H*N-C(=C(C_4H_4))Me) 6.50 (br s, 1H, HNC(=C($C_2H_aH_bC_2H_2$))Me) 6.44 (br s, 1H, HNC(=C($C_2H_aH_bC_2H_2$))Me) 6.23 (br s, 1H, HNC(=C($C_2H_2C_2H_aH_b$))Me) 6.10 (br s, 1H, HNC(=C($C_2H_2C_2H_aH_b$))Me) 2.34 (s, 3H, HN=C*Me*) 2.25 (s, 3H, *H*N-C(=C(C_4H_4))*Me*) 1.70 (s, 15H, C_5Me_5)	228.5 (s,*C*Ph=CH) 185.2 (s, HN=*C*Me) 175.9 (s, HN-*C*(=C(C_4H_4))Me) 150.1 (s, Ph i-C) 135.0 (d, $^1J_{CH}$ = 158.5 Hz, CPh=*C*H) 127.9 (d, $^1J_{CH}$ = 159.2 Hz, Ph) 127.2 (d, $^1J_{CH}$ = 159.0 Hz, Ph) 127.1 (d, $^1J_{CH}$ = 159.0 Hz, Ph) 125.1 (br s, HN-C(=*C*(C_4H_4))Me) 117.8 (br s, HN-C(=C(*C*$_4H_4$))Me) 115.6 (br s, HN-C(=C(*C*$_4H_4$))Me) 115.0 (br s, HN-C(=C(*C*$_4H_4$))Me) 111.7 (s, C_5Me_5) 107.5 (br s, HN-C(=C(*C*$_4H_4$))Me) 23.7 (q, $^1J_{CH}$ = 127.9 Hz, N=C*Me*) 21.2 (q, $^1J_{CH}$ = 128.3 Hz, HN-C(fulv)*Me*) 9.7 (q, $^1J_{CH}$ = 128.0 Hz, C_5Me_5)

Table 3.5 continued.

compd no.	^{1}H NMR[a] δ	^{13}C NMR[a] δ
3.8	7.26 (d, 2H, $^3J_{HH}$ = 6.9 Hz, Ph o-H) 7.14 (t, 2H, $^3J_{HH}$ = 6.9 Hz, Ph m-H) 7.08 (t, 1H, $^3J_{HH}$ = 6.9 Hz, Ph p-H) 6.59 (s, 1H, $^3J_{WH}$ = 14 Hz, CPh=C*H*) 1.95 (s, 3H, HN=C*Me*) 1.51 (s, 15H, C_5Me_5) 1.35 (s, 3H, O-CMe_2) 1.20 (s, 3H, O-CMe_2)	226.2 (s, *C*Ph=CH) 170.7 (s, N=*C*Me) 150.3 (s, Ph i-C) 134.5 (d, $^1J_{CH}$ = 157.5 Hz, CPh=*C*H) 127.5 (d, $^1J_{CH}$ = 158.0 Hz, Ph) 126.8(d, $^1J_{CH}$ = 158.0 Hz, Ph) 126.6(d, $^1J_{CH}$ = 158.0 Hz, Ph) 113.0 (s, C_5Me_5) 99.2 (s, (O*C*Me_2) 30.1 (q, $^1J_{CH}$ = 127.5 Hz, O=C*Me*$_2$) 29.0 (q, $^1J_{CH}$ = 127.5 Hz, O=C*Me*$_2$) 18.3 (q, $^1J_{CH}$ = 127.5 Hz, HN=C*Me*) 9.9 (q, $^1J_{CH}$ = 127.5 Hz, C_5*Me*$_5$)
3.9	7.48 (d, 2H, $^3J_{HH}$ = 7.5 Hz, Ph o-H) 7.32 (vt, 2H, $^3J_{HH}$ = 7.5 Hz, Ph m-H) 7.22 (vt, 1H, $^3J_{HH}$ = 7.3 Hz, Ph p-H) 7.06 (s, 1H, $^3J_{WH}$ = 12.1 Hz, CPh=C*H*) 2.84 (sept, 1H, $^3J_{HH}$ = 6.8 Hz, C*H*Me_2) 1.78 (s, 15H, C_5Me_5) 1.70 (s, 3H, O*C*Me_2) 1.48 (s, 3H, O*C*Me_2) 1.28 (d, 3H, $^3J_{HH}$ = 6.8 Hz, CH*Me*$_2$) 1.26 (d, 3H, $^3J_{HH}$ = 6.8 Hz, CH*Me*$_2$)	226.2 (s, *C*Ph=CH) 180.5 (s, N=*C*^{i}Pr) 150.7 (s, Ph i-C) 129.5 (d, $^1J_{CH}$ = 159.0 Hz, CPh=*C*H) 127.6 (d, $^1J_{CH}$ = 159.0 Hz, Ph) 127.0 (d, $^1J_{CH}$ = 159.0 Hz, Ph) 126.8 (d, $^1J_{CH}$ = 159.0 Hz, Ph) 112.9 (s, C_5Me_5) 99.4 (s, (O*C*Me_2) 32.1 (d, $^1J_{CH}$ = 130.0 Hz, C*C*HMe_2) 30.8 (q, $^1J_{CH}$ = 124.0 Hz, CCH*Me*$_2$) 30.4 (q, $^1J_{CH}$ = 127.0 Hz, CCH*Me*$_2$) 21.6 (q, $^1J_{CH}$ = 127.0 Hz, O=C*Me*$_2$) 20.4 (q, $^1J_{CH}$ = 127.0 Hz, O=C*Me*$_2$) 10.0 (q, $^1J_{CH}$ =.127.3 Hz, C_5*Me*$_5$)
3.10	7.43 (d, 2H, $^3J_{HH}$ = 8.1 Hz, Ph o-H) 7.26 (vt, 2H, $^3J_{HH}$ = 8.4 Hz, Ph m-H) 7.11 (vt, 1H, $^3J_{HH}$ = 7.5 Hz, Ph p-H) 6.83 (s, 1H, CPh=C*H*) 4.73 (br s, 1H, *H*NC(Me)=) 4.45 (s, 1H, NC=CH_aH$_b$) 4.28 (s, 1H, NC=CH$_a$$H_b$) 2.11 (s, 3H, HNC(*Me*)=) 1.73 (s, 15H, C_5Me_5)	191.8 (*C*Ph=CH) 171.1 (NH*C*(Me)=N) 156.1 (N*C*=CH$_2$) 150.9(Ph i-C) 138.8 (d, $^1J_{CH}$ = 127.7 Hz, CPh=*C*H) 127.7 (Ph) 125.4 (Ph) 111.8 (C_5Me_5) 90.6 (NC=*C*H$_2$, $^1J_{CH}$ = 152 Hz) 22.8 (HNC(*Me*)=) 9.9 (C_5*Me*$_5$)

Table 3.5 continued.

compd no.	^{1}H NMR[a] δ	^{13}C NMR[a] δ
3.10-d_6	7.43 (d, 2H, $^3J_{HH}$ = 8.1 Hz, Ph o-H) 7.26 (vt, 2H, $^3J_{HH}$ = 8.4 Hz, Ph m-H) 7.11 (vt, 1H, $^3J_{HH}$ = 7.5 Hz, Ph p-H) 6.83 (s, 1H, CPh=C*H*) 2.11 (s, 3H, DNC(*Me*)=) 1.73 (s, 15H, C_5Me_5)	[b]
3.11	7.61 (d, 2H, $^3J_{HH}$ = 8.4 Hz, Ph o-H) 7.40 (vt, 2H, $^3J_{HH}$ = 8.4 Hz, Ph m-H) 7.37 (vt, 2H, CPh=C*H*, Ph p-H) 4.83 (q, 1H, $^3J_{HH}$ = 7.2 Hz, C=C*H*Me) 4.68 (br s, 1H, NH) 2.62 (dq, 1H, $^2J_{HH}$ = 2.1 Hz, $^3J_{HH}$ = 7.5 Hz, CH_2Me) 2.51 (dq, 1H, $^2J_{HH}$ = 2.1 Hz, $^3J_{HH}$ = 7.5 Hz, CH_2Me) 1.96 d, 3H, $^3J_{HH}$ = 7.2 Hz, C=CH*Me*) 1.85 (s, 15H, C_5Me_5) 1.32 (t, 3H, $^3J_{HH}$ = 7.5 Hz, CH_2Me)	190.1 (s, *C*Ph=CH) 175.2 (s, NH*C*(Et)=N) 151.6 (s, Ph i-C) 149.5 (s, N*C*=CHMe) 134.5 (d, $^1J_{CH}$ = 157.5 Hz, CPh=*C*H) 127.8 (d, $^1J_{CH}$ = 157.5 Hz, Ph) 127.7 (d, $^1J_{CH}$ = 157.5 Hz, Ph) 125.3 (d, $^1J_{CH}$ = 157.5 Hz, Ph) 111.5 (s, C_5Me_5) 102.9 (d, $^1J_{CH}$ = 158.0 Hz, C=*C*HMe) 27.9 (t, $^1J_{CH}$ = 131.5 Hz, *C*H_2Me) 14.2 (q, $^1J_{CH}$ = 126.8 Hz, C=CH*Me*) 9.7 (q, $^1J_{CH}$ = 132.8 Hz, C_5Me_5) 8.7 (t, $^1J_{CH}$ = 131.5 Hz, CH_2Me)
3.12[c]	7.27(d, $^3J_{HH}$ = 7.2 Hz, 2H, Ph-H_{ortho}) 7.11(t, $^3J_{HH}$ = 7.2 Hz, 2H, Ph-H_{meta}) 6.99 (t, $^3J_{HH}$ = 7.2 Hz, 1H, Ph-H_{para}) 6.41 (s, 1H, CPh=C*H*) 1.61 (s, 15H, C5Me5) 1.29 (s, 3H, Me) 1.28 (s, 3H, Me)	[b]

[a] Sample spectra recorded in $CDCl_3$ unless otherwise noted. [b] Spectrum not recorded. [c] Spectrum recorded in acetone-d_6.

3.5 References and Notes

(1) (a) Collman, J. P.; Hegedus, L. S.; Norton, J. R.; Finke, R. G. *Principles and Applications of Organotransition Metal Chemistry*; University Science Books: Mill Valley, CA, 1987, Chapter 9. (b) Crabtree, R. H. *The Organometallic Chemistry of the Transition Metals,* 2nd ed.; Wiley-Interscience: Toronto, 1994, Chapter 6.

(2) Reppe, W.; Schlichting, O.; Klager, K.; Toepel, T. *Liebigs Ann. Chem.* **1948**, *560*, 1.

(3) This field has been reviewed extensively. See, for example: (a) Vollhardt, K. P. C. *Acc. Chem. Res.* **1977**, *10*, 1. (b) Buchwald, S. L.; Nielsen, R. B. *Chem. Rev.* **1988**, *88*, 1047. (c) Carnahan, E. M.; Protasiewicz, J. D.; Lippard, S. J. *Acc. Chem. Res.* **1993**, *26*, 90. (d) Broene, R. D.; Buchwald, S. L. *Science* **1993**, *261*, 1696.

(4) (a) Erker, G. *J. Organomet. Chem.* **1977**, *134*, 189. (b) Erker, G.; Kropp, K. *J. Am. Chem. Soc.* **1979**, *101*, 3659.

(5) Buchwald, S. L.; Watson, B. T.; Huffman, J. C. *J. Am. Chem. Soc.* **1986**, *108*, 7411.

(6) (a) Buchwald, S. L.; Lum, R. T.; Dewan, J. C. *J. Am. Chem. Soc.* **1986**, *108*, 7441. (b) Buchwald, S. L.; Watson, B. T.; Huffman, J. C. *J. Am. Chem. Soc.* **1987**, *109*, 2544.

(7) Debad, J. D.; Legzdins, P.; Lumb, S. A.; Batchelor, R. J.; Einstein, F. W. B. *J. Am. Chem. Soc.* **1995**, *117*, 3288.

(8) Legzdins, P.; Lundmark, P. J.; Rettig, S. J. *Organometallics* **1993**, *12*, 3545.

(9) Crystals of **3.1** are monoclinic of space group $P2_1/c$ a = 7.24217(3) Å, b = 15.3723(7) Å, c = 17.8615(8) Å, β = 98.962(1) °. Dr. V. G. Young solved the structure using the Patterson method and full-matrix least-squares refinement procedures to R_F = 0.0516 for 3457 reflections with $I_o \geq 3\sigma(I_o)$. Tables of fractional atomic coordinates (Table A16) and bond distances and bond angles (Table A17) in the solid-state structure determined for this compound are found in Appendix A.

(10) Carmona, E.; Gutiérrez-Puebla, E.; Monge, A.; Marín, J. M.; Paneque, M.; Poveda, M. *Organometallics* **1989**, *8*, 967.

(11) Peulecke, N.; Ohff, A.; Tillack, A.; Baumann, W.; Kempe, R.; Burlakov, V. V.; Rosenthal, U. *Organometallics* **1996**, *15*, 1340.

(12) Debad, J. D.; Legzdins, P. *Organometallics* **1993**, *12*, 2094.

(13) (a) Ashby, M. T.; Enemark, J. H. *J. Am. Chem. Soc.* **1986**, *108*, 730. (b) Hubbard, J. L.; McVicar, W. K. *Inorg. Chem.* **1992**, *31*, 910.

(14) For a review of this chemistry, see: Yamamoto, A. *Adv. Organomet. Chem.* **1992**, *34*, 111.

(15) Burkey, D. J.; Debad, J. D.; Legzdins, P. *J. Am. Chem. Soc.* **1997**, *119*, 1139.

(16) (a) Lee, J.; Kim, H.; Cha, J. K. *J. Am. Chem. Soc.* **1996**, *118*, 4198. (b) Lee, J.; Kim, H.; Cha, J. K. *J. Am. Chem. Soc.* **1996**, *118*, 291. (c) Corey, E. J.; Rao, A. R.; Noe, M. C. *J.*

Am. Chem. Soc. **1994**, *116*, 9345. (d) Kulinkovich, O. G.; Sviridov, S. V.; Vasilevskii, D. A. *Synthesis* **1991**, *3*, 234.

(17) A recent theoretical analysis describes ring strain and bond enthalpies as the major contributors to the stability of methylcyclopropane relative to methylcyclopropene. See: Johnson, W. T. G.; Borden, W. T. *J. Am. Chem. Soc.* **1997**, *119*, 5930.

(18) (a) Yamamoto, T.; Miyashita, S.; Naito, Y.; Komiya, S.; Ito, T.; Yamamoto, A. *Organometallics* **1982**, *1*, 808. (b) Hayashi, Y.; Yamamoto, T.; Yamamoto, A.; Komiya, S.; Ito T.; Kushi, Y. *J. Am. Chem. Soc.* **1986**, *108*, 385.

(19) Grotjahn, D. B.; Lo, H. C. *Organometallics* **1996**, *15*, 2860.

(20) For other examples of ketone-stabilized vinyl complexes, see: (a) Alt, H. G.; Eichner, M. E.; Jansen, B. M. *Angew. Chem., Int. Ed. Engl.* **1982**, *21*, 861. (b) Alt, H. G.; Hayen, H. I. *J. Organomet. Chem.* **1986**, *103*, 1501. (c) Bianchini, C.; Innocenti, P.; Melli, A.; Sabat, M. *Organometallics* **1986**, *5*, 72. (d) ref 10.

(21) Crystals of **3.3** are monoclinic of space group $P2_1/n$; a = 8.4729(2) Å, b = 21.2313(5) Å, c = 12.106093) Å, β = 97.483(1)°. Dr. V. G. Young solved the structure using the Patterson method and full-matrix least-squares refinement procedures to $R_F = 0.033$ for 3800 reflections with $I_o \geq 3\sigma(I_o)$. Tables of fractional atomic coordinates (Table A18) and bond distances and angles (Table A19) in the solid-state structure determined for this compound are found in Appendix A.

(22) The complex $[Mo(O)(OH)(CN)_4]^{3-}$ has Mo=O = 1.697 (7) Å and Mo-OH = 2.077 (7) Å; see Robinson, P. R.; Schlemper, E. O.; Murmann, R. K. *Inorg. Chem.* **1975**, *14*, 2035. Typical terminal W-oxo bond distances lie in the range 1.68 - 1.72 Å; see, Nugent, W. A.; Mayer, J. M. *Metal Ligand Multiple Bonds*; Wiley: New York, 1988, Chapter 5.

(23) Aromaticity has been invoked for similar aza- and thiapentadienyl iridium systems; see: (a) Alvarado, Y.; Daff, P. J.; Pérez, P. J.; Poveda, M. L.; Sánchez-Delgado, R.; Carmona, E. *Organometallics* **1996**, *15*, 2192. (b) Bleeke, J. R.; Ontwerth, M. F.; Rohde, A. M. *Organometallics* **1995**, *14*, 2813.

(24) Ebsworth, E. A. V.; Rankin, D. W. H.; Cradock, S. *Structural Methods in Inorganic Chemistry*; Blackwell Scientific Publications: London, 1987; pp. 217-218.

(25) Debad, J. D.; Legzdins, P.; Lumb, S. A. *Organometallics* **1995**, *14*, 2543.

(26) (a) Cohen, S. A.; Bercaw, J. E. *Organometallics* **1985**, *4*, 1006. (b) Lorente, P.; Carfagna, C.; Etienne, M.; Donnadieu, B. *Organometallics* **1996**, *15*, 1090. (c) Strickler, J. R.; Wigley, D. E. *Organometallics* **1990**, *9*, 1665. (d) Filippou, A. C.; Völkl, C.; Kiprof, P. *J. Organomet. Chem.* **1991**, *415*, 375. (e) Filippou, A. C.; Völkl, C.; Rogers, R. D. *J. Organomet. Chem.* **1993**, *463*, 135. (f) ref 23a.

(27) Lowry, T. H.; Richardson, K. S. *Mechanism and Theory in Organic Chemistry*, 2nd ed.; Harper & Row: New York, 1981.

(28) Smith, D. P.; Strickler, J. R.; Gray, S. D.; Bruck, M. A.; Holmes, R. S.; Wigley, D. W. *Organometallics* **1992**, *11*, 1275.

(29) Buchwald, S. L.; Watson, B. T.; Lum, R. T.; Nugent, W. A. *J. Am. Chem. Soc.* **1987**, *109*, 7137.

(30) Crystals of **3.7** are monoclinic of space group $P2_1$; a = 7.2125(1) Å, b = 18.4419(1) Å, c = 11.3542(2) Å, β = 100.348(1)°. Dr. V. G. Young solved the structure using the Patterson method and full-matrix least-squares refinement procedures to $R_F = 0.033$ for 4955 reflections with $I_o \geq 3\sigma(I_o)$. Tables of fractional atomic coordinates (Table A20) and bond distances and angles (Table A21) in the solid-state structure determined for this compound are found in Appendix A.

(31) Chiang, J. F.; Bauer, S. H. *J. Am. Chem. Soc.* **1970**, *92*, 261.

(32) Ammon, H. L. *Acta. Crystallogr. Sect. B* **1974**, *30*, 1731.

(33) The rate of a chemical exchange process at the coalescence temperature of the exchanging magnetic environments is given by the equation $k = \pi\Delta\nu / 2^{1/2}$, where $\Delta\nu$ (Hz) is the frequency separation of the two signals at the low-temperature exchange limit. For more details, see: Günther, H. *NMR Spectroscopy;* Wiley: New York, 1980.

(34) The free energy of activation is determined using the Eyring equation, which takes the form $\Delta G^{\ddagger} = -RT\ln(kh/\kappa k_b T)$, where R is the ideal gas constant (8.314 $JK^{-1}mol^{-1}$), T is the

temperature in units of K, k is the rate constant, h is Planck's constant (6.626×10^{-34} J•s), κ is the transmission coefficient (assumed to be 1 for thermochemical processes), and k_b is Boltzmann's constant (1.381×10^{-23} J/K). For more details, see: Connors, K. A. *Chemical Kinetics: The Study of Reaction Rates in Solution;* VCH Publishers: New York, 1990, Chapter 7.

(35) An *intermolecular* exchange cannot be absolutely discounted, but the steric inaccessibility of the fulvene α-H suggests that such a process is unlikely.

(36) Casey, C. P.; O'Connor, J. M.; Haller, K. J. *J. Am. Chem. Soc.* **1985**, *107*, 1241.

(37) O'Connor, J. M.; Casey, C.P. *Chem. Rev.* **1987**, *87*, 307.

(38) Alías, F. M.; Belderraín, T. R., Paneque, M.; Poveda, M. L.; Carmona, E. *Organometallics* **1997**, *16*, 301.

(39) Crystals of **3.9** are monoclinic of space group $P2_1/c$; a = 10.5087(1) Å, b = 15.4352(2) Å, c = 15.1367(1) Å, β = 94.787(1)°. Dr. V. G. Young solved the structure using the Patterson method and full-matrix least-squares refinement procedures to $R_F = 0.033$ for 4064 reflections with $I_o \geq 3\sigma(I_o)$. Tables of fractional atomic coordinates (Table A22) and bond distances and angles (Table A23) in the solid-state structure determined for this compound are found in Appendix A.

(40) (a) ref 3a. (b) Tebbe, F. N.; Parshall, G. W.; Reddy, G. S. *J. Am. Chem. Soc.* **1978**, *100*, 3611. For more recent examples, see: (c) Bruck, M. A.; Copenhaver, A. S.; Wigley, D. E. *J. Am. Chem. Soc.* **1987**, *109*, 6525. (d) Christensen, N. J.; Legzdins, P. *Organometallics* **1991**, *10*, 3070. (e) Yeh, W.-Y.; Ho, C.-L.; Chiang, M. Y.; Chen, I.-T. *Organometallics* **1997**, *16*, 2698 and references cited therein. (f) Yang, S.-M.; Chan, M. C.-W.; Cheung, K.-K.; Che, C.-M.; Peng, S.-M. *Organometallics* **1997**, *16*, 2819.

(41) (a) ref 26a. (b) Meinhart, J. D.; Grubbs, R. H. *Bull. Chem. Soc. Jpn.* **1988**, *61*, 171. (c) Buchwald, S. L.; Grubbs, R. H. *J. Am. Chem. Soc.* **1983**, *105*, 5490. (d) Yasuda, H.; Okamoto, T.; Mashima, K.; Nakamura, A. L. *J. Organomet. Chem.* **1989**, *363*, 61. (e) Beckhaus, R. *J. Chem. Soc., Dalton Trans.* **1997**, 1991.

(42) For a leading reference, see: Kablaoui, N. M.; Hicks, F. A.; Buchwald, S. L. *J. Am. Chem. Soc.* **1997**, *119*, 4424.

(43) See, for example: (a) Cabeza, J. A.; del Río, I.; Franco, J.; Grepioni, F.; Riera, V. *Organometallics* **1997**, *16*, 2763. (b) Cowan, R. L.; Trogler, W. C. *J. Am. Chem. Soc.* **1989**, *111*, 4750. (c) Bryndza, H. E.; Fultz, W. C.; Tam, W. *Organometallics* **1985**, *4*, 939.

(44) Legzdins, P.; Sayers, S. F. *J. Am. Chem. Soc.* **1994**, *116*, 12105.

(45) Nakamoto, K. *Infrared and Raman Spectra of Inorganic and Coordination Compounds*, 4th ed.; Wiley-Interscience: New York, 1986, Chapter 3.

(46) Yeh, W.-Y.; Ting, C.-S.; Chih, C.-F. *J. Organomet. Chem.* **1991**, *427*, 257.

(47) The formal 1,5-tautomerization can also be viewed as two sequential 1,3-H shifts; the first transfer occurs from the methyl group to the internal imine N, and the second from the internal imine N to the terminal amide N. That the tautomerization is shown to be intermolecular renders these labels formal descriptors only.

(48) For an elegant kinetic and mechanistic study of an analogous intermolecular tautomerization process in $(DIPP)_3Ta(\eta^2\text{-}HNC(=CH_2)C(Ph)=CPh)$, see ref 26c.

(49) The results of this crossover experiment only confirm an intermolecular component to this tautomerization. An intramolecular component cannot be ruled out in the absence of the appropriate kinetic studies.

(50) Shriver, D. F.; Atkins, P. W.; Langford, C. H. *Inorganic Chemistry*; W. H. Freeman and Company: New York, 1990, Chapter 6.

(51) Crystals of **3.12** are monoclinic of space group C2/c; a = 52.169(4) Å, b = 10.9755(10) Å, c = 24.861(2) Å, β = 113.791(3)°. Dr. S. J. Rettig solved the structure using the Patterson method and full-matrix least-squares refinement procedures to $R_F = 0.147$ for 16528 reflections with $I_o \geq 3\sigma(I_o)$. Tables of fractional atomic coordinates (Table A24),bond distances (Table A25) and angles (Table A26) in the solid-state structure determined for this compound are found in Appendix A.

(52) Richter-Addo, G. B.; Legzdins, P. *Metal Nitrosyls*; Oxford University Press: New York, 1992, Chapter 2.

(53) (a) Re: Beringhelli, T.; Ciani, G.; D'Alfonso, G.; Molinari, H.; Sironi, A.; Freni, M. *J. Chem. Soc., Chem. Commun.* **1984**, 1327. (b) Mo/Co: Kyba, E. P.; Kerby, M. C.; Kashyap, R. P.; Mountzouris, J. A.; Davis, R. E. *J. Am. Chem. Soc.* **1990**, *112*, 9905.

(54) Chapter 4 describes the scope of the thermal C-H activation chemistry observed for this system in the presence of a variety of hydrocarbons, including a detailed kinetic and mechanistic analysis of these transformations.

(55) Connors, K. A. *Chemical Kinetics: The Study of Reaction Rates in Solution;* VCH Publishers: New York, 1990; Chapter 8.

(56) (a) McCarthy, T. J.; Nuzzo, R. G.; Whitesides, G. M. *J. Am. Chem. Soc.* **1981**, *103*, 3396. (b) Buchanan, J. M.; Stryker, J. F.; Bergman, R. G. *J. Am. Chem. Soc.* **1986**, *108*, 1537.

(57) (a) Legzdins, P.; Rettig, S. J.; Sánchez, L. J.; Bursten, B. E.; Gatter, M. G. *J. Am. Chem. Soc.* **1985**, *107*, 1411. (b) Bursten, B. E.; Cayton, R. H. *Organometallics* **1985**, *6*, 2004.

(58) Lauer, J. W.; Hoffmann, R. *J. Am. Chem. Soc.* **1976**, *98*, 1729.

(59) Ipaktschi, J.; Mirzaei, F.; Demuth-Eberle, G. J.; Beck, J.; Serafin, M. *Organometallics* **1997**, *16*, 3965.

Chapter 4. Hydrocarbon C-H Bond Activation by the Electronically Unsaturated Acetylene Complex, Cp*W(NO)(η^2-PhC≡CH)

4.1 Introduction

The "activation" of an unfunctionalized hydrocarbon C-H bond by an organometallic complex refers to the cleavage of an inert C-H bond under the influence of the transition metal, generating (at least transiently) a reactive metal-carbon linkage. That certain organometallic complexes are capable of this feat under mild conditions (T < 150 °C) is an attractive feature that has driven research in this area over the past 30 years.[1] Substantial developments in this field began with the discovery of phosphine and amine cyclometallation reactions at metal centres in the 1960s.[2] This advance was followed by the discovery of alkane C-H activation by Pt(II) in 1969,[3] and by Pt(IV),[4a] Pd(II),[4b] Ru(IV),[4c] Co(III),[4d] Ir(III)[4e] and Ti(II)[4f] in the early to mid-1970s.[1] In the ensuing 25 years, a massive research effort by a number of groups worldwide has been focused towards the development of homogeneous organometallic systems that effect the functionalization of aliphatic and aromatic hydrocarbons via C-H activation.[1,5]

If the ultimate goal in this field is the development of organometallic systems capable of the catalytic conversion of hydrocarbon feedstocks into more elaborate functionalized, or utilizable, organic compounds, then there exist two main thrusts in the study of hydrocarbon C-H bond activation by organometallic complexes with this task in mind. The first is the systematic investigation of transition-metal systems capable of activating hydrocarbon C-H bonds, with a view towards understanding the physical and chemical requirements of this mode of reactivity. Towards this end, extensive studies of C-H bond activation by metal complexes of nearly every group in the transition series, in addition to complexes of the lanthanides and actinides, have greatly expanded our understanding of the various mechanisms of C-H bond activation.[1,5]

Equally important, the second goal directed towards the derivatization of hydrocarbons requires the application of this amassed knowledge to the design of systems capable not only of

C-H activation but also of chemical elaboration of the resultant hydrocarbyl fragment. At present, the reactivity of many previously studied systems ceases following the C-H activation event, often as a result of the limitations imposed by the metal's valence-electron shell during the activation process. This state of affairs exists because C-H bond activation is often effected by electronically unsaturated intermediates that are generated from saturated or kinetically stable precursors (e.g. eq 4.1). Cleavage of a hydrocarbyl C-H bond then results in the regeneration of a stable, coordinatively saturated metal centre at which no further chemistry can occur.

$$\underset{18e}{L_nM(R)(H)} \xrightarrow{-RH} \underset{16e}{[L_nM]} \xrightarrow{R'H} \underset{18e}{L_nM(R')(H)} \qquad \text{(eq 4.1)}$$

In a few cases, however, electronic unsaturation at the metal centre following C-H bond cleavage permits further reactivity, resulting in the functionalization of the alkane. Examples include the dehydrogenation of an alkane to an alkene[6] and the hydroformylation of an alkane substrate to an aldehyde.[1] Maintaining electronic unsaturation at the metal centre following C-H bond activation is a key concept in the development of catalytic systems capable of hydrocarbon functionalization or elaboration.

In this regard, the dual C-H activation of *n*-pentane, *n*-hexane and diethyl ether by $Cp^*W(NO)(CH_2SiMe_3)(\eta^2\text{-}CPh{=}CH_2)$ (**1**), as described in Chapter 1, Section 1.4.1, not only constitutes a rare example of an intermolecular alkane C-H bond activation at a tungsten metal centre,[7] but also represents a prototypal model of an organometallic system capable of chemically elaborating a hydrocarbon substrate. The result of this dual C-H bond activation

process is the regioselective formation of the tungstenacycles $Cp^*W(NO)(\eta^2\text{-}CH_2CHRCH_2CH(\eta^2\text{-}Ph))$ [R = ^{n}Pr, ^{n}Bu], (eq 4.2).[7c] An inspection of the molecular structures of these complexes reveals that the hydrocarbon fragment, having lost two hydrogen atoms, has undergone a metal-mediated dehydrogenation in a manner described above. However, unique to this system is the chemical elaboration that extends beyond alkane dehydrogenation to encompass the coupling of the vinyl and hydrocarbyl fragments in the metal's coordination sphere.

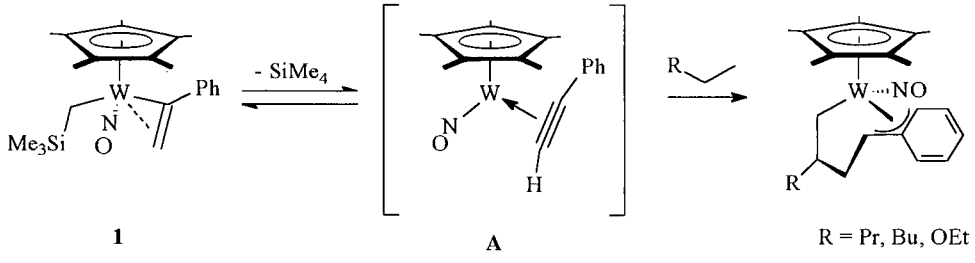

1 A R = Pr, Bu, OEt (eq 4.2)

Since the initial investigations by Dr. Jeff Debad into the thermolytic C-H activation of benzene, pentane, hexane, and diethyl ether by **1**, the scope of this chemistry has been expanded to include other aromatic and aliphatic hydrocarbon substrates. In this Chapter the results of these investigations are described. In addition, kinetic and mechanistic studies lend further support for the intermediacy of acetylene-containing **A** and the mechanism by which it is generated. The results of selectivity experiments shed light on the steric and electronic influences governing the C-H activation event. This Chapter closes with a qualitative frontier-molecular-orbital analysis of acetylene complex **A** which illustrates at a qualitative MO level its capacity to effect hydrocarbon C-H bond activation and, by extension, to effect the reductive coupling of unsaturated, heteroatom-containing substrates, the chemistry of which is the focus of Chapter 3.

4.2 Results and Discussion

Analytical data and a numbering scheme for all compounds discussed in this chapter are presented in Table 4.5. Low- and high-resolution mass spectral data and IR spectral data are collected in Table 4.6. ^{1}H and ^{13}C NMR spectroscopic data for complexes are presented in Table 4.7. These tables are located in Section 4.4 of this Chapter. A discussion of the physical data and other properties of the compounds generated via C-H activation of benzene, *n*-pentane, *n*-hexane, and diethyl ether during Dr. Jeff Debad's investigations are included in this chapter for reference and completeness.

4.2.1 Activation of the C-H Bonds of Benzene, Methyl-substituted Arenes, and Hexamethyldisiloxane

The activation of benzene C-H bonds is described as a representative example of the quantitative thermal activation of **1** in arene solutions. Thermal activation of **1** in neat benzene at temperatures ranging from 40 - 60 °C over periods of 24 – 12 h, respectively, cleanly affords the red-brown phenyl complex **4.1** in >97 % yield (eq 4.3, [W] = Cp*W(NO)) as judged from the ^{1}H NMR spectrum of the final reaction mixture. In addition to signals attributable to the η^2-phenylvinyl ligand analogous to those in **1**, resonances in the aromatic region of the ^{1}H (C_6D_6) and ^{13}C ($CDCl_3$) NMR spectra of **4.1** are readily attributable to the phenyl ligand.

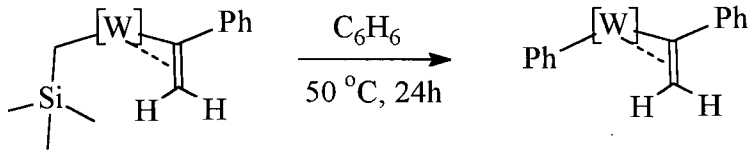

(eq 4.3)

1 **4.1**

Thermolyses of vinyl complex **1** have been conducted in methyl-substituted arenes to assess the selectivity of acetylene complex **A** for the activation of aryl or benzylic C-H bonds. For example, thermolysis of **1** in toluene at 50 °C for 24 h affords the products depicted in eq 4.4 in quantitative yields.

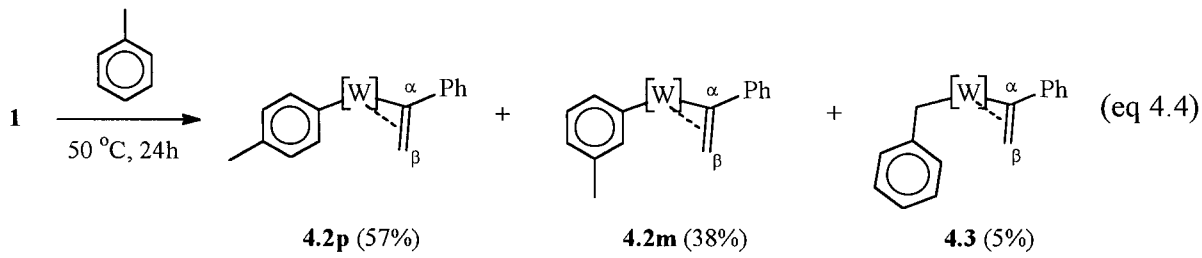

(eq 4.4)

4.2p (57%) **4.2m** (38%) **4.3** (5%)

Complexes **4.2m** and **4.2p** are derived from aryl C-H bond activation of toluene by acetylene complex **A**, whereas aliphatic C-H bond activation of a benzylic C-H bond leads to the red benzyl complex **4.3**, albeit in very low yield. Compounds **4.2m** and **4.2p** co-precipitate, and their physical separation is hampered by their decomposition on chromatographic media. In solution, however, they are readily distinguished by utilizing ^{1}H COSY and NOE NMR data. Identification of benzyl compound **4.3** is facilitated by its alternate route of preparation employing routine metathetical protocol;[8] i.e. utilizing $Cp^*W(NO)Cl_2$ and one equivalent each of $(CH_2{=}CPh)_2Mg{\bullet}$(dioxane) and $Bz_2Mg{\bullet}$(dioxane). The existence of an η^2-vinyl ligand in each

of these three compounds in solution is indicated by the relevant NMR signals in the ^{1}H and ^{13}C NMR spectra for these compounds, as compared to the same data for complex **1** (found in Chapter 1). For example, the vinyl C_{β} signals in the ^{13}C NMR spectra for complexes **4.2p**, **4.2m** and **4.3** appear at δ 80.3, 79.6, and 78.6, respectively, while those of C_{α} occur at 234.6, 233.5, and 207.8 ppm, respectively. It is particularly noteworthy during the above transformation that no products of *ortho*-C-H bond activation are observed. This fact will be discussed in greater detail in Section 4.2.3, which deals with the C-H bond selectivity extant in these conversions.

Scheme 4.1

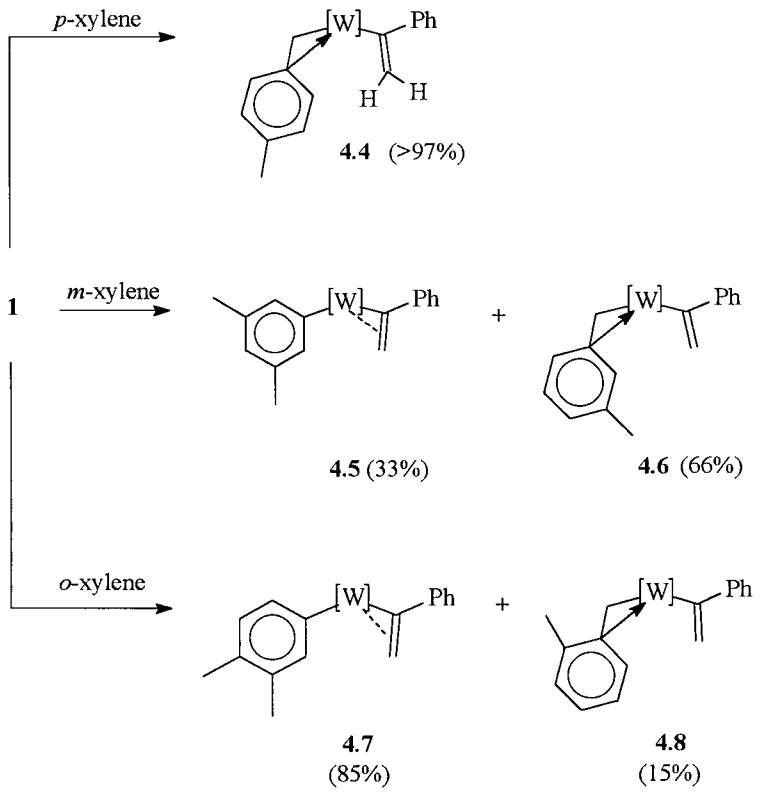

The results of the thermolysis of vinyl complex **1** in *p*-, *m*-, and *o*-xylene at 54 °C are shown in Scheme 4.1 above. Like the thermolysis of **1** in toluene, the analogous thermolysis of **1** in these xylenes yields no products resulting from the activation of an aryl C-H bond in a position on the ring *ortho* to a methyl substituent.

The thermolysis of **1** in *p*-xylene quantitatively affords the 4-methylbenzyl complex **4.4** that results from the activation of a methyl C-H bond. The NMR data for the η^2-benzyl and η^1-vinyl ligands in complex **4.4** contrast to those observed for the η^1-benzyl and η^2-vinyl ligands in benzyl complex **4.3**. By comparison to the same signals for complex **4.3**, both the downfield shift of the vinyl H signals (5.42 and 3.49 ppm) in the ^{1}H NMR spectrum of **4.4** and the shift of the vinyl C_α and C_β signals (194.7 and 115.9 ppm, respectively) into the olefinic region of the ^{13}C NMR spectrum of **4.4** implicate an η^1-bonding mode for the vinyl ligand. In addition, the upfield shift of the benzyl *o*-H signal (6.66 ppm) in the ^{1}H NMR spectrum of **4.4** and the high-field signal for the *ipso*-C of the benzyl ligand (115.5 ppm) in the ^{13}C NMR spectrum attest to the sp^3 character imposed on this carbon nucleus by the η^2-coordination mode of the *p*-xylyl ligand.[9] From these data it can be concluded that the 4-methylbenzyl ligand is the stronger donor in this complex and, therefore, the vinyl ligand is forced to assume the η^1-coordination mode to avoid the expansion of the tungsten valence shell to 20e.

It is intriguing that the coordination modes for the benzyl ligands in complexes **4.3** and **4.4** are so different when the only physical and chemical difference between these ligands is the presence or absence of a methyl substituent in the 4-position of the aromatic ring. When substituent effects in aromatic rings are considered, however, it becomes clear that the presence of an electron-donating methyl substituent increases the electron density at the carbon nucleus in the *para* position of the arene ring.[10] This being the case for the benzyl ligand of complex **4.4**, it

is not surprising that, of the two complexes, **4.4** contains an η^2-benzyl ligand derived from the coordination of the electron-enriched *ipso*-C to W. In addition, VT NMR studies involving the analogous bis(benzyl) complexes of the Cp'W(NO) fragment [Cp' = Cp or Cp*]) reveal that the benzyl ligand oscillates rapidly between the η^1- and η^2-limiting forms.[9] Assuming that the tungsten-η^2-vinyl bonding interaction is similar in strength to that of the W-η^2-benzyl interaction, it is presumably more correct to consider that the solution molecular structure of **4.3** arises because the left-hand side of the equilibrium depicted in eq 4.5 is favoured when R = H, whereas that of **4.4** results from a favouring of the right-hand side when R = Me.

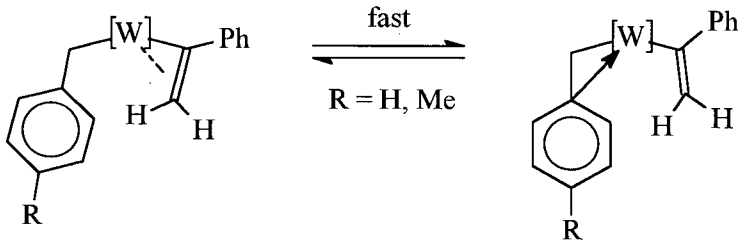

(eq 4.5)

The thermolysis of **1** in *m*-xylene under similar conditions affords aryl complex **4.5** and η^2-benzyl complex **4.6** in a 33 ± 3 : 66 ± 3 ratio. Unlike **4.2m** and **4.2p** described above, **4.5** and **4.6** are readily separable by chromatographic elution of **4.6** with Et_2O on alumina I, albeit at the expense of complex **4.5** which decomposes on this support. ^{1}H NMR spectroscopic data for this latter complex can only be obtained from solutions of the crude mixture. Complex **4.6** readily crystallizes from diethyl ether as red needles. The dihapto bonding of the benzyl ligand to W in **4.6** is clearly apparent by comparison of its NMR spectroscopic data to those of η^2-*p*-xylyl-containing **4.4**.

Aryl complex **4.7** and η^2-benzyl compound **4.8** are formed in an $85 \pm 3 : 15 \pm 3$ ratio during the thermolysis of **1** in *o*-xylene. Complex **4.7** is readily isolated as a red, crystalline solid from the final reaction mixture by fractional crystallization. Complex **4.8**, while not isolated, displays low intensity signals in the ^{1}H and ^{13}C NMR spectra of the crude reaction mixture characteristic of an η^2-benzyl and η^1-vinyl ligand, as detailed above for complexes **4.4** and **4.6**. The availability of a second aryl C-H bond in *o*-xylene relative to *m*-xylene seemingly effects a dramatic reversal in the relative proportion of products derived from aryl and benzyl C-H bond activation. As noted above, the C-H bond selectivity exhibited in these conversions will be discussed in detail in Section 4.2.3.

Analogous to the formation of η^2-benzyl complex **4.4**, the purple silyl ether **4.9** is quantitatively formed via activation of a hexamethyldisiloxane methyl C-H bond during the quantitative thermal decomposition of **1** in solution at 54 °C (eq 4.6). Its NMR spectroscopic features are unremarkable and analogous to those of complex **1**. This complex can be utilized as an analogue of the parent alkyl vinyl complex **1** in the kinetic study of these transformations, as previously described in Chapter 3.

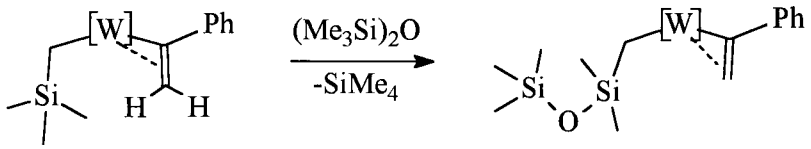

1 **4.9** (>98%) (eq 4.6)

4.2.2 The Mechanism of Hydrocarbon Elimination and C-H Bond Activation

Before describing the kinetic and mechanistic studies conducted with the compounds described in the preceding Section, it is prudent to review the evidence in support of the proposed mechanism by which acetylene-containing **A** is generated via rate-limiting elimination of $SiMe_4$ from **1** under saturation conditions. As described in more detail in Chapter 1, Section 1.4.1, the preliminary mechanistic clues provided by the results of the thermolysis of **1** in C_6D_6 at 50 °C for 24 h in an NMR tube included:

1. A signal at δ 0.00 in the ^1H NMR spectrum of the resultant mixture attributable to $SiMe_4$ in solution.

2. The complete absence of signals attributable to the vinyl protons, due to the incorporation of deuterium into the vinyl positions of the vinyl ligand.

3. The addition of $SiMe_4$ to these reaction mixtures retards the rate of C-H activation.

These observations taken together suggested that $SiMe_4$ is eliminated from the coordination sphere of W, as facilitated by vinyl H elimination, generating an unobserved two-legged piano-stool complex of tungsten containing an η^2-acetylene ligand (**A**). Subsequent C-D bond activation affords deuterium incorporation into the vinyl positions.

The results of the kinetic and mechanistic studies described in Chapter 3 are in support of the proposed mechanism (eq 4.7 below). Three key results that are consistent with the general mechanism depicted in eq 4.7 include:

1. The determination of saturation kinetics for this system, which leads to an independence of the rate of reaction on the nature of the substrate employed in these reductive coupling reactions when the solvent system lies in the saturation regime.

2. The positive activation entropy determined for the $Cp^*W(NO)(CH_2SiMe_3)(\eta^2\text{-}CPh{=}CH_2)$ (**1**) $\rightarrow$ $[Cp^*W(NO)(\eta^2\text{-}PhC{\equiv}CH)]$ (**A**) conversion conducted in EtOAc.

3. Finally, the fact that the products derived from the reductive coupling reactions described in Chapter 3 cannot be interconverted under thermolysis conditions.

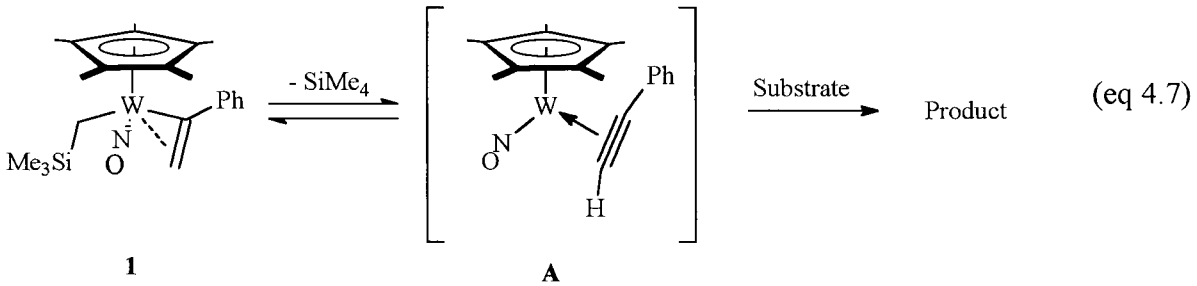

1 **A** (eq 4.7)

The quantitative conversion of **1** to aryl, benzyl, or alkyl vinyl complexes has provided an opportunity to study the vinyl-H elimination / hydrocarbon C-H activation process in detail. The mechanism by which C-H bonds are activated is proposed to involve the same acetylene-containing intermediate **A**. However, studies show that the substrate C-H activation step that follows the hydrocarbon elimination step is reversible, a conclusion that is drawn from the fact that the activation of C-D bonds by **1** in benzene-d_6, p-xylene-d_{10}, and tetramethylsilane-d_{12} solutions results in the deuteration of *both* vinyl positions in the vinyl ligand to afford complexes **4.1**-d_7, **4. 4**-d_{11}, and **1**-d_{13}, respectively (eq 4.8). Further support for this reversibility is given by

the observation that complex **4.1-*d*$_7$**, generated during the thermolysis of **1** in C_6D_6, can be converted back to **4.1** by replacing the C_6D_6 solvent with C_6H_6 and subjecting the resultant sample to a temperature of 50 °C for an additional 24 h.

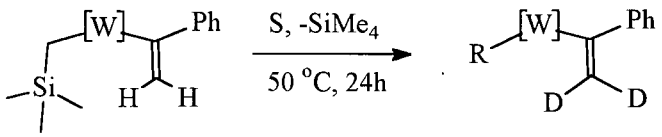

(eq 4.8)

1

1-*d*$_{13}$, S = $SiMe_4$-d_{12}, R = $CD_2Si((CD_3)_3)$
4.1-*d*$_7$, S = C_6D_6, R= C_6D_5
4.4-*d*$_{11}$, S = *p*-xylene-d_{10}, R = η^2-*p*-xylene-d_9

4.2.2.1 Kinetic Studies

Kinetic studies of these conversions were performed in a manner analogous to those described in Chapter 3, Section 3.2.3, utilizing UV-vis spectroscopy to monitor the progress of these reactions. The results of these studies are collected in Table 4.1, and are consistent with the mechanism depicted in eq 4.9 (rds = rate-determining step). This mechanism is analogous to that proposed for the reductive coupling chemistry described in Chapter 3 and depicted in eq 4.7, but it has been demonstrated that "trapping step" involving substrate C-H bond activation is reversible (vide supra). The reversibility of the C-H activation step precludes the possibility of conducting an analogous saturation study employing mixtures of hydrocarbon substrates. As mentioned above, the addition of $SiMe_4$ to these reaction mixtures retards the observed rate of C-H bond activation, qualitatively confirming for the C-H activation process what has been demonstrated quantitatively in Chapter 3; that a reversible, rate-limiting dissociation of hydrocarbon leads to the formation of acetylene-containing **A**. A faster trapping step (either C-H

activation or reductive coupling) generates the observed products discussed in this Chapter and Chapter 3.

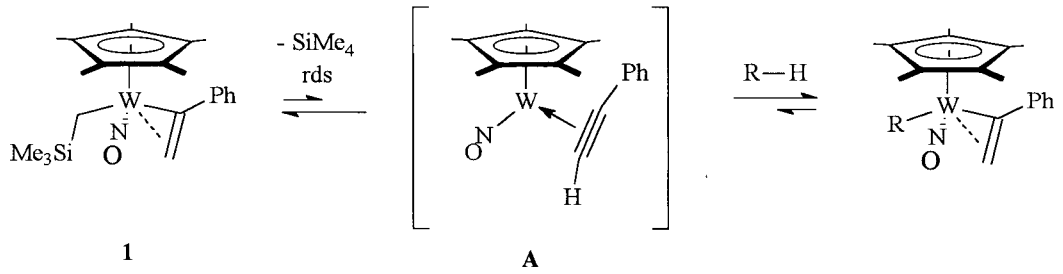

1 A (eq 4.9)

These conversions are first order in [**1**] over the entire experimental concentration range (e.g. Figure 4.1), and the associated rate constants indicate that these conversions are independent of hydrocarbon substrate under saturation conditions (Table entries 1 - 3).

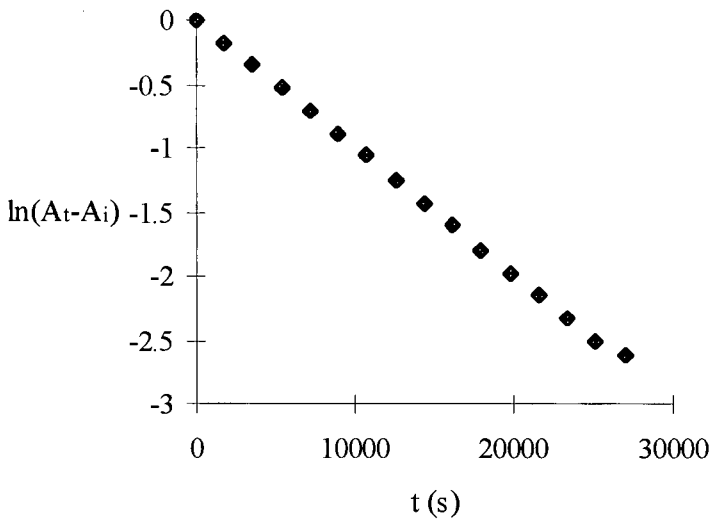

Figure 4.1. A plot of $\ln(A_t-A_i)$ [A_i = absorbance at infinite t] vs. t for the **1** → **4.4** conversion at 327 K ($R^2 = 0.9995$, $k_{obs} = 1.1(1) \times 10^{-4}\ s^{-1}$).

The magnitudes of k_{obs} determined for these conversions compare well with that determined for the activation of **1** in ethyl acetate ($k_{obs} = 1.0(1) \times 10^{-4}$ s^{-1}, see Chapter 3, Section 3.2.3), corroborating the mechanistic proposals made in Chapter 3. Also consistent is the kinetic isotope effect (KIE) of magnitude 1.2(1) determined for the activation of C-H or C-D bonds by **1** under thermolytic conditions in C_6H_6 and C_6D_6 solutions, respectively (Table entries 1 and 2). That this value is not precisely unity suggests the existence of a small, secondary isotope effect which might arise as a result of a solvent effect[11] (cf. Table entries 1 and 3). However, the source of this effect is unknown. One possible reason lies in the greater stability of any deutero-solvated species that lie along the reaction coordinate. Such a species would be slower to react with an incoming reagent relative to a protio-solvated species. The independence of the rate on substrate C-H activation is confirmed by monitoring the progress of the thermolysis of **1** in an equimolar mixture of C_6H_6 and C_6D_6 by ^1H NMR spectroscopy, the results of which yield a KIE of 1.0(1). Strong support for the rate-limiting elimination of hydrocarbon under saturation conditions is given by the KIE of 4.9(4) determined from the η^2-xylyl **4.4** $\rightarrow$ alkyl **4.9** and ***4.4-d*$_{11}$** $\rightarrow$ **4.9** conversions in $(Me_3Si)_2O$ (Table entries 9 and 10). This relatively large intramolecular KIE establishes that the rate of reaction is strongly dependent on vinyl C-H / C-D bond cleavage. Its magnitude is comparable to others determined for such rate-limiting reductive eliminations of hydrocarbon.[12]

An Eyring analysis of the kinetic data obtained for the elimination of $SiMe_4$ from **1** in *p*-xylene solution at different temperatures under saturation conditions (Table entries 3 - 7) yields values for the activation entropy and enthalpy which support a rate-limiting, dissociative process. The moderate, positive value obtained for the activation entropy (18(3) $cal(molK)^{-1}$) is consistent with the dissociative nature of a rate-limiting, alkane-elimination step, and the magnitude of the

activation enthalpy (31.0(8) kcalmol^{-1}) reflects a considerable degree of bond cleavage leading up to the rate-controlling transition state. These values are indistinguishable from the respective activation entropy and enthalpy of 22(3) cal(mol•K)$^{-1}$ and 31.8(6) kcal(mol)$^{-1}$ determined for the thermolysis of **1** in EtOAc over a similar temperature range under similar conditions, as described in more detail in Chapter 3.[13]

Table 4.1. Kinetic data for the thermal activation of vinyl complexes in hydrocarbon solution

Table entry	Cmpd	Extruded Silane Or Hydrocarbon	Substrate	Temp (K)	Average k_{obs} ($\times 10^4$ s^{-1})
1	**1**	$SiMe_4$	benzene	327	1.1(1)
2	**1**	$SiMe_4$	benzene-d_6	327	0.94 (3)
3	**1**	$SiMe_4$	*p*-xylene	327	1.1(1)
4	**1**	$SiMe_4$	*p*-xylene	314	0.12(1)
5	**1**	$SiMe_4$	*p*-xylene	320	0.48(1)
6	**1**	$SiMe_4$	*p*-xylene	340	7.8(2)
7	**1**	$SiMe_4$	*p*-xylene	348	20(1)
8	**4.9**	$(Me_3Si)_2O$	*p*-xylene	327	0.74(1)
9	**4.4**	*p*-xylene	$(Me_3Si)_2O$	327	0.84(2)
10	**4.4-d_{11}**	*p*-xylene-d_{10}	$(Me_3Si)_2O$	327	0.17(1)
11	**4.1**	C_6H_6	$(Me_3Si)_2O$	327	1.3(2)

4.2.2.2 The Intimate Mechanism of Hydrocarbon Elimination and C-H Bond Activation

It has been shown via kinetic and mechanistic studies in Chapter 3 and in this Chapter that hydrocarbon elimination to form acetylene-containing **A** from **4.9** and **1**, respectively, is the rate-controlling process (under saturation conditions) by which coordinated π-ligands are reductively coupled and C-H bonds are activated. The rate-controlling generation of **A**, which to this point has been considered as a single rate-controlling process, actually comprises two events: (1) vinyl-H elimination and (2) reductive elimination of $SiMe_4$ from the coordination sphere of the metal. The determination of the intimate mechanism by which these two elimination events are effected during the formation of **A** is not so easily accomplished and, in reality, the mechanism probably cannot be determined exactly. However, experimental evidence has been accumulated that supports one particular mechanistic pathway over several others. These potential mechanisms and the evidence in support of one in particular are discussed in this Section of the Chapter.

Before considering the intimate mechanism that combines these two elimination processes, a few words regarding the vinyl-H elimination step are prudent at this point. It has been demonstrated in Chapter 2 that the vinyl ligand in complexes bearing a 1e-donor ancillary ligand (such as a chloride or σ-alkyl ligand) binds to the tungsten centre in an η^2-fashion. In addition, recall that deuterium label is incorporated into *both* vinyl positions during the activation of C-D bonds in deuterated substrates. These observations imply that vinyl-H elimination (and vinyl regeneration via C-H activation in the microscopic reverse) must involve an η^2-vinyl ligand, and that both vinyl positions will be deuterated following the activation of two C-D bonds (Scheme 4.2, **I**). This conclusion can be drawn because the alternate scenario involving β-

H elimination from an η^1-vinyl ligand (and regeneration of an η^1-vinyl ligand by C-H activation in the microscopic reverse) only leads to deuterium-label incorporation into the *syn*-vinyl-H position relative to W (Scheme 4.2, **II**).[14] That deuterium-label is incorporated into *both* vinyl positions is only consistent with a mechanism involving an η^2-vinyl ligand.

Scheme 4.2

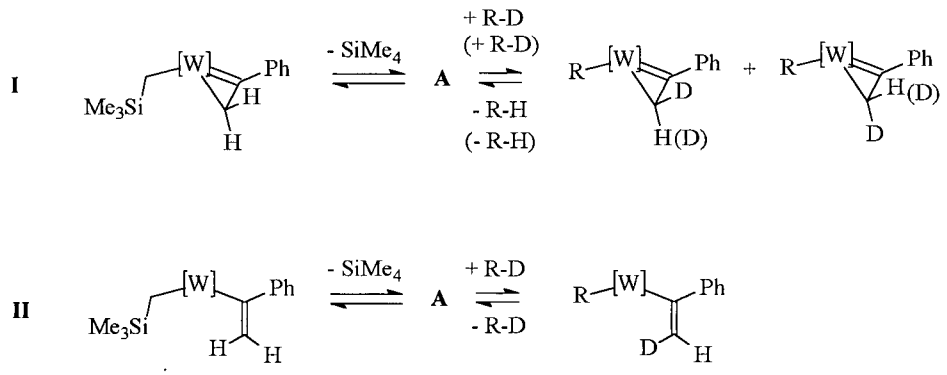

An argument could be made that relies on the equilibration of the two vinyl sites in the η^1-vinyl ligand. Such a rapid $\eta^1 - \eta^2 - \eta^1$ interconversion *could* render both vinyl hydrogens accessible to W and lead to label incorporation into both vinyl sites with equivalent frequency; however, no such equilibration is observed by ^{1}H NMR spectroscopy at reaction temperature. The vinyl magnetic environments remain chemically inequivalent as evinced by the insensitivity of the ^{1}H NMR spectrum of **1** to variation in temperature (up to 60 °C). In addition, a magnetization transfer experiment failed to effect magnetization transfer between the two vinyl H nuclei under the reaction conditions. Nonetheless, a slow exchange process *could* be occurring, and the observed lack of magnetization transfer could arise from a systemic error in the NMR experiment. Thus, an $\eta^2 - \eta^1 - \eta^2$ interconversion could explain the experimental observations. On the other hand, a scenario involving the unselective elimination of H from an η^2-vinyl ligand and addition of D is also consistent with the results of these labeling studies.

Thus, it remains to consider the possible intimate mechanisms by which acetylene complex **A** may be generated. Three limiting forms can be envisioned, as depicted in Scheme 4.3. The associated free energy profiles also depicted in Scheme 4.3 are qualitative in nature and are included only for reasons of clarity. The relative peak heights and well depths that are depicted are intended to imply nothing of the energetics of the species which lie along these profiles (as indicated by the "hash" marks interrupting each profile) apart from the fact that the formation of **A** is rate-limiting under pseudo-first-order conditions and, therefore, one of the peaks preceding **A** must be the highest in energy.

Scheme 4.3

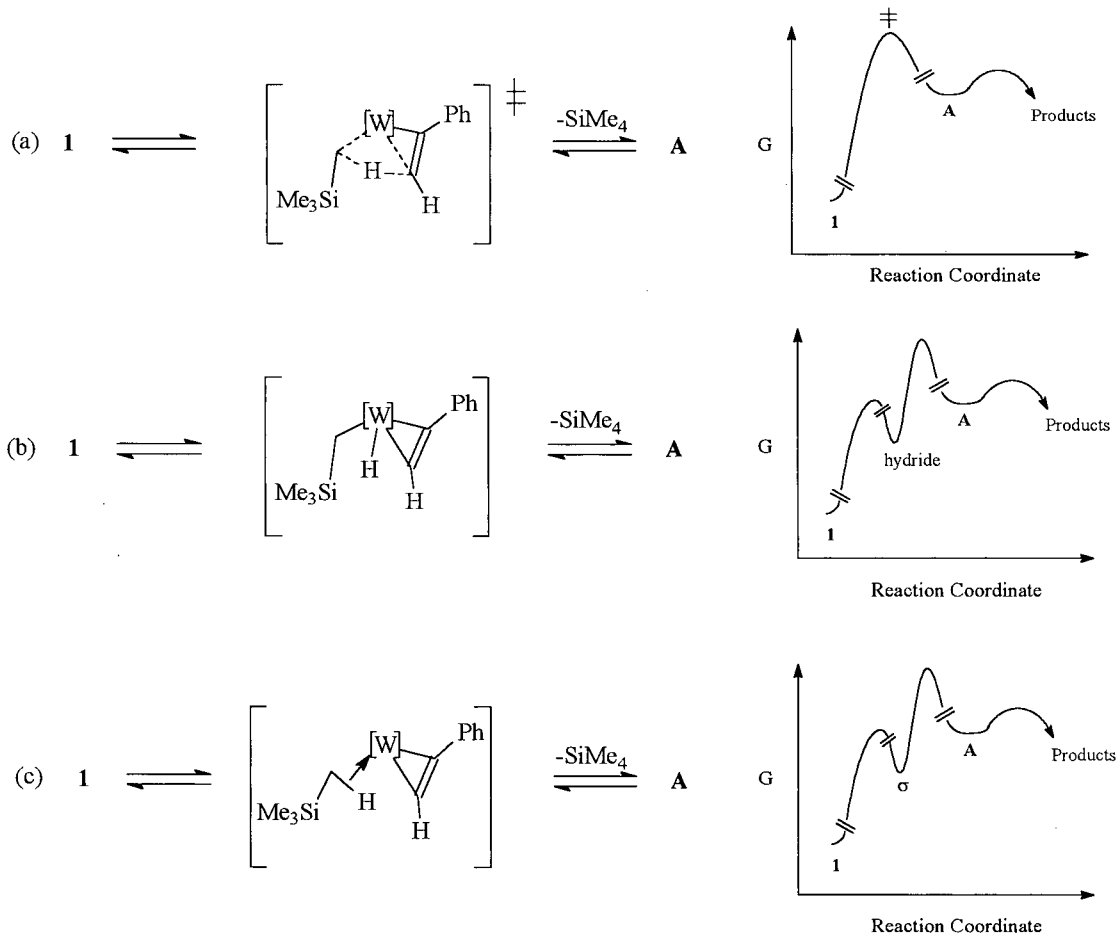

The first path depicts the formation of **A** as a concerted process via a transient, constrained four-centre transition state (Scheme 4.3, (a)). The second depicts the intermediacy of an alkyl-hydride-acetylene species whose formation precedes alkane elimination (Scheme 4.3, (b)). Lastly, vinyl-H elimination to give an intermediate hydrocarbon σ-complex prior to elimination of alkane can also be envisaged as a viable mechanism (Scheme 4.3, (c)).

The accumulated mechanistic and kinetic evidence described thus far in this Chapter is ambiguous in distinguishing the three possible pathways depicted in Scheme 4.3, despite the fact that considerable literature evidence also exists with which to define these pathways. For example, rate-limiting hydrocarbon eliminations by a relatively linear, concerted H-transfer (Scheme 4.3(a)) typically yield large KIEs (ca. 7 – 14),[15] while KIEs for related α-eliminations in reactions which generate alkylidenes are considerably smaller in magnitude (ca. 2.5 – 4).[12c,d] Eliminations of alkanes via hydride intermediates (Scheme 4.3(b)) often also occur with KIEs that are small in magnitude (ca. 3 – 4)[17b,18a] or near unity.[17b] Those that occur from metal-hydride precursors via σ-hydrocarbon intermediates (e.g. Scheme 4.3(c)) often afford inverse KIEs.[15,21] The measured intramolecular KIE of 4.9 for the **4.4** → **4.9** conversion is intermediate to those found in these previously-reported cases, though it deserves mention that a β-elimination of H or D from a thiolate ligand in a Ti(IV) system reported by Buchwald and Neilson yields an intramolecular KIE of similar magnitude (5.2 measured at 80 °C).[12b]

Considering entropic requirements allows one to eliminate the first mechanistic pathway as a potential candidate for the vinyl system described in this Thesis. The concerted mechanism depicted in Scheme 4.3(a) involves a transition state that is more constrained than the starting compound from which it is derived. As such, a negative activation entropy would be expected from an Eyring analysis of the kinetics. An elegant study by Doherty and Bercaw illustrates the

entropic requirements of this process particularly well. They have showed that the reversible insertion of various olefins into the Nb-H bond of $Cp^*_2NbH_3$ occurs with activation entropies ranging from –5.8 to –17.2 eu, all indicative of a constrained, four-centred geometry in the transition state.[16] Likewise, Buchwald and Nielson[12b] and Wolczanski and coworkers[15] have determined by kinetic and mechanistic analysis that the elimination of hydrocarbon in their respective Group 4 systems occurs via a concerted mechanism and yields moderately large and negative activation entropies as a result. In contrast, the positive activation entropy of +18(6) determined for the thermal activation of **1** in *p*-xylene implies that, at the highest point of the energy profile leading to the formation of **A** (i.e. the transition state in the rate-controlling step), there is *greater disorder* relative to the starting material. This finding mitigates against such a concerted H-transfer mechanism as being the rate-limiting process that generates intermediate **A**.

Much stronger evidence consistent with the intermediacy of σ-hydrocarbon complexes (Scheme 4.3, (c)) that also mitigates against pathways (a) and (b) is obtained from the results of mechanistic studies involving (1) the activation of C-D bonds and (2) the thermal interconversion of aryl and benzyl vinyl complexes. Literature evidence for the existence of hydrocarbon σ-complexes in C-H bond activation processes is abundant[17] and has prompted a number of theoretical studies which consider this phenomenon from a computational approach.[18] The mechanistic evidence in support of the intermediacy of σ-complexes prior to the generation of **A** (and prior to C-H activation in the microscopic reverse) is summarized in the following two points.

1. Deuterium label is incorporated into both vinyl positions *simultaneously* during the thermolysis of **1** in deuterated solvents, a feature that is readily determined by monitoring the

reduction in intensity of the vinyl proton signals in the ^{1}H NMR spectrum of **1** in C_6D_6, *p*-xylene-d_{10}, or $SiMe_4$-d_{12} at thermolysis temperature. As illustrated below in eq 4.10, deuterium incorporation into either vinyl position following C-D activation may occur with equal probability, leading to the observed reduction in intensity of both vinyl-H signals. However, monitoring the simultaneous intensity reduction of the two vinyl-H signals of **1** affords a series of NMR spectra in which signals attributable only to **1** and the product containing a doubly-deuterated vinyl ligand are apparent. The mechanisms depicted in Scheme 4.3(a) and (b) necessitate the existence of an intermediate mono-deuterated vinyl species containing the C_6D_5 ligand (**4.1-*d*$_6$** in eq 4.10), yet none is observed during the monitoring of this conversion by ^{1}H, ^{13}C, or ^{2}H NMR spectroscopy. The absence of such an intermediate is inconsistent with the fact that both of these mechanistic scenarios require *two* rate-limiting vinyl elimination processes in order to completely deuterate the vinyl position in each molecule.

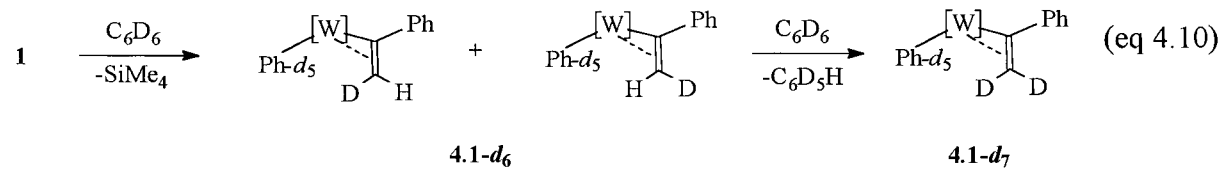

4.1-*d*$_6$ **4.1-*d*$_7$** (eq 4.10)

On the other hand, an equilibrium between the aryl vinyl products and isomeric π- and σ-arene complexes, according to Scheme 4.3(c), leads to the rapid introduction of deuterium into both positions of the vinyl ligand once the deuterated substrate is incorporated into the coordination sphere of tungsten (e.g. Scheme 4.4). Thus, the elimination of hydrocarbon remains as the rate-limiting process, yet isomerization of the mono-deuterated vinyl intermediate to the doubly-deuterated vinyl complex **4.1-*d*$_6$** via arene σ–complexes is rapid, accounting for the equivalent reduction in intensity of the vinyl signals in the ^{1}H NMR spectrum of this reaction mixture. An interesting result of this process is the incorporation of H into the phenyl ring of

4.1-d_6; a phenomenon that is theoretically observable by ^{1}H NMR spectroscopy (and would lend support for these proposals). However, the proton that is incorporated into the phenyl ring is statistically distributed over the 3 positions of local symmetry in the phenyl ring. The statistical reduction of signal intensity and the additional complication of the arene region in the ^{1}H NMR spectrum by the signals of the vinyl phenyl substituent combine to render ambiguous such an observation.

Scheme 4.4

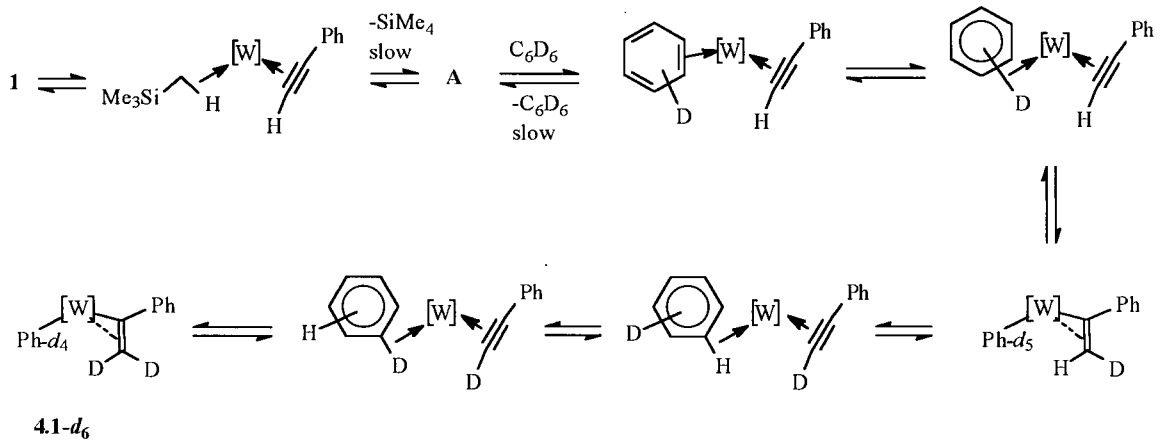

4.1-d_6

2. Attempts to prepare *p*-tolyl-containing **4.2p** by metathesis of Cl^- in chloride-containing **2.1** in the presence of (*p*-tolyl)$_2$Mg affords the target complex cleanly *only* if the work-up is conducted in a timely manner. If the ether solution of crude **4.2p** is left for any length of time (>3 h) at room temperature at any point prior to the isolation of **4.2p** in the solid-state, mixtures of complexes **4.2p** and **4.2m** in variable proportions are obtained instead. This suggests that the former complex is converting into the latter via an isomerization process. If this process occurs via rate-limiting dissociation of toluene in a manner equivalent to that depicted in Scheme 4.3(a) or (b), then the interconversion of **4.2p** and **4.2m** should require

several days to proceed to a measurable level of completion (noting that two weeks were required for the conversion of **1** to **4.1-*d*$_7$** in C_6D_6 at room temperature). However, if the interconversion proceeds via the equilibration of π- and σ-arene complexes in such a way as depicted in Scheme 4.4, then mixtures of the two complexes will be observed at much earlier times.

Monitoring in toluene-d_8 by ^{1}H NMR spectroscopy at 40 °C the conversion of authentic benzyl-containing **4.3** (prepared by synthetic procedures from **2.1** and (benzyl)$_2$Mg) to its aryl isomers, **4.2p** and **4.2m**, yields results that are consistent with the intermediacy of π- and σ-arene complexes. Maintaining the NMR sample at this temperature for 60 min results in the conversion of half of the original amount of complex **4.3** to complexes **4.2p** and **4.2m**. Assuming that this isomerization is unimolecular, an estimate of the associated rate constant of isomerization may be made, based on the relation: $t_{1/2} = \ln(2)/k$. Utilizing a half-life of 3600 s, k is calculated to be 1.9×10^{-4} s^{-1}. This value is more than an order in magnitude *larger* than the rate constant associated with the disappearance of **1** in *p*-xylene at 41 °C under similar pseudo-first order conditions ($k_{obs} = 1.0 \times 10^{-5}$ s^{-1}). The mechanistic scenarios depicted in Scheme 4.3(a) and (b), both of which require the rate-limiting elimination of toluene during this isomerization, cannot account for this discrepancy in rates. Again, it is more likely that the observed isomerization is being facilitated by the rapid interconversion of π- and σ-arene complexes, as depicted in Scheme 4.4 above.

From the results described in points 1 and 2 it can be suggested that the rate-limiting process that affords **A** from **1** under pseudo-first-order conditions involves the intermediacy of hydrocarbyl π- and σ-complexes according to Scheme 4.5. In the microscopic reverse, C-H activation is therefore preceded by the formation of the same hydrocarbyl π- and σ-complexes.

Jones and coworkers describe strong evidence implicating the intermediacy of such π-arene complexes as being the source of label scrambling in their mechanistic studies of C-H activation at Rh(I) centres.[19] However, the intermediacy of such π-arene complexes *alone* cannot account for the observation of label scrambling into the vinyl position during the activation of C-D bonds in $SiMe_4$-d_{12} by **A**, because this substrate lacks a π-system with which to form an intermediate π-complex. Thus, σ-hydrocarbon complexes must also be accessible intermediates along the reaction pathway that affords the observed products.

Scheme 4.5

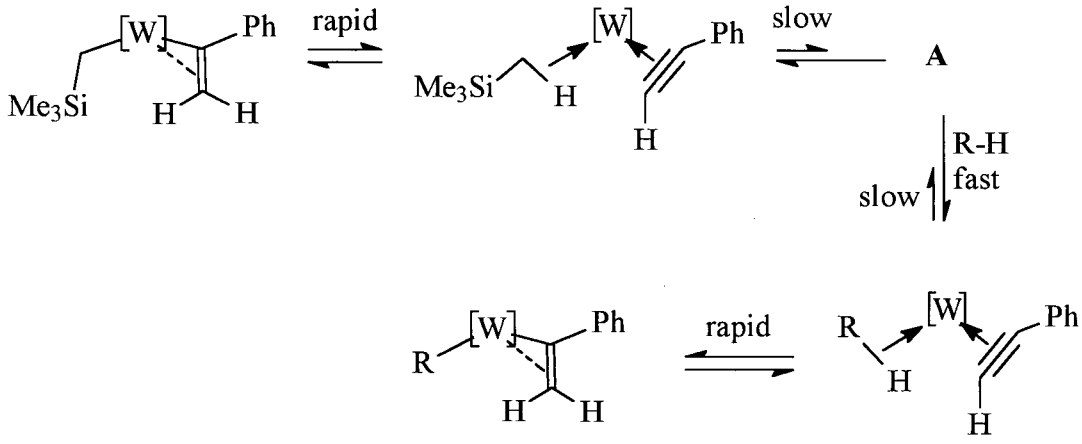

The formation of these σ-complexes and their interconversion is rapid in comparison to the rate-controlling elimination of hydrocarbon, as demonstrated by the results of the mechanistic studies described above. Therefore, in the two-step process that constitutes the formation of acetylene-containing **A** from **1**, the hydrocarbon elimination step must be the rate-controlling one. The consistency of this proposal with the results of the kinetic studies described in Section 4.2.2.1 is called into question. The superposition of a faster isomerization step onto

the rate-controlling hydrocarbon elimination step during the generation of **A** renders it very difficult to formulate *a priori* predictions for such parameters as isotope effects and activation entropies and enthalpies because the observed rate constant for the overall process is a product of the rate constants associated with the individual steps. However, speculation on the origin of the magnitudes of these parameters "after the fact" is certainly valid. For example, the activation enthalpy of 31.0(8) kcal•mol^{-1} appears unusually large,[20] but its magnitude may be considered as arising from the superposition of two energetically demanding steps in the rate-controlling process. Whitesides' group has noted an even larger activation enthalpy (~ 45 kcalmol^{-1}) for an analogous rate-limiting elimination of alkane from a Pt(II) bis(ethyl) complex via β-H elimination.[21a] Bergman *et al.* have postulated that the large activation enthalpy in this latter case arises from the superposition of the β-H elimination process onto the reductive elimination process.[21b] The relatively large and positive activation entropy can only be rationalized if the "pre-equilibrium" step is entropically favourable in conjunction with the rate-limiting, entropically favoured hydrocarbon elimination step that follows. If the entropic demands of the two steps were in conflict, then a small, near-unity overall entropy of activation might be expected.

The measured intramolecular KIE is also consistent with the superposition of the two steps depicted in Scheme 4.5. The equilibrium between vinyl complex and σ-hydrocarbyl complex has associated with it a large, normal isotope effect, due to the fact that a strong sp^2-hybridized C-H bond is being cleaved to form a weaker, σ-complexed sp^3-hybridized C-H bond. Isotopic substitution of ^{2}H at the vinyl positions therefore stabilizes the vinyl-containing starting material to a greater extent relative to the proposed σ-alkane complex. This results in a shift of the equilibrium towards the vinyl complex and a normal and large equilibrium isotope effect.

Since C-H bonds are not being cleaved in the rate-limiting alkane reductive elimination that follows this pre-equilibrium, a near-unity isotope effect is presumed to be associated with this step. The combination of these two steps presumably yields a moderately large, normal isotope effect for the overall rate-controlling process, consistent with experimental findings.

In summary, while the intimate mechanism involving the rate-controlling formation of acetylene-containing **A** perhaps cannot be known unequivocally, one can speculate that the available mechanistic and kinetic evidence strongly implicate an elimination process that involves the intermediacy of hydrocarbon σ-complexes according to Scheme 4.5. Vinyl-H elimination yields the σ-complex in a relatively fast and reversible pre-equilibrium step, followed by a rate-determining elimination of hydrocarbon from the σ-complex to form acetylene-containing **A**.

4.2.3 Selectivity in the Activation of Arene, Benzyl, and Siloxyl C-H Bonds

In considering the selectivity of **A** for the activation of different types of C-H bonds during these conversions, the distinction must be made between intra- and intermolecular C-H bond selectivity. Intramolecular selectivity is exhibited during the activation of chemically inequivalent C-H bonds within the same arene substrate molecule. This selectivity is thermodynamic in nature in the system described in this Thesis due to the presumed interconversion of arene and benzyl σ-complexes under equilibrium conditions (e.g. Scheme 4.4) and is readily quantified by measuring the ratio of products obtained from the thermal activation of **1** in methyl-substituted arene solvents. In contrast, intermolecular selectivity describes the preference displayed by **A** for the C-H bonds of one substrate over those of another. The

intermolecular selectivity for ethyl acetate or hexamethyldisiloxane by **A** has already been quantified in a saturation kinetics study described in Chapter 3. In this Section the intermolecular selectivity for arene, benzyl and siloxyl C-H bonds in benzene, *p*-xylene, and hexamethyldisiloxane, respectively, is measured by determining the relative proportions of products that result from the generation of **A** in 1:1 (mol:mol) mixtures of these hydrocarbons. Kinetic distributions of products are expected at short reaction times ($< 0.5 \times t_{1/2}$, when the amount of the reverse reaction is minimal), while at long reaction times ($>20 \times t_{1/2}$) thermodynamic distributions of products are expected (due to the inherent reversibility of the elementary steps in this mechanism).

4.2.3.1 Intramolecular C-H Bond Selectivity

The intramolecular C-H bond selectivity exhibited by **A** in the presence of methyl-substituted arenes is considered first. As noted in Section 4.2.1, no products of *ortho*-C-H bond activation are observed in any of the cases studied. This selectivity is not unprecedented,[15,22] and arises as a result of the steric shielding of the *ortho*-C-H bonds by the steric bulk of the methyl substituent[10] in each case.

Mixtures of aryl and benzyl products are obtained during the thermolytic decomposition of **1** in toluene, and *o*- and *m*- xylene, presumably from equilibria that arise as a result of the interconversion of σ- and π-arene complexes (as described in Section 4.2.2.2 and depicted in Scheme 4.4). The associated equilibrium constants for these equilibria are derived from the ratios of products. A "per C-H bond" ratio and equilibrium constant are calculated by correcting the amount of each product for the number of symmetry-equivalent substrate C-H bonds that

lead to its formation. Once in hand, the equilibrium constants permit the estimation of the associated free energies of these equilibria.[23] The pertinent data are collected in Table 4.2. In the case of toluene C-H bond activation, the equilibrium between the three co-dependent species (**4.3**, **4.2m** and **4.2p**) is difficult to analyze.[11] However, if the yield of benzyl complex **4.3** is considered to be minimal, then, as a first approximation, an equilibrium can be described between **4.2m** and **4.2p**. On the other hand, the toluene system can also be simplified by describing an equilibrium between the combined products of aryl C-H activation and those of benzyl C-H activation.

Table 4.2. Equilibrium constants and free energies for the equilibria between C- H activation products derived from intramolecular equilibration.

Equilibrium	K_{eq}	K_{eq} **(per C-H bond)**	$\Delta G°_{327K}$ **(per C-H bond, kcalmol^{-1})**
aryl **4.2m** ⇌ aryl **4.2p**	1.5(2)	3.0(0.4)	-0.7(0.1)
aryl [**4.2m** + **4.2p**] ⇌ benzyl **4.3**	0.05(0.02)	0.05(0.02)	1.9(0.2)
aryl **4.5** ⇌ benzyl **4.6**	0.18(0.04)	0.06(0.01)	1.8(0.1)
aryl **4.7** ⇌ benzyl **4.8**	2.0(0.2)	0.33(0.04)	0.7(0.1)

That aryl C-H bond activation is favored in these equilibria (as evinced by the preponderance of aryl C-H bond activation products) is surprising, considering the greater strength of the aryl C-H bond relative to the benzyl C-H bond. However, Bergman *et al.* have shown that the stronger C-H bond gives rise to the stronger M-C bond upon C-H bond cleavage,

and therefore it is the relative strength of the C-H bonds being activated that is the predominant factor which influences the product distributions in these types of equilibria.[15,21b]

A noteworthy general trend in these conversions is the increased proportion of benzylic C-H bond activation that is observed as the methyl substituents in these xylenes become further separated in space, shielding a greater number of arene C-H bonds. The relative amount of benzyl C-H activation follows the trend: *p*-xylene > *m*-xylene > *o*-xylene ≈ toluene. Considering the data presented in Table 4.2, it is only when three of the four arene C-H bonds in *m*-xylene are blocked to activation by **A** by the methyl substituents does the activation of the benzyl C-H bonds become competitive with aryl C-H bond activation. Even in this case, the greater proportion of benzyl C-H activation remains a statistical effect, due to the number of symmetry-equivalent benzyl C-H bonds. An analysis of the energetics of these equilibria on a "per C-H bond" basis reveals that aryl C-H activation remains the energetically favorable process in all cases.

It is intriguing to note that the equilibrium between the accessible aryl and benzyl C-H bonds of toluene and *o*-xylene afford statistically identical equilibrium constants and corresponding standard free energies. For the two equilibria to be similar, the methyl substituents in the two arenes must influence the strength of the M-C bonds formed in the two products to a similar extent and, hence, shift equally the two equilibria towards the preferential formation of the product derived from $C\text{-}H_{para}$ activation. This is reasonable if one considers that each of the two accessible arene C-H bonds in *o*-xylene is stabilized only by the inductive effect of the *para*-disposed Me substituent. As a result, the net stabilizing effect of the two methyl substituents in *o*-xylene on the strength of the $W\text{-}C_{aryl}$ bond formed in **4.7** is similar to that of the single Me substituent in toluene on the $W\text{-}C_{para}$ bond in **4.2p**. Utilizing a similar argument it is

noteworthy that the energy differential in the equilibrium between the aryl and benzyl products of *m*-xylene C-H bond activation is *decreased* relative to the energy differential between the aryl and benzyl products derived from toluene and *o*-xylene. This is presumably due to the fact that the *meta*-Me substituents exert no inductive effect on the strength of the single accessible arene C-H bond (and hence the resultant W-C_{aryl} bond).

Thus, two conclusions may be drawn from these equilibrium studies which consider the intramolecular isomerization of methyl-substituted aryl complexes. It is clear that aryl C-H bond activation dominates these equilibria, due to the formation of the stronger W-C_{aryl} bond in the product vinyl complexes. Thus, *para*-C-H bond activation is favoured in cases in which more than one type of aryl C-H bond is accessible, again a reflection of the thermodynamic preference for the formation of the stronger M-C_{aryl} bond.

4.2.3.2 Intermolecular Competition Experiments

Competition studies employed to assess the intermolecular kinetic selectivity of **A** for *p*-xylene, hexamethyldisiloxane, and benzene C-H bonds also reveal a preference for substrates containing stronger C-H bonds (Table 4.3). The k_2/k_1 rate-ratios for these competition experiments have been determined by quantifying the proportion of C-H activation products that result from the generation of **A** irreversibly in 1:1 (mol:mol) mixtures of hydrocarbon solvents. The thermal equilibration of the product distributions at early reactions times (at approximately 20% conversion) is presumed to be minimal and hence, the ratios of products should reflect a kinetic selectivity by **A**. A "per-C-H-bond" rate-ratio is calculated for each competition by adjusting the amount of each complex for the number of symmetry-equivalent C-H bonds.

A glance at the range of data obtained for the kinetic C-H bond selectivity expressed by **A** reveals a surprising lack of discrimination between aryl sp^2-C-H bonds and alkane sp^3-C-H bonds. However, accounting for the statistical influence of the number of symmetry-identical C-H bonds in each hydrocarbon molecule leads to normalized rate-ratios that reflect a preference for the stronger C-H bond in benzene. In the context of this bond-strength argument, the rate-ratio determined for the *p*-xylene / hexamethyldisiloxane mixture seems contradictory, since benzylic C-H bonds are weaker than methyl C-H bonds. However, steric influences presumably also affect the kinetic selectivity by **A** for different C-H bonds,[24] and the unusual preference for the weaker benzyl C-H bond might arise as a result of the smaller steric profile for *p*-xylene, as compared to the bulkier hexamethyldisiloxane. In addition, the ability of the arene substrates to engage in π-interactions with the unsaturated acetylene-containing **A** may also lead to the preferential activation of arene C-H bonds by **A**. Thus, it can be stated that arene C-H bonds are probably favored on steric grounds as well as electronic grounds, over either alkyl or benzyl C-H bonds. The resulting relative kinetic selectivity scale for C-H bond activation takes the order sp^2 > sp^3-alkyl ≈ sp^3-benzyl.

Table 4.3. Intermolecular kinetic selectivity exhibited by **A** for hydrocarbyl C-H bonds

Competition	k_2 / k_1	k_2 / k_1 **(per C-H bond)**
p-xylyl **4.4** $\overset{k_1}{\longleftarrow}$ **A** $\overset{k_2}{\longrightarrow}$ phenyl **4.1**	1.4(1)	1.4(1)
p-xylyl **4.4** $\overset{k_1}{\longleftarrow}$ **A** $\overset{k_2}{\longrightarrow}$ alkyl **4.9**	1.4(1)	0.49(3)
alkyl **4.9** $\overset{k_1}{\longleftarrow}$ **A** $\overset{k_2}{\longrightarrow}$ phenyl **4.**	1.0(1)	3.1(2)

Thermal equilibration is accomplished by heating these mixtures at 327 K over a period of 96 h. The equilibrium distributions of products that are observed reflect the relative stability of the complexes, and the determination of the equilibrium constants for these equilibria permits the approximation of the associated $\Delta G°(327K)$ values based upon a single-point calculation (Table 4.4). Correction of $\Delta G°(327K)$ for the entropic contribution made by the number of equivalent C-H bonds in each substrate permits the calculation of $\Delta G°_{corr}(327K)$, the value of which reflects the equilibrium preference on a "per-C-H-bond" basis.

Table 4.4. Approximate equilibrium free energies for mixtures of various vinyl complexes.

Equilibrium	K_{eq}	$\Delta G°$ (327K) (kcalmol^{-1})	$\Delta G°_{corr}$(327K) (kcalmol^{-1})
p-xylyl **4.4** $\rightleftharpoons$ phenyl **4.1**	1.4(1)	-0.8(1)	-0.8 (1)
p-xylyl **4.4** $\rightleftharpoons$ alkyl **4.9**	1.4(1)	-0.9(1)	-0.2(1)
phenyl **4.1** $\rightleftharpoons$ alkyl **4.9**	1.1 (1)	-0.3(2)	+0.7(1)

The stability of the complexes, which are largely influenced by the M-C bond strengths as described above, follow the trend of the conjugate C-H bond strengths. Thus, the stability trend for the hydrocarbyl vinyl complexes takes the expected form: Ph > alkyl ≈ benzyl.[15] In measuring these thermodynamic equilibria, however, one must keep in mind that the bonding of the vinyl ligand to W is a variable which contributes to the stability of these complexes. For example, in the case of the phenyl and alkyl vinyl complexes (**4.1** and **4.9**, respectively), the vinyl ligand is η^2-bound, whereas the η^2-*p*-xylyl ligand in **4.4** forces the vinyl into an η^1-bonding

mode. Thus, the strength of the substrate C-H bond (and resultant M-C bond) presumably is not the sole influence on the position of these equilibria.

4.2.3.3 The Nature of the Kinetic and Thermodynamic Selectivity Exhibited by A

It has been previously proposed that the degree of *kinetic* C-H bond selectivity expressed during the activation of hydrocarbon C-H bonds by a transition metal is proportional to the strength of the M-C interaction in the selectivity step. In cases where the selectivity event is the formation of a hydrocarbon σ-complex, M-C bond formation is minimal and the selectivity expressed is quite subtle, due to the weakness of the (C-H)→M interaction. The C-H bond selectivity observed by Jones' group during the generation of transient $Cp^*Rh(PMe_3)$ in hydrocarbon solution illustrates this case particularly well.[19] Where C-H bond breakage actually occurs during the selectivity step, the degree of M-C bond formation is much greater, and a more distinctive selectivity is exhibited. Such is the case for C-H bond activation by the Ti=NR fragment studied by Wolzcanski *et al.*[15] From the data presented in Tables 4.2 - 4.4 it is clear that acetylene-containing **A** displays small kinetic and thermodynamic preferences for substrate C-H bonds. The subtle kinetic C-H bond selectivity that is exhibited is consistent with the intermediacy of hydrocarbon σ-complexes along the postulated C-H bond activation pathway.

As mentioned above, the *thermodynamic* selectivity in these reactions is proposed to be governed by the relative strengths of the two metal-carbon bonds formed in competition during C-H bond activation, with the stronger C-H bond being activated preferentially to afford the more stable organometallic complex.[15,21b] That the intermolecular thermodynamic selectivity determined for this system is statistically identical to the intermolecular kinetic selectivity seems

initially troublesome. However, if the energy differences between the two barriers that lead to σ-formation between R-H or R'-H and **A** (i.e. the source of the observed intermolecular *kinetic* selectivity) are similar to the energy differential between the products of R-H and R'-H bond activation (the source of intermolecular *thermodynamic* selectivity) then the observed selectivities will be the same. Thus, it could be coincidence that the two types of selectivity yield similar results for the system described in this Chapter.

A few remarks regarding the effect of temperature on these thermodynamic selectivities is worthwhile at this point. The thermal C-H activation reactions presented in this Chapter are conducted at relatively low temperatures (45 – 55 °C); other analogous organometallic C-H activation systems for which thermodynamic selectivity data are available typically operate at much higher temperatures, ca. 90 – 140 °C. Thus, the $T\Delta S°$ contribution to $\Delta G°$ associated with such equilibria is substantially larger. As a result, a larger differential in product distribution is observed. For example, Wolczanski and Bennett have determined entropic contributions of -2.8 to -6.8 cal(mol•K)$^{-1}$ to the free energy of the equilibrium between (^{t}BuSiO)$_2$(^{t}Bu$_3$SiNH)TiR and (^{t}BuSiO)$_2$(^{t}Bu$_3$SiNH)TiR' in mixtures of RH / R'H at 90 °C (R / R' = Me / Et; CH_2SiMe_3 / Me).[15a] Assuming that, to a first approximation, the entropic contributions in the equilibria described in this Chapter are similar to those in the equilibria described by Wolczanski and Bennett, then an increase in the temperature employed for the studies described in this Chapter to 90 - 140 °C from 54 °C corresponds to an increase in $\Delta G°$ of 0.25 - 0.5 kcalmol^{-1}, respectively (employing –6.8 cal(molK)$^{-1}$ as the entropic contribution to the free energy). While these increases are not large in absolute magnitude terms, they increase the free energies of equilibria collected in Tables 4.2 and 4.4 by a factor of 1.3 – 3.5 (employing the highest and lowest value of K_{eq} in the two Tables). If the kinetic and thermodynamic selectivities exhibited by this system

indeed are coincidentally similar in energy at 54 °C, as suggested above, then higher temperatures such as those employed in other studies are required for the exhibition of a substantial thermodynamic selectivity towards different types of C-H bonds.

4.2.4 Dual C-H Bond Activation in Aliphatic Hydrocarbons

Since our initial report of the double C-H activation of *n*-pentane and *n*-hexane by **1** under thermolysis conditions,[7c] thermolyses of **1** in the presence of a variety of other hydrocarbons have been performed in an attempt to determine the scope and limitations of this activation process. The results of these investigations are summarized in Scheme 4.6.

Scheme 4.6

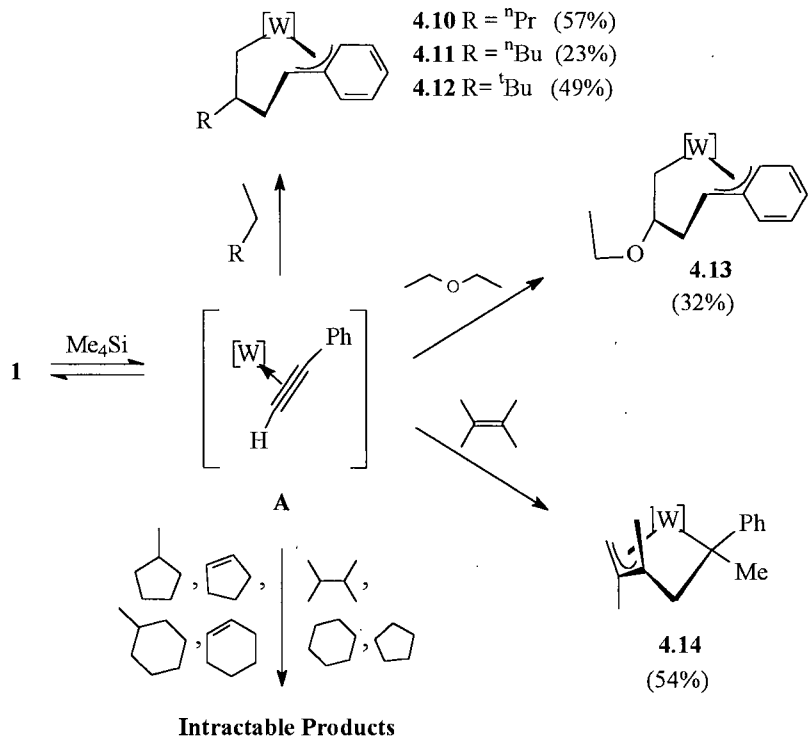

[W] = Cp*W(NO)

Thermolysis of **1** in the presence of *n*-pentane, *n*-hexane, 2,2-dimethylbutane, and diethyl ether results in their double C-H bond activation, yielding the η^3-benzyl metallacycles **4.10**, **4.11**, **4.12**, and **4.13,** respectively. These complexes are isolated in moderate yields as yellow or yellow-brown crystals, the ^{1}H NMR spectra of the reaction mixtures revealing that the crude yields fall in the range 50-70 %. These complexes are moderately air-stable in the solid-state, persisting for up to 24 hours in air with little measurable decomposition.

Characterization of these metallacycles is facilitated by the solid-state molecular structure of **4.10** (Figure 4.2) which has been established by an X-ray crystallographic analysis.[25]

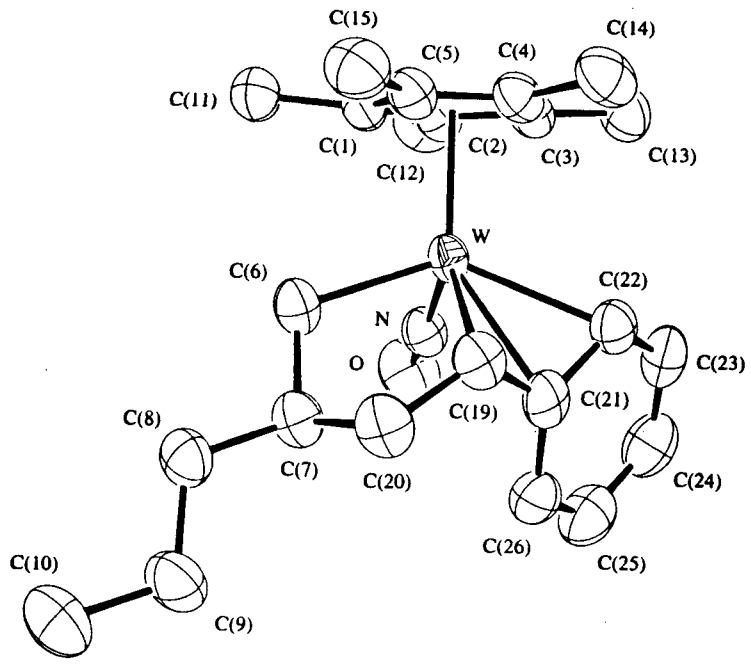

Figure 4.2. The solid-state molecular structure of complex **4.10**. Thermal ellipsoids represent the 50% probability level.

Clearly, a molecule of pentane has been incorporated into the coordination sphere of the metal via two C-H bond cleavage processes, i.e. one at the terminal position binding the molecule to the metal, and the second in the β-position facilitating its fusion to the vinyl ligand. Single M-C and C-C[26] bonding contacts in the W-C(19) and C(19)-C(20) links (2.301(5) and 1.510(5) Å, respectively) implicate that the vinyl fragment has been hydrogenated to yield the saturated W-CHPh-CH_2 fragment. The hydrocarbyl and vinyl fragments are fused by a single bond of distance 1.535(7) Å between C(7) and C(20). These metallacycles are stabilized as 18e species by virtue of a W-η^3-benzyl interaction, as evinced by the W contacts at C(19), C(21), and C(22) of 2.301(4), 2.381(1), and 2.371(4) Å, respectively. The W-C(19)-C(21) angle of 75.5(3)° is nearly identical to the M-C_α-Ph angle found in other η^3-benzyl complexes.[27] In addition to these features, the lengthened C(21)-C(22) distance (1.432(5) Å) and the shortened C(19)-C(21) distance (1.419(5) Å) are indicative of a substantial degree of π-delocalization in the allyl fragment. Other literature examples of η^3-benzyl interactions at transition-metal centres display comparable asymmetric structural features.[27]

Remarkable in the ^1H and ^{13}C NMR spectra of these complexes (Table 4.7) is the broadness or complete lack of signals attributable to the ^1H and ^{13}C nuclei involved in the η^3-benzyl interaction. It has been proposed previously that complexes of this type undergo a rapid η^3-η^1-η^3 interconversion (shown below) that equilibrates the *ortho / ortho'* and *meta / meta'* H and C magnetic environments.[28]

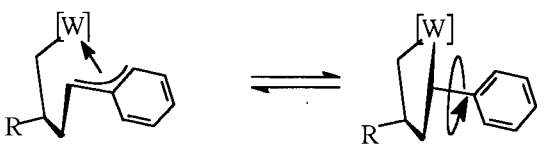

[W] = Cp*W(NO)

For reasons of clarity, the VT behavior of *t*-butyl complex **4.12** has been examined in detail as a representative example (Figure 4.3), though each η^3-benzyl complex behaves similarly. At 313 K, the ^{1}H NMR spectrum (CD_2Cl_2) of complex **4.12** displays broadened downfield signals attributable to the protons in the phenyl ring. Triplets at 7.10 and 6.70 ppm integrating for 2 H and 1 H are tentatively assigned as being due to the *meta*- and *para*-H protons, respectively. The *ortho* proton signals are distinctly absent at this temperature. Cooling of the sample results in the collapse of the triplets at 7.10 ppm and 6.70 to sets of doublets of doublets, while signals at 6.90 and 3.43 ppm become apparent and intensify with a lowering of the temperature. Fine structure is evident in all four signals at 253 K, and no further change occurs in the spectrum with cooling to 233 K.

The rate of this fluxional process at the coalescence temperature may be determined utilizing the separation of the H_m and $H_{m'}$ signals in the low temperature ^{1}H NMR spectrum recorded at 233 K. The 67(1) Hz separation of these two signals corresponds to a rate of rotation of 149(2) Hz at coalescence (T = 290 K).[29] The activation energy for this process at coalescence (290 K) is 14.1(1) kcalmol^{-1}, consistent with a rotation of the phenyl ring that is hindered by the stabilizing effect of the η^3-benzyl interaction.

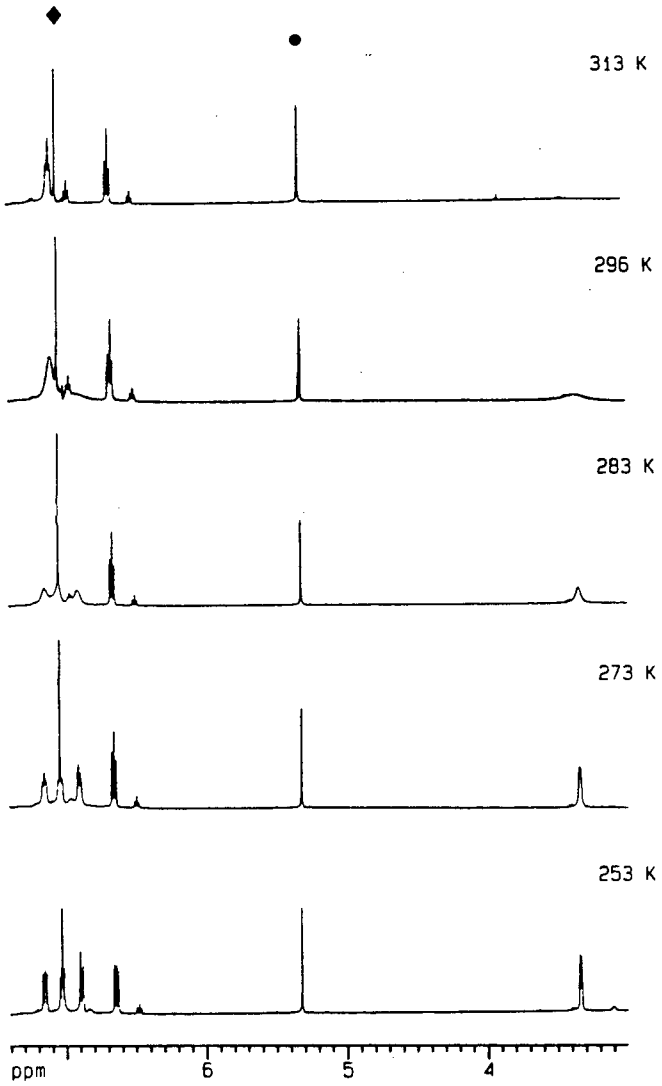

Figure 4.3. The temperature dependence of the signals in the ^{1}H NMR spectrum (CD_2Cl_2) attributable to the η^3-benzyl interaction in **4.12** (♦ ≡ solvent impurity, • = $CHDCl_2$).

A ^{1}H COSY experiment recorded at 233 K affords the conclusive assignment of the five signals (Figure 4.4). The upfield doublet at 3.43 ppm is assigned to the *ortho*-H nucleus α to the W centre and bound to the pseudo-tetrahedral allylic C_α. H_o couples strongly to H_m, which in turn couples to the doublet of doublets ascribable to H_p. H_p couples to both sets of doublets of

doublets, each attributed to H_m and H_m', and the H_m' signal displays coupling to the doublet that is attributable to H_o'.

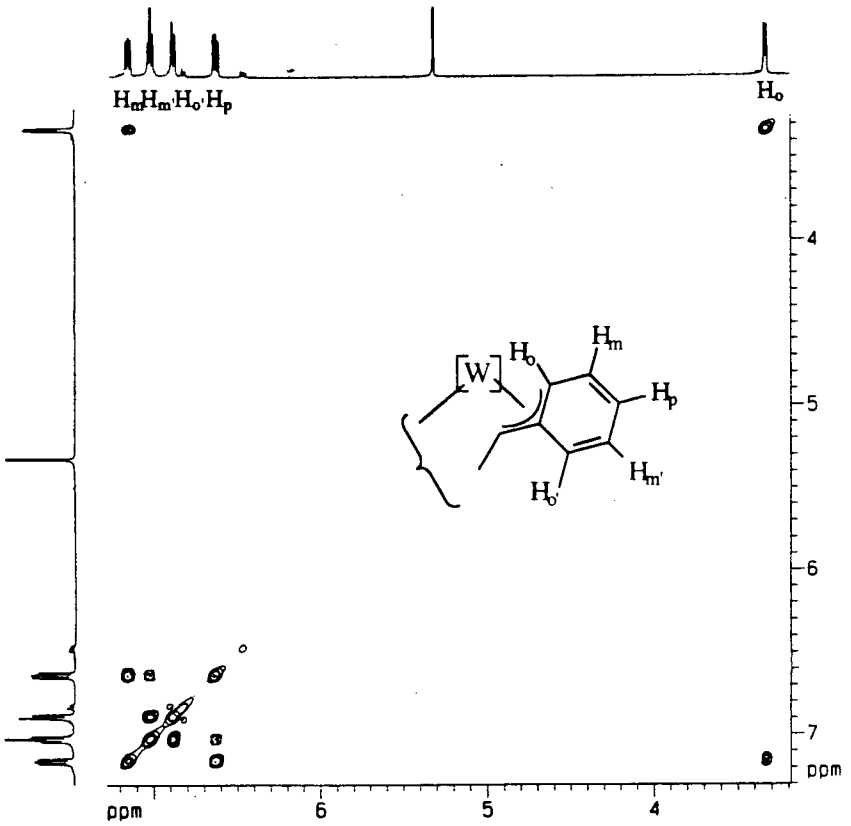

Figure 4.4. The downfield region of the ^1H COSY spectrum of complex **4.12** (CD_2Cl_2) recorded at 233 K.

4.2.5 Selectivity in the Dual C-H Activation of Saturated Hydrocarbons

In discussing the microscopic nature of the selectivity that yields the η^3-benzyl metallacycles **4.10-4.13**, the proposed mechanism by which they are formed must be considered (Scheme 4.7).[7c] Initiation of the dehydrogenation process occurs with terminal C-H bond activation of the hydrocarbon substrate by **A**. β-H elimination in the resultant alkyl-containing **B**

completes the dehydrogenation of the hydrocarbyl fragment. Transfer of the β-H to the vinyl α-C yields the bis(η^2-olefin) intermediate **C**, and coupling of the two metal-bound olefins affords the observed 18e metallacycles. Numerous attempts were made to prepare these intermediate compounds by synthetic methods to establish their existence along the reaction pathway. For example, attempts were made to prepare analogues to **B** via metathesis of the chloride ligand in vinyl-chloride-containing **2.1** utilizing alkylating reagents such as lithium-, magnesium-, and zinc-hydrocarbyls as well as lithium organocuprates. In each case, intractable oils containing unidentifiable compounds were obtained. Likewise, attempts to replace the olefin ligands generated in **C** with other olefins and acetylenes in substitution reactions during the thermolysis of **1** in pentane also failed. Nonetheless, ample literature precedents exist to support the mechanism depicted in Scheme 4.7 and the individual transformations which comprise it.[30]

Scheme 4.7

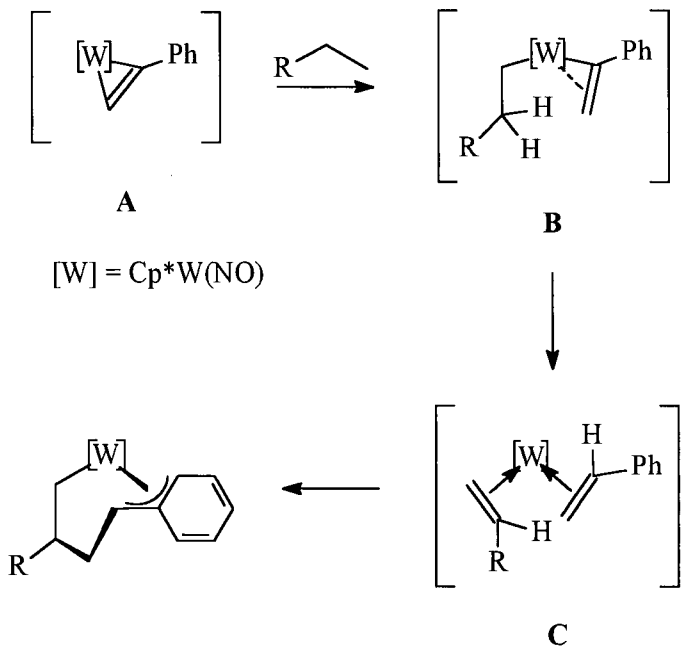

The selectivity exhibited in this chemistry for alkane C-H bonds has been assessed by conducting these thermolyses in the presence of a variety of aliphatic substrates. It is worth noting that all the products of dual C-H bond activation arise from the activation of C-H bonds at the terminal and β-position in the hydrocarbon fragment. Thus, one can conclude that the reaction exhibits a selectivity for terminal C-H bonds. Such a conclusion raises a question regarding the necessity of a terminal methyl substituent in the hydrocarbyl substrate for the clean conversion of **1** to tractable product. The answer to that question is illustrated in Scheme 4.6. In contrast to the moderately clean formation of **4.10** – **4.13**, the thermolyses of alkyl vinyl complex **1** in cyclopentane, cyclopentene, cyclohexane, and cyclohexene each lead to the formation of a plethora of intractable products, as evinced by the number of Cp* methyl resonances in the ^{1}H NMR spectra of the resulting reaction mixtures. Thus, primary C-H bonds in the hydrocarbon substrate are requisite for the clean conversion of **1** to tractable metallacyclic products.

As the results of the thermolysis of **1** in methylcyclopentane, methylcyclohexane and 2,3-dimethylbutane indicate (Scheme 4.6), the presence of a methyl substituent is not sufficient for the clean conversion of **1** to these metallacyclic products. The thermolysis of **1** in these latter methyl-substituted alkane substrates also affords mixtures of intractable products, despite the presence of a methyl substituent in each of the substrates employed. The formation of the 18e metallacyclic products appears to be sensitive to the substitution at the β-C nucleus proximal to the terminal site of C-H activation as well. For example, only an oily tar is obtained from the thermal decomposition of **1** in 2,3-dimethylbutane, yet complex **4.12** is generated in good yields during the thermolysis of **1** in 2,2-dimethylbutane (Scheme 4.8).

Scheme 4.8

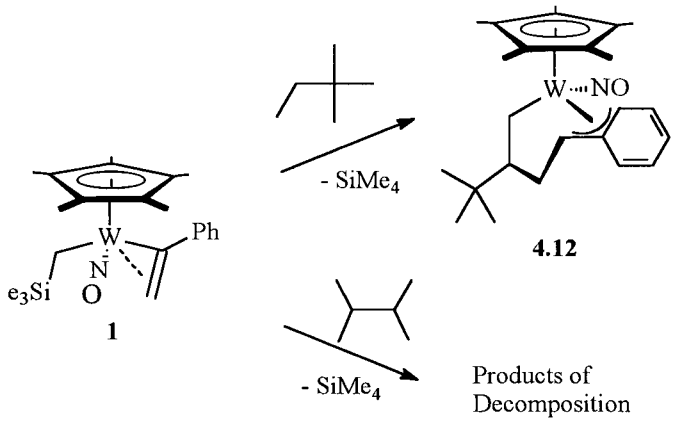

The selectivity exhibited in these reactions is proposed to arise as a result of steric interactions that come into play during the formation and subsequent isomerization of bis(olefin) **C**, and is not regarded as a manifestation of an ability or inability by **A** to activate particular C-H bonds. This concept is illustrated in Figure 4.5 below.

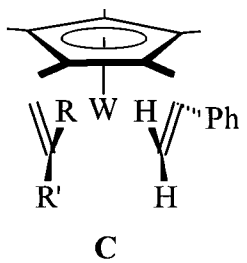

Figure 4.5. Steric interactions in the proposed bis(olefin) intermediate **C** [R, R' = H or hydrocarbyl]. The NO ligand is eclipsed by the W centre.

Thus, the dehydrogenation of an alkane containing a terminal ethyl substituent affords an α-olefin CH_2=CHR (R' = H) to which the η^2-CHPh=CH_2 ligand cleanly couples in **C**. On the other hand, branched or cyclic aliphatic substrates yield multi-substituted, internal olefins upon

dehydrogenation (R, R' ≠ H). In these cases, unfavourable steric interactions between the substituents of the internal olefin and the other ligands in the W coordination sphere lead to the decomposition of **C**, presumably by encouraging dissociation of the olefin or by slowing the rate of reductive coupling so that decomposition pathways become kinetically competitive.

The regioselectivity extant in the formation of metallacycles **4.10 – 4.13** is also worth noting. The 3,5-substitution in the metallacycle ring is typical of such metal-mediated couplings of asymmetric olefins or acetylenes.[31,11b] More striking is the stereoselectivity apparent in the coupling of the two hydrocarbyl fragments; it is only the *re* face of the η^2-CHPh=CH_2 ligand and the *si* face of the η^2-CH_2=CHR ligand that are coupled together in the metallacyclic products. The former enantiofacial selectivity presumably arises due to the steric interactions between the Cp* ring and the phenyl substituent that are minimized when the *re* face of the η^2-CHPh=CH_2 ligand is presented to the metal. The reason for the *si*-η^2-CH_2=CHR enantiofacial selectivity is less obvious, but an inspection of the product structures that result from the coupling of either enantioface of the η^2-CH_2=CHR ligand (Figure 4.6) clarifies the observed selectivity on steric grounds.

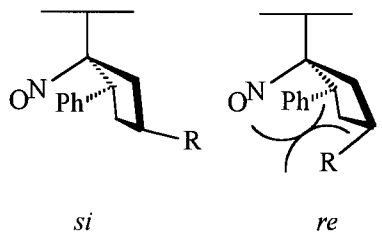

Figure 4.6. The steric interactions that result from the coupling of the *si* or *re* face of the primary olefin to the styrene ligand in intermediate **C**.

Steric conflict between the R substituent and the NO ligand and Ph substituent in the complex that results from *re* enantiofacial coupling probably renders this pathway a higher-energy process than the coupling of the η^2-CH_2=CHR ligand *si* face to the η^2-CHPh=CH_2 ligand; hence, *si*-enantiofacial coupling predominates.

4.2.6 Dual C-H bond Activation in an Olefinic Substrate

The thermolysis of alkyl vinyl complex **1** in 2,3-dimethyl-2-butene, a hydrocarbon substrate lacking β-hydrogens, leads to an alternate mode of reactivity. In this instance, moderate yields of yellow, crystalline *endo*-allyl complex **4.14** are obtained (eq 4.11). Fusion of the olefinic fragment to the vinyl fragment has occurred in a manner reminiscent of the formation of compounds **4.10-4.13**, though the two C-H bond activations in this case occur at the mutually-*trans*-γ positions.

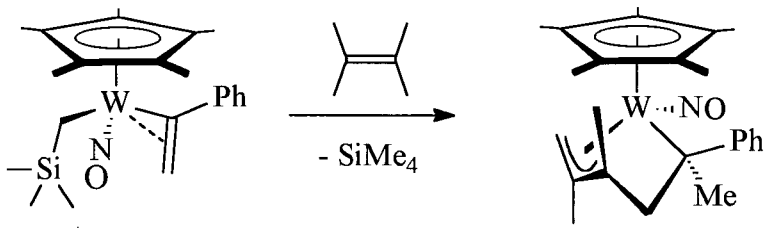

(eq 4.11)

1 **4.14**

The solid-state molecular structure of **4.14** has been established by an X-ray crystallographic analysis and is illustrated in Figure 4.7.[32] The allylic W-C(11), W-C(12), and W-C(13) bond lengths of 2.249(7), 2.331(7), and 2.353(7) Å, as well as the respective C(11)-

C(12) and C(12)-C(13) contacts of 1.425(11) and 1.397(10) Å, are nearly identical to those extant in similar structurally characterized allyl nitrosyl complexes of tungsten.[33]

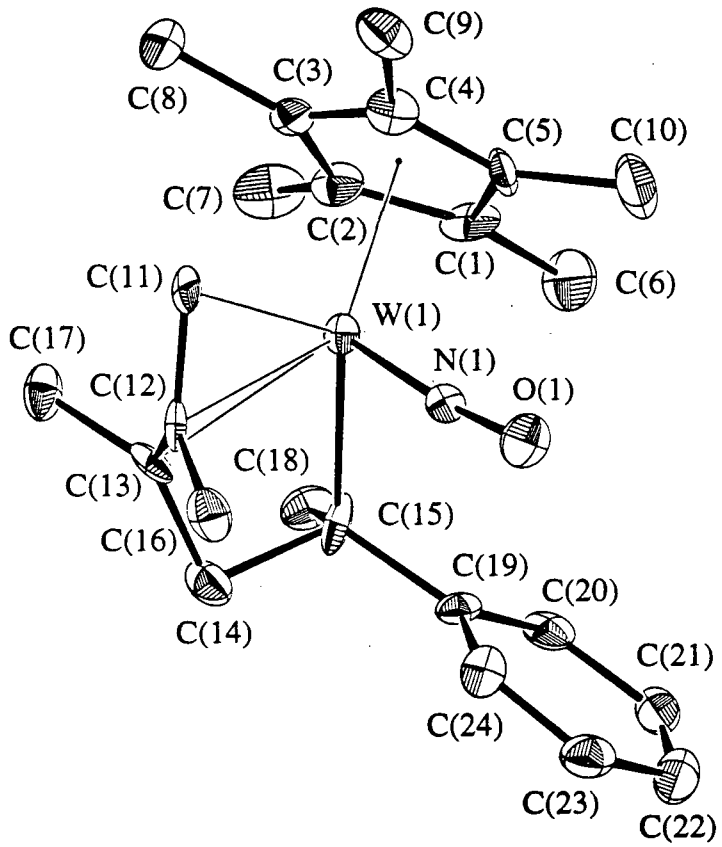

Figure 4.7. The solid-state molecular structure of complex **4.14**, with thermal ellipsoids depicting the 50% probability level.

The C(15)-C(18) bond distance of 1.535(10) Å implies that saturation of the vinyl fragment has occurred, and the W-C(15) distance of 2.353(7) Å is indicative of a long W-C single bond. Of

note is the acute C(13)-C(14)-C(15) angle of 99.0(7)° in the constrained pseudo-four-membered ring that results from the fusion of the two hydrocarbyl fragments. In the ^{1}H NMR spectrum of **4.14**, the signals for the corresponding methylene protons at C(14) display a large two-bond coupling of 13.2 Hz, consistent with the geometric distortion existing about the sp^3-hybridized C(14) nucleus.

Scheme 4.9

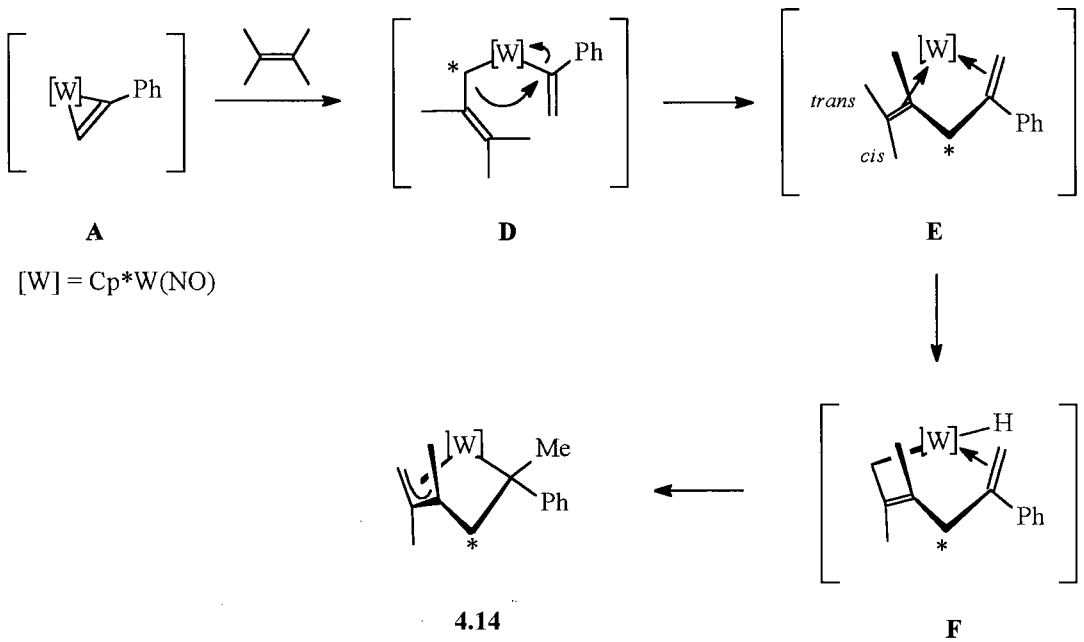

The case of the dual C-H activation of 2,3-dimethyl-2-butene is unique in that, in the absence of accessible β-C-H bonds, an entirely different mode of reactivity results (Scheme 4.9). The observation that $SiMe_4$ is liberated in this reaction implicates an initial step that involves the elimination of $SiMe_4$ and the activation of a methyl C-H bond, thereby affording an intermediate allyl vinyl complex (**D**). For reasons of clarity, the allyl α-C in **D** has been highlighted as a point of reference. At this point it is proposed that the allyl and vinyl ligands couple to yield a diene

complex (**E**) in a process similar to that recently reported by Ipaktschi and co-workers for a CpW(NO) allyl/acetylide system.[33a] Activation of a *trans*-methyl C-H bond in the resultant diene ligand yields an allyl olefin hydride intermediate (**F**), and transfer of the hydride to the olefin affords complex **4.14**.

Two points regarding the formation of complex **4.14** are worth mentioning. It is interesting that the intermediate η^4-diene-containing **F** postulated above is *not* isolable, given that stable, isolable η^4-*trans*-butadiene complexes of the CpW(NO) fragment have been reported previously by the Legzdins group.[34] It is the combination of the accessible butadiene frontier molecular orbitals and the *trans* conformation of the butadiene ligand that stabilizes the formation of these latter complexes. Such attributes in the non-conjugated η^4-diene ligand postulated to exist in **F** are lacking, and presumably contribute to its instability. Secondly, only the least-substituted allyl fragment is formed in the final product. While the second C-H bond activation that affords the allyl function *could* occur at the endocyclic position (*) in **F** (as observed in the CpW(NO)-based system reported by Ipaktschi and coworkers[33a]), the internal-allyl-containing complex is not observed as a byproduct. The constrained geometry of the metallacyclic fragment and the considerable ring strain that must be overcome to cleave one of the endocyclic methylene C-H bonds at the W centre probably render this pathway energetically inaccessible.

4.2.7 The Electronic Nature of Cp*W(NO)(η^2- PhC≡CH)

To the best of our knowledge, Cp*W(NO)(η^2-PhC≡CH) is the first acetylene complex postulated to activate alkane C-H bonds in an intermolecular fashion.[35] Such acetylene

complexes are often invoked as reactive intermediates in transition-metal-mediated transformations, the reductive coupling chemistry mediated by the Group 4 metallocenes being an excellent example.[36] In contrast, stable acetylene complexes of the transition metals are also quite abundant,[37] and those of Mo and W have been especially well-studied.[38] Consequently, a consideration of the frontier molecular orbitals extant in **A** aids in understanding its reactivity towards C-H bonds.

As a starting point, the relationship between Cp*W(NO)(η^2-PhC≡CH) and Cp*W(NO)(PPh_3) is considered. Burkey *et al.* recently reported the fully-characterized η^2-ethyl acetate adduct of this latter fragment.[39] The formation of this ester adduct has been attributed to the synergism of the strong σ-acceptor, π-donor character inherent to the W centre in the 16e Cp*W(NO)(PPh_3) fragment, by analogy to the $[CpRe(NO)(PR_3)]^+$ system of Gladysz's group.[40] It is proposed herein that σ-complexation of a hydrocarbon C-H bond is facilitated by the same synergic donor/acceptor ability in the Cp*W(NO)(η^2-PhC≡CH) fragment. To clarify this proposal, a comparison of the valence-molecular-orbital structure of Cp*W(NO)(η^2-HC≡CH) and Cp*W(NO)(PPh_3) is presented below.

Before considering the MO architecture of the Cp*W(NO)L fragment [L = PR_3, HC≡CH], it is worthwhile noting that unlike the unsaturated Cp*W(NO)(PPh_3) fragment, acetylene complex **A** is an 18e, closed-shell species if one assumes that the acetylene ligand functions as a 4e donor. σ-Complexation of a C-H bond by **A**, on the other hand, can only occur if the metal centre is electronically unsaturated. Thus, it is reasonable to assume that **A** must exist transiently as a 16e intermediate with the acetylene ligand functioning as a 2e donor only.

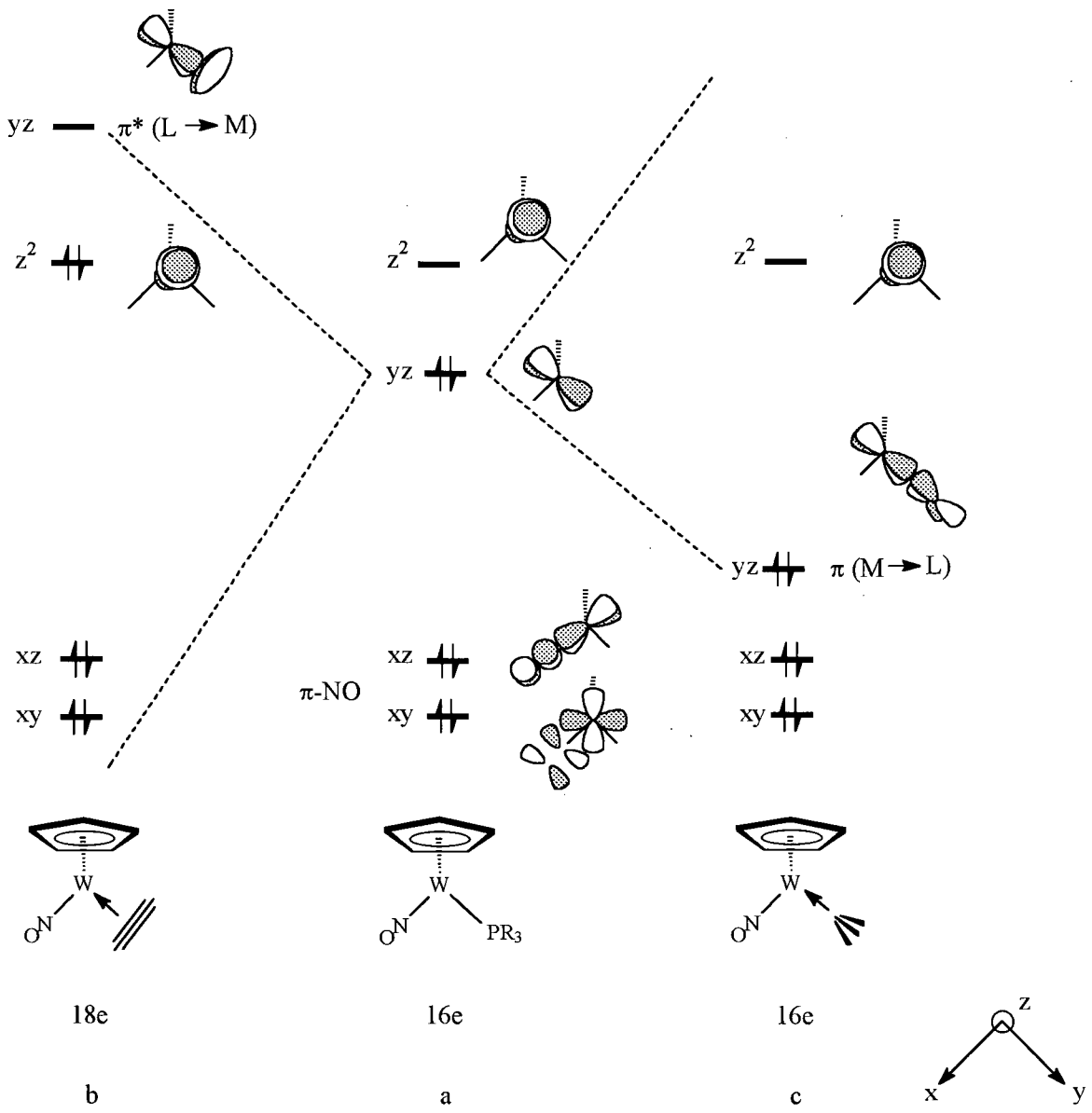

Figure 4.8. A qualitative MO diagram depicting the valence-orbital interactions in CpW(NO)(L) fragments [L = PR_3, HC≡CH].

A qualitative MO diagram depicting the W d-orbital interactions in the Cp*W(NO)L fragment is presented in Figure 4.8. The Cp*W(NO)L fragment is depicted as pyramidal-at-

metal, based on a recent computational study that describes the conformational dependence of two-legged piano-stool complexes on the nature of the ancillary ligands.[41] The results of this study reveal that the pyramidal-at-metal conformation is energetically preferred in complexes bearing strong-field ligands such as CO, CS, or NO^+. The four highest-energy, tungsten-based d-type orbitals[42] of the pyramidal 16e $Cp^*W(NO)PR_3$ fragment take the form and order depicted in Figure 4.8a, according to theoretical studies of similar systems.[43] The d_{xy} an d_{xz}-type orbitals are lowest in energy as a result of W π-back-donation to the NO ligand. The HOMO is essentially a metal-centred, non-bonding, d_{yz}-type orbital of π-symmetry with respect to the PR_3 ligand, and the LUMO is a metal-centred, d_{z^2}-type orbital of σ–symmetry with respect to the PR_3 ligand. With respect to the open coordination axis (along the z-axis) the HOMO and LUMO are also π- and σ-symmetric, respectively.

Replacement of the PR_3 ligand by an acetylene ligand introduces an orientational dependence into the metal-acetylene bonding interaction (Figure 4.8b (acetylene in the page plane) and 4.8c (acetylene perpendicular to the page plane). Though the alkyne possesses the ability to do so, it cannot act as both a π-donor and π-acceptor in this system because the two requisite π-symmetric, mutually-orthogonal metal d-orbitals are unavailable.[44] Aligning the acetylene longitudinal axis coplanar with the W-NO vector (Figure 4.8b) allows the acetylene ligand to function as a 4e π-donor via a ligand→metal bonding interaction with the π-symmetric d_{yz}-type orbital. The metal d_{yz} orbital is destabilized and the d_{z^2} orbital becomes doubly-occupied as a result. The acetylene functioning as a 4e donor in this way affords an 18e intermediate in which all bonding and non-bonding metal-based orbitals are doubly-occupied, with the filled, non-bonding metal orbital remaining high in energy. It has been suggested that the presence of such a higher-energy, metal-centred orbital in species of this type has led to the

paucity of such isolable, low-valent two-legged piano-stool complexes.[45] Despite being coordinatively unsaturated, the acetylene complex depicted in Figure 4.8b is electronically saturated and as a result, σ-complex formation is blocked by the absence of an empty metal-centred orbital of σ-symmetry with respect to the coordination axis.

In contrast, when the acetylene longitudinal axis is oriented perpendicular to the M-NO vector (Figure 4.8c), the acetylene functions as a π-acceptor, stabilizing the W d_{yz}-type orbital via tungsten → acetylene π–back-donation. The symmetry of the metal-centred d_{z^2} orbital precludes its interaction with the acetylene ligand and it remains non-bonding. Hence, the acetylene ligand functions as a 2e donor only and the resulting acetylene complex, containing 16 valence electrons, is both electronically and coordinatively unsaturated. Its HOMO and LUMO are ideally arranged for the complexation of σ-basic, π-acidic species. Thus, the (η^2-C-H)→W interaction is facilitated by C-H σ-donation into the σ-symmetric LUMO and stabilized by π-back-donation by the HOMO into the π-symmetric C-H σ* orbital. In the manner reported for the complexation of nitriles and esters by Cp*W(NO)(PPh_3),[39] it is also proposed that the reductive coupling chemistry which comprises Chapter 3 arises due to the ability of **A** to complex esters and nitriles via the same synergic σ–π interaction. DFT modeling of the CpW(NO)(η^2-HC≡CH) fragment is currently being conducted by Drs. Rinaldo Poli and Kevin Smith.[46]

4.3 Epilogue and Future Work

The activation of C-H bonds in a wide range of hydrocarbon substrates has been demonstrated to occur following the thermal decomposition of $Cp^*W(NO)(CH_2SiMe_3)(CPh{=}CH_2)$ (**1**) to the acetylene complex, $Cp^*W(NO(\eta^2\text{-}PhC{\equiv}CH)$ (**A**). In cases where only one C-H bond is activated, the conversions are clean and quantitative. Thus, the activation of a benzene C-H bond yields the corresponding phenyl vinyl complex. In the case of methyl-substituted arenes, mixtures of aryl and benzyl complexes are obtained. In these reactions, no products of *ortho*-C-H bond activation are observed, presumably due to the steric shielding of the *ortho*-C-H bond by the methyl substituent.

The mechanisms by which RH is eliminated from $Cp^*W(NO)(R)(CPh{=}CH_2)$ and hydrocarbon C-H bond activation is accomplished in the resultant acetylene complex **A** have been investigated. Kinetic and mechanistic studies are consistent with those reported in Chapter 3, where reductive coupling reactions between coordinated substrate and acetylene were studied. Thus, hydrocarbon elimination affords acetylene-containing **A** in a rate-limiting, reversible step. Hydrocarbon C-H bond activation "traps" **A** in a faster reversible step, affording the observed hydrocarbyl products. Rapid scrambling of deuterium label into the vinyl positions and the rapid appearance of equilibrium mixtures of aryl C-H bond activation products at short reaction times are consistent with the transiency of hydrocarbon σ-complexes prior to both the rate-limiting elimination of hydrocarbon to afford **A** and to the activation of a substrate C-H bond by **A** in the microscopic reverse.

The proportion of aryl and benzyl C-H bond activation is dependent upon the relative number of accessible aryl and benzyl C-H bonds. Intramolecular competition studies reveal that, statistically, the stronger C-H bond is preferentially activated and gives rise to the greater proportion of product. This feature is also manifested in the kinetic and thermodynamic intermolecular C-H bond selectivity exhibited by **A**. While the observed trends follow those reported previously (the stronger C-H bond being the preferred site of activation), the expression of kinetic selectivity is reduced during the formation of hydrocarbon σ-complexes. This is consistent with the proposed mechanism of C-H activation and contrasts to the selectivities that are observed for cases where C-H bond cleavage occurs during the selectivity event.

The dual C-H bond activation of aliphatic hydrocarbons represents a unique case in which the dehydrogenation of a hydrocarbon molecule is facilitated by the vinyl ligand functioning as an intramolecular hydrogen acceptor. Elaboration of the hydrocarbyl fragment is afforded by the reductive coupling of the resultant olefin ligands in the metal's coordination sphere. In these conversions, tractable products are only obtained in the presence of aliphatic substrates which contain an ethyl substituent. This selectivity is presumed to result from steric constraints within the bis(olefin) reductive coupling step. Thus, the α-olefin CH_2=CHR that results from the dehydrogenation of CH_3CH_2R cleanly couples to the styrene ligand to afford the observed η^3-benzyl products. On the other hand, the activation of branched or cyclic hydrocarbons leads to a plethora of products. It is assumed that the internal olefins that result from the dehydrogenation of these latter substrates couple to the vinyl fragment with difficulty, due to unfavourable steric interactions between the coordinated olefins and ancillary ligands in the coordination sphere of W. Decomposition pathways presumably become kinetically competitive, and mixtures of intractable products are obtained. The regio- and enantioselectivity

extant in these cyclizations are proposed to arise as a result of steric interactions between the coordinated olefin ligands and the Cp*W(NO) fragment during coupling of the hydrocarbyl fragments. The dual C-H activation of 2,3-dimethyl-2-butene represents a unique case in which the absence of β-hydrogens in the hydrocarbyl fragment enforces an alternate mode of reactivity.

An MO scheme for the W-acetylene bonding interaction aids in rationalizing the activity of acetylene-containing **A** towards substrate C-H bonds. An acetylene orientational dependence is apparent upon inspection of the molecular orbitals in this intermediate complex. When the acetylene ligand is oriented parallel to the W-NO vector in pyramidal **A**, the two-legged piano-stool complex is electronically saturated. However, in an orientation perpendicular to the W-NO vector, the acetylene ligand functions as a 2e donor only, and the intermediate complex is both electronically and coordinatively unsaturated. We propose that the resultant σ-symmetric metal-centred LUMO and π-symmetric metal-centred HOMO render this 16e acetylene complex both strongly Lewis acidic and Lewis basic, facilitating the binding and cleavage of a substrate C-H bond.

There are two key factors to the viability of this dual C-H activation process. The first is the ability of **A** to activate hydrocarbon C-H bonds, and the second is the ability of both the acetylene ligand in **A** and the vinyl ligand that is generated in the C-H activation event to function as hydrogen acceptors. It remains to generalize this chemistry so as to introduce functionality into the vinyl ligand. Thus, new routes to the preparation of organometallic vinyl transfer agents are required. Before this stoichiometric process can be rendered catalytic, a ligand set must be devised that can function not only as a hydrogen acceptor, but also a hydrogen donor. Because the dehydrogenation of the hydrocarbon substrate generates two equivalents of H, a means of temporarily storing these H atoms and then returning them to the hydrocarbyl

fragment after functionalization must be devised so as to avoid the build-up of a surplus of hydrogen in the system. In the past, this has been accomplished by using an external hydrogen acceptor such as *tert*-butylethylene (TBE) to "absorb" the two equivalents of hydrogen generated in each alkane dehydrogenation cycle.[47] These systems are not truly catalytic in all reagents, because a stoichiometric amount of TBE is required for the success of the catalytic cycle. Goldman and coworkers have eliminated the build-up of hydrogen in such a catalytic cycle by designing an organometallic reagent with a bulky coordination environment that promotes reductive elimination of H_2 from the metal centre.[48] Conducting these dehydrogenation reactions under reflux effects the elimination of H_2 from the system as a gas. An advance on this capability could be made with the incorporation of an intramolecular, reversible hydrogen acceptor into the organometallic complex. Such a Lewis-basic site would function as a temporary hydrogen storage device following C-H activation of the hydrocarbon substrate. Functionalization of the hydrocarbyl fragment at the metal centre would then be followed by the return of the hydrogen to the functionalized fragment during its elimination from the metal's coordination sphere. However, much work is required to develop and incorporate such a system into a viable catalytic cycle.

4.4 Experimental Procedures

4.4.1 General Methods.

All reactions and subsequent manipulations were performed under anaerobic and anhydrous conditions either under high vacuum or an atmosphere of dinitrogen or argon. General procedures routinely employed in this research are described in detail in Chapter 2, Section 2.4.1. Where appropriate, ^{1}H homonuclear decoupling experiments, COSY, NOE, HMQC, HMBC, VT ^{1}H and ^{13}C experiments, and gate-decoupled ^{13}C NMR experiments were performed to facilitate ^{1}H and ^{13}C spectral assignments.

4.4.2 Reagents

Benzene, toluene, *o*-, *m*-, and *p*-xylene, hexane, pentane, diethyl ether, 2,2-dimethylbutane, 2,3-dimethylbutane, 2,3-dimethylbutene, cylcohexane, methylcyclohexane, cyclopentane, cyclopentene, and hexamethyldisiloxane (Aldrich) were distilled or vacuum transferred from sodium or sodium/benzophenone ketyl. Benzene-d_6, tetramethylsilane-d_{12}, and *p*-xylene-d_{10} were vacuum transferred from sodium or sodium/benzophenone ketyl.

4.4.3 Kinetic Studies

Kinetic studies were performed using gas-tight quartz cells and an HP8452 UV-vis spectrometer equipped with a thermostatted cell holder connected to a VWR1150 constant-

temperature bath which was accurate to ± 0.05 °C. At least three replicate kinetic runs were employed in the determination of k_{obs} for a given set of experimental conditions. Typical kinetic runs monitored the product band at 350 or 360 nm arising from the thermolysis of 0.1 - 1 mg of **1** or **4.4** dissolved in 3 mL of solvent over not less than 3.5 half-lives, unless otherwise noted. Absorbence values for t_∞ were obtained by optimization of the squared residual, R^2, for the regression line fitted to the data through a first-order analysis. The optimized A_∞ values agreed within 8% with those determined experimentally for selected kinetic runs.

4.4.4 Competition Experiments

A sample of Cp*W(NO)(CH_2SiMe_3)(CPh=CH_2) (8 mg, 15 μmol) was dissolved in a 1:1 (mol:mol) mixture of the appropriate solvents (0.5 mL) which was prepared by weighing equimolar volumes of solvent into a vial prior to addition of the solid organometallic reagent. The resulting solution was heated at 54 °C in an NMR tube equipped with a Rotaflo Teflon valve. After 1 h the volatiles were removed under vacuum, C_6D_6 was added, and the ^1H NMR spectrum was recorded utilizing relaxation delays in excess of 90 s to ensure full relaxation of all proton environments prior to excitation. The ratios of products were determined by multiple integration of the appropriate vinyl and/or methyl signals. The absolute errors in these integrations were assumed to be 5%. The per-C-H-bond selectivities were calculated analogously, but the amount of each species was corrected for the number of symmetry equivalent C-H bonds in each case.

4.4.5 Equilibration of Cp*W(NO)(R^2)(CPh=CH_2) and Cp*W(NO)(R^1)(CPh=CH_2)

Solutions of Cp*W(NO)(CH_2SiMe_3)(CPh=CH_2) (8 mg, 15 μmol), dissolved in a 1:1 (mol:mol) mixture (0.5 mL) of the appropriate solvents as in the previous case, were heated at 54 °C in an NMR tube equipped with a Rotaflo Teflon valve. After 96 h the volatiles were removed under vacuum, the residue was dissolved in C_6D_6, and the ^1H NMR spectrum was recorded. The equilibrium constant K_{eq} (327 K) was determined in each case as the ratio [Cp*W(NO)(R^2)(CPh=CH_2)] / [Cp*W(NO)(R^1)(CPh=CH_2)]. A single-point calculation utilizing $\Delta G°$ (327 K) = -RTln(K_{eq}) afforded approximate values of the equilibrium free energy for each of the equilibria. Additionally, the amounts of Cp*W(NO)(R^2)(CPh=CH_2) and Cp*W(NO)(R^1)(CPh=CH_2) were corrected for the number of symmetry-equivalent C-H bonds in each case, thereby yielding the per-C-H bond equilibrium expression.

4.4.6 Thermolyses of Cp*W(NO)(CPh=CH_2)(CH_2SiMe_3) (1) in Hydrocarbon Solvents

The thermolyses of complex **1** in various solvents were performed in a similar manner throughout. Compounds **4.1**-**4.9** crystallize readily from hydrocarbon or ethereal solvents and may be isolated in yields ranging from 70-85%. The preparation of **4.1** via the thermolysis of **1** in benzene is described as a representative example. In an inert atmosphere glovebox a thick-walled glass bomb was charged with **1** (135 mg, 0.25 mmol). The bomb was removed from the glovebox and connected to an inert atmosphere/vacuum line, whereupon benzene (ca. 5 mL) was vacuum transferred onto the crystalline solid cooled to –196 °C. Warming of the bomb to room temperature yielded a burgundy solution of **1**. The bomb was then placed in a constant-temperature oil-bath and maintained at 54 °C for 24 h, during which time the solution lightened

in color to a deep red-brown. When the thermolysis was deemed to be complete, the bomb was removed from the bath and cooled to room temperature. The solvent was subsequently removed under high vacuum, and the remaining oily solids were maintained under high vacuum for 1 h. After this time the bomb was taken into the inert-atmosphere glovebox and the contents were dissolved in a minimum of diethyl ether. The resulting red-brown solution was filtered through a column of Celite (0.5 × 3.0 cm), the column was rinsed with diethyl ether (1 × 1 mL), and the filtrate was concentrated *in vacuo*. Cooling of the filtrate for 24 h at –30 °C resulted in the deposition of analytically pure **4.1** as red-brown blocks. Complexes **4.2m** and **4.2p** and **4.8** were prepared in an analogous manner.

4.4.6.1 Preparation of 4.4, 4.9 and Metallacycles 4.10-4.14

These compounds were prepared in a manner analogous to that described for the preparation of **1** above by employing the appropriate solvent. However, in each case the ether extract was passed through alumina I instead of Celite. Concentration and cooling of the yellow-orange eluates afforded analytically pure, crystalline solids in each case. Complexes **4.10, 4.11, 4.13,** and **4.14** were recrystallized from 1:1 Et_2O/hexanes, hexanes, 1:1 Et_2O/hexanes, and Et_2O, respectively.

4.4.6.2 Preparation of Xylyl Complexes 4.5 and 4.6

These complexes were prepared in a manner analogous to that employed for the synthesis of **1**. Concentration and cooling of the diethyl ether filtrate resulted in the co-crystallization of

4.5 and **4.6** as red-brown irregular blocks. In an independent preparation, benzyl complex **4.6** was isolated as analytically pure red crystals by concentration and cooling of the Et_2O eluate that resulted from passing an extracted mixture of **4.5** and **4.6** through a column of alumina I (1 cm × 3 cm).

4.4.6.3 Independent Preparation of Benzyl Complex 4.3

Authentic **4.3** was prepared by metathetical methods employing $Cp^*W(NO)Cl_2$ (420 mg, 1 mmol), and $(CH_2{=}CPh)_2Mg{\bullet}x(dioxane)$ and $(PhCH_2)_2Mg{\bullet}x(dioxane)$ (210 mg and 155 mg, respectively, 1 equiv each). The organometallic dichloride complex and bis(phenylvinyl)magnesium were mixed in a 25-mL Erlenmeyer flask which was subsequently immersed in a glovebox cold-well and cooled to ~ -180 °C. THF (10 mL) was added in a dropwise fashion down the sides of the flask, whereupon it froze upon contacting the cooled solids. The solid puck was allowed to warm slowly to room temperature with stirring, whereupon the solids dissolved and a burgundy-black solution resulted. The reaction mixture was cooled to –30 °C, and a cooled, THF solution of the bis(benzyl)magnesium reagent (-30 °C) was added dropwise with concomitant agitation of the reaction flask. The contents were then allowed to warm to room temperature with stirring. After the reaction mixture was stirred for 0.5 h at room temperature, the THF was removed from the mixture under vacuum, and the remaining red solids were maintained under high vacuum for 2 h. The solids were extracted with diethyl ether (35 mL), and the extracts were passed down a column of alumina I. The red band that developed was collected. Concentration of the eluate and subsequent cooling afforded **4.3** as a red crystalline solid (typical yields 70-75 %).

Table 4.5. Numbering scheme, yield, and analytical data for complexes **1** and **4.1-4.14**

Complex	Cmpd no.	Colour (yield[a], %)	Anal. found (calcd) C	H	N
Cp*W(NO)(CPh=CH_2)(CH_2SiMe_3)	**1**	red, (72)[b]	49.30 (48.98)	6.29 (6.17)	2.52 (2.60)
Cp*W(NO)(CPh=CD_2)($CD_2Si(CD_3)_3$)	**1-d_{13}**	brown, (>97)	[c]		
Cp*W(NO)(CPh=CH_2)(Ph)	**4.1**	brown, (>97)	54.46 (54.76)	5.14 (5.36)	2.65 (2.42)
Cp*W(NO)(CPh=CD_2)(Ph-d_5)	**4.1-d_7**	brown, (>97)	[c]		
Cp*W(NO)(CPh=CH_2)(*p*-tolyl)	**4.2p**	red-brown, (57)	[d]54.94 (55.26)	5.28 (5.38)	2.43 (2.58)
Cp*W(NO)(CPh=CH_2)(*m*-tolyl)	**4.2m**	red-brown, (38)	[d]54.94 (55.26)	5.28 (5.38)	2.43 (2.58)
Cp*W(NO)(CPh=CH_2)(CH_2Ph)	**4.3**	red, (78)	55.20 (55.26)	5.18 (5.38)	2.57 (2.58)
Cp*W(NO)(CPh=CH_2)(η^2-$CH_2C_6H_4$-*p*-Me)	**4.4**	orange, (>97)	56.16 (56.03)	5.63 (5.61)	2.60 (2.51)
Cp*W(NO)(CPh=CD_2)(η^2-$CD_2C_6D_4$-*p*-CD_3)	**4.4-d_{11}**	red (>97)	[c]		
Cp*W(NO)(CPh=CH_2)(C_6H_3-*m*-Me_2)	**4.5**	red (33)	[c]		
Cp*W(NO)(CPh=CH_2)(η^2-$CH_2C_6H_4$-*m*-Me)	**4.6**	orange (66)	56.27 (56.03)	5.51 (5.61)	2.43 (2.51)
Cp*W(NO)(CPh=CH_2)(C_6H_4-*m,p*-Me_2)	**4.7**	burgundy (85)	56.26 (56.03)	5.51 (5.61)	2.50 (2.51)
Cp*W(NO)(CPh=CH_2)(η^2-$CH_2C_6H_4$-*o*-Me)	**4.8**	burgundy (15)	[c]		
Cp*W(NO)(CPh=CH_2)($CH_2SiMe_2OSiMe_3$)	**4.9**	mauve, (>97)	47.13 (46.98)	6.21 (6.41)	2.26 (2.28)
Cp*W(NO)(η^2-*C*H(η^2-Ph)CH_2CH(^{n}Pr)*C*H_2)	**4.10**	brown (57)[b]	52.18 (52.78)	6.48 (6.36)	2.60 (2.68)
Cp*W(NO)(η^2-*C*H(η^2-Ph)CH_2CH(^{n}Bu)*C*H_2)	**4.11**	brown (23)[b]	53.90 (53.46)	6.61 (6.57)	2.54 (2.61)
Cp*W(NO)(η^2-*C*H(η^2-Ph)CH_2CH(^{t}Bu)*C*H_2)	**4.12**	brown (59)[b]	[c]		
Cp*W(NO)(η^2-*C*H(η^2-Ph)CH_2CH(OEt)*C*H_2)	**4.13**	brown (63)[b]	50.30 (50.29)	5.91 (5.95)	2.58 (2.67)
Cp*W(NO)(η^3-*endo*-*C*H_2*C*(Me)*C*(Me)CH_2(η^1-*C*PhMe))	**4.14**	yellow (68)[b]	[c]		

[a] Yield as indicated in the ^{1}H NMR spectrum of the reaction mixture unless otherwise noted. [b] Isolated yield. [c] Satisfactory analysis could not be obtained [d] Determined as a mixture of **4.2m** and **4.2p**.

Table 4.6. Mass spectrometric and IR spectral data for complexes **1** and **4.1-4.14**

Compd no.	MS (m/z)[a]	probe temp[b] (°C)	IR (Nujol, cm^{-1})
1	539	180	1539 (ν_{NO})
1-d_{13}	552	180	[c]
4.1	529	120	1572, 1562, 1553
4.1-d_7	536	120	[c]
4.2p	[d]544	150	1565 (ν_{NO})
4.2m	[d]544	150	1565 (ν_{NO})
4.3	544	150	1591 (ν_{NO})
4.4	557	250	1593, 1569, 1545
4.4-d_{11}	568	150	[c]
4.5	557	250	1626 (ν_{NO})
4.6	[c]	[c]	[c]
4.7	557	150	1573 (ν_{NO})
4.8	[c]	[c]	[c]
4.9	598 [P+ - Me] 451 [P+ - $C_6H_{17}OSi_2$]	150	1580 (ν_{NO})
4.10	523	100	1571 (ν_{NO})
4.11	537	150	1572 (ν_{NO})
4.12	[e]537.22364 (537.22284) [P+] 507.22783 (507.22482) [P+ - NO]	150	1568 (ν_{NO})
4.13	525	120	1560 (ν_{NO})
4.14	[e]535.20809 (535.20715) [P+]	120	1542 (ν_{NO})

[a] Values for the highest intensity peak of the calculated isotopic cluster (^{184}W). [b] Probe temperatures. [c] Not recorded. [d] Spectra recorded as a mixture of **4.2m** and **4.2p**. [e] High-resolution EI mass spectrum, found (calcd).

Table 4.7. ^{1}H and ^{13}C NMR spectroscopic data for complexes **1** and **4.1-4.14**

cmpd no.	^{1}H NMR[a] δ	^{13}C NMR[a] δ
1	7.87 (dd, $^{3}J_{HH}$ = 8.0 Hz, $^{4}J_{HH}$ = 1.2 Hz, 2H, Ph-H_{ortho}) 7.29 (t, $^{3}J_{HH}$ = 8.0 Hz, 2H, Ph-H_{meta}) 7.11 (t, $^{3}J_{HH}$ = 8.0 Hz, 1H, Ph-H_{para}) 3.88 (dd, $^{2}J_{HH}$ = 5.4 Hz, $^{5}J_{HH}$ = 1.2 Hz, 1H, CPh=CH_aH$_b$) 3.56 (dd, $^{2}J_{HH}$ = 5.4 Hz, $^{5}J_{HH}$ = 1.2 Hz, 1H, CPh=CH$_a$$H_b$) 1.50 (s, 15H, C_5Me_5) 0.69 (d, $^{2}J_{HH}$ = 12.6 Hz, 1H, CH_aH$_b$SiMe$_3$) 0.59 (s, 9H, SiMe$_3$) 0.21 (d, $^{2}J_{HH}$ = 12.6 Hz, 1H, CH$_a$$H_b$SiMe$_3$)	227.9 (s, $^{1}J_{WC}$ = 99 Hz, *C*Ph=CH$_2$) 145.3 (s, Ph-C_{ipso}) 129.6 (d, $^{1}J_{CH}$ = 157 Hz, Ph) 128.8 (d, $^{1}J_{CH}$ = 157 Hz, Ph) 127.6 (d, $^{1}J_{CH}$ = 157 Hz, Ph) 109.6 (s, C_5Me_5) 83.1 (dd, $^{1}J_{CH}$ = 146 Hz, $^{2}J_{WC}$ = 13 Hz, CPh=*C*H$_2$) 35.5 (t, $^{1}J_{CH}$ = 111 Hz, *C*H$_2$SiMe$_3$) 9.5 (q, $^{1}J_{CH}$ = 127 Hz, C_5Me_5) 3.4 (q, $^{1}J_{CH}$ = 126 Hz, CH$_2$Si*Me*$_3$)
1-d_{13}	7.87 (dd, $^{3}J_{HH}$ = 8.0 Hz, $^{4}J_{HH}$ = 1.2 Hz, 2H, Ph-H_{ortho}) 7.29 (t, $^{3}J_{HH}$ = 8.0 Hz, 2H, Ph-H_{meta}) 7.11 (t, $^{3}J_{HH}$ = 8.0 Hz, 1H, Ph-H_{para}) 1.50 (s, 15H, C_5Me_5)	[b]
4.1	7.99 (d, $^{3}J_{HH}$ = 7.8 Hz, 2H, Ph-H_{ortho}) 7.90 (d, $^{3}J_{HH}$ = 7.8 Hz, 2H, Ph-H_{ortho}) 7.27 (m, 4H, Ph-H_{meta}) 7.18 (m, 2H, Ph-H_{para}) 4.28 (d, $^{2}J_{HH}$ = 6.9 Hz, J_{WH} = 6.3 Hz, 1H, CPh=CH_aH$_b$) 3.71 (d, $^{2}J_{HH}$ = 6.9 Hz, J_{WH} = 6.3 Hz, 1H, CPh=CH$_a$$H_b$) 1.54 (s, 15H, C_5Me_5)	225.1 (*C*Ph=CH$_2$) 179.0 (Ph-C_{ipso}) 143.3 (Ph-C_{ipso}) 140.8, 130.3, 129.3, 128.9, 127.5, 126.4 (Ar) 110.2 (s, C_5Me_5) 78.6 (CPh=*C*H$_2$) 9.6 (C_5Me_5)
4.1-d_7	7.90 (d, $^{3}J_{HH}$ = 7.8 Hz, 2H, Ph-H_{ortho}) 7.27 (t, $^{3}J_{HH}$ = 7.8 Hz, 4H, Ph-H_{meta}) 7.18 (t, $^{3}J_{HH}$ = 7.6 Hz, 1H, Ph-H_{para}) 1.54 (s, 15H, C_5Me_5)	[b]
4.2p	7.99 (d, $^{3}J_{HH}$ = 7.7 Hz, 2H, Ar-H_{ortho}) 7.92 (d, $^{3}J_{HH}$ = 7.4 Hz, 2H, Ar-H_{ortho}) 7.27 (t, $^{3}J_{HH}$ = 8.1 Hz, 1H, Ar-H_{para}) 7.14 (m, 2H, Ar-H_{meta}) 7.01 (t, $^{3}J_{HH}$ = 7.4 Hz, 1H, Ar-H_{para}) 4.30 (d, $^{2}J_{HH}$ = 6.6 Hz, 1H, CPh=CH_aH$_b$) 3.76 (d, $^{2}J_{HH}$ = 6.6 Hz, 1H, CPh=CH$_a$$H_b$) 2.18 (s, 3H, Ar(*Me*)) 1.56 (s, 15H, C_5Me_5)	[c]234.6 (*C*Ph=CH$_2$) 233.6 (*C*Ph=CH$_2$) 178.2 (Ar-C_{ipso}) 175.1 (Ar-C_{ipso}) 144.2 (Ar-C_{ipso}) 139.5 (Ar-C_{ipso}) 142.2, 141.6, 138.4 (Ar) 137.9 (Ar-*C*(Me))

Table 4.7 continued.

cmpd no.	^{1}H NMR[a] δ	^{13}C NMR[a] δ
4.2m	7.98 (s, 1H, Ph-H_{ortho}) 7.92 (d, $^3J_{HH}$ = 7.4 Hz, 2H, Ph-H_{ortho}) 7.78 (d, $^3J_{HH}$ = 7.3 Hz, 2H, Ph-H_{ortho}) 7.27 (d, $^3J_{HH}$ = 8.1 Hz, 2H, Ph-H_{meta}) 7.14 (m, 2H, Ph) 7.01 (t, $^3J_{HH}$ = 7.4 Hz, 1H, Ph-H_{para}) 4.33 (d, $^2J_{HH}$ = 6.6 Hz, 1H, CPh=CH_aH$_b$) 3.79 (d, $^2J_{HH}$ = 6.6 Hz, 1H, CPh=CH$_a$$H_b$) 2.25 (s, 3H, Ar(*Me*)) 1.56 (s, 15H, C_5Me_5)	137.2 (Ar-*C*(Me)) 130.9, 130.8, 130.4, 130.3, 130.2, 129.9, 129.8, 129.3, 129.2, 128.8, 128.2 (Ar) 110.9 (C_5Me_5) 80.3 (CPh=*C*H$_2$) 79.6 (CPh=*C*H$_2$) 21.6 (Ar*Me*) 21.5 (Ar*Me*) 9.9 (C_5Me_5)
4.3	7.56 (d, $^3J_{HH}$ = 7.8 Hz, 2H, Ph-H_{ortho}) 7.30 (t, $^3J_{HH}$ = 7.8 Hz, 4H, Ph-H_{meta}) 7.11 (m, 4H, Ph-H_{meta}, -H_{ortho}) 6.99 (t, $^3J_{HH}$ = 7.8 Hz, 1H, Ph-H_{para}) 4.76 (s, 1H, CPh=CH_aH$_b$) 3.54 (s, 1H, CPh=CH_aH$_b$) 3.08 (d, $^2J_{HH}$ = 8.1 Hz, 1H, CH_aH$_b$Ph) 2.60 (d, $^2J_{HH}$ = 8.1 Hz, 1H, CH$_a$$H_b$Ph) 1.54 (s, 15H, C_5Me_5)	207.8 (*C*Ph=CH$_2$) 149.9 (Ph-C_{ipso}) 132.6 (Ph-C_{ortho}) 130.8 (Ph-C_{ipso}) 129.1, 128.8, 128.2, 127.6, 126.9 (Ph) 110.2 (s, C_5Me_5) 78.6 (CPh=*C*H$_2$) 9.6 (C_5Me_5)
4.4	7.39 (m, 4H, Ar-H_{ortho}, -H_{meta}) 7.10 (tt, $^3J_{HH}$ = 6.9 Hz, $^4J_{HH}$ = 1.8 Hz, Ar-H_{para}) 6.88 (d, $^3J_{HH}$ = 7.2 Hz, 2H, Ar-H_{meta}) 6.66 (d, $^3J_{HH}$ = 7.2 Hz, 2H, Ar-H_{ortho}) 5.42 (d, $^3J_{HH}$ = 0.9 Hz, 1H, CPh=CH_aH$_b$) 3.49 (d, $^3J_{HH}$ = 0.9 Hz, 1H, CPh=CH$_a$$H_b$) 3.17 (d, $^2J_{HH}$ = 6.6 Hz, 1H, CH_aH$_b$Ar) 2.32 (d, $^2J_{HH}$ = 6.6 Hz, 1H, CH$_a$$H_b$Ar) 1.91 (s, 3H, Ar(*Me*)) 1.59 (s, 15H, C_5Me_5)	194.7 (*C*Ph=CH$_2$) 152.6 (Ar-C_{ipso}) 141.9, 134.6, 130.1, 127.8, 127.3, 125.2 (Ar) 115.9 (CPh=*C*H$_2$) 115.5 (Ar-C_{ipso}) 108.8 (C_5Me_5) 47.5 (CH_2Ar) 22.1 (Ar(*Me*)) 10.6 (C_5Me_5)
4.4-d_{11}	7.39 (m, 4H, Ar-H_{ortho}, -H_{meta}) 7.10 (tt, $^3J_{HH}$ = 6.9 Hz, $^4J_{HH}$ = 1.8 Hz, Ar-H_{para}) 1.59 (s, 15H, C_5Me_5)	[b]

Table 4.7 continued.

cmpd no.	^{1}H NMR[a] δ	^{13}C NMR[a] δ
4.5	7.92 (s, 1H, Ar-H_{ortho}) 7.90 (s, 1H, Ar-H_{ortho}) 7.75 (s, 1H, Ar-H_{para}) 7.58 (d, $^3J_{HH}$ = 7.8 Hz, 2H, Ar-H_{ortho}) 7.37 (t, $^3J_{HH}$ = 7.8 Hz, 2H, Ar-H_{meta}) 7.17 (t, $^3J_{HH}$ = 7.9 Hz, 1H, Ar-H_{para}) 4.40 (d, 1H, CPh=CH_aH$_b$) 3.86 (d, 1H, CPh=CH$_a$$H_b$) 2.38 (s, 3H, Ar(*Me*)) 1.61 (s, 15H, C_5Me_5) 1.52 (s, 3H, Ar(*Me*))	233.5 (*C*Ph=CH_2) 179.8 (Ar-C_{ipso}) 151.9 (Ar-C_{ipso}) 138.6 (Ar-*C*(Me)) 137.6 (Ar-*C*(Me)) 134.4, 131.1, 130.2, 128.7 128.2 127.2 (Ar) 110.3 (C_5Me_5) 80.9 (CPh=*C*H_2) 21.6 (Ar-C(*Me*)) 21.3 (Ar-C(*Me*)) 9.7 (C_5*Me*$_5$)
4.6	7.27 (m, 4H, Ar-H_{ortho}) 7.17 (m, 1H, Ar-H_{para}) 7.16 (d, 1H, Ar-H_{para}) 6.95 (br t, 1H, Ar-H_{meta}) 6.79 (br d, 1H, Ar-H_{ortho}) 6.70 (br s, 1H, Ar-H_{ortho}) 4.88 (s, 1H, CPh=CH_aH$_b$) 3.79 (s, 1H, CPh=CH$_a$$H_b$) 2.80 (d, $^3J_{HH}$ = 12.4 Hz, CH_aH$_b$Ar) 2.68 (d, $^3J_{HH}$ = 12.4 Hz, CH$_a$$H_b$Ar) 2.23 (s, 3H, Ar(Me)) 1.91 (s, 15H, C_5Me_5)	208.7 (*C*Ph=CH_2) 139.8 (Ar-C_{ipso}) 134.5, 132.3 (Ar) 131.8 (Ar-*C*(Me)) 129.9, 129.5, 129.2, 128.3, 127.5 (Ar) 110.2 (C_5Me_5) 109.5 (Ar-C_{ipso}) 104.0 (CPh=*C*H_2) 52.3 (*C*H_2Ar) 21.6 (Ar-C(*Me*)) 10.8 (C_5*Me*$_5$)
4.7	8.04 (s, 1H, Ar-H_{ortho}) 7.93 (d, $^3J_{HH}$ = 7.5 Hz, 2H, Ar-H_{ortho}) 7.81 (d, $^3J_{HH}$ = 7.5 Hz, 2H, Ar-H_{ortho}) 7.28 (t, $^3J_{HH}$ = 7.2 Hz, 2H, Ar-H_{meta}) 7.15 (t, $^3J_{HH}$ = 7.2 Hz, 2H, Ar-H_{para}) 7.12 (d, $^3J_{HH}$ = 7.5 Hz, 2H, Ar-H_{meta}) 4.37 (d, $^2J_{HH}$ = 6.3 Hz, 1H, CPh=CH_aH$_b$) 3.90 (d, $^2J_{HH}$ = 6.3 Hz, 1H, CPh=CH$_a$$H_b$) 2.17 (s, 3H, Ar*Me*) 2.09 (s, 3H, Ar*Me*) 1.59 (s, 15H, C_5Me_5)	232.8 (*C*Ph=CH_2) 177.8 (s, Ar-C_{ipso}) 144.2 (s, Ar-C_{ipso}) 142.5, 138.8, 138.6 (d, $^1J_{CH} \approx 156$ Hz, Ar) 135.7 (s, Ar-*C*(Me)) 135.2 (s, Ar-*C*(Me)) 130.1, 129.9, 129.5, (d, $^1J_{CH} \approx 156$ Hz, Ar) 129.1, 128.8 (d, $^1J_{CH} \approx 156$ Hz, Ar) 111.8 (s, C_5Me_5) 82.2 (dd, $^1J_{CH}$ = 152 Hz, CPh=*C*H_2) 19.9, 19.8 (q, $^1J_{CH}$ = 126 Hz, Ar(*Me*)) 10.6 (q, $^1J_{CH}$ = 127 Hz, C_5*Me*$_5$)

Table 4.7 continued.

cmpd no.	^{1}H NMR[a] δ	^{13}C NMR[a] δ
4.8	6.82, 6.61, 6.40 (br, Ar) 5.31 (s, CPh=CH_aH$_b$) 3.77 (s, CPh=CH$_a$$H_b$) 3.10 (d, C$H_aH_b$Ar) 2.25 (d, CH$_a$$H_b$Ar) 2.02 (s, Ar*Me*) 1.54 (s, C_5Me_5)	[b]
4.9	7.93(d, $^3J_{HH}$ = 7.2 Hz, 2H, Ph-H$_{ortho}$) 7.29 (t, $^3J_{HH}$ = 7.2 Hz, 2H, Ph-H$_{meta}$) 7.13 (t, $^3J_{HH}$ = 7.5 Hz, 1H, Ph-H$_{para}$) 3.84 (dd, $^2J_{HH}$ = 6.0 Hz, $^5J_{HH}$ = 1.0 Hz, 1H, CPh=CH_aH$_b$) 3.57 (dd, $^2J_{HH}$ = 6.0 Hz, $^5J_{HH}$ = 1.0 Hz, 1H, CPh=CH$_a$$H_b$) 1.50 (s, 15H, C_5Me_5) 0.79 (d, $^3J_{HH}$ = 12.6 Hz, CH_aH$_b$SiMe$_2$OSiMe$_3$) 0.54 (s, 3H, Si*Me$_a$*Me$_b$OSiMe$_3$) 0.31 (d, $^3J_{HH}$ = 12.6 Hz, CH$_a$$H_b$SiMe$_2$OSiMe$_3$) 0.28 (s, 3H, SiMe$_a$*Me$_b$*OSiMe$_3$) 0.20 (s, 9H, OSiMe$_3$)	228.0 (*C*Ph=CH$_2$) 145.0 (Ph-C$_{ipso}$) 131.4, 129.7, 129.0 (Ph) 109.6 (C_5Me_5) 82.1 (CPh=*C*H$_2$) 35.3 (*C*H$_2$SiMe$_2$OSiMe$_3$) 9.6 (C_5*Me$_5$*) 4.6 (*C*H$_2$Si*Me$_a$*Me$_b$OSiMe$_3$) 4.4(*C*H$_2$SiMe$_a$*Me$_b$*OSiMe$_3$) 2.5 (OSiMe$_3$)
4.10	6.97 (br, 2H, Ar) 6.64 (t, 1H, Ar) 2.98 (m, 1H, CH$_2$CH(^{n}Pr)CH_2CHAr) 2.51 (m, 1H, CH$_2$CH(^{n}Pr)CH$_2$CHAr) 1.83 (m, 1H, CH$_2$CH(^{n}Pr)CH$_2$CHAr) 1.67 (m, 1H, CH_2CH(^{n}Pr)CH$_2$CHAr) 1.4-1.6 (m, 5H) 1.58 (s, 15H, C_5Me_5) 1.10 (m, 1H, CH_2CH(^{n}Pr)CH$_2$CHAr) 0.98 (t, $^3J_{HH}$ = 7.0 Hz, 3H, CH$_3$)	121.3, 121.0 (Ar) 106.5 (C_5Me_5) 71.3 (W*C*HAr, $^1J_{CW}$ = 15 Hz) 52.7 (WCH$_2$*C*H(^{n}Pr)) 44.2 (*C*H$_2$CH$_2$CH$_3$) 36.1 (WCH$_2$*C*H(^{n}Pr)), $^1J_{CW}$ = 88 Hz) 35.3 (CH$_2$CH(^{n}Pr)*C*H$_2$CHAr) 22.4 (CH$_2$*C*H$_2$CH$_3$) 15.1 (CH$_2$CH$_2$*C*H$_3$) 10.1 (C_5*Me$_5$*)
4.11	7.00 (br, 2H, ArH) 6.68 (t, $^3J_{HH}$ = 7 Hz, 1H, ArH) 3.02 (m, 2H, WCHPhCH_2CH) 2.54 (m, 1H, WCH$_2$CH) 1.4 - 1.8 (m, 6H) 1.59 (s, 15H, C_5Me_5) 1.15 (m, 2H) 1.02 (m, 1H) 0.97 (t, $^3J_{HH}$ = 7.6 Hz, 3H, CH$_3$)	122.0, 121.1 (C$_{aryl}$) 106.5 (C_5Me_5) 71.3 (W*C*HPh) 53.1 (WCH$_2$*C*H) 41.9 (CH$_3$CH$_2$CH$_2$CH$_2$) 36.3 (WCH$_2$) 34.1 (CH$_3$CH$_2$*C*H$_2$) 31.7 (CH*C*H$_2$CH) 23.9 (CH$_3$*C*H$_2$) 14.6 (CH$_3$) 10.1 (C_5*Me$_5$*)

Table 4.7 continued.

cmpd no.	^{1}H NMR[a] δ	^{13}C NMR[a] δ
4.12	7.17 (app t, 1H, W(H_{meta}) 7.04 (app t, 1H, $H_{meta'}$) 6.89 (d, 1H, $H_{ortho'}$) 6.64 (d, 1H, H_{para}) 3.33 (d, 1H, η^2-C-H_{ortho}) 2.67 (m, 1H, WCH_aH$_b$) 1.88 (obscured, $WCH_2CH(^tBu)$) 1.85 (br d, 1H, $WCH_2CH(^tBu)CH_aH_b$) 1.78 (m 1H, WCH_aH_b) 1.31 (br dt, 1H, $WCH_2CH(^tBu)CH_aH_b$) 1.10 (dd, 1H, $WCH_2CH(^tBu)CH_2CH(\eta^2$-Ph) 0.82 (s, 9H, ^{t}Bu)	136, 131, 123 (br, Ar) 121.3, 120.8 (Ar) 107.7 (C_5Me_5) 70.7 (WCHPh) 62.4 (WCH_2CH) 35.8 ($C(CH_3)_3$) 29.9 (WCH_2) 27.9 ($C(CH_3)_3$) 27.5 ($WCH_2CH(^tBu)CH_2$) 10.3 (C_5Me_5)
4.13	6.95 (br, 2H, ArH) 6.65 (t, $^3J_{HH}$ = 7 Hz, 1H, ArH) 3.99 (m, 1H, WCH) 3.72 (m, 1H, OCH_2CH_3) 3.52 (m, 1H, OCH_2CH_3) 3.43 (m, 1H, $CHCH_2CH$) 2.15 (m, 1H, $CHCH_2CH$) 2.02 (m, 1H, WCH_2) 1.54 (s, 15H, C_5Me_5) 1.35 (m, 2H, WCH_2CH) 1.30 (t, $^3J_{HH}$ = 8.5 Hz, 3H, OCH_2CH_3)	136, 131, 123 (br, Ar) 121.25, 120.83 (Ar) 107.72 (C_5Me_5) 87.46 (WCHPh) 68 (br) 64.33 (OCH_2CH_3) 58.20 (WCH_2CH) 33.15 (WCH_2, $^1J_{WC}$ = 109 Hz,) 31.36 ($CHCH_2CH$) 16.02 (CH_3) 10.43 (C_5Me_5)
4.14	7.46 (d, $^3J_{HH}$ = 6.9 Hz, 2H, Ph-H_{ortho}) 7.32 (t, $^3J_{HH}$ = 6.9 Hz, 2H, Ph-H_{meta}) 7.00 (d, $^3J_{HH}$ = 6.9 Hz, 1H, Ph-H_{para}) 4.04 (d, $^2J_{HH}$ = 13 Hz, 1H, η^3-$CH_2C(Me)C(Me)CH_aH_bPhMe$) (d, $^2J_{HH}$ = 13 Hz, 1H, η^3-$CH_2C(Me)C(Me)CH_aH_bPhMe$) 3.51 (d, $^2J_{HH}$ = 4.1 Hz, 1H, 3.52 η^3-$CH_aH_bC(Me)C(Me)CH_2PhMe$) 2.42 (s, 3H, η^3-$CH_2C(Me)C(Me)CH_2PhMe$) 1.76 (s, 3H, η^3-$CH_2C(Me)C(Me)CH_2PhMe$) 1.52 (s, 15H, C_5Me_5) 1.36 (s, 3H, η^3-$CH_2C(Me)C(Me)CH_2PhMe$) 1.29 (d, $^2J_{HH}$ = 4.1 Hz, 1H, η^3-$CH_aH_bC(Me)C(Me)CH_2PhMe$)	157.8 (Ph-C_{ipso}) 137.2 (η^3-$CH_2C(Me)C(Me)CH_2CPhMe$) 128.8 (Ph-H_{ortho}) 127.2 (Ph-H_{meta}) 121.9 (Ph-H_{para}) 119.5 (η^3-$CH_2C(Me)C(Me)CH_2CPhMe$) 113.6 (η^3-$CH_2C(Me)C(Me)CH_2CPhMe$) 109.3 (C_5Me_5) 62.7 (η^3-$CH_2C(Me)C(Me)CH_2CPhMe$) 48.5 (η^3-$CH_2C(Me)C(Me)CH_2CPhMe$) 33.8 (η^3-$CH_2C(Me)C(Me)CH_2CPhMe$) 23.3(η^3-$CH_2C(Me)C(Me)CH_2CPhMe$) 21.1(η^3-$CH_2C(Me)C(Me)CH_2CPhMe$) 10.6 (C_5Me_5)

[a] ^{1}H NMR spectra recorded in C_6D_6 at RT unless otherwise noted, and ^{13}C NMR spectra recorded in $CDCl_3$ at RT unless otherwise noted. [b] Spectrum not recorded. [c] Data combined for aryl compounds **4.2m** and **4.2p**. [d] Spectrum recorded at -20 °C in CD_2Cl_2 solvent.

4.5 Notes and References

(1) Shilov, A. E.; Shul'pin, G. B. *Chem. Rev.* **1997**, *97*, 2879.

(2) (a) Kleiman, J. P.; Dubeck, M. *J. Am. Chem. Soc.* **1963**, *85*, 1544. (b) Chatt, J.; Davidson, J. M. *J. Chem. Soc.* **1965**, 843.

(3) Goldschleger, N. F.; Tyabin, M. B.; Shilov, A. E.; Shteinman, A. A. *Zh. Fiz. Khim.* **1969**, *43*, 2174.

(4) (a) Gol'dschleger, N. F.; Es'kova, V. V.; Shilov, A. E.; Shteinman, A. A. *Zh. Fiz. Khim.* **1972**, *46*, 1353. (b) Rudakov, E. S.; Zamashchikov, V. V.; Belyayeva, N. P.; Rudakova, R. I. *Zh. Fiz. Khim.* **1973**, *47*, 2732. (c) Tret'akov, V. P.; Arzamaskova, L. N.; Ermakov, Yu. I. *Kinet. Katal.* **1974**, *15*, 538. (d) Hanotier, J.; Cameran, P.; Hanotier-Bridoux, M.; De Radzitsky, P. *J. Chem. Soc., Perkin Trans. 2.* **1972**, 2247. (e) Garnett, J. L.; Long, M. A.; Peterson, K. B. *Aust. J. Chem.* **1974**, *27*, 1823. (f) Grigoryan, E. A.; D'ychkovskiy, F. S.; Mullagaliev, I. R. *Dauk. Akad. Nauk. SSR* **1975**, *224*, 859.

(5) This field has been reviewed comprehensively. See, for example: (a) reference 1. (b) Hill, C. L., Ed., *Activation and Functionalization of Alkanes*; Wiley-Interscience: New York; 1989. (c) Arndtsen, B. A.; Bergman, R. G.; Mobley, A.; Peterson, T. H. *Acc. Chem. Res.* **1995**, *28*, 154. (d) Bergman, R. G. *J. Organomet. Chem.* **1990**, *400*, 273.

(6) (a) Gupta, M.; Hagen, C.; Kaska, W. C.; Cramer, R. E.; Jensen, C. M. *J. Am. Chem. Soc.* **1997**, *119*, 840, and references cited therein. (b) Vigalok, A.; Kraatz, H.-B.; Konstantinovsky, L.; Milstein, D. *Chem. Eur. J.* **1997**, *3*, 253. (c) Arndtsen, B. A.;

Bergman, R. G. *Science* **1995**, *270*, 1970. (d) McNeill, K.; Andersen, R. A.; Bergman, R. G. *J. Am. Chem. Soc.* **1997**, *119*, 11244.

(7) (a) Waltz, K. M.; Hartwig, J. F. *Science* **1997**, *277*, 211. (b) Tran, E.; Legzdins, P. *J. Am. Chem. Soc.* **1997**, *119*, 5071. (c) Debad, J. D.; Legzdins, P.; Lumb, S. A.; Batchelor, R. J.; Einstein, F. W. B. *J. Am. Chem. Soc.* **1995**, *117*, 3288. (d) Green, M. L.; Berry, M.; Couldwell, C.; Prout, K. *Nouv. J. de Chim.* **1977**, *1*, 187.

(8) Debad, J. D.; Legzdins, P.; Batchelor, R. J.; Einstein, F. W. B. *Organometallics* **1993**, *12*, 2094.

(9) (a) Dryden, N. H.; Legzdins, P.; Sayers, S. F.; Trotter, J.; Yee, V. C. *Can. J. Chem.* **1995**, *73*, 1035. (b) Legzdins, P.; Jones, R. H.; Phillips, E. C.; Yee, V. C.; Trotter, J.; Einstein, F. W. B. *Organometallics* **1991**, *10*, 986. (c) Dryden, N. H.; Legzdins, P.; Trotter, J.; Yee, V. C. *Organometallics* **1991**, *10*, 2857. (d) Dryden, N. H.; Legzdins, P.; Phillips, E. C.; Trotter, J.; Yee, V. C. *Organometallics* **1990**, *9*, 882.

(10) Sykes, P. *Mechanism in Organic Chemistry*, 6th ed; John Wiley and Sons: New York; 1985, Chapter 6.

(11) Connors, K. A. *Chemical Kinetics*; VCH: New York; 1990, Chapter 6.

(12) (a) Caulton, K. G.; Chisholm, M. H.; Streib, W. E.; Xue, Z. *J. Am. Chem. Soc.* **1991**, *113*, 6082. (b) Buchwald, S. L.; Nielson, R. B. *J. Am. Chem. Soc.* **1988**, *110*, 3171. (c) Schrock, R. R.; Fellmann, J. D. *J. Am. Chem. Soc.* **1978**, *100*, 3359. (d) Freundlich, J. S.; Schrock, R. R.; Davis, W. M. *J. Am. Chem. Soc.* **1996**, *118*, 3643. (e) Luinstra, G. A.; Teuben, J. H. *Organometallics* **1992**, *11*, 1793.

(13) (a) Chapter 3, Section 2.3. (b) Legzdins, P.; Lumb, S. A.; Young, V. G. *Organometallics* **1998**, *17*, 854.

(14) Assuming unimolecularity.

(15) (a) Bennett, J. L.; Wolczanski, P. T. *J. Am. Chem. Soc.* **1997**, *119*, 10696. (b) Schaller, C. P.; Cummins, C. C.; Wolczanski, P. T. *J. Am. Chem. Soc.* **1996**, *118*, 591.

(16) Doherty, N. M.; Bercaw, J. E. *J. Am. Chem. Soc.* **1985**, *107*, 2670.

(17) (a) Lian, T.; Bromberg, S. E.; Yang, H.; Proulx, G.; Bergman, R. G.; Harris, C. B. *J. Am. Chem. Soc.* **1996**, *118*, 3769. (b) Jones, W. D.; Hessell, E. T. *J. Am. Chem. Soc.* **1992**, *114*, 6087. (c) Bullock, R. M.; Headford, C. E. L.; Hennessy, K. M.; Kegley, S. E.; Norton, J. R. *J. Am. Chem. Soc.* **1989**, *111*, 3897. (d) Periana, R. A.; Bergman, R. G. *J. Am. Chem. Soc.* **1986**, *108*, 7332.

(18) For example, see: (a) Hinderling, C.; Feichtinger, D.; Plattner, D. A.; Chen, P. *J. Am. Chem. Soc.* **1997**, *119*, 10793. (b) Su, M.-D.; Chu, S.-Y. *J. Am. Chem. Soc.* **1997**, *119*, 5373. (c) Siegbahn, P. E. M.; Crabtree, R. H. *J. Am. Chem. Soc.* **1996**, *118*, 4442. (d) Siegbahn, P. E. M. *J. Am. Chem. Soc.* **1996**, *118*, 1487. (e) Abu-Hasanayn, F.; Krogh-Jespersen, K.; Goldman, A. S. *J. Am. Chem. Soc.* **1993**, *115*, 8019.

(19) Jones, W. D.; Feher, F. J. *J. Am. Chem. Soc.* **1986**, *108*, 4814.

(20) Enthalpies of activation of magnitude 20-27 kcal•mol^{-1} are commonly determined for single-step reductive elimination reactions. See, for example, references 12, 15, 17,and 19.

(21) (a) McCarthy, T. J.; Nuzzo, R. G.; Whitesides, G. M. *J. Am. Chem. Soc.* **1981**, *103*, 3396. (b) Buchanan, J. M.; Stryker, J. F.; Bergman, R. G. *J. Am. Chem. Soc.* **1986**, *108*, 1537.

(22) Burger, P.; Bergman, R. G. *J. Am. Chem. Soc.* **1993**, *115*, 10462.

(23) While Van't Hoff analyses yield more accurate free energy determinations, the slight thermal instability of the aryl vinyl complexes introduces error into the high temperature equilibrium data, obviating the accuracy of such an analysis.

(24) Janowicz, A. H.; Bergman, R. G. *J. Am. Chem. Soc.* **1983**, *105*, 3929.

(25) Crystals of complex **4.10** are monoclinic of space group C_2/c; a = 19.5492(12) Å, *b* = 17.8193(20) Å, *c* = 13.9719(9) Å, β = 117.112(6)°. The solid-state molecular structure was solved by Drs. F. W. B. Einstein and R. J. Batchelor of Simon Fraser University using the Patterson method and full-matrix least-squares refinement procedures to R_F = 0.017 for 3800 reflections with $I_o \geq 3\sigma(I_o)$. Tables of fractional atomic coordinates (Table A27) and bond distances and angles (Table A28) in the molecular stucture of this compound are found in Appendix A.

(26) Pauling, L. *The Nature of the Chemical Bond*, 3rd ed.; Cornell University Press: Ithaca, New York, 1960, Chapter 7.

(27) (a) Carmona, E.; Marin, J. M.; Paneque, M.; Poveda, M. L. *Organometallics* **1987**, *6*, 1757. (b) Bleeke, J. R.; Burch, R. R.; Coulman, C. L.; Schardt, B. C. *Inorg. Chem.* **1981**, *20*, 1316. (c) Burch, R. R.; Muetterties, E. L.; Day, V. W. *Organometallics* **1982**, *1*, 188.

(28) (a) Cotton, F. A.; Marks, T. J. *J. Am. Chem. Soc.* **1969**, *91*, 1339. (b) Cotton, F. A.; LaPrade, M. D. *J. Am. Chem. Soc.* **1968**, *90*, 5418.

(29) Utilizing NMR spectroscopy, the rate of a chemical exchange process at the coalescence temperature of the exchanging magnetic environments is given by the equation $k = \pi\Delta\nu / 2^{1/2}$, where $\Delta\nu$ (Hz) is the frequency separation of the two signals at the low-temperature exchange limit. For more details, see: Günther, H. *NMR Spectroscopy;* Wiley: New York, 1980.

(30) See, for example: (a) McDade, C.; Bercaw, J. E. *J. Organomet. Chem.* **1985**, *279*, 281. (b) Doherty, N. M.; McDade, C.; Bercaw, J. E. in *Organometallic Compounds. Synthesis, Structure, and Reactivity, Vol. 1*, Shapiro, B. L., ed.; Texas A & M University Press: College Station, Texas, 1983.

(31) (a) Hill, J. E.; Balaich, G.; Fanwick, P. E.; Rothwell, I. P. *Organometallics* **1993**, *12*, 2911.

(32) Crystals of **4.14** are triclinic of space group P1; a = 8.392(2) Å, b = 9.714(1) Å, c = 13.155(3) Å, α = 94.060(6)°, β = 99.371(4)°, γ = 91.896(4)°. Dr. S. J. Rettig solved the structure using the Patterson method and full-matrix least-squares refinement procedures to $R_F = 0.048$ for 3798 reflections with $I_o \geq 3\sigma(I_o)$. Tables of fractional atomic coordinates (Table A29), bond distances (Table A30) and angles (Table A31) in the molecular stucture of this compound are found in Appendix A.

(33) (a) Ipaktschi, J.; Mirzaei, F.; Demuth-Eberle, G. J.; Beck, J.; Serafin, M. *Organometallics* **1997**, *16*, 3965. (b) Greenhough, T. J.; Legzdins, P.; Martin, D. T.; Trotter, J. *Inorg. Chem.* **1979**, *18*, 3268.

(34) (a) Christensen, N. J.; Legzdins, P.; Einstein, F. W. B.; Jones, R. H. *Organometallics* **1991**, *10*, 3070. (b) Christensen, N. J.; Hunter, A. D.; Legzdins, P. *Organometallics* **1989**, *8*, 930.

(35) (a) The hydromethylation of acetylene to propylene has been observed for complexes of iron, nickel and platinum in the presence of methane, though the mechanism of this conversion is unknown and the homogeneity of these reactions is purported to be suspect. See Shilov, A. E. in *Activation and Functionalization of Alkanes*; Hill, C. L., Ed.; John Wiley & Sons: New York, 1989, Chapter 1. (b) A zirconocene acetylene complex has been reported to activate the C-H bonds of the Cp ligand. See Rosenthal, U.; Ohff, A.; Michalik, M.; Görls, H.; Burlakov, V. V.; Shur, V. B. *Angew. Chem,. Int. Ed. Engl.* **1993**, *32*, 1193. (c) A zirconocene benzyne complex has been reported to activate benzene C-H bonds. See Erker, G. *J. Organomet. Chem.* **1977**, *134*, 189.

(36) (a) Buchwald, S. L.; Nielsen, R. B. *Chem. Rev.* **1988**, *88*, 1047. (b) Broene, R. D.; Buchwald, S. L. *Science* **1993**, *261*, 1696. (c) Negishi, E.-I.; Takahashi, T. *Acc. Chem. Res.* **1994**, *27*, 124.

(37) (a) Casey, C. P.; Carino, R. S.; Hayashi, R. K.; Schladetzky, K. D. *J. Am. Chem. Soc.* **1996**, *118*, 1617. (b) Wong, K. L. T.; Thomas, J. L.; Brintzinger, H. H. *J. Am. Chem. Soc.* **1974**, *96*, 3694. (c) reference 35b.

(38) Templeton, J. L. *Adv. Organomet. Chem.* **1989**, *29*, 1.

(39) Burkey, D. J.; Debad, J. D.; Legzdins, P. *J. Am. Chem. Soc.* **1997**, *119*, 1139.

(40) (a) Czech, P. T.; Gladysz, J. A.; Fenske, R. F. *Organometallics* **1989**, 8, 1806. (b) Bodner, G. S.; Smith, D. E.; Hatton, D. E.; Heah, P. C.; Georgiou, S.; Rheingold, A. L.; Geib, S. J.; Hutchinson, J. P.; Gladysz, J. A. *J. Am. Chem. Soc.* **1987**, *109*, 7688.

(41) Ward, T. R.; Schafer, O.; Daul, C.; Hofmann, P. *Organometallics* **1997**, *16*, 3207.

(42) The labels applied to these d-orbitals are arbitrary due to the low symmetry of the complexes under scrutiny.

(43) (a) Schilling, B. E. R.; Hoffmann, R.; Faller, J. W. *J. Am. Chem. Soc.* **1979**, *101*, 592. (b) Johnson, T. J.; Folting, K.; Streib, W. E.; Martin, J. D.; Huffman, J. C.; Jackson, S. A.; Eisenstein, O.; Caulton, K. G. *Inorg. Chem.* **1995**, *34*, 488.

(44) (a) Gibson, V. C. *J. Chem. Soc., Dalton Trans.* **1994**, 1607. (b) Huber, S. R.; Baldwin, T. C.; Wigley, D. E. *Organometallics* **1993**, *12*, 91.

(45) Bursten, B. E.; Gatter, M. G.; Goldberg, K. I. *Polyhedron* **1990**, *9*, 2001.

(46) Legzdins. P.; Poli, R.; Smith, K. M., manuscript in preparation.

(47) (a) Gupta, M.; Hagen, C.; Kaska, W. C.; Cramer, R. E.; Jensen, C. M. *J. Am. Chem. Soc.* **1997**, *119*, 840. (b) Crabtree, R. H.; Parnell, C. P.; Uriarte, R. J. *Organometallics* **1987**, *6*, 696.

(48) Maquire, J. A.; Petrillo, A.; Goldman, A. S. *J. Am. Chem. Soc.* **1992**, *114*, 9492.

Appendix A. Tables of Fractional Atomic Coordinates, Bond Distances, and Angles Determined for the Structurally Characterized Complexes Described in this Thesis

Table A1. Fractional atomic coordinates in the solid-state molecular structure determined for complex **1.**

atom	x	y	z	B(eq)
W(1)	0.28432(2)	0.49183(2)	0.255895(11)	1.663(4)
Si(1)	0.3080(2)	0.31214(15)	0.44105(8)	2.67(3)
O(1)	0.1404(4)	0.2420(4)	0.2210(2)	3.46(9)
N(1)	0.2135(5)	0.3316(4)	0.2420(2)	2.28(8)
C(1)	0.2614(5)	0.7692(5)	0.2268(3)	2.03(9)
C(2)	0.0998(6)	0.7734(5)	0.2594(3)	2.31(10)
C(3)	0.0384(5)	0.6822(5)	0.2083(3)	2.20(10)
C(4)	0.1606(6)	0.6252(5)	0.1424(3)	2.44(10)
C(5)	0.2982(5)	0.6804(5)	0.1543(3)	2.12(9)
C(6)	0.3661(7)	0.8558(5)	0.2614(3)	3.19(12)
C(7)	0.0040(7)	0.8718(6)	0.3308(3)	3.55(12)
C(8)	--0.1277(7)	0.6611(6)	0.2171(4)	4.04(14)
C(9)	0.1484(8)	0.5313(6)	0.0710(3)	3.89(14)
C(10)	0.4432(7)	0.6605(6)	0.0965(3)	3.12(12)
C(11)	0.5377(6)	0.3692(5)	0.2180(3)	2.09(10)
C(12)	0.6107(6)	0.4224(5)	0.2752(3)	2.33(10)
C(13)	0.6334(6)	0.2303(5)	0.1661(3)	2.26(10)
C(14)	0.5505(6)	0.1422(5)	0.1296(3)	2.56(11)
C(15)	0.6440(8)	0.0109(6)	0.0809(3)	3.96(14)
C(16)	0.8190(9)	-0.0348(6)	0.0675(4)	4.65(15)
C(17)	0.8979(7)	0.0533(7)	0.1039(4)	4.48(15)
C(18)	0.8092(6)	0.1839(6)	0.1521(3)	3.22(11)
C(19)	0.2381(6)	0.5077(5)	0.3850(3)	2.11(10)
C(20)	0.1420(8)	0.2207(6)	0.4341(3)	3.83(14)
C(21)	0.5203(7)	0.1602(6)	0.4050(3)	4.41(14)
C(22)	0.3289(8)	0.3552(6)	0.5489(3)	4.10(14)

Table A2. Bond distances (Å) in the solid-state molecular structure of complex **1**.

atom-atom-distance		atom-atom-distance	
W(1)-N(1)	1.760(3)	W(1)-C(1)	2.447(4)
W(1)-C(2)	2.411(4)	W(1)-C(3)	2.301(4)
W(1)-C(4)	2.300(4)	W(1)-C(5)	2.400(4)
W(1)-C(11)	2.076(5)	W(1)-C(12)	2.615(5)
W(1)-C(19)	2.173(5)	W(1)-CP	2.04
Si(1)-C(19)	1.870(4)	Si(1)-C(20)	1.867(5)
Si(1)-C(21)	1.877(6)	Si(1)-C(22)	1.878(6)
O(1)-N(1)	1.237(4)	C(1)-C(2)	1.429(6)
C(1)-C(5)	1.416(6)	C(1)-C(6)	1.506(6)
C(2)-C(3)	1.423(6)	C(2)-C(7)	1.505(7)
C(3)-C(4)	1.434(7)	C(3)-C(8)	1.478(6)
C(4)-C(5)	1.438(6)	C(4)-C(9)	1.497(7)
C(5)-C(10)	1.479(7)	C(11)-C(12)	1.342(6)
C(11)-C(13)	1.470(7)	C(13)-C(14)	1.391(6)
C(13)-C(18)	1.390(6)	C(14)-C(15)	1.392(7)
C(15)-C(16)	1.383(9)	C(16)-C(17)	1.365(8)
C(17)-C(18)	1.374(8)		

Table A3. Bond angles (°) in the solid-state molecular structure determined for complex **1.**

atom-atom-atom-angle		atom-atom-atom-angle	
N(1)-W(1)-C(11)	96.8(2)	N(1)-W(1)-C(12)	118.33(15)
N(1)-W(1)-C(19)	96.0(2)	N(1)-W(1)-CP	120.2
C(11)-W(1)-C(12)	30.6(2)	C(11)-W(1)-C(19)	114.9(2)
C(11)-W(1)-CP	113.3	C(12) W(1)-CP	112.6
C(12)-W(1)-C(19)	89.8(2)	C(19)-W(1)-CP	113.7
C(19)-Si(1)-C(20)	109.1(2)	C(19)-Si(1)-C(21)	114.4(2)
C(19)-Si(1)-C(22)	108.4(2)	C(20)-Si(1)-C(21)	108.7(3)
C(20)-Si(1)-C(22)	109.3(3)	C(21)-Si(1)-C(22)	106.9(3)
W(1)-N(1)-O(1)	166.2(3)	C(2)-C(1)-C(5)	108.3(4)
C(2)-C(1)-C(6)	125.1(5)	C(5)-C(1)-C(6)	126.5(4)
C(1)-C(2)-C(3)	108.4(4)	C(1)-C(2)-C(7)	125.2(5)
C(3)-C(2)-C(7)	126.1(4)	C(2)-C(3)-C(4)	107.6(4)
C(2)-C(3)-C(8)	126.7(5)	C(4)-C(3)-C(8)	125.5(5)
C(3)-C(4)-C(5)	107.8(4)	C(3)-C(4)-C(9)	127.6(5)
C(5)-C(4)-C(9)	124.5(5)	C(1)-C(5)-C(4)	107.9(4)
C(1)-C(5)-C(10)	126.5(4)	C(4)-C(5)-C(10)	125.4(5)
W(1)-C(11)-C(12)	97.5(4)	W(1)-C(11)-C(13)	137.1(3)
C(12)-C(11)-C(13)	123.0(4)	C(11)-C(13)-C(14)	120.9(4)
C(11)-C(13)-C(18)	120.9(4)	C(14)-C(13)-C(18)	118.2(5)
C(13)-C(14)-C(15)	119.9(5)	C(14)-C(15)-C(16)	121.5(5)
C(15)-C(16)-C(17)	117.6(6)	C(16)-C(17)-C(18)	122.3(6)
C(13)-C(18)-C(17)	120.5(5)	W(1)-C(19)-Si(1)	116.5(2)

Table A4. Fractional atomic coordinates in the solidstate molecular structure determined for complex **2.1.**

atom	x	y	z	B(eq)
W(1)	0.60200(2)	0.28831(1)	0.17738(2)	2.605(3)
Cl(1)	0.7880(1)	0.41459(9)	0.1252(2)	4.17(3)
O(1)	0.5432(4)	0.1342(3)	-0.1570(4)	4.58(8)
N(1)	0.5631(4)	0.2025(3)	-0.0326(4)	3.12(7)
C(1)	0.5539(5)	0.1873(3)	0.3931(6)	3.35(9)
C(2)	0.5732(5)	0.2832(3)	0.4913(5)	3.32(9)
C(3)	0.7274(5)	0.3363(3)	0.5224(5)	3.20(8)
C(4)	0.8056(5)	0.2730(3)	0.4488(6)	3.43(9)
C(5)	0.6990(5)	0.1808(3)	0.3687(6)	3.41(9)
C(6)	0.4149(6)	0.1043(4)	0.3480(7)	4.9(1)
C(7)	0.4520(6)	0.3183(4)	0.5585(7)	5.0(1)
C(8)	0.8006(7)	0.4393(4)	0.6249(7)	5.2(1)
C(9)	0.9769(6)	0.2974(5)	0.4679(7)	5.2(1)
C(10)	0.7371(7)	0.0916(4)	0.2882(7)	5.3(1)
C(11)	0.3745(5)	0.3058(3)	0.1009(5)	3.00(8)
C(12)	0.4125(5)	0.4025(4)	0.1312(7)	4.1(1)
C(13)	0.2159(5)	0.2451(3)	-0.0029(5)	3.03(8)
C(14)	0.1887(5)	0.1505(4)	-0.0986(7)	4.2(1)
C(15)	0.0368(6)	0.0949(4)	-0.1886(8)	5.4(1)
C(16)	--0.0898(5)	0.1302(4)	-0.1805(7)	4.7(1)
C(17)	--0.0654(5)	0.2231(4)	-0.0882(7)	4.6(1)
C(18)	0.0848(5)	0.2805(4)	0.0004(6)	3.9(1)

Table A5. Bond distances (Å) in the solid-state molecular structure of complex **2.1.**

atom-atom	distance	atom-atom	distance
W(1)-Cl(1)	2.375(1)	W(1)-N(1)	1.770(3)
W(1)-C(1)	2.331(4)	W(1)-C(2)	2.416(4)
W(1)-C(3)	2.416(4)	W(1)-C(4)	2.354(4)
W(1)-C(5)	2.310(4)	W(1)-C(11)	2.071(4)
W(1)-CP	2.04	O(1)-N(1)	1.214(4)
C(1)-C(2)	1.431(6)	C(1)-C(5)	1.421(6)
C(1)-C(6)	1.487(6)	C(2)-C(3)	1.409(6)
C(2)-C(7)	1.501(6)	C(3)-C(4)	1.422(6)
C(3)-C(8)	1.502(6)	C(4)-C(5)	1.421(6)
C(4)-C(9)	1.507(6)	C(5)-C(10)	1.497(6)
C(11)-C(12)	1.331(6)	C(11)-C(13)	1.469(6)
C(13)-C(14)	1.394(6)	C(13)-C(18)	1.403(6)
C(14)-C(15)	1.385(7)	C(15)-C(16)	1.373(7)
C(16)-C(17)	1.369(8)	C(17)-C(18)	1.381(7)

Table A6. Bond angles (°) in the solid-state molecular structure determined for complex **2.1.**

atom-atom-atom	angle	atom-atom-atom	angle
Cl(1)-W(1)-N(1)	99.3(1)	Cl(1)-W(1)-C(11)	115.4(1)
Cl(1)-W(1)-CP	112.8	N(1)-W(1)-C(11)	93.8(1)
N(1)-W(1)-CP	120.7	C(11)-W(1)-CP	113.2
W(1)-N(1)-O(1)	170.0(3)	C(2)-C(1)-C(5)	108.0(4)
C(2)-C(1)-C(6)	126.5(4)	C(5)-C(1)-C(6)	125.1(4)
C(1)-C(2)-C(3)	108.3(4)	C(1)-C(2)-C(7)	125.3(4)
C(3)-C(2)-C(7)	126.3(4)	C(2)-C(3)-C(4)	107.6(4)
C(2)-C(3)-C(8)	126.7(4)	C(4)-C(3)-C(8)	125.6(4)
C(3)-C(4)-C(5)	108.8(4)	C(3)-C(4)-C(9)	125.3(4)
C(5)-C(4)-C(9)	125.7(4)	C(1)-C(5)-C(4)	107.3(4)
C(1)-C(5)-C(10)	126.5(4)	C(4)-C(5)-C(10)	126.0(4)
W(1)-C(11)-C(12)	96.4(3)	W(1)-C(11)-C(13)	137.0(3)
C(12)-C(11)-C(13)	124.7(4)	C(11)-C(13)-C(14)	122.7(4)
C(11)-C(13)-C(18)	119.6(4)	C(14)-C(13)-C(18)	117.6(4)
C(13)-C(14)-C(15)	120.5(4)	C(14)-C(15)-C(16)	121.0(5)
C(15)-C(16)-C(17)	119.3(5)	C(16)-C(17)-C(18)	120.8(4)
C(13)-C(18)-C(17)	120.7(5)		

Table A7. Fractional atomic coordinates in the solid-state molecular structure determined for complex **2.2**

Atom		x/a	y/b	z/c	Uiso/eq
W	0.21854(2)		0.13901(2)	0.14836(1)	0.0440
	O(1)	0.3221(5)	0.2002(5)	0.2587(3)	0.0906
	O(2)	0.2673(4)	0.0053(3)	0.1684(2)	0.0553
	O(3)	0.3215(4)	0.0703(3)	0.0882(2)	0.0548
	N	0.2884(5)	0.1762(4)	0.2094(3)	0.0593
	C(1)	0.0840(6)	0.0997(6)	0.2023(4)	0.0501
	C(2)	0.0771(6)	0.1910(6)	0.1952(5)	0.0558
	C(3)	0.0617(6)	0.2074(6)	0.1336(5)	0.0502
	C(4)	0.0572(5)	0.1264(6)	0.1021(4)	0.0505
	C(5)	0.0701(5)	0.0600(5)	0.1445(5)	0.0553
	C(6)	0.2535(6)	0.2475(5)	0.0868(4)	0.0490
	C(7)	0.2624(6)	0.2262(6)	0.0283(4)	0.0659
	C(8)	0.3222(6)	0.0033(5)	0.1220(4)	0.0491
	C(11)	0.0914(6)	0.0511(7)	0.2610(5)	0.0835
	C(12)	0.0795(7)	0.2593(7)	0.2447(5)	0.0910
	C(13)	0.0357(6)	0.2944(6)	0.1065(5)	0.0690
	C(14)	0.0351(7)	0.1163(6)	0.0355(4)	0.0838
	C(15)	0.0644(7)	-0.0375(6)	0.1317(5)	0.0827
	C(61)	0.2680(6)	0.3416(5)	0.1040(5)	0.0576
	C(62)	0.3082(6)	0.3682(6)	0.1573(5)	0.0685
	C(63)	0.3202(8)	0.4548(7)	0.1717(6)	0.0889
	C(64)	0.295(1)	0.5178(8)	0.1311(8)	0.0923
	C(65)	0.254(1)	0.4957(8)	0.0772(8)	0.1040
	C(66)	0.2406(6)	0.4075(6)	0.0637(6)	0.0767
	C(81)	0.3854(6)	-0.0727(5)	0.1088(3)	0.0457
	C(82)	0.4620(6)	-0.0627(6)	0.0692(4)	0.0595
	C(83)	0.5221(6)	-0.1330(6)	0.0566(4)	0.0676
	C(84)	0.5047(7)	-0.2131(6)	0.0826(4)	0.0659
	C(85)	0.4276(8)	-0.2233(6)	0.1214(5)	0.0701
	C(86)	0.3684(6)	-0.1534(5)	0.1358(4)	0.0562

Table A8. Selected bond distances (Å) in the solid-state molecular structure of complex **2.2.**

atom-atom-	distance	atom-atom	distance
W-O(2)	2.187(5)	W-C(3)	2.403(8)
W-O(3)	2.195(5)	W-C(4)	2.433(8)
W-N	1.741(7)	W-C(5)	2.359(7)
W-C(1)	2.267(9)	W-C(6)	2.188(8)
W-C(2)	2.327(9)	W-Cp	2.034
O(1)-N	1.232(10)	C(6)-C(61)	1.496(11)
O(2)-C(8)	1.266(10)	C(8)-C(81)	1.472(11)
O(3)-C(8)	1.262(10)	C(61)-C(62)	1.355(14)
C(1)-C(2)	1.403(13)	C(61)-C(66)	1.389(14)
C(1)-C(5)	1.421(14)	C(62)-C(63)	1.366(14)
C(1)-C(11)	1.491(14)	C(63)-C(64)	1.356(19)
C(2)-C(3)	1.392(15)	C(64)-C(65)	1.350(24)
C(2)-C(12)	1.505(14)	C(65)-C(66)	1.387(16)
C(3)-C(4)	1.416(13)	C(81)-C(82)	1.369(12)
C(3)-C(13)	1.495(13)	C(81)-C(86)	1.385(11)
C(4)-C(5)	1.386(13)	C(82)-C(83)	1.376(13)
C(4)-C(14)	1.503(13)	C(83)-C(84)	1.369(14)
C(5)-C(15)	1.512(12)	C(84)-C(85)	1.363(14)
C(6)-C(7)	1.331(12)	C(85)-C(86)	1.373(12)

Table A9. Selected bond angles (°) in the solid-state molecular structure determined for complex **2.2.**

atom-atom-atom	angle	atom-atom-atom	angle
O(2)-W-O(3)	58.86(20)	N-W-C(6)	96.4(3)
O(2)-W-N	88.9(3)	N-W-Cp	119.5
O(2)-W-C(6)	139.54(25)	C(6)-W-Cp	106.1
O(2)-W-Cp	105.8	W-O(2)-C(8)	92.3(5)
O(3)-W-N	105.6(3)	W-O(3)-C(8)	92.0(5)
O(3)-W-C(6)	81.21(25)	W-N-O(1)	68.1(7)
O(3)-W-Cp	132.6	O(2)-C(8)-O(3)	116.8(7)
C(2)-C(1)-C(5)	108.2(8)	O(2)-C(8)-C(81)	121.7(7)
C(2)-C(1)-C(11)	126.4(9)	O(3)-C(8)-C(81)	121.6(7)
C(5)-C(1)-C(11)	124.9(9)	C(6)-C(61)-C(62)	123.9(8)
C(1)-C(2)-C(3)	107.3(8)	C(6)-C(61)-C(66)	119.7(9)
C(1)-C(2)-C(12)	127.0(9)	C(62)-C(61)-C(66)	116.4(8)
C(3)-C(2)-C(12)	125.6(8)	C(61)-C(62)-C(63)	122.5(9)
C(2)-C(3)-C(4)	109.0(8)	C(62)-C(63)-C(64)	120.0(12)
C(2)-C(3)-C(13)	125.6(9)	C(63)-C(64)-C(65)	120.4(12)
C(4)-C(3)-C(13)	124.5(9)	C(64)-C(65)-C(66)	118.9(13)
C(3)-C(4)-C(5)	107.6(8)	C(61)-C(66)-C(65)	121.8(12)
C(3)-C(4)-C(14)	125.0(8)	C(8)-C(81)-C(82)	119.1(7)
C(5)-C(4)-C(14)	127.2(9)	C(8)-C(81)-C(86)	121.0(7)
C(1)-C(5)-C(4)	107.9(8)	C(82)-C(81)-C(86)	119.9(8)
C(1)-C(5)-C(15)	126.2(9)	C(81)-C(82)-C(83)	119.9(8)
C(4)-C(5)-C(15)	125.8(10)	C(82)-C(83)-C(84)	120.4(9)
W-C(6)-C(7)	115.7(6)	C(83)-C(84)-C(85)	119.8(9)
W-C(6)-C(61)	126.6(6)	C(84)-C(85)-C(86)	120.7(9)
C(7)-C(6)-C(61)	117.7(8)	C(81)-C(86)-C(85)	119.4(8)

Table A10. Fractional atomic coordinates in the solid-state molecular structure determined for complex **2.6.**

atom	x	y	z	B(eq)
W(1)	0.14315(1)	0.13070(4)	0.35219(2)	3.075(6)
Cl(1)	0.19540(7)	-0.0586(2)	0.3024(1)	4.85(6)
O(1)	0.0992(2)	-0.1273(8)	0.4264(3)	7.5(2)
N(1)	0.1121(2)	0.1217(8)	0.2421(3)	4.1(2)
N(2)	0.1145(2)	-0.0253(7)	0.3898(3)	4.1(2)
C(1)	0.1998(3)	0.1544(9)	0.4399(4)	3.9(2)
C(2)	0.2180(3)	0.2431(10)	0.3861(4)	4.1(2)
C(3)	0.1903(3)	0.371(1)	0.3712(4)	4.6(2)
C(4)	0.1543(3)	0.370(1)	0.4164(4)	4.9(2)
C(5)	0.1599(3)	0.236(1)	0.4587(4)	4.6(2)
C(6)	0.2212(3)	0.012(1)	0.4747(5)	6.9(3)
C(7)	0.2641(3)	0.209(1)	0.3554(5)	5.6(3)
C(8)	0.1986(4)	0.504(1)	0.3212(6)	8.0(3)
C(9)	0.1230(3)	0.508(1)	0.4280(6)	8.1(3)
C(10)	0.1307(3)	0.197(1)	0.5170(5)	8.2(3)
C(11)	0.0657(2)	0.1675(10)	0.2642(4)	4.6(2)
C(12)	0.0767(2)	0.2633(8)	0.3277(4)	3.4(2)
C(13)	0.1283(3)	0.255(1)	0.1995(4)	5.0(2)
C(14)	0.1750(3)	0.234(1)	0.1751(5)	5.6(3)
C(15)	0.1844(3)	0.251(1)	0.1115(5)	7.4(3)
C(16)	0.1097(3)	-0.024(1)	0.1981(5)	5.3(3)
C(17)	0.0908(4)	-0.168(1)	0.2309(5)	6.5(3)
C(18)	0.0562(4)	-0.251(2)	0.2072(7)	10.3(4)
C(19)	0.0362(3)	0.275(1)	0.3716(4)	3.6(2)
C(20)	0.0144(3)	0.418(1)	0.3814(4)	5.0(2)
C(21)	--0.0230(3)	0.431(1)	0.4205(5)	6.3(3)
C(22)	--0.0391(3)	0.297(2)	0.4511(5)	6.5(3)
C(23)	--0.0198(3)	0.154(1)	0.4416(5)	5.9(3)
C(24)	0.0183(3)	0.142(1)	0.4022(4)	5.1(2)

Table A11. Bond distances (Å) in the solid-state molecular structure of complex **2.6**.

atom-atom-distance		atom-atom-distance	
W(1)-Cl(1)	2.451(2)	W(1)-N(1)	2.310(6)
W(1)-N(2)	1.747(6)	W(1)-C(1)	2.325(8)
W(1)-C(2)	2.426(8)	W(1)-C(3)	2.460(8)
W(1)-C(4)	2.398(8)	W(1)-C(5)	2.313(8)
W(1)-C(12)	2.255(7)	W(1)-CP	2.06
O(1)-N(2)	1.227(7)	N(1)-C(11)	1.491(8)
N(1)-C(13)	1.497(10)	N(1)-C(16)	1.507(9)
C(1)-C(2)	1.43(1)	C(1)-C(5)	1.42(1)
C(1)-C(6)	1.50(1)	C(2)-C(3)	1.36(1)
C(2)-C(7)	1.53(1)	C(3)-C(4)	1.42(1)
C(3)-C(8)	1.53(1)	C(4)-C(5)	1.41(1)
C(4)-C(9)	1.50(1)	C(5)-C(10)	1.51(1)
C(11)-C(12)	1.51(1)	C(12)-C(19)	1.509(9)
C(13)-C(14)	1.48(1)	C(14)-C(15)	1.31(1)
C(16)-C(17)	1.49(1)	C(17)-C(18)	1.29(1)
C(19)-C(20)	1.38(1)	C(19)-C(24)	1.39(1)
C(20)-C(21)	1.38(1)	C(21)-C(22)	1.38(1)
C(22)-C(23)	1.35(1)	C(23)-C(24)	1.40(1)

Table A12. Bond angles (°) in the solid-state molecular structure determined for complex **2.6.**

atom-atom-atom	angle	atom-atom-atom	angle
Cl(1)-W(1)-N(1)	79.2(2)	Cl(1)-W(1)-N(2)	90.2(2)
Cl(1)-W(1)-C(12)	141.1(2)	Cl(1)-W(1)-CP	105.9
N(1)-W(1)-N(2)	102.1(3)	N(1)-W(1)-C(12)	62.3(2)
N(1)-W(1)-CP	139.7	N(2)-W(1)-C(12)	92.4(3)
N(2)-W(1)-CP	117.6	C(12)-W(1)-CP	107.1
W(1)-N(1)-C(11)	91.2(4)	W(1)-N(1)-C(13)	112.9(5)
W(1)-N(1)-C(16)	125.0(5)	C(11)-N(1)-C(13)	107.1(6)
C(11)-N(1)-C(16)	111.8(6)	C(13)-N(1)-C(16)	106.9(6)
W(1)-N(2)-O(1)	168.4(7)	C(2)-C(1)-C(5)	106.7(7)
C(2)-C(1)-C(6)	126.8(8)	C(5)-C(1)-C(6)	126.2(8)
C(1)-C(2)-C(3)	109.6(7)	C(1)-C(2)-C(7)	124.7(8)
C(3)-C(2)-C(7)	125.4(8)	C(2)-C(3)-C(4)	107.9(8)
C(2)-C(3)-C(8)	127.4(8)	C(4)-C(3)-C(8)	124.3(9)
C(3)-C(4)-C(5)	108.4(8)	C(3)-C(4)-C(9)	124.8(10)
C(5)-C(4)-C(9)	125.2(9)	C(1)-C(5)-C(4)	107.3(7)
C(1)-C(5)-C(10)	127.0(9)	C(4)-C(5)-C(10)	125.5(9)
N(1)-C(11)-C(12)	103.6(6)	W(1)-C(12)-C(11)	92.7(4)
W(1)-C(12)-C(19)	126.4(5)	C(11)-C(12)-C(19)	112.5(6)
N(1)-C(13)-C(14)	115.0(7)	C(13)-C(14)-C(15)	123.3(9)
N(1)-C(16)-C(17)	114.5(7)	C(16)-C(17)-C(18)	125(1)
C(12)-C(19)-C(20)	121.2(7)	C(12)-C(19)-C(24)	121.6(7)
C(20)-C(19)-C(24)	117.2(7)	C(19)-C(20)-C(21)	122.2(8)
C(20)-C(21)-C(22)	119.0(8)	C(21)-C(22)-C(23)	121.0(8)
C(22)-C(23)-C(24)	119.8(10)	C(19)-C(24)-C(23)	120.8(9)

Table A13. Fractional atomic coordinates in the solid-state molecular structure determined for complex **2.7.**

Atom	x	y	z	B(Eq)
W(1)	0.46795(3)	0.7509(1)	0.36735(2)	5.51(2)
W(2)	0.71736(4)	0.4981(1)	0.11180(3)	6.37(2)
P(1)	0.4524(2)	0.6888(5)	0.2805(1)	5.5(1)
P(2)	0.6939(2)	0.5729(6)	0.0241(1)	6.3(1)
O(1)	0.5098(6)	0.461(2)	0.4154(4)	8.4(5)
O(2)	0.7615(6)	0.786(2)	0.1617(4)	8.9(5)
N(1)	0.4872(6)	0.578(2)	0.3891(4)	6.5(5)
N(2)	0.7383(7)	0.675(2)	0.1365(5)	7.1(5)
C(1)	0.5144(10)	0.976(2)	0.3969(7)	7.0(6)
C(2)	0.4608(10)	1.006(2)	0.3857(6)	7.3(6)
C(3)	0.4448(8)	0.924(2)	0.4166(6)	6.8(6)
C(4)	0.4918(8)	0.846(2)	0.4480(5)	6.6(5)
C(5)	0.5343(8)	0.877(2)	0.4341(6)	6.4(5)
C(6)	0.5513(9)	1.069(2)	0.3791(6)	11.4(8)
C(7)	0.4262(9)	1.129(3)	0.3508(7)	10.2(7)
C(8)	0.3864(8)	0.936(2)	0.4185(6)	10.4(7)
C(9)	0.4896(8)	0.746(2)	0.4895(5)	9.3(6)
C(10)	0.5931(8)	0.816(3)	0.4613(6)	11.1(7)
C(11)	0.3748(6)	0.718(2)	0.3343(5)	5.6(5)
C(12)	0.3401(7)	0.817(2)	0.3023(6)	8.1(6)
C(13)	0.3463(7)	0.587(2)	0.3475(6)	6.8(5)
C(14)	0.3709(7)	0.515(2)	0.3922(6)	7.4(6)
C(15)	0.3448(9)	0.396(3)	0.4043(6)	8.9(7)
C(16)	0.2932(10)	0.348(3)	0.3706(9)	11.1(8)
C(17)	0.2698(9)	0.410(4)	0.3263(8)	14(1)
C(18)	0.2933(8)	0.530(3)	0.3129(6)	10.7(7)
C(19)	0.3917(6)	0.576(2)	0.2372(5)	5.6(5)
C(20)	0.3730(8)	0.458(2)	0.2558(6)	6.8(6)
C(21)	0.3294(9)	0.364(2)	0.2265(8)	9.2(7)
C(22)	0.3008(9)	0.396(3)	0.1759(9)	10.6(9)
C(23)	0.3216(9)	0.504(3)	0.1580(7)	9.7(7)
C(24)	0.3656(8)	0.598(2)	0.1848(6)	8.4(6)
C(25)	0.5115(6)	0.582(2)	0.2762(5)	5.2(4)
C(26)	0.5459(7)	0.487(2)	0.3131(6)	6.7(5)
C(27)	0.5878(7)	0.406(2)	0.3087(6)	7.3(5)
C(28)	0.5966(8)	0.418(2)	0.2674(7)	8.2(6)
C(29)	0.5626(9)	0.508(3)	0.2293(7)	10.7(8)
C(30)	0.5198(8)	0.586(2)	0.2329(6)	8.8(6)

Table A13 continued.

C(31)	0.4515(10)	0.868(2)	0.2484(6)	5.9(5)
C(32)	0.4986(10)	0.938(3)	0.2543(7)	8.5(7)
C(33)	0.498(1)	1.074(4)	0.236(1)	11(1)
C(34)	0.451(2)	1.144(3)	0.209(1)	12(1)
C(35)	0.399(1)	1.074(4)	0.1987(9)	10.6(10)
C(36)	0.3985(10)	0.933(3)	0.2184(8)	8.0(7)
C(37)	0.768(1)	0.280(3)	0.1385(9)	10.7(10)
C(38)	0.714(1)	0.223(3)	0.1253(9)	10.3(9)
C(39)	0.6984(9)	0.305(2)	0.1585(8)	8.5(7)
C(40)	0.7424(9)	0.391(2)	0.1916(6)	7.6(6)
C(41)	0.7877(10)	0.375(3)	0.1780(8)	10.5(9)
C(42)	0.812(1)	0.209(3)	0.1216(9)	20(1)
C(43)	0.683(2)	0.108(3)	0.0895(9)	26(1)
C(44)	0.644(1)	0.274(3)	0.1634(7)	13.2(9)
C(45)	0.7409(8)	0.488(2)	0.2344(6)	9.7(7)
C(46)	0.8475(9)	0.458(4)	0.2058(8)	18(1)
C(47)	0.6276(9)	0.531(3)	0.0870(6)	12.5(9)
C(48)	0.5905(9)	0.435(3)	0.0496(7)	12.5(9)
C(49)	0.5957(8)	0.626(3)	0.1033(6)	8.0(6)
C(50)	0.540(1)	0.636(4)	0.087(1)	19(1)
C(51)	0.516(1)	0.741(4)	0.105(1)	23(1)
C(52)	0.541(1)	0.833(4)	0.1414(8)	11(1)
C(53)	0.594(1)	0.830(3)	0.1571(9)	11.6(9)
C(54)	0.6218(9)	0.725(3)	0.1374(8)	11.5(9)
C(55)	0.6297(7)	0.682(2)	-0.0135(6)	6.7(5)
C(56)	0.595(1)	0.664(3)	-0.0642(8)	11.4(8)
C(57)	0.5479(10)	0.755(4)	-0.0884(9)	13(1)
C(58)	0.5315(10)	0.852(4)	-0.064(1)	15(1)
C(59)	0.567(1)	0.879(3)	-0.015(1)	11.8(9)
C(60)	0.6148(9)	0.790(2)	0.0107(7)	8.3(7)
C(61)	0.7489(7)	0.687(2)	0.0164(6)	6.9(5)
C(62)	0.7910(8)	0.762(2)	0.0545(6)	7.8(6)
C(63)	0.8315(7)	0.848(2)	0.0461(6)	8.3(6)
C(64)	0.8280(8)	0.857(2)	0.0000(7)	8.0(7)
C(65)	0.7860(9)	0.790(3)	-0.0382(7)	9.7(8)
C(66)	0.7450(8)	0.706(2)	-0.0315(6)	7.6(6)
C(67)	0.6903(8)	0.404(2)	-0.0126(6)	6.9(5)
C(68)	0.7406(8)	0.345(2)	-0.0091(6)	8.2(6)
C(69)	0.7429(10)	0.208(3)	-0.0318(8)	8.2(8)
C(70)	0.693(1)	0.131(3)	-0.0563(8)	11.0(9)
C(71)	0.645(1)	0.189(3)	-0.0593(9)	12(1)
C(72)	0.6416(10)	0.320(3)	-0.0376(8)	10.1(8)

Table A14. Bond distances (Å) in the solid-state molecular structure of complex **2.7.**

atom-atom	distance	atom-atom	distance
W(1)-P(1)	2.519(3)	W(1)-N(1)	1.66(2)
W(1)-C(1)	2.31(2)	W(1)-C(2)	2.36(2)
W(1)-C(3)	2.39(1)	W(1)-C(4)	2.38(1)
W(1)-C(5)	2.30(2)	W(1)-C(11)	2.21(1)
W(1)-CP(1)	2.04	W(2)-P(2)	2.517(4)
W(2)-N(2)	1.72(1)	W(2)-C(37)	2.29(2)
W(2)-C(38)	2.49(3)	W(2)-C(39)	2.40(2)
W(2)-C(40)	2.39(2)	W(2)-C(41)	2.32(2)
W(2)-C(47)	2.15(2)	W(2)-CP(2)	2.06
P(1)-C(19)	1.85(2)	P(1)-C(25)	1.86(1)
P(1)-C(31)	1.86(2)	P(2)-C(55)	1.84(2)
P(2)-C(61)	1.85(2)	P(2)-C(67)	1.84(2)
O(1)-N(1)	1.28(2)	O(2)-N(2)	1.23(2)
C(1)-C(2)	1.32(2)	C(1)-C(5)	1.34(2)
C(1)-C(6)	1.53(2)	C(2)-C(3)	1.37(2)
C(2)-C(7)	1.51(3)	C(3)-C(4)	1.37(2)
C(3)-C(8)	1.55(2)	C(4)-C(5)	1.37(2)
C(4)-C(9)	1.55(2)	C(5)-C(10)	1.49(2)
C(11)-C(12)	1.33(2)	C(11)-C(13)	1.52(2)
C(13)-C(14)	1.37(2)	C(13)-C(18)	1.42(2)
C(14)-C(15)	1.39(2)	C(15)-C(16)	1.36(2)
C(16)-C(17)	1.32(3)	C(17)-C(18)	1.37(3)
C(19)-C(20)	1.37(2)	C(19)-C(24)	1.43(2)
C(20)-C(21)	1.38(2)	C(21)-C(22)	1.40(3)
C(22)-C(23)	1.33(3)	C(23)-C(24)	1.36(2)
C(25)-C(26)	1.37(2)	C(25)-C(30)	1.41(2)
C(26)-C(27)	1.36(2)	C(27)-C(28)	1.36(2)
C(28)-C(29)	1.36(2)	C(29)-C(30)	1.36(2)
C(31)-C(32)	1.32(2)	C(31)-C(36)	1.41(2)
C(32)-C(33)	1.33(3)	C(33)-C(34)	1.30(4)
C(34)-C(35)	1.41(4)	C(35)-C(36)	1.38(3)
C(37)-C(38)	1.40(3)	C(37)-C(41)	1.36(3)
C(37)-C(42)	1.56(3)	C(38)-C(39)	1.42(3)
C(38)-C(43)	1.45(3)	C(39)-C(40)	1.38(2)
C(39)-C(44)	1.52(2)	C(40)-C(41)	1.41(2)
C(40)-C(45)	1.56(2)	C(41)-C(46)	1.60(3)
C(47)-C(48)	1.41(3)	C(47)-C(49)	1.42(2)
C(49)-C(50)	1.32(2)	C(49)-C(54)	1.30(2)
C(50)-C(51)	1.36(3)	C(51)-C(52)	1.29(3)

Table A14 continued.

C(52)-C(53)	1.27(3)	C(53)-C(54)	1.44(3)
C(55)-C(56)	1.40(2)	C(55)-C(60)	1.36(2)
C(56)-C(57)	1.39(3)	C(57)-C(58)	1.32(4)
C(58)-C(59)	1.38(3)	C(59)-C(60)	1.39(3)
C(61)-C(62)	1.37(2)	C(61)-C(66)	1.41(2)
C(62)-C(63)	1.41(2)	C(63)-C(64)	1.34(2)
C(64)-C(65)	1.33(2)	C(65)-C(66)	1.39(2)
C(67)-C(68)	1.37(2)	C(67)-C(72)	1.38(2)
C(68)-C(69)	1.41(2)	C(69)-C(70)	1.36(3)
C(70)-C(71)	1.34(3)	C(71)-C(72)	1.35(3)

Table A15. Bond angles (°) in the solid-state molecular structure determined for complex **2.7.**

atom-atom-atom	angle	atom-atom-atom	angle
P(1)-W(1)-N(1)	95.1(4)	P(1)-W(1)-C(11)	81.5(3)
P(1)-W(1)-CP(1)	141.4	N(1)-W(1)-C(11)	98.2(6)
N(1)-W(1)-CP(1)	118.7	C(11)-W(1)-CP(1)	109.1
P(2)-W(2)-N(2)	95.6(5)	P(2)-W(2)-C(47)	82.1(4)
P(2)-W(2)-CP(2)	141.3	N(2)-W(2)-C(47)	97.0(9)
N(2)-W(2)-CP(2)	118.8	C(47)-W(2)-CP(2)	108.5
W(1)-P(1)-C(19)	123.5(5)	W(1)-P(1)-C(25)	114.5(5)
W(1)-P(1)-C(31)	107.9(5)	C(19)-P(1)-C(25)	99.0(6)
C(19)-P(1)-C(31)	106.7(9)	C(25)-P(1)-C(31)	103.4(8)
W(2)-P(2)-C(55)	121.8(5)	W(2)-P(2)-C(61)	115.0(6)
W(2)-P(2)-C(67)	109.6(5)	C(55)-P(2)-C(61)	100.5(8)
C(55)-P(2)-C(67)	105.3(9)	C(61)-P(2)-C(67)	102.5(8)
W(1)-N(1)-O(1)	166(1)	W(2)-N(2)-O(2)	167(1)
C(2)-C(1)-C(5)	109(1)	C(2)-C(1)-C(6)	124(2)
C(5)-C(1)-C(6)	124(2)	C(1)-C(2)-C(3)	108(1)
C(1)-C(2)-C(7)	124(2)	C(3)-C(2)-C(7)	125(2)
C(2)-C(3)-C(4)	106(1)	C(2)-C(3)-C(8)	125(2)
C(4)-C(3)-C(8)	127(1)	C(3)-C(4)-C(5)	106(1)
C(3)-C(4)-C(9)	120(1)	C(5)-C(4)-C(9)	132(1)
C(1)-C(5)-C(4)	108(1)	C(1)-C(5)-C(10)	129(1)
C(4)-C(5)-C(10)	122(1)	W(1)-C(11)-C(12)	120(1)
W(1)-C(11)-C(13)	123(1)	C(12)-C(11)-C(13)	116(1)
C(11)-C(13)-C(14)	122(1)	C(11)-C(13)-C(18)	120(1)
C(14)-C(13)-C(18)	116(1)	C(13)-C(14)-C(15)	122(1)
C(14)-C(15)-C(16)	119(2)	C(15)-C(16)-C(17)	119(2)
C(16)-C(17)-C(18)	123(2)	C(13)-C(18)-C(17)	118(1)
P(1)-C(19)-C(20)	118(1)	P(1)-C(19)-C(24)	123(1)
C(20)-C(19)-C(24)	117(1)	C(19)-C(20)-C(21)	122(1)
C(20)-C(21)-C(22)	118(1)	C(21)-C(22)-C(23)	117(2)
C(22)-C(23)-C(24)	126(2)	C(19)-C(24)-C(23)	116(1)
P(1)-C(25)-C(26)	122(1)	P(1)-C(25)-C(30)	120(1)
C(26)-C(25)-C(30)	116(1)	C(25)-C(26)-C(27)	121(1)
C(26)-C(27)-C(28)	120(1)	C(27)-C(28)-C(29)	120(1)
C(28)-C(29)-C(30)	119(1)	C(25)-C(30)-C(29)	121(1)
P(1)-C(31)-C(32)	122(1)	P(1)-C(31)-C(36)	118(1)
C(32)-C(31)-C(36)	119(1)	C(31)-C(32)-C(33)	122(2)
C(32)-C(33)-C(34)	122(3)	C(33)-C(34)-C(35)	118(3)

Table A15 continued.

C(34)-C(35)-C(36)	119(2)	C(31)-C(36)-C(35)	117(2)
C(38)-C(37)-C(41)	115(2)	C(38)-C(37)-C(42)	123(3)
C(41)-C(37)-C(42)	118(3)	C(37)-C(38)-C(39)	99(2)
C(37)-C(38)-C(43)	129(3)	C(39)-C(38)-C(43)	130(2)
C(38)-C(39)-C(40)	113(2)	C(38)-C(39)-C(44)	121(2)
C(40)-C(39)-C(44)	123(2)	C(39)-C(40)-C(41)	105(1)
C(39)-C(40)-C(45)	126(1)	C(41)-C(40)-C(45)	127(2)
C(37)-C(41)-C(40)	105(2)	C(37)-C(41)-C(46)	131(2)
C(40)-C(41)-C(46)	123(2)	W(2)-C(47)-C(48)	117(1)
W(2)-C(47)-C(49)	132(1)	C(48)-C(47)-C(49)	109(2)
C(47)-C(49)-C(50)	129(2)	C(47)-C(49)-C(54)	119(2)
C(50)-C(49)-C(54)	111(2)	C(49)-C(50)-C(51)	122(2)
C(50)-C(51)-C(52)	127(2)	C(51)-C(52)-C(53)	112(2)
C(52)-C(53)-C(54)	121(2)	C(49)-C(54)-C(53)	125(2)
P(2)-C(55)-C(56)	126(1)	P(2)-C(55)-C(60)	116(1)
C(56)-C(55)-C(60)	117(1)	C(55)-C(56)-C(57)	120(2)
C(56)-C(57)-C(58)	120(2)	C(57)-C(58)-C(59)	118(2)
C(58)-C(59)-C(60)	121(2)	C(55)-C(60)-C(59)	120(2)
P(2)-C(61)-C(62)	123(1)	P(2)-C(61)-C(66)	118(1)
C(62)-C(61)-C(66)	118(1)	C(61)-C(62)-C(63)	120(1)
C(62)-C(63)-C(64)	119(1)	C(63)-C(64)-C(65)	121(1)
C(64)-C(65)-C(66)	120(1)	C(61)-C(66)-C(65)	119(1)
P(2)-C(67)-C(68)	117(1)	P(2)-C(67)-C(72)	124(1)
C(68)-C(67)-C(72)	117(1)	C(67)-C(68)-C(69)	122(1)
C(68)-C(69)-C(70)	117(2)	C(69)-C(70)-C(71)	119(2)
C(70)-C(71)-C(72)	123(2)	C(67)-C(72)-C(71)	119(2)

Table A16. Fractional atomic coordinates in the solid-state molecular structure determined for complex **3.1**.

Atom	x	y	z	U(eq)
W(1)	1967(1)	3767(1)	3280(1)	21(1)
C(1)	5186(15)	4176(7)	3580(6)	30(2)
C(2)	4929(15)	3440(6)	3069(6)	31(3)
C(3)	3926(13)	3742(7)	2369(5)	27(2)
C(4)	3568(13)	4632(6)	2440(6)	27(2)
C(5)	4331(14)	4905(6)	3200(6)	27(2)
C(6)	6306(16)	4142(7)	4366(6)	40(3)
C(7)	5816(17)	2552(7)	3233(7)	42(3)
C(8)	3553(16)	3226(8)	1658(6)	41(3)
C(9)	2837(14)	5248(7)	1824(6)	33(3)
C(10)	4252(16)	5812(6)	3486(6)	36(3)
C(11)	-618(14)	6076(6)	4153(6)	29(2)
O(1)	1041(9)	4783(4)	4009(4)	28(2)
C(12)	-225(15)	5302(6)	3696(6)	29(2)
C(13)	-1105(13)	5108(6)	2952(6)	24(2)
C(14)	-365(12)	4461(6)	2596(6)	20(2)
C(15)	-1179(13)	4303(7)	1771(6)	26(2)
C(16)	-1363(15)	3480(7)	1455(6)	34(3)
C(17)	-2129(15)	3366(7)	696(6)	34(3)
C(18)	-2696(16)	4073(8)	239(7)	40(3)
C(19)	-2553(16)	4887(8)	549(6)	42(3)
C(20)	-1808(14)	5015(7)	1312(6)	33(3)
O(2)	2499(10)	3344(4)	4351(4)	30(2)
C(21)	2331(17)	2470(7)	4557(6)	40(3)
N(1)	992(12)	2760(5)	2940(5)	29(2)
O(3)	522(11)	2032(4)	2680(5)	41(2)

Table A17. Bond distances (Å) and angles (°) in the solid-state molecular structure of complex **3.1.**

W(1)-N(1)	1.769(8)
W(1)-O(2)	2.001(7)
W(1)-C(14)	2.200(9)
W(1)-O(1)	2.203(6)
W(1)-C(2)	2.290(10)
W(1)-C(3)	2.320(9)
W(1)-C(1)	2.393(11)
W(1)-C(4)	2.430(9)
W(1)-C(5)	2.467(9)
C(1)-C(5)	1.403(14)
C(1)-C(2)	1.447(14)
C(1)-C(6)	1.51(2)
C(2)-C(3)	1.423(14)
C(2)-C(7)	1.518(14)
C(3)-C(4)	1.401(13)
C(3)-C(8)	1.486(14)
C(4)-C(5)	1.446(14)
C(4)-C(9)	1.485(14)
C(5)-C(10)	1.490(13)
C(11)-C(12)	1.496(13)
O(1)-C(12)	1.277(12)
C(12)-C(13)	1.413(14)
C(13)-C(14)	1.337(12)
C(14)-C(15)	1.519(14)
C(15)-C(16)	1.38(2)
C(15)-C(20)	1.400(14)
C(16)-C(17)	1.392(14)
C(17)-C(18)	1.38(2)
C(18)-C(19)	1.37(2)
C(19)-C(20)	1.400(14)
O(2)-C(21)	1.403(12)
N(1)-O(3)	1.240(10)

N(1)-W(1)-O(2)	92.9(3)
N(1)-W(1)-C(14)	90.1(4)
O(2)-W(1)-C(14)	134.9(3)
N(1)-W(1)-O(1)	132.9(3)
O(2)-W(1)-O(1)	72.3(3)
C(14)-W(1)-O(1)	73.0(3)
N(1)-W(1)-C(2)	94.9(4)
O(2)-W(1)-C(2)	92.3(3)
C(14)-W(1)-C(2)	132.3(4)
O(1)-W(1)-C(2)	129.2(3)
N(1)-W(1)-C(3)	90.0(4)
O(2)-W(1)-C(3)	128.2(3)
C(14)-W(1)-C(3)	96.8(3)
O(1)-W(1)-C(3)	134.6(3)
C(2)-W(1)-C(3)	36.0(4)
N(1)-W(1)-C(1)	129.0(4)
O(2)-W(1)-C(1)	80.5(3)
C(14)-W(1)-C(1)	129.3(3)
O(1)-W(1)-C(1)	93.3(3)
C(2)-W(1)-C(1)	35.9(4)
C(3)-W(1)-C(1)	58.7(3)
N(1)-W(1)-C(4)	118.0(4)
O(2)-W(1)-C(4)	136.8(3)
C(14)-W(1)-C(4)	77.9(3)
O(1)-W(1)-C(4)	101.3(3)
C(2)-W(1)-C(4)	58.0(3)
C(3)-W(1)-C(4)	34.2(3)
C(1)-W(1)-C(4)	56.8(3)
N(1)-W(1)-C(5)	147.5(3)
O(2)-W(1)-C(5)	104.7(3)
C(14)-W(1)-C(5)	96.0(3)
O(1)-W(1)-C(5)	79.0(3)
C(2)-W(1)-C(5)	58.0(3)
C(3)-W(1)-C(5)	57.7(3)
C(1)-W(1)-C(5)	33.5(3)
C(4)-W(1)-C(5)	34.3(3)
C(5)-C(1)-C(2)	108.4(9)
C(5)-C(1)-C(6)	127.7(10)
C(2)-C(1)-C(6)	123.8(10)
C(5)-C(1)-W(1)	76.1(6)
C(2)-C(1)-W(1)	68.2(6)
C(6)-C(1)-W(1)	124.3(7)
C(3)-C(2)-C(1)	107.3(9)
C(3)-C(2)-C(7)	127.3(10)
C(1)-C(2)-C(7)	125.0(10)
C(3)-C(2)-W(1)	73.1(6)

Table A17 continued.

C(1)-C(2)-W(1)	75.9(6)	C(4)-C(5)-W(1)	71.4(5)
C(7)-C(2)-W(1)	123.0(7)	C(10)-C(5)-W(1)	125.4(7)
C(4)-C(3)-C(2)	108.4(9)	C(12)-O(1)-W(1)	116.5(6)
C(4)-C(3)-C(8)	125.9(10)	O(1)-C(12)-C(13)	117.9(9)
C(2)-C(3)-C(8)	125.2(10)	O(1)-C(12)-C(11)	116.2(10)
C(4)-C(3)-W(1)	77.2(5)	C(13)-C(12)-C(11)	125.8(9)
C(2)-C(3)-W(1)	70.9(5)	C(14)-C(13)-C(12)	116.7(9)
C(8)-C(3)-W(1)	124.0(7)	C(13)-C(14)-C(15)	117.1(9)
C(3)-C(4)-C(5)	108.6(9)	C(13)-C(14)-W(1)	115.2(7)
C(3)-C(4)-C(9)	127.3(10)	C(15)-C(14)-W(1)	127.6(6)
C(5)-C(4)-C(9)	123.4(9)	C(16)-C(15)-C(20)	118.3(10)
C(3)-C(4)-W(1)	68.6(5)	C(16)-C(15)-C(14)	122.7(9)
C(5)-C(4)-W(1)	74.2(5)	C(20)-C(15)-C(14)	119.0(9)
C(9)-C(4)-W(1)	131.1(6)	C(15)-C(16)-C(17)	120.8(10)
C(1)-C(5)-C(4)	107.4(9)	C(18)-C(17)-C(16)	120.8(10)
C(1)-C(5)-C(10)	128.2(11)	C(19)-C(18)-C(17)	118.9(11)
C(4)-C(5)-C(10)	124.4(9)	C(18)-C(19)-C(20)	121.1(10)
C(1)-C(5)-W(1)	70.3(6)	C(15)-C(20)-C(19)	120.1(10)
		C(21)-O(2)-W(1)	123.4(6)
		O(3)-N(1)-W(1)	172.2(8)

Table A18. Fractional atomic coordinates in the solid-state molecular structure determined for complex **3.3.**

Atom	x	y	z	U(eq)
W(1)	7071(1)	960(1)	8942(1)	17(1)
N(1)	5463(4)	942(1)	10177(3)	22(1)
C(1)	5211(4)	1443(2)	10738(3)	24(1)
C(2)	3908(5)	1489(2)	11466(4)	32(1)
C(3)	6258(4)	1960(2)	10602(3)	25(1)
C(4)	7271(4)	1883(2)	9822(3)	21(1)
C(5)	8387(5)	2412(2)	9685(3)	23(1)
C(6)	9946(5)	2312(2)	9460(3)	26(1)
C(7)	10986(5)	2816(2)	9401(3)	33(1)
C(8)	10494(5)	3435(2)	9557(3)	34(1)
C(9)	8951(5)	3537(2)	9753(3)	33(1)
C(10)	7914(5)	3039(2)	9823(3)	28(1)
O(1)	6739(3)	15(1)	9237(2)	24(1)
N(2)	9149(4)	852(1)	9318(3)	22(1)
O(2)	10600(3)	753(1)	9458(3)	35(1)
C(11)	4765(4)	1265(2)	7623(3)	27(1)
C(12)	5265(5)	668(2)	7317(3)	30(1)
C(13)	6856(5)	721(2)	7056(3)	26(1)
C(14)	7316(4)	1367(2)	7169(3)	20(1)
C(15)	6014(4)	1704(2)	7518(3)	20(1)
C(16)	3165(5)	1447(3)	7932(4)	48(1)
C(17)	4284(7)	74(2)	7242(5)	54(2)
C(18)	7812(7)	204(2)	6601(4)	49(1)
C(19)	8830(5)	1641(2)	6851(3)	32(1)
C(20)	5811(5)	2404(2)	7544(3)	31(1)
N(101)	9330(6)	1036(3)	4090(4)	70(2)
C(101)	9349(6)	967(2)	3167(4)	41(1)
C(102)	9389(7)	878(3)	1980(4)	54(1)

Table A19. Bond distances (Å) and angles (°) in the solid-state molecular structure of complex **3.3.**

W(1)-N(2)	1.775(3)	C(7)-C(8)	1.398(6)
W(1)-O(1)	2.064(2)	C(8)-C(9)	1.376(6)
W(1)-N(1)	2.150(3)	C(9)-C(10)	1.385(6)
W(1)-C(4)	2.227(4)	N(2)-O(2)	1.238(4)
W(1)-C(13)	2.323(4)	C(11)-C(12)	1.401(6)
W(1)-C(14)	2.348(3)	C(11)-C(15)	1.428(5)
W(1)-C(12)	2.411(4)	C(11)-C(16)	1.503(6)
W(1)-C(15)	2.422(4)	C(12)-C(13)	1.429(6)
W(1)-C(11)	2.444(4)	C(12)-C(17)	1.508(6)
N(1)-C(1)	1.295(5)	C(13)-C(14)	1.427(5)
C(1)-C(3)	1.434(5)	C(13)-C(18)	1.510(6)
C(1)-C(2)	1.503(5)	C(14)-C(15)	1.425(5)
C(3)-C(4)	1.366(5)	C(14)-C(19)	1.504(5)
C(4)-C(5)	1.491(5)	C(15)-C(20)	1.497(5)
C(5)-C(6)	1.400(5)	N(101)-C(101)	1.129(7)
C(5)-C(10)	1.406(5)	C(101)-C(102)	1.454(7)
C(6)-C(7)	1.395(5)		

N(2)-W(1)-O(1)	89.04(12)	N(1)-W(1)-C(15)	107.30(12)
N(2)-W(1)-N(1)	121.11(13)	C(4)-W(1)-C(15)	76.37(13)
O(1)-W(1)-N(1)	75.52(11)	C(13)-W(1)-C(15)	57.90(13)
N(2)-W(1)-C(4)	88.83(14)	C(14)-W(1)-C(15)	34.72(12)
O(1)-W(1)-C(4)	140.97(12)	C(12)-W(1)-C(15)	56.64(13)
N(1)-W(1)-C(4)	72.45(12)	N(2)-W(1)-C(11)	152.06(13)
N(2)-W(1)-C(13)	99.90(14)	O(1)-W(1)-C(11)	104.79(12)
O(1)-W(1)-C(13)	87.85(12)	N(1)-W(1)-C(11)	86.21(12)
N(1)-W(1)-C(13)	134.75(13)	C(4)-W(1)-C(11)	94.81(14)
C(4)-W(1)-C(13)	130.83(13)	C(13)-W(1)-C(11)	57.46(14)
N(2)-W(1)-C(14)	94.51(13)	C(14)-W(1)-C(11)	57.57(12)
O(1)-W(1)-C(14)	123.08(12)	C(12)-W(1)-C(11)	33.53(14)
N(1)-W(1)-C(14)	141.42(12)	C(15)-W(1)-C(11)	34.14(12)
C(4)-W(1)-C(14)	95.93(13)	C(1)-N(1)-W(1)	120.9(3)
C(13)-W(1)-C(14)	35.57(13)	N(1)-C(1)-C(3)	114.9(3)
N(2)-W(1)-C(12)	132.8(2)	N(1)-C(1)-C(2)	123.1(4)
O(1)-W(1)-C(12)	78.77(12)	C(3)-C(1)-C(2)	122.0(3)
N(1)-W(1)-C(12)	99.83(13)	C(4)-C(3)-C(1)	116.2(3)
C(4)-W(1)-C(12)	128.10(14)	C(3)-C(4)-C(5)	116.9(3)
C(13)-W(1)-C(12)	35.07(14)	C(3)-C(4)-W(1)	114.8(3)
C(14)-W(1)-C(12)	58.04(13)	C(5)-C(4)-W(1)	128.3(3)
N(2)-W(1)-C(15)	121.92(13)	C(6)-C(5)-C(10)	117.2(4)
O(1)-W(1)-C(15)	135.34(11)	C(6)-C(5)-C(4)	122.4(3)
		C(10)-C(5)-C(4)	120.4(3)

Table A19 continued.

C(7)-C(6)-C(5)	120.8(4)	C(12)-C(13)-C(18)	126.2(4)
C(6)-C(7)-C(8)	120.9(4)	C(14)-C(13)-C(18)	125.5(4)
C(9)-C(8)-C(7)	118.5(4)	C(12)-C(13)-W(1)	75.8(2)
C(8)-C(9)-C(10)	121.0(4)	C(14)-C(13)-W(1)	73.2(2)
C(9)-C(10)-C(5)	121.5(4)	C(18)-C(13)-W(1)	122.7(3)
O(2)-N(2)-W(1)	172.7(3)	C(15)-C(14)-C(13)	107.4(3)
C(12)-C(11)-C(15)	108.3(3)	C(15)-C(14)-C(19)	126.9(4)
C(12)-C(11)-C(16)	127.7(4)	C(13)-C(14)-C(19)	125.4(3)
C(15)-C(11)-C(16)	123.9(4)	C(15)-C(14)-W(1)	75.5(2)
C(12)-C(11)-W(1)	71.9(2)	C(13)-C(14)-W(1)	71.3(2)
C(15)-C(11)-W(1)	72.1(2)	C(19)-C(14)-W(1)	123.8(3)
C(16)-C(11)-W(1)	125.1(3)	C(14)-C(15)-C(11)	108.0(3)
C(11)-C(12)-C(13)	108.4(3)	C(14)-C(15)-C(20)	126.9(3)
C(11)-C(12)-C(17)	126.1(4)	C(11)-C(15)-C(20)	123.9(4)
C(13)-C(12)-C(17)	125.5(4)	C(14)-C(15)-W(1)	69.8(2)
C(11)-C(12)-W(1)	74.6(2)	C(11)-C(15)-W(1)	73.8(2)
C(13)-C(12)-W(1)	69.1(2)	C(20)-C(15)-W(1)	131.7(3)
C(17)-C(12)-W(1)	123.4(3)	N(101)-C(101)-C(102)	179.5(6)
C(12)-C(13)-C(14)	107.9(3)		

Table A20. Fractional atomic coordinates in the solid-state molecular structure determined for complex **3.7.**

Atom	x	y	z	U(eq)
W(1)	1444(1)	2510(1)	2188(1)	20(1)
N(1)	290(7)	2812(3)	3365(5)	26(1)
O(1)	-400(7)	3029(3)	4204(4)	39(1)
N(2)	95(8)	1646(3)	1088(5)	27(1)
C(1)	-827(10)	378(4)	773(7)	39(2)
C(2)	58(9)	1003(3)	1507(6)	26(1)
C(3)	896(9)	919(4)	2742(6)	28(2)
C(4)	1774(9)	1506(4)	3291(6)	27(1)
C(5)	2732(9)	1414(4)	4563(6)	30(2)
C(6)	3384(10)	734(4)	5004(7)	38(2)
C(7)	4105(12)	628(5)	6201(7)	47(2)
C(8)	4287(12)	1202(5)	6992(7)	47(2)
C(9)	3724(11)	1876(5)	6594(7)	41(2)
C(10)	2960(10)	1988(4)	5395(6)	35(2)
N(3)	-625(8)	3042(3)	869(5)	22(1)
C(11)	-1652(9)	3642(3)	794(6)	25(1)
C(12)	-1743(9)	4058(4)	1920(6)	27(1)
C(13)	-2639(9)	3910(4)	-309(6)	27(2)
C(14)	-2757(10)	3578(4)	-1470(6)	35(2)
C(15)	-3838(11)	4024(5)	-2308(7)	44(2)
C(16)	-4368(10)	4639(4)	-1720(7)	38(2)
C(17)	-3667(10)	4576(4)	-523(7)	31(2)
C(18)	4170(10)	2329(3)	1227(6)	27(2)
C(19)	3368(10)	3001(4)	868(6)	26(2)
C(20)	3433(9)	3449(3)	1894(6)	22(1)
C(21)	4384(9)	3054(4)	2898(6)	21(1)
C(22)	4819(8)	2356(3)	2495(6)	22(2)
C(23)	4456(11)	1696(4)	428(7)	38(2)
C(24)	2675(10)	3229(4)	-418(6)	31(2)
C(25)	2940(9)	4246(4)	1864(7)	29(2)
C(26)	5038(9)	3370(4)	4144(6)	26(1)
C(27)	6046(9)	1791(3)	3188(6)	28(2)
N(101)	1869(20)	4718(6)	5079(11)	112(4)
C(101)	1363(15)	4372(5)	5742(10)	63(3)
C(102)	954(14)	3888(5)	6635(8)	54(2)
N(201)	-708(12)	1759(5)	8354(7)	66(2)
C(201)-	856(12)	1567(5)	7405(8)	48(2)
C(202)-	1129(15)	1351(8)	6170(9)	87(4)

Table A21. Bond distances (Å) and angles (°) in the solid-state molecular structure of complex **3.7.**

W(1)-N(1)	1.785(5)	C(101)-C(102)	1.421(14)
W(1)-N(2)	2.147(6)	N(201)-C(201)	1.121(11)
W(1)-N(3)	2.151(5)	C(201)-C(202)	1.436(12)
W(1)-C(4)	2.224(6)	N(1)-W(1)-N(2)	116.3(2)
W(1)-C(20)	2.311(6)	N(1)-W(1)-N(3)	91.2(2)
W(1)-C(21)	2.354(6)	N(2)-W(1)-N(3)	75.4(3)
W(1)-C(19)	2.396(7)	N(1)-W(1)-C(4)	81.7(2)
W(1)-C(22)	2.413(6)	N(2)-W(1)-C(4)	72.6(2)
W(1)-C(18)	2.437(6)	N(3)-W(1)-C(4)	139.7(2)
N(1)-O(1)	1.219(7)	N(1)-W(1)-C(20)	105.1(2)
N(2)-C(2)	1.280(9)	N(2)-W(1)-C(20)	134.4(2)
C(1)-C(2)	1.496(9)	N(3)-W(1)-C(20)	85.9(2)
C(2)-C(3)	1.432(10)	C(4)-W(1)-C(20)	134.3(2)
C(3)-C(4)	1.348(9)	N(1)-W(1)-C(21)	97.1(2)
C(4)-C(5)	1.495(10)	N(2)-W(1)-C(21)	143.3(2)
C(5)-C(6)	1.400(10)	N(3)-W(1)-C(21)	120.9(2)
C(5)-C(10)	1.408(10)	C(4)-W(1)-C(21)	99.4(2)
C(6)-C(7)	1.379(10)	C(20)-W(1)-C(21)	35.5(2)
C(7)-C(8)	1.379(12)	N(1)-W(1)-C(19)	138.7(2)
C(8)-C(9)	1.359(12)	N(2)-W(1)-C(19)	99.8(2)
C(9)-C(10)	1.390(10)	N(3)-W(1)-C(19)	78.4(2)
N(3)-C(11)	1.327(8)	C(4)-W(1)-C(19)	130.6(3)
C(11)-C(13)	1.414(9)	C(20)-W(1)-C(19)	35.1(2)
C(11)-C(12)	1.503(10)	C(21)-W(1)-C(19)	57.7(2)
C(13)-C(17)	1.432(10)	N(1)-W(1)-C(22)	121.5(2)
C(13)-C(14)	1.441(10)	N(2)-W(1)-C(22)	109.7(2)
C(14)-C(15)	1.388(10)	N(3)-W(1)-C(22)	135.2(2)
C(15)-C(16)	1.403(11)	C(4)-W(1)-C(22)	79.5(2)
C(16)-C(17)	1.367(10)	C(20)-W(1)-C(22)	58.2(2)
C(18)-C(19)	1.396(10)	C(21)-W(1)-C(22)	34.6(2)
C(18)-C(22)	1.433(10)	C(19)-W(1)-C(22)	56.8(2)
C(18)-C(23)	1.515(10)	N(1)-W(1)-C(18)	154.2(2)
C(19)-C(20)	1.422(9)	N(2)-W(1)-C(18)	87.5(2)
C(19)-C(24)	1.516(10)	N(3)-W(1)-C(18)	105.4(2)
C(20)-C(21)	1.421(9)	C(4)-W(1)-C(18)	97.2(2)
C(20)-C(25)	1.511(9)	C(20)-W(1)-C(18)	57.7(2)
C(21)-C(22)	1.420(9)	C(21)-W(1)-C(18)	57.5(2)
C(21)-C(26)	1.524(9)	C(19)-W(1)-C(18)	33.6(2)
C(22)-C(27)	1.496(9)	C(22)-W(1)-C(18)	34.4(2)
N(101)-C(101)	1.098(13)	O(1)-N(1)-W(1)	176.3(5)

Table A21 continued.

C(2)-N(2)-W(1)	120.6(5)	C(22)-C(18)-C(23)	125.0(6)
N(2)-C(2)-C(3)	115.5(6)	C(19)-C(18)-W(1)	71.6(4)
N(2)-C(2)-C(1)	122.8(7)	C(22)-C(18)-W(1)	71.9(3)
C(3)-C(2)-C(1)	121.6(6)	C(23)-C(18)-W(1)	125.5(5)
C(4)-C(3)-C(2)	116.5(6)	C(18)-C(19)-C(20)	109.0(6)
C(3)-C(4)-C(5)	117.0(6)	C(18)-C(19)-C(24)	125.1(7)
C(3)-C(4)-W(1)	114.4(5)	C(20)-C(19)-C(24)	125.8(6)
C(5)-C(4)-W(1)	128.5(5)	C(18)-C(19)-W(1)	74.9(4)
C(6)-C(5)-C(10)	116.3(7)	C(20)-C(19)-W(1)	69.2(4)
C(6)-C(5)-C(4)	120.9(7)	C(24)-C(19)-W(1)	125.4(5)
C(10)-C(5)-C(4)	122.8(6)	C(21)-C(20)-C(19)	107.4(6)
C(7)-C(6)-C(5)	121.5(8)	C(21)-C(20)-C(25)	126.4(6)
C(6)-C(7)-C(8)	120.5(7)	C(19)-C(20)-C(25)	125.0(6)
C(9)-C(8)-C(7)	119.8(7)	C(21)-C(20)-W(1)	73.9(3)
C(8)-C(9)-C(10)	120.3(8)	C(19)-C(20)-W(1)	75.7(4)
C(9)-C(10)-C(5)	121.5(7)	C(25)-C(20)-W(1)	125.6(4)
C(11)-N(3)-W(1)	137.3(5)	C(22)-C(21)-C(20)	108.0(5)
N(3)-C(11)-C(13)	122.3(6)	C(22)-C(21)-C(26)	126.6(6)
N(3)-C(11)-C(12)	118.8(6)	C(20)-C(21)-C(26)	125.0(6)
C(13)-C(11)-C(12)	118.9(6)	C(22)-C(21)-W(1)	75.0(4)
C(11)-C(13)-C(17)	127.8(7)	C(20)-C(21)-W(1)	70.6(3)
C(11)-C(13)-C(14)	126.8(6)	C(26)-C(21)-W(1)	126.2(4)
C(17)-C(13)-C(14)	105.4(6)	C(21)-C(22)-C(18)	107.7(5)
C(15)-C(14)-C(13)	108.0(7)	C(21)-C(22)-C(27)	127.3(6)
C(14)-C(15)-C(16)	108.7(7)	C(18)-C(22)-C(27)	124.0(5)
C(17)-C(16)-C(15)	108.7(6)	C(21)-C(22)-W(1)	70.4(3)
C(16)-C(17)-C(13)	109.3(7)	C(18)-C(22)-W(1)	73.8(3)
C(19)-C(18)-C(22)	107.8(6)	C(27)-C(22)-W(1)	130.1(4)
C(19)-C(18)-C(23)	127.1(7)	N(101)-C(101)-C(102)	172.5(13)
		N(201)-C(201)-C(202)	176.8(11)

Table A22. Fractional atomic coordinates in the solid-state molecular structure determined for complex **3.9.**

atom	x	y	z	U(eq)
W(1)	7324(1)	2281(1)	1807(1)	19(1)
C(1)	8110(4)	1610(3)	486(3)	27(1)
C(2)	7459(4)	2392(3)	214(3)	24(1)
C(3)	8146(4)	3097(3)	665(3)	26(1)
C(4)	9272(4)	2739(3)	1187(3)	26(1)
C(5)	9241(4)	1827(3)	1077(3)	26(1)
C(6)	7808(5)	718(3)	137(3)	41(1)
C(7)	6275(5)	2491(3)	-458(3)	37(1)
C(8)	7860(5)	4052(3)	548(3)	38(1)
C(9)	10359(4)	3287(3)	1648(3)	36(1)
C(10)	10305(4)	1191(3)	1390(3)	39(1)
O(1)	5339(3)	2312(2)	1309(2)	26(1)
C(11)	4849(4)	1535(3)	1673(3)	26(1)
C(12)	4307(4)	917(3)	943(3)	37(1)
C(13)	3813(4)	1740(3)	2322(3)	35(1)
N(2)	6111(3)	1256(2)	2161(2)	21(1)
C(14)	6492(4)	615(3)	2667(3)	23(1)
C(15)	5695(4)	-192(3)	2795(3)	28(1)
C(16)	6150(5)	-899(3)	2181(4)	46(1)
C(17)	5786(5)	-508(4)	3749(3)	51(2)
C(18)	7820(4)	781(3)	3088(3)	24(1)
C(19)	8435(4)	1537(3)	2885(3)	21(1)
C(20)	9691(4)	1774(3)	3413(3)	22(1)
C(21)	10650(4)	1148(3)	3679(3)	29(1)
C(22)	11808(4)	1366(3)	4199(3)	35(1)
C(23)	12023(4)	2218(3)	4464(3)	35(1)
C(24)	11084(4)	2847(3)	4214(3)	33(1)
C(25)	9939(4)	2632(3)	3689(3)	29(1)
N(3)	7255(3)	3209(2)	2510(2)	25(1)
O(2)	7362(3)	3923(2)	2880(2)	37(1)

Table A23. Bond distances (Å) and angles (°) in the solid-state molecular structure of complex **3.9.**

W(1)-N(3)	1.789(4)	O(1)-W(1)-C(19)	133.56(13)
W(1)-O(1)	2.075(3)	N(2)-W(1)-C(19)	71.90(14)
W(1)-N(2)	2.095(3)	N(3)-W(1)-C(3)	92.4(2)
W(1)-C(19)	2.219(4)	O(1)-W(1)-C(3)	96.17(13)
W(1)-C(3)	2.345(4)	N(2)-W(1)-C(3)	147.46(14)
W(1)-C(4)	2.351(4)	C(19)-W(1)-C(3)	129.29(14)
W(1)-C(5)	2.405(4)	N(3)-W(1)-C(4)	94.1(2)
W(1)-C(2)	2.433(4)	O(1)-W(1)-C(4)	131.05(13)
W(1)-C(1)	2.442(4)	N(2)-W(1)-C(4)	148.4(2)
C(1)-C(2)	1.419(6)	C(19)-W(1)-C(4)	93.7(2)
C(1)-C(5)	1.427(6)	C(3)-W(1)-C(4)	35.63(14)
C(1)-C(6)	1.496(6)	N(3)-W(1)-C(5)	125.4(2)
C(2)-C(3)	1.432(6)	O(1)-W(1)-C(5)	128.57(13)
C(2)-C(7)	1.509(6)	N(2)-W(1)-C(5)	113.8(2)
C(3)-C(4)	1.437(6)	C(19)-W(1)-C(5)	79.23(14)
C(3)-C(8)	1.509(6)	C(3)-W(1)-C(5)	58.2(2)
C(4)-C(5)	1.418(6)	C(4)-W(1)-C(5)	34.66(14)
C(4)-C(9)	1.506(6)	N(3)-W(1)-C(2)	122.8(2)
C(5)-C(10)	1.500(6)	O(1)-W(1)-C(2)	76.69(12)
O(1)-C(11)	1.425(5)	N(2)-W(1)-C(2)	112.86(14)
C(11)-N(2)	1.478(5)	C(19)-W(1)-C(2)	134.34(14)
C(11)-C(13)	1.524(6)	C(3)-W(1)-C(2)	34.81(14)
C(11)-C(12)	1.527(6)	C(4)-W(1)-C(2)	57.69(14)
N(2)-C(14)	1.290(5)	C(5)-W(1)-C(2)	56.77(14)
C(14)-C(18)	1.453(5)	N(3)-W(1)-C(1)	149.1(2)
C(14)-C(15)	1.503(6)	O(1)-W(1)-C(1)	94.56(13)
C(15)-C(17)	1.520(6)	N(2)-W(1)-C(1)	97.11(14)
C(15)-C(16)	1.528(6)	C(19)-W(1)-C(1)	101.8(2)
C(18)-C(19)	1.368(6)	C(3)-W(1)-C(1)	57.7(2)
C(19)-C(20)	1.484(5)	C(4)-W(1)-C(1)	57.5(2)
C(20)-C(21)	1.400(6)	C(5)-W(1)-C(1)	34.24(14)
C(20)-C(25)	1.405(6)	C(2)-W(1)-C(1)	33.84(14)
C(21)-C(22)	1.391(6)	C(2)-C(1)-C(5)	107.8(4)
C(22)-C(23)	1.387(6)	C(2)-C(1)-C(6)	127.3(4)
C(23)-C(24)	1.385(6)	C(5)-C(1)-C(6)	124.4(4)
C(24)-C(25)	1.383(6)	C(2)-C(1)-W(1)	72.7(2)
N(3)-O(2)	1.237(4)	C(5)-C(1)-W(1)	71.5(2)
N(3)-W(1)-O(1)	96.54(13)	C(6)-C(1)-W(1)	127.6(3)
N(3)-W(1)-N(2)	113.60(14)	C(1)-C(2)-C(3)	108.4(4)
O(1)-W(1)-N(2)	63.06(12)	C(1)-C(2)-C(7)	126.9(4)
N(3)-W(1)-C(19)	91.1(2)	C(3)-C(2)-C(7)	124.6(4)

Table A23 continued.

C(1)-C(2)-W(1)	73.4(2)	N(2)-C(11)-C(13)	110.1(3)
C(3)-C(2)-W(1)	69.2(2)	O(1)-C(11)-C(12)	111.1(4)
C(7)-C(2)-W(1)	124.7(3)	N(2)-C(11)-C(12)	114.8(4)
C(2)-C(3)-C(4)	107.2(4)	C(13)-C(11)-C(12)	112.0(4)
C(2)-C(3)-C(8)	127.4(4)	C(14)-N(2)-C(11)	136.1(4)
C(4)-C(3)-C(8)	125.1(4)	C(14)-N(2)-W(1)	125.5(3)
C(2)-C(3)-W(1)	75.9(2)	C(11)-N(2)-W(1)	98.4(2)
C(4)-C(3)-W(1)	72.4(2)	N(2)-C(14)-C(18)	110.0(4)
C(8)-C(3)-W(1)	122.4(3)	N(2)-C(14)-C(15)	125.2(4)
C(5)-C(4)-C(3)	108.0(4)	C(18)-C(14)-C(15)	124.8(4)
C(5)-C(4)-C(9)	128.3(4)	C(14)-C(15)-C(17)	113.4(4)
C(3)-C(4)-C(9)	123.1(4)	C(14)-C(15)-C(16)	108.9(4)
C(5)-C(4)-W(1)	74.8(2)	C(17)-C(15)-C(16)	110.6(4)
C(3)-C(4)-W(1)	71.9(2)	C(19)-C(18)-C(14)	117.9(4)
C(9)-C(4)-W(1)	125.5(3)	C(18)-C(19)-C(20)	118.1(4)
C(4)-C(5)-C(1)	108.4(4)	C(18)-C(19)-W(1)	113.4(3)
C(4)-C(5)-C(10)	127.2(4)	C(20)-C(19)-W(1)	128.5(3)
C(1)-C(5)-C(10)	123.7(4)	C(21)-C(20)-C(25)	117.6(4)
C(4)-C(5)-W(1)	70.6(2)	C(21)-C(20)-C(19)	121.3(4)
C(1)-C(5)-W(1)	74.3(2)	C(25)-C(20)-C(19)	121.0(4)
C(10)-C(5)-W(1)	128.7(3)	C(22)-C(21)-C(20)	121.4(4)
C(11)-O(1)-W(1)	101.1(2)	C(23)-C(22)-C(21)	119.7(4)
O(1)-C(11)-N(2)	97.4(3)	C(24)-C(23)-C(22)	119.9(4)
O(1)-C(11)-C(13)	110.6(4)	C(25)-C(24)-C(23)	120.3(5)
		C(24)-C(25)-C(20)	121.0(4)
		O(2)-N(3)-W(1)	167.5(3)

Table A24. Fractional atomic coordinates in the solid-state molecular structure determined for complex **3.12.**

atom	x	y	z	B(eq)
W(1)	0.412541(8)	0.55629(4)	0.28870(2)	2.142(8)
W(2)	0.401882(8)	0.75375(3)	0.447780(15)	1.922(8)
W(3)	0.322010(7)	0.66628(4)	0.273893(15)	1.932(8)
O(1)	0.41837(13)	0.6078(6)	0.4127(2)	2.17(14)
O(2)	0.34360(13)	0.6720(6)	0.3692(2)	2.17(14)
O(3)	0.36911(14)	0.5134(6)	0.2664(3)	2.33(14)
O(4)	0.39309(14)	0.6482(6)	0.2147(3)	2.80(15)
O(5)	0.43063(14)	0.8311(6)	0.4288(3)	2.42(15)
O(6)	0.32231(13)	0.8393(6)	0.2926(3)	2.35(14)
N(1)	0.4151(2)	0.6055(7)	0.3582(4)	2.5(2)
N(2)	0.36837(15)	0.7168(7)	0.3962(3)	2.0(2)
N(3)	0.35096(14)	0.5941(7)	0.2691(3)	1.53(15)
C(1)	0.4152(3)	0.3495(10)	0.3124(5)	3.6(3)
C(2)	0.4056(3)	0.3496(12)	0.2519(5)	4.3(3)
C(3)	0.4258(3)	0.3962(11)	0.2354(5)	3.9(3)
C(4)	0.4512(2)	0.4299(11)	0.2885(5)	3.8(3)
C(5)	0.4432(2)	0.3919(11)	0.3368(4)	3.3(3)
C(6)	0.4015(4)	0.3077(13)	0.3478(7)	6.7(5)
C(7)	0.3775(3)	0.3077(13)	0.2051(7)	6.3(4)
C(8)	0.4257(4)	0.4140(14)	0.1735(5)	5.9(4)
C(9)	0.4791(3)	0.4573(15)	0.2923(7)	6.9(4)
C(10)	0.4632(3)	0.3941(14)	0.4010(6)	5.8(4)
C(11)	0.3995(3)	0.6061(10)	0.5120(4)	3.2(3)
C(12)	0.4286(3)	0.6236(11)	0.5298(4)	4.1(3)
C(13)	0.4356(2)	0.7438(10)	0.5507(4)	3.0(2)
C(14)	0.4117(2)	0.8015(10)	0.5497(4)	2.9(2)
C(15)	0.3889(2)	0.7206(11)	0.5257(4)	3.0(2)
C(16)	0.3827(4)	0.4935(12)	0.4913(5)	5.6(4)
C(17)	0.4490(3)	0.5273(13)	0.5284(5)	5.7(4)
C(18)	0.4651(3)	0.7975(14)	0.5733(5)	4.8(3)
C(19)	0.4116(4)	0.9183(12)	0.5788(5)	6.1(4)
C(20)	0.3596(3)	0.7380(13)	0.5231(5)	4.7(3)
C(21)	0.3013(2)	0.4797(10)	0.2845(6)	3.8(3)
C(22)	0.2921(2)	0.5588(10)	0.3151(4)	2.9(2)
C(23)	0.2748(2)	0.6479(11)	0.2756(5)	3.5(3)
C(24)	0.2726(2)	0.6167(12)	0.2205(5)	3.9(3)
C(25)	0.2887(2)	0.5155(10)	0.2217(5)	3.4(3)

Table A24 continued.

C(26)	0.3194(3)	0.3659(13)	0.3069(8)	6.2(4)
C(27)	0.2988(3)	0.5493(14)	0.3794(5)	5.0(3)
C(28)	0.2611(3)	0.7503(12)	0.2935(7)	5.8(4)
C(29)	0.2520(3)	0.6787(15)	0.1650(6)	5.6(4)
C(30)	0.2890(4)	0.4461(14)	0.1711(7)	6.3(4)
C(31)	0.4435(2)	0.6902(11)	0.2880(4)	3.2(2)
C(32)	0.4332(2)	0.7675(11)	0.2423(4)	3.2(3)
C(33)	0.4033(2)	0.7508(9)	0.1975(4)	2.7(2)
C(34)	0.3854(2)	0.8584(11)	0.1970(5)	3.8(3)
C(35)	0.4034(2)	0.7297(12)	0.1357(5)	3.8(3)
C(36)	0.4721(2)	0.7169(11)	0.3336(4)	3.3(2)
C(37)	0.4779(2)	0.7086(11)	0.3946(5)	3.2(2)
C(38)	0.5045(2)	0.7386(11)	0.4360(5)	3.7(3)
C(39)	0.5254(2)	0.7722(13)	0.4185(5)	4.5(3)
C(40)	0.5199(2)	0.7832(15)	0.3598(6)	5.4(4)
C(41)	0.4928(3)	0.760(2)	0.3189(5)	5.9(4)
C(42)	0.3922(2)	0.9474(8)	0.4438(4)	2.4(2)
C(43)	0.4080(2)	1.0163(9)	0.4286(4)	2.8(2)
C(44)	0.4315(2)	0.9568(10)	0.4184(5)	3.1(2)
C(45)	0.4607(3)	1.0112(11)	0.4554(5)	4.2(3)
C(46)	0.4267(3)	0.9726(11)	0.3516(5)	4.5(3)
C(47)	0.3666(2)	1.0058(9)	0.4486(4)	2.5(2)
C(48)	0.3397(2)	0.9548(10)	0.4222(4)	3.1(2)
C(49)	0.3171(2)	1.0139(12)	0.4240(5)	4.1(3)
C(50)	0.3197(3)	1.1230(12)	0.4522(6)	4.6(3)
C(51)	0.3460(3)	1.1736(12)	0.4803(5)	4.6(3)
C(52)	0.3693(2)	1.1175(10)	0.4775(5)	3.2(2)
C(53)	0.3141(2)	0.7615(9)	0.1917(4)	2.0(2)
C(54)	0.3133(2)	0.8805(9)	0.1948(4)	2.3(2)
C(55)	0.3175(2)	0.9379(9)	0.2528(5)	2.8(2)
C(56)	0.3438(3)	1.0188(10)	0.2771(5)	3.9(3)
C(57)	0.2917(3)	1.0120(11)	0.2491(6)	4.6(3)
C(58)	0.3113(2)	0.7054(10)	0.1331(4)	2.5(2)
C(59)	0.3292(2)	0.6188(11)	0.1303(4)	3.3(3)
C(60)	0.3268(2)	0.5646(11)	0.0769(5)	3.7(3)
C(61)	0.3038(3)	0.6057(13)	0.0246(5)	4.3(3)
C(62)	0.2863(3)	0.6918(13)	0.0274(5)	4.1(3)
C(63)	0.2893(2)	0.7449(11)	0.0804(4)	3.3(3)

Table A25. Bond distances (Å) in the solid-state molecular structure of complex **3.12.**

atom-atom	distance	atom-atom	distance
W(1)-O(3)	2.156(6)	W(1)-O(4)	1.982(6)
W(1)-N(1)	1.764(8)	W(1)-C(1)	2.335(11)
W(1)-C(2)	2.419(12)	W(1)-C(3)	2.461(10)
W(1)-C(4)	2.450(9)	W(1)-C(5)	2.388(9)
W(1)-C(31)	2.190(11)	W(1)-CP(1)	2.08
W(2)-O(1)	2.161(6)	W(2)-O(5)	1.939(6)
W(2)-N(2)	1.748(7)	W(2)-C(11)	2.313(10)
W(2)-C(12)	2.418(10)	W(2)-C(13)	2.452(9)
W(2)-C(14)	2.431(9)	W(2)-C(15)	2.326(9)
W(2)-C(42)	2.178(9)	W(2)-CP(2)	2.06
W(3)-O(2)	2.176(5)	W(3)-O(6)	1.954(6)
W(3)-N(3)	1.751(7)	W(3)-C(21)	2.378(10)
W(3)-C(22)	2.481(10)	W(3)-C(23)	2.488(10)
W(3)-C(24)	2.436(10)	W(3)-C(25)	2.373(9)
W(3)-C(53)	2.181(8)	W(3)-CP(3)	2.12
O(1)-N(1)	1.296(9)	O(2)-N(2)	1.289(9)
O(3)-N(3)	1.318(9)	O(4)-C(33)	1.385(11)
O(5)-C(44)	1.408(12)	O(6)-C(55)	1.419(11)
C(1)-C(2)	1.38(2)	C(1)-C(5)	1.42(2)
C(1)-C(6)	1.41(2)	C(2)-C(3)	1.37(2)
C(2)-C(7)	1.53(2)	C(3)-C(4)	1.49(2)
C(3)-C(8)	1.550(15)	C(4)-C(5)	1.480(15)
C(4)-C(9)	1.45(2)	C(5)-C(10)	1.51(2)
C(11)-C(12)	1.42(2)	C(11)-C(15)	1.467(15)
C(11)-C(16)	1.48(2)	C(12)-C(13)	1.41(2)
C(12)-C(17)	1.51(2)	C(13)-C(14)	1.386(15)
C(13)-C(18)	1.53(2)	C(14)-C(15)	1.412(15)
C(14)-C(19)	1.47(2)	C(15)-C(20)	1.52(2)
C(21)-C(22)	1.362(15)	C(21)-C(25)	1.48(2)
C(21)-C(26)	1.53(2)	C(22)-C(23)	1.421(15)
C(22)-C(27)	1.498(15)	C(23)-C(24)	1.37(2)
C(23)-C(28)	1.49(2)	C(24)-C(25)	1.38(2)
C(24)-C(29)	1.53(2)	C(25)-C(30)	1.48(2)
C(31)-C(32)	1.345(15)	C(31)-C(36)	1.494(13)
C(32)-C(33)	1.517(14)	C(33)-C(34)	1.505(15)
C(33)-C(35)	1.555(14)	C(36)-C(37)	1.424(14)
C(36)-C(41)	1.354(15)	C(37)-C(38)	1.392(14)
C(38)-C(39)	1.38(2)	C(39)-C(40)	1.38(2)
C(40)-C(41)	1.39(2)	C(42)-C(43)	1.281(14)

Table A25 continued.

C(42)-C(47)	1.528(14)	C(43)-C(44)	1.501(14)
C(44)-C(45)	1.544(15)	C(44)-C(46)	1.587(15)
C(47)-C(48)	1.403(14)	C(47)-C(52)	1.400(14)
C(48)-C(49)	1.364(14)	C(49)-C(50)	1.37(2)
C(50)-C(51)	1.38(2)	C(51)-C(52)	1.386(15)
C(53)-C(54)	1.310(13)	C(53)-C(58)	1.533(13)
C(54)-C(55)	1.507(14)	C(55)-C(56)	1.537(15)
C(55)-C(57)	1.543(14)	C(58)-C(59)	1.355(14)
C(58)-C(63)	1.419(13)	C(59)-C(60)	1.413(14)
C(62)-C(63)	1.390(15)		

Table A26. Bond angles (°) in the solid-state molecular structure determined for complex **3.12.**

Atom-atom-atom	angle	Atom-atom-atom	angle
O(3)-W(1)-O(4)	77.4(3)	O(3)-W(1)-N(1)	88.6(3)
O(3)-W(1)-C(31)	147.9(3)	O(3)-W(1)-CP(1)	100.4
O(4)-W(1)-N(1)	124.2(3)	O(4)-W(1)-C(31)	75.8(3)
O(4)-W(1)-CP(1)	119.1	N(1)-W(1)-C(31)	92.1(4)
N(1)-W(1)-CP(1)	116.5	C(31)-W(1)-CP(1)	107.9
O(1)-W(2)-O(5)	75.7(2)	O(1)-W(2)-N(2)	88.6(3)
O(1)-W(2)-C(42)	145.9(3)	O(1)-W(2)-CP(2)	102.2
O(5)-W(2)-N(2)	124.4(3)	O(5)-W(2)-C(42)	75.5(3)
O(5)-W(2)-CP(2)	117.3	N(2)-W(2)-C(42)	92.8(4)
N(2)-W(2)-CP(2)	118.0	C(42)-W(2)-CP(2)	107.1
O(2)-W(3)-O(6)	76.2(3)	O(2)-W(3)-N(3)	90.3(3)
O(2)-W(3)-C(53)	145.6(3)	O(2)-W(3)-CP(3)	101.1
O(6)-W(3)-N(3)	122.1(3)	O(6)-W(3)-C(53)	74.8(3)
O(6)-W(3)-CP(3)	117.8	N(3)-W(3)-C(53)	89.7(3)
N(3)-W(3)-CP(3)	120.0	C(53)-W(3)-CP(3)	108.5
W(2)-O(1)-N(1)	122.1(5)	W(3)-O(2)-N(2)	123.2(5)
W(1)-O(3)-N(3)	122.8(5)	W(1)-O(4)-C(33)	125.7(6)
W(2)-O(5)-C(44)	124.1(6)	W(3)-O(6)-C(55)	126.3(6)
W(1)-N(1)-O(1)	163.1(7)	W(2)-N(2)-O(2)	165.0(6)
W(3)-N(3)-O(3)	164.7(6)	C(2)-C(1)-C(5)	108.7(10)
C(2)-C(1)-C(6)	128.8(14)	C(5)-C(1)-C(6)	122.3(12)
C(1)-C(2)-C(3)	110.1(11)	C(1)-C(2)-C(7)	129.8(14)
C(3)-C(2)-C(7)	120.1(12)	C(2)-C(3)-C(4)	110.1(10)
C(2)-C(3)-C(8)	130.4(12)	C(4)-C(3)-C(8)	119.5(12)
C(3)-C(4)-C(5)	101.9(10)	C(3)-C(4)-C(9)	128.3(11)
C(5)-C(4)-C(9)	127.4(11)	C(1)-C(5)-C(4)	109.0(9)
C(1)-C(5)-C(10)	127.5(11)	C(4)-C(5)-C(10)	123.4(11)
C(12)-C(11)-C(15)	105.6(1	C(12)-C(11)-C(16)	129.1(12)
C(15)-C(11)-C(16)	124.8(12)	C(11)-C(12)-C(13)	109.0(10)
C(11)-C(12)-C(17)	125.2(12)	C(13)-C(12)-C(17)	125.8(13)
C(12)-C(13)-C(14)	109.1(11)	C(12)-C(13)-C(18)	124.5(11)
C(14)-C(13)-C(18)	126.3(10)	C(13)-C(14)-C(15)	108.6(9)
C(13)-C(14)-C(19)	124.8(12)	C(15)-C(14)-C(19)	125.7(12)
C(11)-C(15)-C(14)	107.7(10)	C(11)-C(15)-C(20)	124.5(11)
C(14)-C(15)-C(20)	127.2(10)	C(22)-C(21)-C(25)	108.1(10)
C(22)-C(21)-C(26)	128.4(12)	C(25)-C(21)-C(26)	123.3(12)
C(21)-C(22)-C(23)	108.8(9)	C(21)-C(22)-C(27)	124.8(11)

Table A26 continued.

C(23)-C(22)-C(27)	126.4(11)	C(22)-C(23)-C(24)	106.9(11)
C(22)-C(23)-C(28)	124.1(11)	C(24)-C(23)-C(28)	128.9(13)
C(23)-C(24)-C(25)	111.9(11)	C(23)-C(24)-C(29)	122.5(13)
C(25)-C(24)-C(29)	125.2(12)	C(21)-C(25)-C(24)	104.1(9)
C(21)-C(25)-C(30)	127.4(13)	C(24)-C(25)-C(30)	127.7(13)
W(1)-C(31)-C(32)	112.5(7)	W(1)-C(31)-C(36)	129.8(8)
C(32)-C(31)-C(36)	117.1(10)	C(31)-C(32)-C(33)	119.2(9)
O(4)-C(33)-C(32)	106.3(8)	O(4)-C(33)-C(34)	109.0(8)
O(4)-C(33)-C(35)	109.8(9)	C(32)-C(33)-C(34)	111.2(9)
C(32)-C(33)-C(35)	109.3(9)	C(34)-C(33)-C(35)	111.1(8)
C(31)-C(36)-C(37)	120.9(10)	C(31)-C(36)-C(41)	121.5(10)
C(37)-C(36)-C(41)	117.4(10)	C(36)-C(37)-C(38)	119.5(10)
C(37)-C(38)-C(39)	120.6(10)	C(38)-C(39)-C(40)	120.5(10)
C(39)-C(40)-C(41)	118.2(11)	C(36)-C(41)-C(40)	123.5(11)
W(2)-C(42)-C(43)	115.2(8)	W(2)-C(42)-C(47)	126.8(7)
C(43)-C(42)-C(47)	117.4(9)	C(42)-C(43)-C(44)	117.4(9)
O(5)-C(44)-C(43)	107.7(9)	O(5)-C(44)-C(45)	111.6(9)
O(5)-C(44)-C(46)	107.2(8)	C(43)-C(44)-C(45)	114.1(9)
C(43)-C(44)-C(46)	109.5(9)	C(45)-C(44)-C(46)	106.4(10)
C(42)-C(47)-C(48)	122.4(8)	C(42)-C(47)-C(52)	119.9(9)
C(48)-C(47)-C(52)	117.6(9)	C(47)-C(48)-C(49)	120.7(10)
C(48)-C(49)-C(50)	121.7(11)	C(49)-C(50)-C(51)	118.9(11)
C(50)-C(51)-C(52)	120.6(11)	C(47)-C(52)-C(51)	120.5(10)
W(3)-C(53)-C(54)	114.9(7)	W(3)-C(53)-C(58)	127.4(7)
C(54)-C(53)-C(58)	117.6(8)	C(53)-C(54)-C(55)	118.5(8)
O(6)-C(55)-C(54)	105.4(8)	O(6)-C(55)-C(56)	106.8(8)
O(6)-C(55)-C(57)	110.3(9)	C(54)-C(55)-C(56)	112.4(9)
C(54)-C(55)-C(57)	112.0(9)	C(56)-C(55)-C(57)	109.7(9)
C(53)-C(58)-C(59)	121.8(9)	C(53)-C(58)-C(63)	119.2(9)
C(59)-C(58)-C(63)	119.0(9)	C(58)-C(59)-C(60)	122.8(10)
C(59)-C(60)-C(61)	116.2(11)	C(60)-C(61)-C(62)	120.9(10)
C(61)-C(62)-C(63)	121.9(11)	C(58)-C(63)-C(62)	119.1(11)

Table A27. Fractional atomic coordinates in the solid-state molecular structure determined for complex **4.10.**

Atom	x	y	z	Ueq
W	0.222924(8)	0.029129(8)	0.087827(11)	0.03626
O	0.12441(19)	0.06250(20)	0.15560(28)	0.0696
N	0.16722(18)	0.02819(17)	0.12874(25)	0.0448
C(1)	0.22651(22)	0.15172(21)	0.15249(25)	0.0450
C(2)	0.14922(20)	0.13633(22)	0.07510(29)	0.0452
C(3)	0.14892(20)	0.12735(22)	0.02578(28)	0.0452
C(4)	0.22508(22)	0.13964(22)	0.01134(28)	0.0448
C(5)	0.27222(19)	0.15437(22)	0.09747(29)	0.0460
C(11)	0.25072(26)	0.17423(24)	0.26779(28)	0.0595
C(12)	0.07956(22)	0.13229(25)	0.09458(37)	0.0610
C(13)	0.07759(23)	0.11674(25)	0.13124(32)	0.0611
C(14)	0.25023(25)	0.14335(26)	0.09894(32)	0.0583
C(15)	0.35553(20)	0.17574(25)	0.14559(36)	0.0636
C(6)	0.32041(22)	0.01446(22)	0.25141(30)	0.0464
C(7)	0.35846(22)	0.06215(23)	0.26508(30)	0.0462
C(8)	0.42623(22)	0.07286(22)	0.37767(31)	0.0503
C(9)	0.45705(24)	0.15260(25)	0.40250(36)	0.0607
C(10)	0.52175(30)	0.16125(30)	0.51575(41)	0.0795
C(19)	0.31733(22)	0.03879(22)	0.07196(32)	0.0453
C(20)	0.38146(22)	0.06955(25)	0.17413(32)	0.0522
C(21)	0.24867(22)	0.07929(23)	0.00999(29)	0.0436
C(22)	0.18748(24)	0.03868(23)	0.07391(32)	0.0475
C(23)	0.11398(24)	0.07282(26)	0.12874(33)	0.0551
C(24)	0.10078(27)	0.14171(29)	0.10073(39)	0.0645
C(25)	0.16084(29)	0.18213(27)	0.01810(40)	0.0647
C(26)	0.23181(25)	0.15291(23)	0.03629(33)	0.0522

Table A28. Selected bond distances (Å) and angles (°) in the solid-state molecular structure of complex **4.10.**

atom-atom	distance	atom-atom	distance
W-N	1.767(4)	W-Cp [b]	2.051
W-C(1)	2.353(4)	W-C(6)	2.226(3)
W-C(2)	2.350(4)	W-C(19)	2.301(5)
W-C(3)	2.363(4)	W-C(21)	2.381(4)
W-C(4)	2.419(4)	W-C(22)	2.371(4)
W-C(5)	2.410(4)	O-N	1.225(6)
C(1)-C(2)	1.428(5)	C(1)-C(11)	1.512(5)
C(1)-C(5)	1.420(7)	C(2)-C(12)	1.507(7)
C(2)-C(3)	1.416(6)	C(3)-C(13)	1.509(4)
C(3)-C(4)	1.425(6)	C(4)-C(14)	1.514(7)
C(4)-C(5)	1.397(5)	C(5)-C(15)	1.500(5)
C(6)-C(7)	1.524(6)	C(7)-C(20)	1.535(7)
C(7)-C(8)	1.538(5)	C(19)-C(20)	1.510(5)
C(8)-C(9)	1.520(6)	C(19)-C(21)	1.419(5)
C(9)-C(10)	1.518(6)	C(23)-C(24)	1.349(7)
C(21)-C(22)	1.432(5)	C(24)-C(25)	1.412(6)
C(21)-C(26)	1.440(6)	C(25)-C(26)	1.346(6)
C(22)-C(23)	1.421(6)		

atom-atom-atom	angle	atom-atom-atom	angle
N-W-C(6)	88.02(15)	C(6)-W-Cp	108.35
N-W-C(19)	111.51(15)	C(19)-W-C(21)	35.23(13)
N-W-C(21)	88.19(16)	C(19)-W-C(22)	62.53(14)
N-W-C(22)	93.34(16)	C(19)-W-Cp	124.72
N-W-Cp	123.76	C(21)-W-C(22)	35.08(12)
C(6)-W-C(19)	71.82(16)	C(21)-W-Cp	139.03
C(6)-W-C(21)	96.51(13)	C(22)-W-Cp	110.82
C(6)-W-C(22)	131.34(15)	W-N-O	174.3(3)
W-C(6)-C(7)	111.99(24)	C(19)-C(21)-C(26)	124.8(3)
W-C(19)-C(20)	117.2(3)	C(22)-C(21)-C(26)	117.8(3)
W-C(19)-C(21)	75.5(3)	W-C(22)-C(21)	72.84(23)
C(20)-C(19)-C(21)	122.6(4)	W-C(22)-C(23)	121.1(4)
C(7)-C(20)-C(19)	108.7(4)	C(21)-C(22)-C(23)	119.2(4)

Table A28 continued.

W-C(21)-C(19)	69.31(25)	C(22)-C(23)-C(24)	120.9(4)
W-C(21)-C(22)	72.07(25)	C(23)-C(24)-C(25)	120.2(4)
W-C(21)-C(26)	120.1(4)	C(24)-C(25)-C(26)	121.5(5)
C(19)-C(21)-C(22)	116.6(4)	C(21)-C(26)-C(25)	120.3(4)
C(6)-C(7)-C(8)	112.5(3)	C(8)-C(7)-C(20)	113.3(4)
C(6)-C(7)-C(20)	106.5(3)	C(7)-C(8)-C(9)	114.6(3)
C(2)-C(1)-C(5)	107.8(3)	C(8)-C(9)-C(10)	112.8(4)
C(2)-C(1)-C(11)	124.6(4)	C(4)-C(3)-C(13)	126.7(4)
C(5)-C(1)-C(11)	126.8(3)	C(3)-C(4)-C(5)	108.1(4)
C(1)-C(2)-C(3)	107.4(4)	C(3)-C(4)-C(14)	126.5(3)
C(1)-C(2)-C(12)	127.1(4)	C(5)-C(4)-C(14)	125.1(4)
C(3)-C(2)-C(12)	125.5(3)	C(1)-C(5)-C(4)	108.5(3)
C(2)-C(3)-C(4)	108.2(3)	C(1)-C(5)-C(15)	126.0(3)
C(2)-C(3)-C(13)	124.7(4)	C(4)-C(5)-C(15)	125.3(4)

[a] Distances as corrected by a rigid-body model for thermal motion of the molecule.
[b] Cp represents thecenter of mass of the C5-ring of Cp*.
[c] The oxygen atom displays excess thermal motion beyond that accounted for by the rigid-body model. A more reasonable corrected distance of ~1.240 Å for the N-O bond length is estimated based upon a riding model.

Table A29. Fractional atomic coordinates in the solid-state molecular structure determined for complex **4.14.**

atom	x	y	z	B(eq)
W(1)	0.20735(3)	0.34389(4)	0.28874(2)	1.146(6)
O(1)	0.5663(6)	0.3451(7)	0.3330(4)	2.26(13)
N(1)	0.4177(6)	0.3377(7)	0.3180(4)	1.17(13)
C(1)	0.1309(10)	0.3827(9)	0.1108(6)	1.9(2)
C(2)	--0.0182(9)	0.3961(10)	0.1519(6)	2.0(2)
C(3)	0.0108(8)	0.5103(9)	0.2256(6)	1.6(2)
C(4)	0.1717(9)	0.5672(9)	0.2306(6)	1.9(2)
C(5)	0.2416(8)	0.4903(9)	0.1570(6)	1.7(2)
C(6)	0.1544(11)	0.2884(12)	0.0181(7)	3.2(2)
C(7)	--0.1774(9)	0.3257(11)	0.1135(7)	2.9(2)
C(8)	--0.1174(9)	0.5770(10)	0.2808(7)	2.3(2)
C(9)	0.2387(10)	0.7006(10)	0.2919(7)	2.5(2)
C(10)	0.4103(10)	0.5157(12)	0.1318(7)	3.3(3)
C(11)	0.1908(8)	0.4477(9)	0.4448(5)	1.4(2)
C(12)	0.2176(8)	0.3068(9)	0.4628(5)	1.4(2)
C(13)	0.1053(9)	0.2086(9)	0.4071(5)	1.5(2)
C(14)	0.1521(9)	0.0695(9)	0.3694(6)	2.0(2)
C(15)	0.1758(8)	0.1025(9)	0.2557(6)	1.9(2)
C(16)	0.3749(9)	0.2751(10)	0.5276(6)	2.0(2)
C(17)	--0.0813(8)	0.2309(9)	0.3993(6)	2.0(2)
C(18)	0.0217(9)	0.0476(9)	0.1828(6)	2.0(2)
C(19)	0.3251(8)	0.0371(8)	0.2228(6)	1.4(2)
C(20)	0.3220(9)	-0.0270(9)	0.1242(6)	1.8(2)
C(21)	0.4544(10)	-0.0903(9)	0.0943(7)	2.3(2)
C(22)	0.5942(9)	-0.0958(10)	0.1647(7)	2.3(2)
C(23)	0.6012(9)	-0.0338(9)	0.2637(7)	2.2(2)
C(24)	0.4707(8)	0.0332(9)	0.2910(6)	1.8(2)

Table A30. Bond distances (Å) in the solid-state molecular structure of complex **4.14.**

atom-atom	distance	atom-atom	distance
W(1)-N(1)	1.748(5)	W(1)-C(1)	2.384(8)
W(1)-C(2)	2.483(8)	W(1)-C(3)	2.438(7)
W(1)-C(4)	2.363(9)	W(1)-C(5)	2.365(8)
W(1)-C(11)	2.249(7)	W(1)-C(12)	2.331(7)
W(1)-C(13)	2.353(7)	W(1)-C(15)	2.353(9)
W(1)-CP	2.08	O(1)-N(1)	1.230(7)
C(1)-C(2)	1.447(11)	C(1)-C(5)	1.410(11)
C(1)-C(6)	1.516(11)	C(2)-C(3)	1.408(11)
C(2)-C(7)	1.477(11)	C(3)-C(4)	1.431(10)
C(3)-C(8)	1.529(10)	C(4)-C(5)	1.397(11)
C(4)-C(9)	1.517(12)	C(5)-C(10)	1.522(10)
C(11)-C(12)	1.425(11)	C(12)-C(13)	1.397(10)
C(12)-C(16)	1.504(10)	C(13)-C(14)	1.493(12)
C(13)-C(17)	1.576(10)	C(14)-C(15)	1.593(11)
C(15)-C(18)	1.535(10)	C(15)-C(19)	1.534(9)
C(19)-C(20)	1.394(10)	C(19)-C(24)	1.397(10)
C(20)-C(21)	1.386(11)	C(21)-C(22)	1.377(12)
C(22)-C(23)	1.387(12)	C(23)-C(24)	1.377(10)

Table A31. Bond angles (°) in the solid-state molecular structure determined for complex **4.14.**

atom-atom-atom	angle a	tom-atom-atom	angle
N(1)-W(1)-C(11)	92.6(3)	N(1)-W(1)-C(12)	83.9(2)
N(1)-W(1)-C(13)	105.7(3)	N(1)-W(1)-C(15)	92.1(3)
N(1)-W(1)-CP	118.9	C(11)-W(1)-C(12)	36.2(3)
C(11)-W(1)-C(13)	62.9(3)	C(11)-W(1)-C(15)	121.6(3)
C(11)-W(1)-CP	108.8	C(12)-W(1)-C(13)	34.7(3)
C(12)-W(1)-C(15)	86.8(3)	C(12)-W(1)-CP	142.4
C(13)-W(1)-C(15)	59.9(3)	C(13)-W(1)-CP	135.2
C(15)-W(1)-CP	119.0	W(1)-N(1)-O(1)	173.5(6)
C(2)-C(1)-C(5)	108.9(7)	C(2)-C(1)-C(6)	125.8(7)
C(5)-C(1)-C(6)	124.1(8)	C(1)-C(2)-C(3)	105.2(7)
C(1)-C(2)-C(7)	128.6(8)	C(3)-C(2)-C(7)	125.3(7)
C(2)-C(3)-C(4)	110.1(7)	C(2)-C(3)-C(8)	125.0(7)
C(4)-C(3)-C(8)	124.3(8)	C(3)-C(4)-C(5)	107.0(7)
C(3)-C(4)-C(9)	124.8(7)	C(5)-C(4)-C(9)	127.4(7)
C(1)-C(5)-C(4)	108.6(6)	C(1)-C(5)-C(10)	125.3(8)
C(4)-C(5)-C(10)	126.0(8)	W(1)-C(11)-C(12)	75.0(4)
W(1)-C(12)-C(11)	68.8(4)	W(1)-C(12)-C(13)	73.5(4)
W(1)-C(12)-C(16)	120.1(4)	C(11)-C(12)-C(13)	116.7(7)
C(11)-C(12)-C(16)	117.4(7)	C(13)-C(12)-C(16)	125.3(8)
W(1)-C(13)-C(12)	71.8(4)	W(1)-C(13)-C(14)	99.5(5)
W(1)-C(13)-C(17)	108.6(5)	C(12)-C(13)-C(14)	122.4(7)
C(12)-C(13)-C(17)	120.1(7)	C(14)-C(13)-C(17)	116.6(7)
C(13)-C(14)-C(15)	99.0(7)	W(1)-C(15)-C(14)	96.5(5)
W(1)-C(15)-C(18)	116.2(6)	W(1)-C(15)-C(19)	113.1(5)
C(14)-C(15)-C(18)	106.8(6)	C(14)-C(15)-C(19)	112.8(7)
C(18)-C(15)-C(19)	110.5(6)	C(15)-C(19)-C(20)	122.1(6)
C(15)-C(19)-C(24)	122.0(7)	C(20)-C(19)-C(24)	115.9(6)
C(19)-C(20)-C(21)	122.8(7)	C(20)-C(21)-C(22)	119.7(8)
C(21)-C(22)-C(23)	119.0(7)	C(22)-C(23)-C(24)	120.5(7)
C(19)-C(24)-C(23)	122.0(7)		

Appendix B. Derivation of the Saturation Rate Expression Discussed in Chapter 3

Before deriving a rate equation for the conversion of **4.9** to **3.2**, the system and a mechanism for the conversion must be defined. Thus, let

A = [Cp*W(NO)($CH_2SiOSiMe_3$)(η^2-CPh=CH_2)]
B = [Cp*W(NO)(η^2-CPh≡CH)]
C = [$Me_3SiOSiMe_3$]
D = [EtOAc]
E = [Cp*W(NO)(OEt)(η^2-*O*=CMeCH=*C*Ph)].

The formation of E may be described in the following elementary steps:

$$A \underset{k_{-1}}{\overset{k_1}{\rightleftharpoons}} B + C$$

$$B + D \xrightarrow{k_2} E$$

From this mechanism, the rate expression for the loss of A may be derived. Knowing that

$$-dA/dt = k_1A - k_{-1}BC \qquad (1)$$

and

$$dB/dt = k_1A - k_{-1}BC - k_2BD \qquad (2),$$

the steady-state approximation is applied to B, i.e. dB/dt = 0. One obtains from this approximation an expression for B:

$$B = \frac{k_1A}{k_{-1}C + k_2D} \qquad (3)$$

By mass balance, under steady-state conditions, $-dA/dt = dE/dt = k_2BD$ (4).

Substituting (3) into (4), one obtains an expression for dE/dt that is dependent upon known and measurable quantities:

$$-dA/dt = dE/dt = \frac{k_1 k_2 AD}{k_{-1}C + k_2 D} \quad , \text{and } k_{obs} = \frac{k_1 k_2 D}{k_{-1}C + k_2 D} \qquad (5)$$

Thus, a rate dependence on both C and D exists in this derivation. Inverting the expression for k_{obs} yields

$$1 / k_{obs} = \frac{k_{-1}C}{k_1 k_2 D} + \frac{1}{k_1}$$

Thus, a plot of $1/k_{obs}$ vs. C/D affords a line of slope k_{-1}/k_1k_2 and intercept $1/k_1$. The k_1 rate constant is calculated from the intercept of the line and its value is employed in the expression for the k_{-1}/k_2 ratio utilizing the magnitude of the slope. This ratio expresses the selectivity by B for the k_{-1} and k_2 steps; in essence, it is a measure of the selectivity by B for one reagent over another.